# Biochemical analysis of Tribbles 2 pseudokinase using repurposed kinase inhibitors

Daniel M. Foulkes

**Thesis submitted in accordance with the requirements of the University of Liverpool for the degree of Doctor in Philosophy**

SEPTEMBER 28, 2018

THE UNIVERSITY OF LIVERPOOL

# Acknowledgements

Undertaking a PhD project in Pat Eyers' lab was challenging, fraught with difficulty but exciting. The learning curve from undergraduate to PhD level was steep but Pat helped me to achieve my potential. Pat would always be understanding and be there for me whenever I needed him. As a supervisor he would give you nothing less than 100% and inspired passion. I can honestly say that I enjoyed writing this thesis, which was due to the excellent support network and continuous contact with Pat and Dom.

Dom Byrne dedicated so much of his time to training me; he witnessed all of my mistakes, and aside from occasional satire, was the paragon of a kind and patient person. Dom is someone I aspire to, who puts others before himself and is motivated only by the enjoyment of his work. He was someone I could always depend on and over the four years of my PhD, he has become one of my closest friends.

Sam Ferries and I began our PhD journeys together. We became good friends during our training and could always depend on each other for both moral and experimental support. Thank you Sam, for all the hours of work you put into TRIB2 mass spectrometry.

My wife Imogen never ceased to amaze in her unyielding support of me during the entirety of the last four years. She would take me to and from the lab at inordinate times, was patient when I was poorly tempered and took pride in my achievements. Finally, I give thanks to my sister Jessica, mother Lorraine and father Warren, for their support and belief in my abilities. Although my mother could never grasp the correct pronunciation of 'pseudokinase', she would always show interest and want to hear about my work.

# Publications

Some of the work described in this thesis has been published.

1. Foulkes, D.M., et al., Covalent inhibitors of EGFR family protein kinases induce degradation of human Tribbles 2 (TRIB2) pseudokinase in cancer cells. Sci Signal, 2018. 11(549).

2. Byrne, D.P., D.M. Foulkes, and P.A. Eyers, Pseudokinases: update on their functions and evaluation as new drug targets. Future Med Chem, 2017. 9(2): p. 245-265.

3. Foulkes, D.M., et al., Tribbles pseudokinases: novel targets for chemical biology and drug discovery? Biochem Soc Trans, 2015. 43(5): p. 1095-103.

# Abstract

Pseudokinases make up ~10% of the human kinome and lack one or more of the evolutionary conserved amino acids that are typically required to hydrolyse ATP and phosphorylate protein substrates. Overexpression of the Tribbles 2 pseudokinase (TRIB2) has been identified in subsets of acute myeloid and acute lymphoblastic leukaemia as well as drug-resistant solid tumours, marking it out as an important new target for drug discovery. TRIB2 is the most ancestral of the three human TRIB pseudokinase homologues, which have evolved features distinguishing them from all other protein kinases. They are uniquely defined by an unusual αC-helix, which forms a binding site for an E3 ubiquitin ligase binding motif in the Tribbles C-terminal tail. The pseudokinase domain also retains a binding platform for substrates, such as the myeloid transcription factor C/EBPα, which are ubiquitinated by context-specific E3 ligases. TRIB2 has also been reported to induce AKT phosphorylation at Ser473, promoting cell survival. A lack of target-validated small molecule ligands with which to probe signalling functions has hindered the analysis of Tribbles pseudokinases.

This thesis describes a kinase inhibitor-repurposing approach to discover novel TRIB2 chemical ligands, in order to probe TRIB2 biochemical mechanisms *in vitro* and analyse TRIB2 signalling mechanisms in human cells. By employing a simple thermal shift assay, recombinant TRIB2 protein was screened using the Published Kinase Inhibitor Set (PKIS), and distinct families of stabilising and destabilising chemical ligands were discovered and analysed. The clinically-approved covalent EGFR/HER2 inhibitors afatinib and neratinib were found to bind covalently to two unique cysteine residues in the αC-helix of the TRIB2 pseudokinase domain, causing it to become uncoupled from its own C-terminal tail region. Cellular afatinib exposure led to rapid proteasome-mediated degradation of both exogenous and endogenously expressed TRIB2 in human cell lines. Mutation of the two Cys residues responsible for covalent compound-binding *in vitro* also resulted in TRIB2 stabilisation in cells in the presence of afatinib, alongside the maintenance of high levels of pSer473 AKT. Afatinib and neratinib were also highly cytotoxic in the TRIB2 overexpressing leukaemia U937 cell model, downstream of TRIB2 degradation and the induction of apoptosis. The work reported in this thesis suggests new potential therapeutic approaches for the treatment of TRIB2-associated diseases.

# Contents

# List of figures and tables

# List of abbreviations

| | |
|---|---|
| ACC | Acetyl Co enzyme A carboxylase |
| AcLDL | Acetylated low density lipoprotein |
| ADP | Adenosine diphosphate |
| AFA | Afatinib |
| AGC | Protein kinase A, G and C families |
| ALL | Acute lymphoblastic leukaemia |
| Alphascreen | Amplified Luminescent Proximity Homogeneous Assay Screen |
| AML | Acute myeloid leukaemia |
| AMPK | AMP-activated protein kinase |
| AST | Active site thether |
| ATP | Adenosine triphosphate |
| BME | β-mecaptoethanol |
| BOR | Bortezomib |
| BSA | Bovine serum albumin |
| BTK | Bruton's tyrosine kinase |
| C/EBPα | CCAAT enhancer-binding protein alpha |
| CAMK | Calmodulin dependent kinases |
| CAN | Canertinib |
| CD | Cicular dichrosim |
| CDC25 | M-phase inducer phosphatase |
| CDK | Cyclin dependent kinase |
| CETSA | Cellular thermal shift assay |
| CLL | Chronic lymphoid leukaemia |
| CLT | C-terminal tether |
| CMGC | cyclin-dependent kinase, map kinase, glycogen synthase kinase 3 and CDK2-like kinases |
| CML | Chronic myeloid leukaemia |
| COP1 | Constitutive photomorphogenic protein 1 |
| CRISPR | Clustered regularly interspaced short palindromic repeats |
| C-terminal | Carboxly-terminus |
| Da | Dalton |

| | |
|---|---|
| DMEM | Dulbecco’s Modified Eagle medium |
| DMSO | Dimethyl sulphoxide |
| DNA | Deoxyribonucleaic acid |
| DSF | Differential scanning fluorimetry |
| DSLS | Differential static light scattering |
| DTT | Dithiothreitol |
| EGFR | Epidermal growth factor receptor |
| ERK | Extracellular signal regulated kinase |
| ERL | Erlotinib |
| FBS | Foetal bovine serum |
| FDA | Food and drug administration |
| FITC | Fluorescence isothiocyanate |
| FOXO | Forkhead/winged helix class O transcription factors |
| GAPDH | Glyceraldehyde 3-phosphate dehydrogenase |
| GEF | Gefitinib |
| GPCR | G-protein coupled receptor |
| GSK3 | Glycogen synthase kinase 3 |
| GST | Glutathione-S-transferase |
| HCD | Higher-energy collisional dissociation |
| HER2 | Human epidermal growth factor recetor 2 |
| HER3 | Human epidermal growth factor recetor 3 |
| HER4 | Human epidermal growth factor recetor 4 |
| HM | Hydrophobic motif |
| HPLC | High performance liquid chromatography |
| HSP | Heat shock protein |
| IGF1 | Insulin-like growth factor |
| IL-8 | Interleukin-8 |
| IMAC | Immobalised metal affinity chromatography |
| IM-MS | Ion-mobility Mass spectrometry |
| IP | Immunoprecipitation |
| IPTG | Isopropyl-1-thio-β-D-galactosidase |
| ITC | Isothermal titration calorimetry |
| JAK | Janus kinase |

| | |
|---|---|
| JH | Janus homology domain |
| JM | Juxtamembrane domain |
| kDa | Kilodalton |
| KSR | Kinase suppressor of Ras |
| L | Litre |
| LAP | Lapatinib |
| LB | Luria-Bertani |
| LIC | Ligation independent cloning |
| MAPK | Mitogen activated protein kinases |
| MBP | Maltose binding protein |
| MDS | Myelodysplastic syndrome |
| MEF | Mouse embryonic fibroblasts |
| mg | micro gram |
| mL | Millilitre |
| MLKL | Mixed lineage kinase like protein |
| MO25 | Calcium-binding protein 39 |
| Mr | Relative molecular mass |
| MS | Mass spectrometry |
| MST | Micoscale thermophoresis |
| mTORC1 | Mammalian target of rapamycin complex 1 |
| mTORC2 | Mammalian target of rapamycin complex 2 |
| MTT | 3-(4,5-dimethylthiazol-2-yl)-2,5-diphenyltetrazolium bromide |
| NER | Neratinib |
| ng | nano gram |
| NLT | N-terminal tether |
| NSCLC | Non-small cell lung cancer |
| NTA | Nitrilotriacetate |
| N-terminal | Amino-terminus |
| OD | Optical density |
| OSI | Osimertinib |
| OSR1 | oxidative stress response kinase |
| PBS | Phosphate buffered saline |
| PCR | Polymerase chain reaction |

| | |
|---|---|
| PDB | Protein data bank |
| PDK1 | 3-phosphoinositide-dependent protein kinase 1 |
| PH | Pleckstrin homology |
| PI3K | Phosphatidylinositol 3-kinase |
| PIF | PDK1-interacting fragment |
| PIP2 | Phosphatidylinositol 4,5-bisphosphate |
| PIP3 | phosphatidylinositol 3,4,5-triphosphate |
| PKA | Protein kinase A |
| PKB/AKT | RAC-alpha serine/threonine-protein kinase |
| PKC | Protein kinase C |
| PKIS1 | Protein kinase inhibitor set 1 |
| PLK | Polo like kinase |
| PRK2 | Serine/threonine-protein kinase N |
| RNA | Ribonucleaic acid |
| S6K | S6 kinase beta |
| SDS-PAGE | Sodium dodecyl sulphate-polyacrylamide electrophoresis |
| SEC | Size exclusion chromatography |
| SH | Src homology domain |
| shRNA | Short hairpin RNA |
| SOS | Son of sevenless |
| SPR | Surface plasmon resonance |
| STE | homologues of yeast Sterile 7/11/20 kinases |
| STRADα | STE20 Related kinase Adapter |
| T-ALL | T-cell acute lymphoblastic leukaemia |
| TBS-T | Tris-buffered saline and 0.1% Tween 20 |
| TCEP | Tris(2-carboxyethyl)phosphine) |
| TdCD | Temperature depedent circular dichroism |
| TDD | Tribbles degradation domain |
| TET | Tetracycline |
| TFA | Trifluoroacetic acid |
| TGF | Transforming growth factor |
| TIE-2 | Angiopoietin-1 receptor |
| TK | Tyrosine kinase |

| | |
|---|---|
| TKL | Tyrosine kinase like |
| Tm | Melting temperature |
| TNF | Tumour necrosis factor |
| TRIB | Tribbles |
| TSA | Thermal shift assay |
| TYK | Non-receptor tyrosine-protein kinase TYK2 |
| U | Enzymatic unit of activity |
| UC | Ulcerative colitis |
| Ve | Volume of elution |
| VEGF | Vasular endothelial growth factor |
| Vo | Void volume |
| VRK3 | Inactive serine/threonine-protein kinase VRK3 |
| WNK | With no lysine kianses |
| YFP | yellow fluorescent protein |
| ΔTm | Relative difference in melting temperature |
| λPP | Lambda phosphatase |
| µL | Microlitre |

## List of amino acids

| Amino acid | 3 letter code | single letter code |
|---|---|---|
| alanine | ala | A |
| arginine | arg | R |
| asparagine | asn | N |
| aspartic acid | asp | D |
| cysteine | cys | C |
| glutamine | gln | Q |
| glutamic acid | glu | E |
| glycine | gly | G |
| histidine | his | H |
| isoleucine | ile | I |
| leucine | leu | L |
| lysine | lys | K |
| methionine | met | M |
| phenylalanine | phe | F |
| proline | pro | P |
| serine | ser | S |
| threonine | thr | T |
| tryptophan | trp | W |
| tyrosine | tyr | Y |
| valine | val | V |

# Chapter 1: Introduction

## Background

In our cells thousands of chemical reactions are being controlled at every instant both spatially and temporally. In the 1960s it was realised that the proteins, encoded within our genome, carry out these diverse and specialised functions [1]. Adenosine triphosphate (ATP), which is commonly referred to as 'the molecular currency' drives many vital functions in cells, providing energy for muscle contraction, nerve impulse propagation and chemical synthesis [2]. ATP is also the substrate for protein kinases in cellular signalling, which regulate nearly all aspects of cellular life. Kinases catalyse the transfer of the negatively charged ATP gamma phosphate to a specific serine, threonine or tyrosine amino acid residue on a target substrate. The localised negative charge exerted by the attached phosphate influences the target proteins architecture and molecular dynamics, therefore allowing/disallowing the target to perform a particular function or interact with another specified protein(s). 2% of the entire genome codes for kinases and pseudokinases [3]. The pseudokinase complement of the human kinome consists of approximately 60 signalling proteins, which lack one or more of the amino acids in the highly conserved motifs typically required to correctly align ATP and divalent metal ions, and phosphorylate protein substrates. Recent studies in the pseudokinase field have begun to expose the biological relevance of pseudokinases, which are now thought to perform a diverse range of physiological roles and are connected to a multitude of human diseases. Like canonical kinases, pseudokinases drive conformation-dependent signalling associated with both physiology and disease [4, 5]. The human 'pseudokinome' includes cancer-associated signalling proteins such as human epidermal growth factor receptor 3 (HER3), Janus kinase 2 (JAK2; JH2 domain) and Tribbles 2 (TRIB2), which have received much less attention than conventional kinases. Growing evidence suggests that pseudokinase domains represent rational targets for drug discovery, capable of binding small molecule kinase inhibitors [6]. Discovering or repurposing biologically and/or clinically-active compounds that target atypical-conformations of canonical kinases or pseudokinases, is an active area of research [4, 5, 7-11]. With the benefit of decades of kinase research and the food and drug administration (FDA) approval of over 40

clinical kinase inhibitors for cancer and inflammatory diseases [12, 13], the field of pseudokianse research is in a strong position to understand how ATP-competitive, allosteric, or covalent inhibitors might influence pseudokinase-based signalling mechanisms that are relevant to health and disease [5, 14].

## 1.1 Protein kinases

Kinases bind to ATP and catalyse hydrolysis, transferring the gamma phosphate to a target substrate (Figure 1.1). The phosphorylation of a protein substrate is the best understood method that kinases use to transfer information within a cell, elicit cellular responses and to adequately respond to extracellular stimuli. For instance response to growth factors, which stimulate EGFR autophosphorylation, activation of mitogen activated protein kinases (MAPK) and phosphoinositide 3-kinase (PI3K) cascades to induce cellular proliferation (Figure 1.2). Protein kinases are divided into eight superfamilies, based on their evolutionary relationships: Tyrosine kinases (TK), tyrosine kinase-like (TLK), cyclin-dependent kinases (CDK), homologues of yeast Sterile 7, Sterile 11, and Sterile 20 kinases (STE), cyclin-dependent kinase, map kinase, glycogen synthase kinase 3 and CDK2-like kinases (CMGC), calcium/calmodulin-dependent protein kinase (CAMK), the AGC kinases (named after the protein kinase A, G and C families and the Atypical protein kinases (Figure 1.3). Pseudokinases are found within all of the kinase superfamilies (Figure 1.3B). In order to function, kinases have evolved common ancestral structural features in the catalytic domain but have also independently evolved diverse mechanisms to regulate cellular signalling processes that are not solely based on catalysis [15].

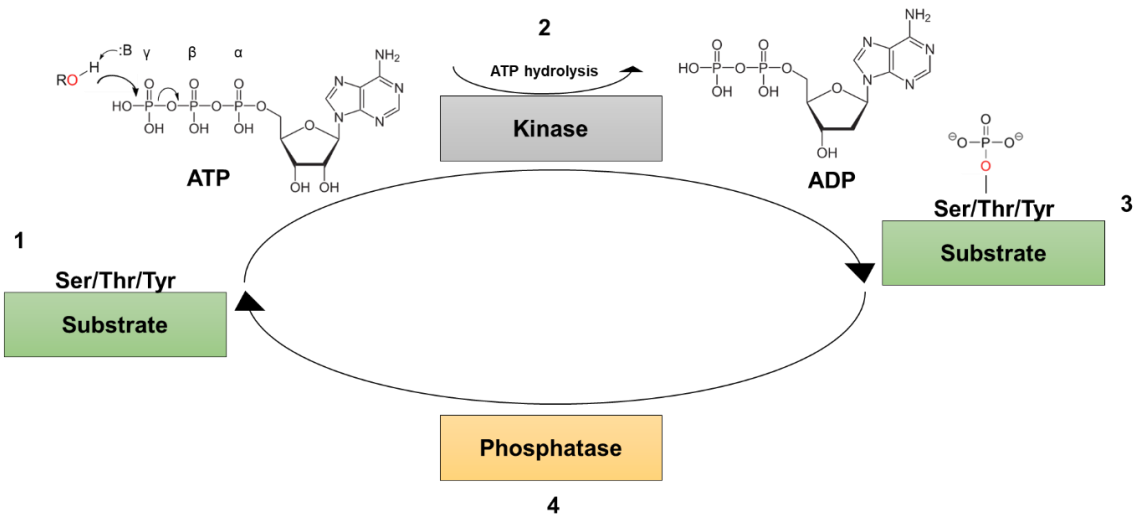

**Figure 1.1: Simplified mechanism of ATP hydrolysis and phosphate transfer by protein kinases.** The unmodified substrate (1) possesses an exposed Ser, Thr or Tyr residue amenable to modification. Kinases (2) bind to ATP and the substrate to catalyse transfer of the ATP γ-phophate, yielding a covalently modified substrate with a negatively charged phosphate group bound to a target Ser, Thr or

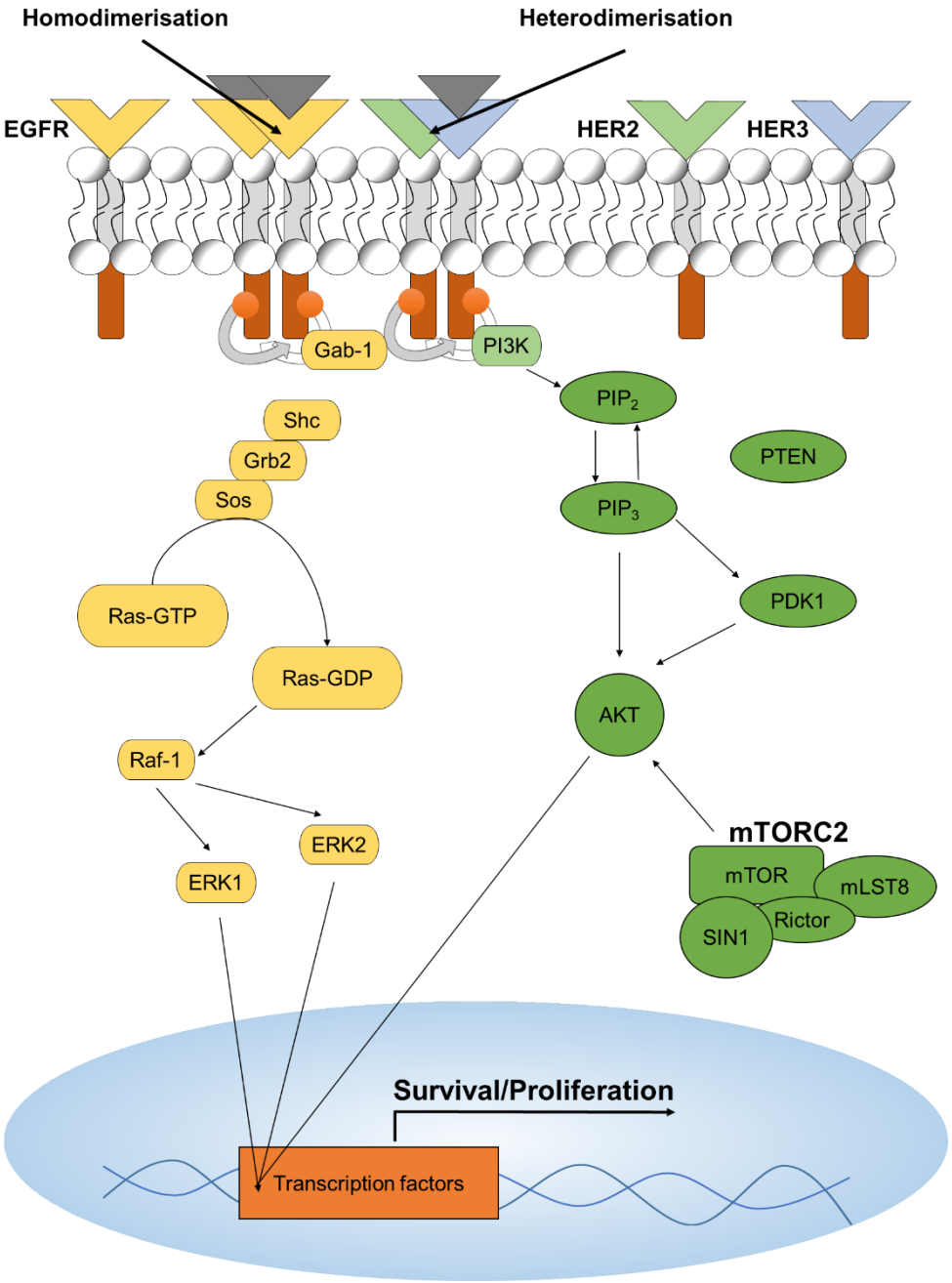


Tyr residue and ADP as a biproduct. Phosphatases (4) perform the opposite role to kinases and catalyse the removal of the previously attached phosphate group.

**Figure 1.2: General explanation of signal transduction.** Extracellular ligands bind to the receptor domains of EGFR kinases, including EGFR, HER3 and HER4 (HER2 cannot bind extracellular ligands

but can activate other EGFR family members), resulting in dimerization of the intracellular kinase domain, *trans* autophosphorylation and activation of MAPK and PI3K/AKT signalling cascades.

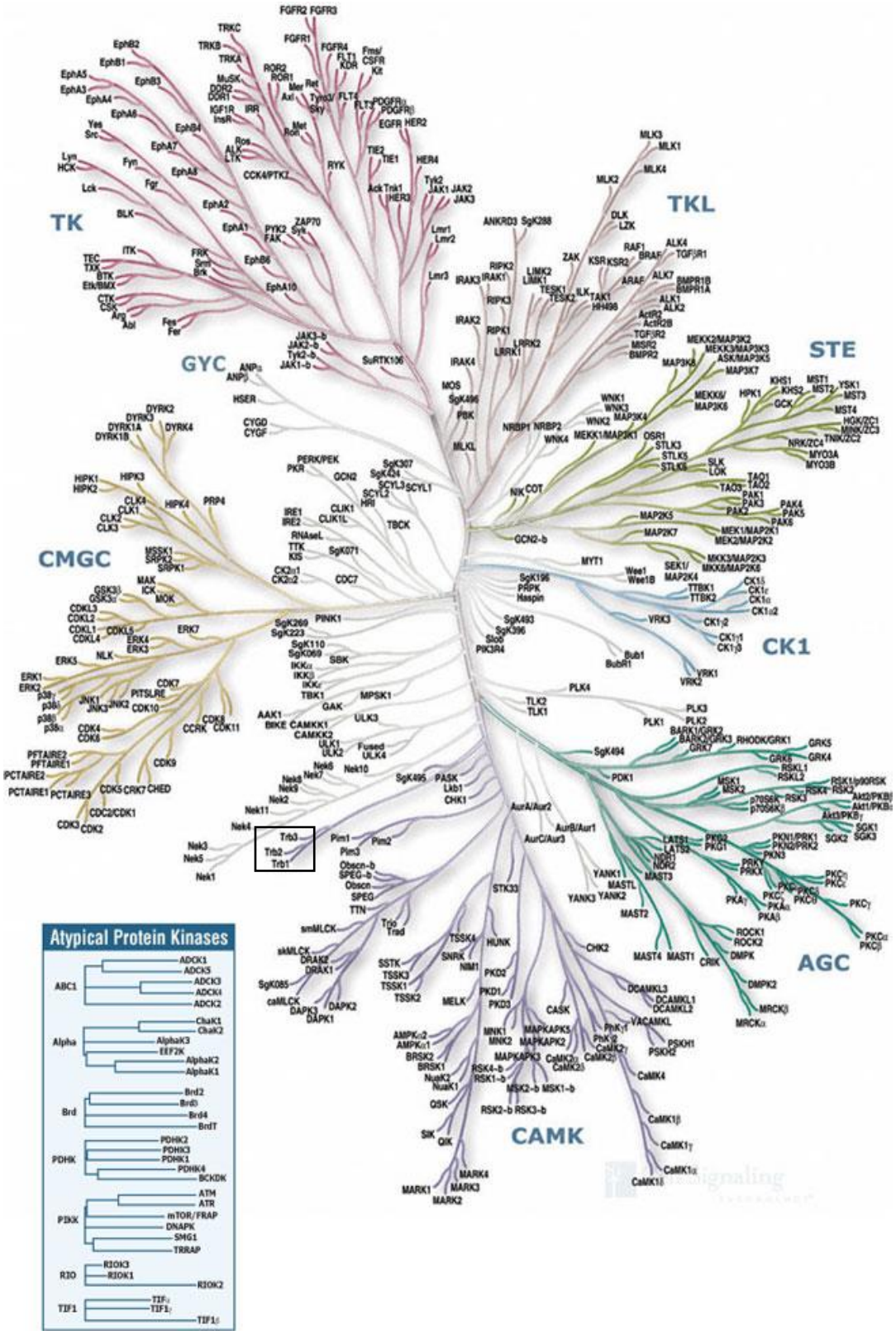

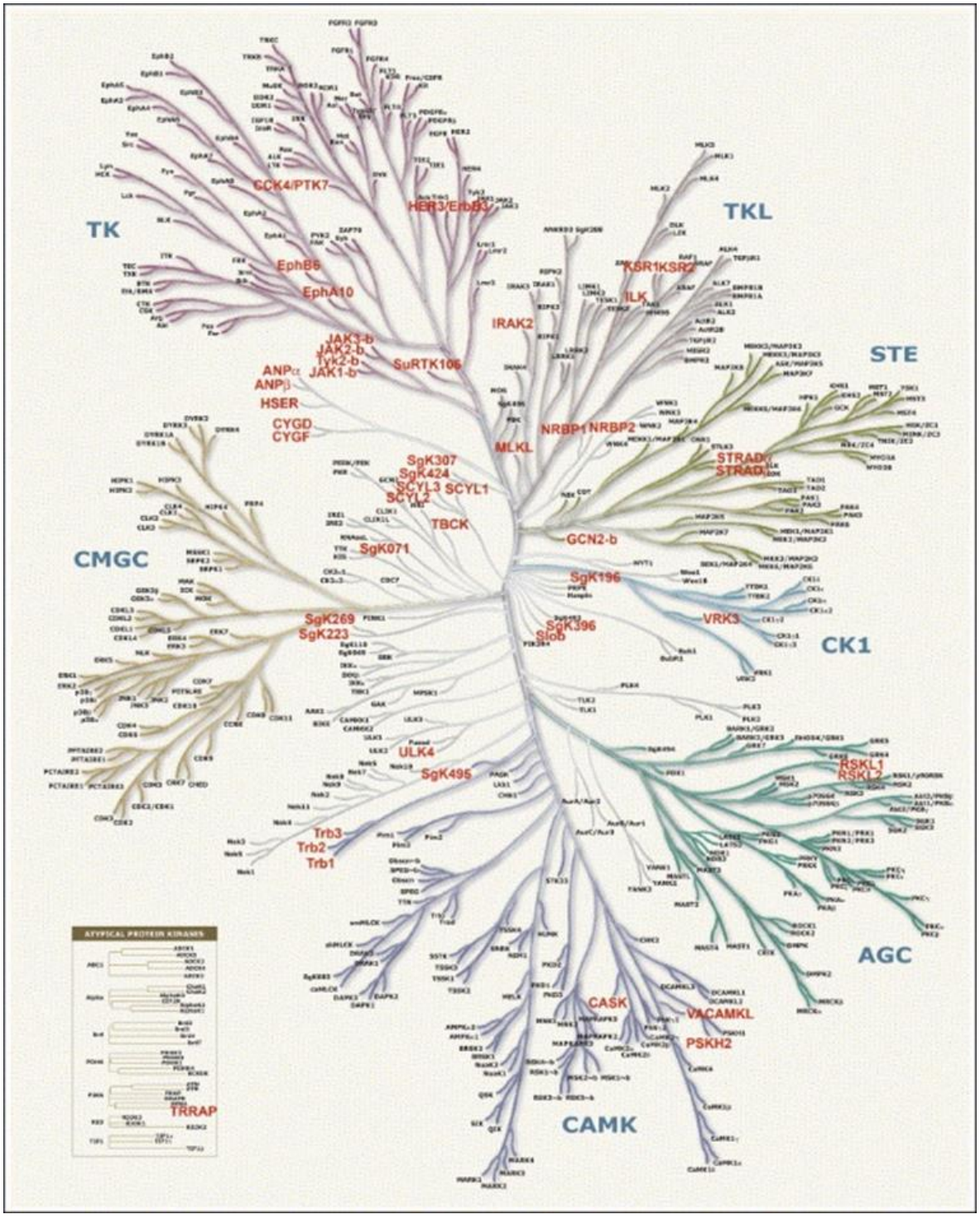


**Figure 1.3: The human kinome. (A)** Depicts the eight major kinase. A black box highlights TRIB1, TRIB2 and TRIB3, which flank the close relative SgK495 (also known as STK40). Illustration obtained from www.cellsignal.com. (B) Highlights all pseudokinases (red) and depicts their evolutionary relationships to canonical kinases. From Boueau *etl al* (2006) [15].

### 1.1.1 Mechanism of ATP hydrolysis and gamma phosphate transfer

PKA was the first crystal structure of a kinase to be solved, in 1991 [16]. Amino acid sequence alignments from genomic data and local spatial pattern alignments from structural data have helped to identify certain key motifs within the designated kinase domain, that are pivotal for binding and hydrolysis of ATP [3]. The kinase domain is bilobal consisting of a small N-terminal lobe and a large C-terminal lobe. The N-terminal lobe typically contains 5 anti-parallel β-pleated sheets and an αC-helix. The C-lobe is mainly α-helical, containing the designated αF helix and catalytic loop, which are vital for aligning the regulatory spine and for the hydrolysis of ATP. The interface of the αC-helix between the N-lobe and the C-lobe forms a cleft, which is the binding surface for ATP and the substrate to which phosphate is transferred [17] (Figure 1.4A). Other structural aspects of the kinase domain are the glycine-rich loop, a conserved lysine in the β3 sheet, the αC helix, the catalytic motif, the activation segment and the hydrophobic αF-helix (Figure 1.4B).

#### 1.1.1.1 The glycine rich loop

In subdomain I the consensus sequence GxGxxG forms the glycine rich loop, which occurs within a β-turn-β motif between the β1 and β2 strands of the N-lobe. The second Gly residue is the most highly conserved throughout the kinome and considered to be the most important [18]. This motif is inherently flexible as there is reduced steric hindrance from the hydrogen R group of the glycine amino acids. Furthermore, as highlighted in blue (Figure1.4A), this loop is offered space as it faces down into the cleft between the N and C-lobes. Upon ATP binding, and a conformational change of the kinase from an inactive to an active conformation, the glycine rich loop closes down upon the ATP and correctly orientates the γ-phosphate, priming transfer to a target substrate [19].

A

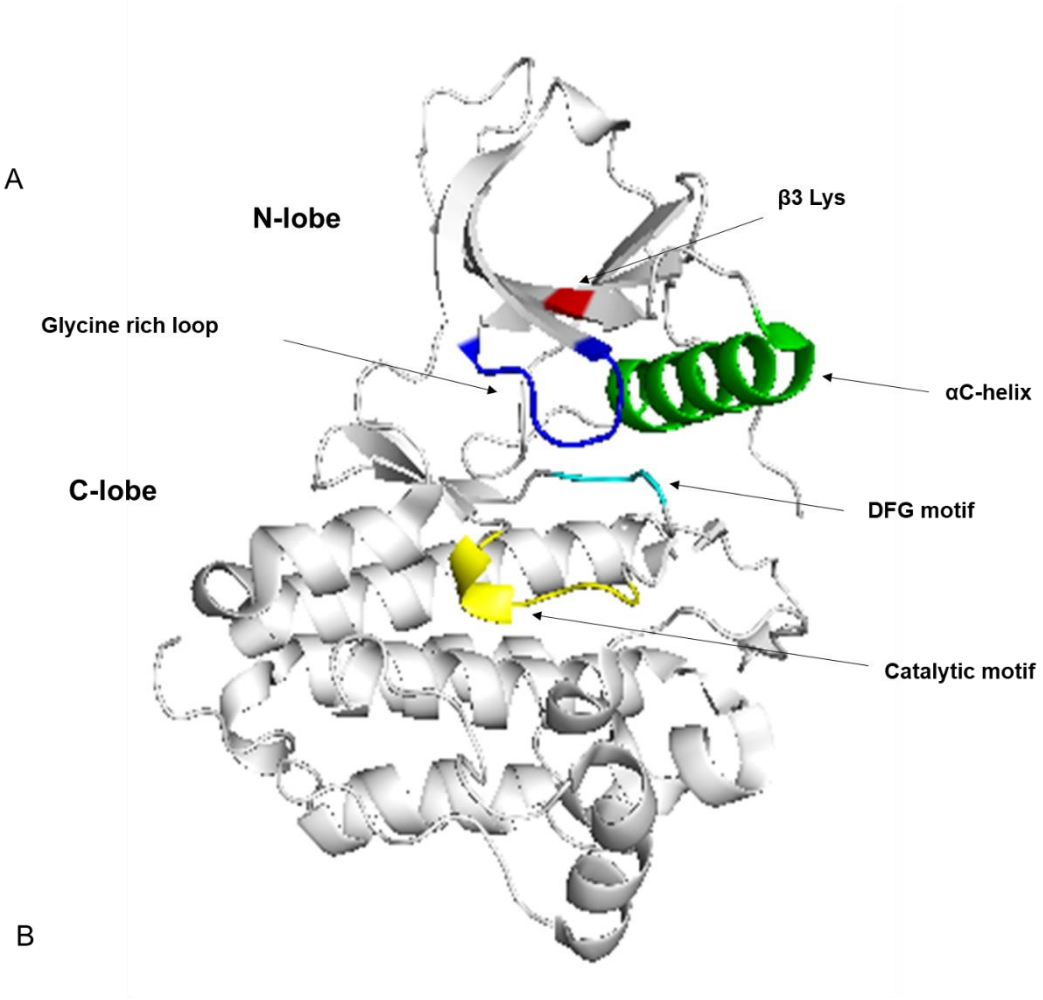


B

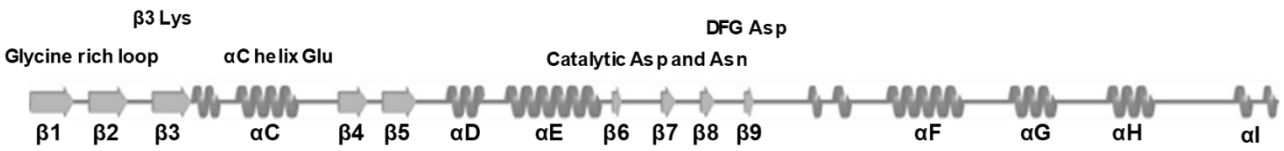


Secondary structure of PKA

| Glycine rich loop | β3 Lys | αC helix Glu | Catalytic Asp and Asn | DFG Asp | Kinase |
|---|---|---|---|---|---|
| $_{719}$VLGSGAFG | $_{743}$VAIKE | $_{761}$DEA | $_{835}$HRDLAARN | $_{855}$DFG | EGFR |
| $_{775}$VLGSGAFG | $_{750}$VAIKV | $_{769}$DEA | $_{843}$HRDLAARN | $_{863}$DFG | HER2 |
| $_{714}$VLGSGVFG | $_{739}$VCIKV | $_{757}$DHM | $_{832}$HRNLAARN | $_{852}$DFG | HER3 |
| $_{723}$VLGSGAFG | $_{748}$VAIKI | $_{767}$DEA | $_{841}$HRDLAARN | $_{861}$DFG | HER4 |
| $_{49}$TLGTGSFG | $_{69}$YAMKI | $_{90}$NEK | $_{164}$YRDLKPEN | $_{184}$DFG | PKA |
| $_{155}$LLGKGTFG | $_{176}$YAMKI | $_{197}$TEN | $_{272}$YRDLKLEN | $_{291}$DFG | PKB/AKT1 |
| $_{344}$VLGKGSFG | $_{365}$YAIKI | $_{386}$VEK | $_{461}$YRDLKLDN | $_{481}$DFG | PKC |

**Figure 1.4: Structure of EGFR kinase domain with highlighted conserved motifs**. (A) The EGFR kinase domain (PDB ID: 1M14) with the glycine-rich loop highlighted in blue, the β3 Lys in red, the αC-helix in green, the catalytic loop in yellow, the magnesium DFG motif in cyan. (B) (Top) The secondary structure of PKA represented with key motifs highlighted along with their relative positions. (Bottom) A comparison of the conserved kinase domain motifs for EGFR family (pseudo)kinases EGFR, HER2, HER3 and HER4. Comparison of the conserved kinase domain motifs for AGC kinases PKA, PKB/AKT and PKC, with conserved residues highlighted in red.

#### 1.1.1.2 The β3 lysine

In subdomain II the positively charged β3 lysine (highlighted in red) coordinates to the ATP α and β phosphates. This helps to stabilise the ATP molecule as the glycine rich loop clamps down, exposing the γ phosphate. As described for the structure of PKA, the VAIK motif additionally stabilises the adenosine ring of ATP [18]. On movement of the kinase from an inactive to active conformation the β3 lysine forms an ionic salt-bridge with a conserved Glu residue within the αC-helix in order to help correctly orientate ATP for catalysis. In biochemical studies, mutation of the β3 Lys to a residue with an uncharged side chain (such Ala or Met) reduces the activity of many protein kinases [20].

#### 1.1.1.3 The αC-helix

The positioning of the αC-helix, the only conserved helix in the β sheet-rich N lobe, is an important mediator of conformational changes that take place within the catalytic centre [18]. The aforementioned salt-bridge between the β3 Lys and Glu within the αC-helix helps coordinate α and β phosphates of ATP. In addition the αC helix also makes direct contact with the N-terminal region of the activation loop [21]. Conformation of the αC-helix in/out is also governed by the interaction with the DFG motif [22]. The position of the αC-helix can be allosterically modulated by interactions with regulatory peptides. In many AGC kinases, the dynamic nature of the αC helix, can be modulated through activating or inhibitory regulatory mechanisms. In many AGC kinases, including protein kinase A (PKA), RAC-alpha serine/threonine-protein kinase (PKB/AKT1), protein kinase C (PKC) and 3-phosphoinositide-dependent protein kinase 1 (PDK1) there is the presence of a hydrophobic motif (HM), which is a C-terminal tail sequence of 50–60 amino acids after the conserved catalytic core [23, 24]. This HM, consisting of the general motif F/Y-X-X-F/Y-S/T/E/D-F/Y, docks to a co-evolved hydrophobic surface in the N-lobe created by the αC-helix, known as the

PDK1-interacting fragment (PIF)-pocket [25]. Phosphorylation of AKT at Ser473, within the HM, results in enhanced binding of the HM to the PIF pocket *in-cis* and helps to stabilise the kinase in an active conformation [20, 26]. Conversely, Src tyrosine kinase can be inactivated by a complex of Src-homology domains SH2 and SH3 that bind to the αC-helix and to an inhibitory p-tyrosine in the C-terminal tail, stabilising it in the inactive conformation [27, 28].

The cyclin-dependent kinase (CDK) family also provides an example of allosteric regulation of catalytic activity via the αC-helix. CDKs are catalytically inactive until binding cognate cyclins [29]. In the absence of cyclin, the αC helix serves as a conserved cyclin recognition motif that is rotated to an outward state [29]. In this conformation the conserved Glu51 of CDK2 cannot form an ionic bond with β3 Lys33. However, binding of cyclin directly to the αC helix induces rotation to an inward state thus restoring the Lys33-Glu51 ion pair [30].

#### 1.1.1.4 Magnesium binding DFG motif

The DFG motif (Figure 1.4A, cyan) forms a loop within the catalytic spine. The highly conserved Asp is responsible for coordinating a positively charged $Mg^{2+}$ ion, which stabilises the negative charges of the ATP phosphate groups and makes polar contacts with all three ATP phosphates [31]. In cases of incorrect positioning of the DFG motif, the active site is sterically blocked from binding ATP. Structural analysis of AKT revealed that the DFG Phe flips over and occupies the position in the catalytic-spine that is usually filled by the adenine ring of ATP in the active conformation [26]. This has been designated as a 'DFG-out' conformation, and this serves as a structural signature of the inactive form for many kinases. The hydrophobic Phe makes contacts with the catalytic motif and αC-helix when the kinase lobes close and the DFG loop faces inwards (DFG-in conformation), which stimulates the formation of the aforementioned β3 Lys-Glu ionic bond [32]. Finally the Gly stimulates correct positioning of the Asp residue through formation of a hydrogen bond. In the DFG-out conformation, this hydrogen bond is disrupted and the flexibility of movement offered within the DFG loop is a hindrance to $Mg^{2+}$ ion binding [31].

#### 1.1.1.5 The catalytic motif

The Asp in the HRD of the catalytic motif becomes protonated by accepting a hydrogen from the hydroxyl group from the R group of the substrate amino acid (either Ser, thr

or Tyr) [21]. The Asn residue helps to orientate the catalytic Asp by coordinating an $Mg^{2+}$ ion (therefore two $Mg^{2+}$ ions can be coordinated in collaboration with the DFG motif). The His at the beginning of the motif is highly conserved, serving as a central scaffold for the catalytic spine, which binds to the carbonyl of the DFG aspartate and makes a hydrophobic contact with the DFG Phe [31]. The HRD Arg is also prevalent in most kinases that require phosphorylation of the activation loop for activation. The positively charged Arg interacts with the phosphorylated activation loop residue to support a link between the catalytic motif, activation loop and the DFG motif [33].

#### 1.1.1.6 Activation loop phosphorylation

Normally, kinases with a HRD catalytic motif (as opposed to HxD motif) require phosphorylation of the activation loop. For instance phosphorylation of the Thr197 residue of PKA, which is adjacent to the catalytic HRD Asp, is required for full catalytic activity. The phosphate group from the phospho-Thr197 coordinates the αC-helix (His87), the catalytic motif (Arg165) and the β9 sheet (Lys189), allowing conformational movement from a DFG-out to a DFG-in catalytically active orientation [34].

Phosphorylation of the activation loop of fibroblast growth factor receptors (FGFRs) and insulin-like growth factor receptors (IGFRs) occurs upon dimerization and *trans*-autophosphorylation [35, 36]. This autophosphorylation relieves the inhibition caused by the activation loop, which would otherwise occlude the active site and prevent substrate from binding [36].

#### 1.1.1.7 The αF-helix

The αF-helix serves as a central scaffold for coordination and assembly of catalytic and regulatory spines (Figure 1.5), which anchors all the elements important for catalysis [18]. The αC-helix and the Activation Loop, can be very mobile, which allows the hydrophobic spine to be dynamically assembled or disassembled thereby regulating the protein kinase activity and was thus designated as the regulatory Spine [21]. One of the regulatory spine residues in the C-lobe, is part of the HRD motif of the Catalytic Loop. In most kinases this is a histidine whereas in PKA and most of the AGC subfamily the His is replaced by a Tyr [37] (Figure 1.3B). The backbone of the His/Tyr is anchored to the F-helix through a conserved aspartate (Asp220 of PKA), which serves as the base of the regulatory spine. The second hydrophobic spine also

encompasses residues from the N and C-lobes, but is completed by the adenine ring of ATP and was thus termed the catalytic spine. The catalytic spine is formed from the Ala residue in the VAIK motif in the β3 sheet and this interacts with the adenine ring of ATP [18].

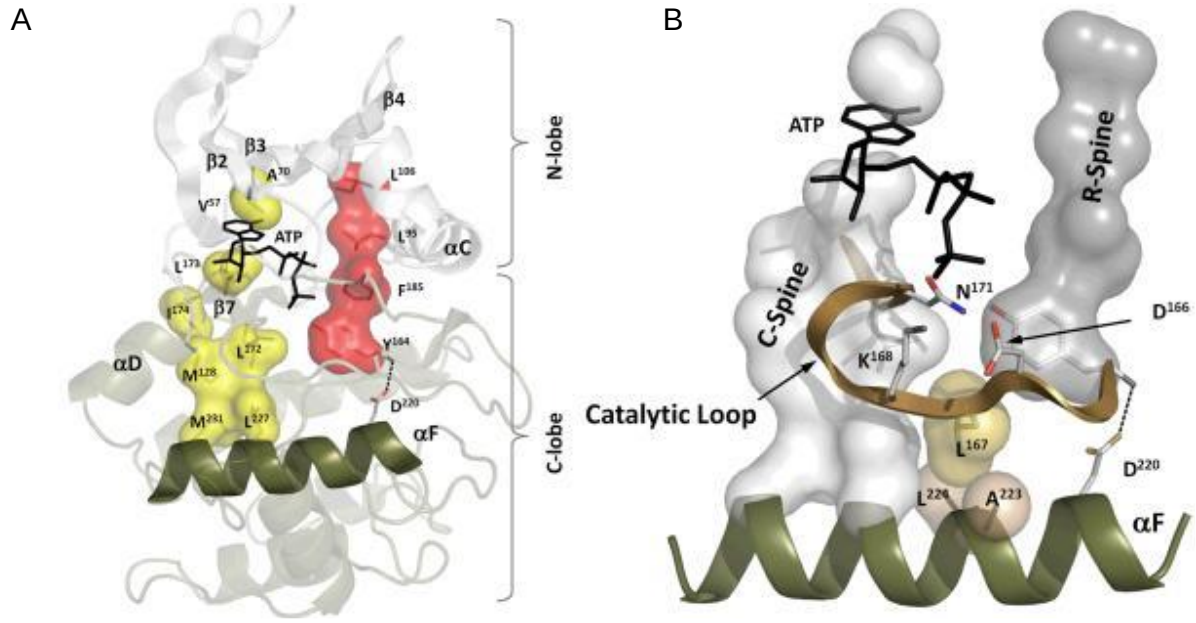


**Figure 1.5: The F-helix and two hydrophobic Spines define the kinase architecture.** (A) The regulatory spine (red) and catalytic spines (yellow) are connected to the αF-helix (tan) in the centre of the C-lobe. ATP completes the catalytic spine and provides a connection between the N and C-lobes. (B) Highlighted elements of the catalytic machinery, which are anchored to the αF-helix directly or via spines. Figure obtained from [18].

## 1.2 Mechanisms of kinase domain activation

### 1.2.1 C-terminal tail interactions to control activity of AGC kinases

The mechanism by which protein kinases perform ATP hydrolysis and phospho transfer to regulate target proteins in cell signalling has been discussed. However, protein kinases are intracellular mediators of signals and have evolved multiple regulatory mechanisms to efficiently phosphorylate specific substrates at the time and location needed. Certain AGC kinases are regulated by interactions with regulatory domains or inhibitory subunits, which can modulate their localisation and ability to interact with substrates. Certain kinases from various superfamilies, including many AGC kinases, exploit *in cis* interactions of a C-terminal polypeptide tail with the

catalytic domain in order to control substrate binding and catalytic activity. They are regulated, in part, allosterically through the interaction of the C-terminal tail with a regulatory site by the αC-helix in the N-lobe known as the PDK1 interacting fragment-(PIF)-pocket [23, 24, 38]. The PIF-pocket acts like an ON-OFF switch in AGC kinases with different modes of regulation. The PIF-pocket was first shown in the crystal structure of PKA as the site where the Phe residues, within a hydrophobic motif (HM) with the consensus F-T-E-F-COOH in the C-terminal tail, dock to a surface created by the αC-helix (PDB 1ATP). Interaction of the HM with the PIF-pocket allosterically affects the ATP-binding site and the peptide substrate binding site [26, 39, 40].

#### 1.2.1.1 Regulation of AKT activity

AKT is a main effector downstream of PI3K stimulation (Figure 1.2), with the key downstream signalling nodes glycogen synthase kinase 3 (GSK3), forkhead/winged helix class O transcription factors (FOXO) and mammalian target of rapamycin complex 1 (mTORC1). The vast circuitry of the dynamically branching signalling networks stemming from AKT stimulation is ubiquitous to nearly every cell in the body. Mouse and human genetic studies have also revealed physiological roles for the AKT network in nearly every organ system. There are 3 isoforms of the Ser/Thr kinase (AKT1, AKT2 and AKT3) and comprehension of their regulatory functions is particularly important, given the consequences of AKT dysfunction in various diseases, including cancer, cardiovascular disease, insulin resistance, inflammatory and autoimmune disorders, and neurological disorders [38, 41-43].

AKT is phosphorylated in the activation loop (Thr308 in AKT1) by PDK1, but requires phosphorylation at a Ser473 residue, in the HM, by the mTORC2 complex for full activation [26, 42]. *In vitro* AKT from HEK293 cells is inactive, but phosphorylation by PDK1 increases activity by ~100 fold [44]. Subsequent phosphorylation of AKT at Ser473 by MAPKAP kinase-2 AKT resulted in up to 1000-fold increased activity *in vitro* compared to the inactive form of AKT. When only the Ser473 residue is phosphorylated by MAPKAP kinase-2, the total kinase activity of AKT is increased ~6 fold [44]. AKT has an N-terminal Pleckstrin homology (PH) domain which binds, *in cis*, to the kinase domain, stabilising an inactive conformation and sterically hindering binding of PDK1. On growth factor stimulation of receptor tyrosine kinases (RTKs) or G-protein-coupled receptors (GPCRs), PI3K is recruited to the plasma membrane,

where it phosphorylates phosphatidylinositol 4,5-bisphosphate ($PIP_2$), producing phosphatidylinositol (3,4,5)-trisphosphate ($PIP_3$). [45]. $PIP_3$ binds to the PH domain of AKT, thereby disrupting the inhibitory interaction between the N-terminal and catalytic domains. Binding of $PIP_3$ to the PH domain also serves to localise AKT to the plasma membrane with PDK1 (Figure 1.6A). PDK1 is then able to bind and phosphorylate AKT1 at Thr308. In contrast, the HM of ribosomal protein S6 kinase beta (S6K) is required to bind *in trans* to the PIF pocket of PDK1 to be phosphorylated (Figure 1.6B). After phosphorylation of the activation loop by PDK1, S6K does not require phosphorylation of the HM to interact *in cis* to fully activate the kinase domain [46]. The HM of AKT does not bind *in trans* to PDK1. Deleting the PH domain (ΔPH-AKT) negates phosphorylation at Thr308 by PDK1. However, replacing the C-terminal tail of AKT with the C-terminal tail of PRK2 results in AKT phosphorylation at Thr308 [26].

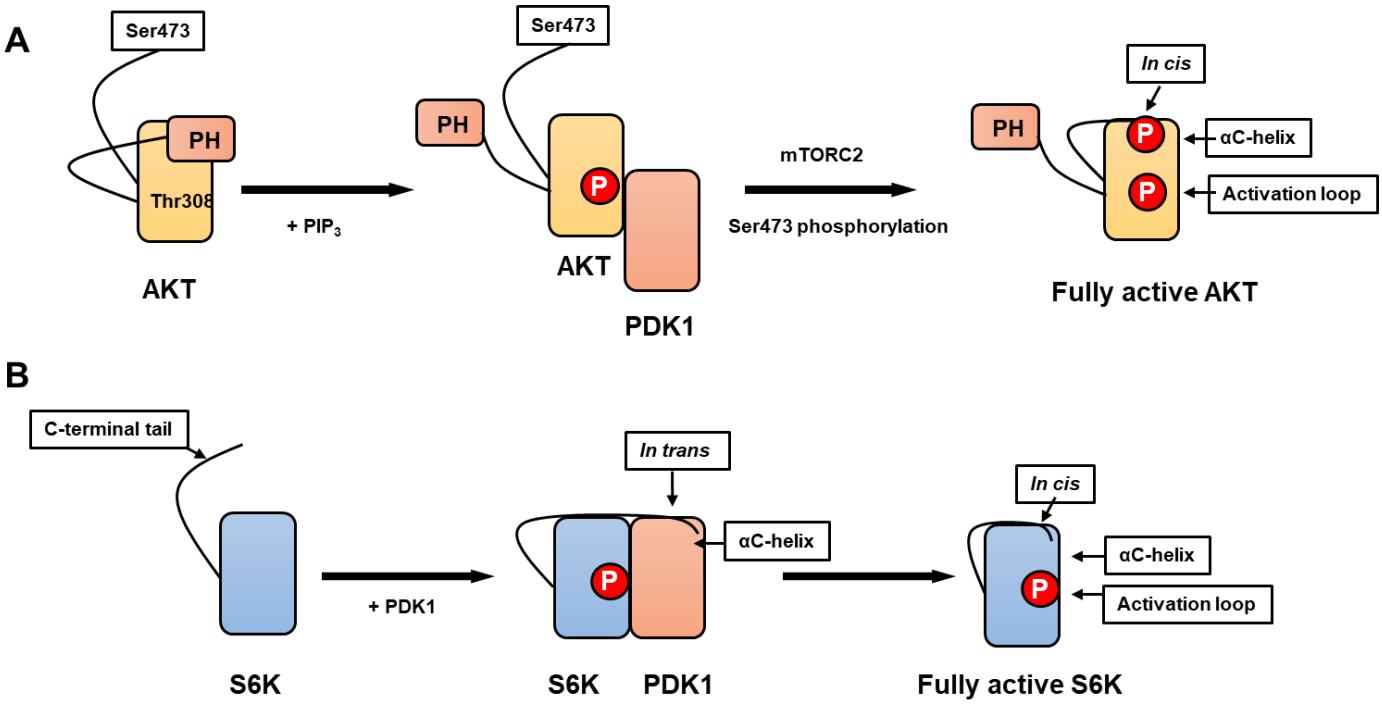


**Figure 1.6: Mechanisms of AKT and S6K activation by PDK1.** (A) The PH domain of AKT inhibits the kinase domain until binding of $PIP_3$ to the PH domain interrupts this interaction and sequesters AKT to the plasma membrane where it is phosphorylated by PDK1 at the activation loop Thr308. Subsequently, after phosphorylation of Ser473 by mTORC2, intramolecular binding between the HM and the αC-helix of the AKT kinase domain leads to full activation. (B) The C-terminal tail of S6K binds *in trans* to the αC-helix PIF pocket of PDK1 resulting in phosphorylation of S6K by PDK1. Subsequently PDK1 dissociates and the HM in the C-terminal tail of S6K binds to the the αC-helix *in cis* resulting in activation.

#### 1.2.1.2 PRK2 forms an inactive dimer and is regulated by the C-terminal tail

Serine/threonine-protein kinase N (PRK) kinases are closely related to PKCs and are described to mediate physiological effects downstream of Rho, such as Rho-dependent cell migration [47]. They are also implicated in the aetiology of prostate cancer [48]. PRK2 is auto-inhibited by dimerization of the kinase domain, mediated through the N-terminal pseudosubstrate PLK domains and not intramolecular interactions [49]. This prevents the interaction with upstream kinase PDK1. Interaction of the N-terminal Rho-binding domains with GTP-Rho stimulates interaction with PDK1. The HM motif of PRK2, which has a negatively charged Asp in place of a phosphorylation site, then binds *in trans* with the PIF pocket of PDK1 [50]. Phosphorylation by PDK1 results in dissociation and supports the formation of an active PRK2 monomer with an *in cis* HM intramolecular interaction with the PIF-pocket.

### 1.2.2 Activation by intermolecular interaction

#### 1.2.2.1 Activation of Aurora kinases

Aurora kinases are not thought to have N or C-terminal extensions that bind *in cis* with the kinase domain, however there is a regulatory site by the αC-helix in Aurora A that binds to TPX2 and similarly where INCENP binds to Aurora B [51-53]. Binding of TPX2 leads to activation Aurora A *in vitro* [52], enhancing autophosphorylation of Thr288 (in the activation loop). When TPX2 is absent, the activation segment of Aurora A is orientated in an inactive conformation. However, binding of TPX2 induces a 10 Å shift of the phosphorylated Thr288 from an exposed to a buried position. Thus, TPX2 synergises with Aurora A to increase phosphorylation and dephosphorylation is inhibited [51, 52].

#### 1.2.2.2 Activation of Polo like kinases (PLKs)

Domains that flank the kinase domain are important for modulating regulatory interactions and activity. Polo-like kinases (PLKs) are mitotic kinases that are close relatives to the AGC superfamily of kinases. PLKs have two C-terminal polo-box domains (PBDs) that bind to specific target sequences when phosphorylated in order to regulate activity and the localisation of the kinase [54]. The crystal structure of the PBD shows that the two polo boxes have identical folds comprising of a six-stranded

antiparallel β-sheet covered by a single α-helix, with the binding site for a cognate phospho-peptide located at the interface of the two polo boxes [54].

#### 1.2.2.3 Activation of EGFR family kinases

The Epidermal growth factor receptors (EGFR) are members of the RTK family of kinases, which include EGFR, HER2, HER3 and HER4. They are all composed of an extracellular domain, a transmembrane lipophilic domain and an intracellular tyrosine kinase domain. With HER2 being the only exception, the extracellular domain is responsible for binding to extracellular ligands, such as growth factors, to relay information into the cell. The ligands epidermal growth factor (EGF) and transforming growth factor-α (TGF-α) selectively bind to EGFR, which induces translocation and homodimerisation (with other EGFR proteins) and heterodimerisation (with different EGFR members, such as HER2) of the intracellular kinase domain, which leads to *in trans* autophosphorylation at specific tyrosine residues [55]. The activated kinase domains stimulate major signalling pathways, including the Ras/Raf/mitogen-activated protein kinase pathway to activate extracellular signal regulated kinase (ERK)1 and ERK2, or the PI3K/AKT pathway (Figure 1.2). ERK1 and ERK2 regulate cell growth and proliferation, whereas AKT signalling regulates cell survival and apoptosis [56].

Rather than employing phosphorylation mediated switches for catalytic activation, the kinase domain of EGFR proteins move into an active conformation when stimulated by allosteric intermolecular interactions following asymmetrical dimerization, whereby one kinase domain activates the other. In the cytoplasmic domain, in the N-terminal region flanking the kinase domain there is a juxtamembrane segment that links the kinase domain to the transmembrane domain. The juxtamembrane domain (JM) has two segments; the JM-A segment links to the transmembrane domain and the JM-B segment, which on dimerization binds to the C-lobe of the ‘activator kinase’, which allosterically stimulates the N-lobe of the ‘receiver kinase’ (Figure 1.7) [57]. In this way, the JM-B segment of the juxtamembrane domain forms what is referred to as a ‘juxtamembrane-latch’. Dimerization, induced by extracellular ligand binding, stabilises the helical JM-A dimer, which in turn stabilises the kinase domain dimer, thereby activating the kinase domain. In the absence of ligand, alternative dimer formation does not lead to activation as the C-terminal tails of the kinase domains inhibit the formation of the juxtamembrane latch [57] .

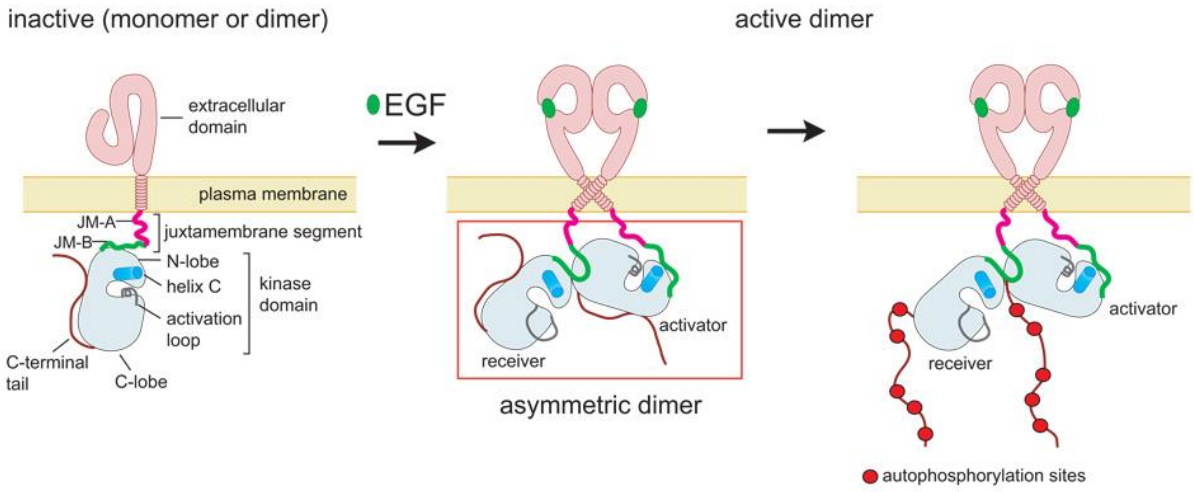


**Figure 1.7: Activation of EGFR by EGF results in the formation of an asymmetric kinase domain dimer.** The JM-B region of the juxtamembtrane segment of one of the EGFR monomers binds to the C-lobe of the adjacent EFGR monomer forming a dimer. The "receiver" kinase domain is subsequently activated by phosphorylation. Obtained from [57].

## 1.3 Protein pseudokinases

In contrast to kinases, pseudokinases are far less-well characterised and lack one or more of the previously described key motifs required for ATP binding and phosphotransfer. Pseudokinases appear within all kinase superfamilies in humans and are components of essentially all sequenced eukaryote kinomes [3, 15]. Pseudokinases are scattered throughout the distinct protein kinase subfamilies, suggesting that they have evolved from active kinases. Furthermore, there are pseudokinase homologues in humans, mice, worms, flies and yeast that lack the equivalent catalytic residues [15].

Increasing biological and structural information have revealed that many pseudokinases have evolved unique and interesting mechanisms of controlling cellular signalling [6]. The substrates and interactome of pseudokinases are often unknown, in both *in vitro* and *in vivo* circumstances. Therefore, the ability of signalling molecules to be modulated by interacting partners and ligands means that pseudoenzymes, with little or no detectable catalytic potential, might still carry out essential signalling roles. Pseudokianse signalling could be propagated through either low levels of catalysis, made possible by an alternative active site geometry, via nucleotide binding-driven allosteric transitions, and/or through the direct modulation of binding surfaces [6].

Although many pseudokinases are not catalytically active, the ability to bind to and/or hydrolyse ATP (sometimes very weakly) can be detected in a number of cases [58]. Examples include CASK [59], TRIB2 [60], JAK2 [61], HER3 [62], with-no-lysine kinases (WNK1-4) [63], STE20-related kinase adapter protein alpha (STRADα) [64], Mixed lineage kinase domain-like protein (MLKL) [65] and kinase suppressor of ras 1 and 2 (KSR1/2) [66], all of which will be discussed in more detail below. A retained affinity for ATP indicates that nucleotide-dependent switching mechanisms may have been preserved in the fold in order to regulate a proportion of pseudokinase-dependent signalling. ATP binding is now understood to be essential for the biological activities of non-catalytic pseudokinases such as STRADα [64] and HER3 [62].The pseudokinase VRK3 has a diverse interactome, but cannot bind to ATP [67]. The VRK3 pseudokinase domain has been crystalised in a constitutively in an active conformation and exerts its role as a signalling enzyme perhaps as an allosteric modulator, inducing phosphorylation of various nuclear proteins [67]. Indeed, some kinases retain full catalytic capabilities in order to exert their signalling potential; WNK pseudokinases do not possess the critical $Mg^{2+}$ coordinating β3 lysine, but have evolved an alternate, unique, lysine to coordinate $Mg^{2+}$, which appears in place of the terminal Gly residue of the glycine-rich loop (GRGSFK) [63]. Following a review of mechanistic functions of pseudokinases in biology [6], signalling mechanisms can simplified within 5 distinct groups (Figure 1.8).

1. Allosteric modulator: Regulate the activity of binding partner by forming intermolecular interactions to stimulate activation.
2. Competitor: Competes for binding of particular substrates with other active proteins to control signalling output.
3. Spatial anchor: Forms intramolecular interactions with binding partners to control localisation to particular cellular compartments.
4. Scaffold: To bind to multiple target substrates to instigate signalling activity within protein complexes.

5. Catalyst: Perform ATP hydrolysis and phosphate transfer, analogous to a canonical kinase.

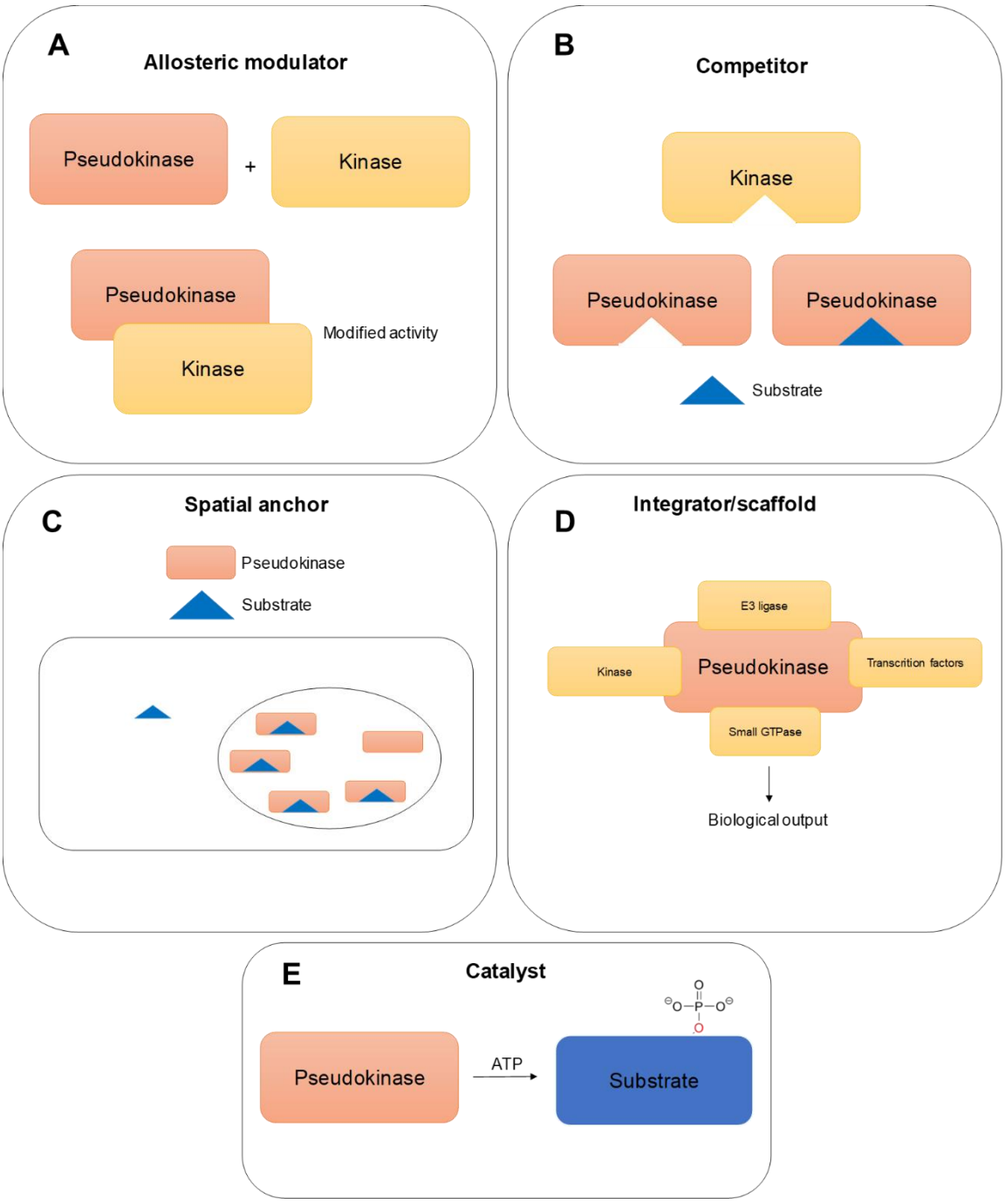


**Figure 1.8: Five mechanisms potentially employed by pseudokinases to modulate cell signalling.** (A) The pseudokinase forms intermolecular interactions with binding partners to influence activity. (B) The pseudokinase binds to a common substrate and directly competes with other proteins. (C) The pseudokinase dictates localisation of a binding partner by sequestering it to a particular cellular compartment. (D) The pseudokianse binds to multiple proteins, forming functional regulatory complexes and bridging certain signalling networks. (E) The pseudokinase functioning with non-canonical catalytic activity to transfer a phosphate group to a protein substrate.

Throughout the last decade it has become increasing clear that rate-limiting cellular outputs are not restricted to catalytic turnover. The prospect that many pseudokinases still retain (perhaps both regulatory and vestigial) ATP binding activity outlines them as potentially valuable new drug targets for small molecule ATP competitive kinase inhibitors. Approximately two thirds of pseudokinases have been implicated in range of human diseases [6]. In the following section I will briefly discuss the pseudokinases currently of most interest, whose biological activities may be susceptible to therapeutic intervention with small molecule chemical ligands.

## 1.4 Pseudokinases in disease

### 1.4.1 Janus kinases

The JAK family of non-receptor tyrosine kinases consist of JAK1, JAK2, JAK3 and TYK2, which share homologous regions of sequence termed Janus homology (JH) domains [68]. Janus, the roman deity of beginnings and transitions and of passageways and endings, is normally depicted as having two faces. Janus kinases, aptly named, have two opposing JH domains. The JH1 domain comprises a canonical catalytically active kinase domain that becomes activated upon stimulation by type I/II cytokine receptors [68]. This regulates a variety of biological processes including haematopoiesis and immune response [68]. Normally, the JH1 is negatively regulated by intramolecular interactions with the JH2 domain, which contains a pseudokinase domain lacking the catalytic Asp residue of the HRD motif [69]. Homology modelling analysis suggests that that JAK2 JH1 kinase activity is inhibited due to allosteric interactions with the JH2 domain. The JH2 Cys618 residue was predicted to occupy a loop between two N-lobe β strands, which restricts conformational flexibility of the JH1 activation loop by forming interactions with Val1000 and Pro1002 [70]. Furthermore, mutation of V617F, which is next to this site, is a highly prevalent oncogenic driver in the bone marrow disorder polycythaemia Vera [71].

Biochemical evidence suggests that the JH2 domain of JAK2 has signalling potential with the occurrence of weak catalytic activity. In JAK2, residues Ser523 and Tyr570, of the JH1 domain, are potentially phosphorylated by the JH2 domain [72]. Although targeted inactivation of the JH1 domain abolishes Tyr570 phosphorylation *in vitro*, therefore indicating the JH1 to be rate-limiting in this process. Despite retaining the

ability to bind to ATP, the JH2 domain of JAK1 and TYK2 are catalytically inactive *in vitro*, and neither possess the JH1 domain Ser523 or Tyr570 residues, which is potentially indicative of a lack phosphorylation driven regulation [73]. Interestingly, ATP binding stabilises the JH2 domain of TYK2 (without significant structural rearrangement), which allosterically regulates the JH1 domain by evoking stabilisation of the inactive conformation [73]. Indeed, deletion of the JH2 domain causes enhanced kinase activity in JAK2 and JAK3 [74].

Janus kinases have arguably been the most intensively studied pseudokinases to date and this can be directly attributed to the occurrence of multiple disease-driving somatic mutations in JH2 domains [75]. A prominent gain of function oncogenic variant of JAK2 (V617F) [76], that has been strongly implicated in multiple myeloproliferative neoplasms and is used diagnostically to guide therapeutic intervention strategies owing to its occurrence in approximately 95% of polycythaemia Vera and approximately 60% of essential thrombocythemia and primary myelofibrosis cases [71]. This amino acid substitution consequently results in hyperactivation of JAK2 and constitutive downstream STAT signalling due to a presumed destabilisation of the auto-inhibitory JH1–JH2 interaction [77]. Interestingly, ATP binding to the pseudokinase domain of JAK2 was recently shown to be essential for the hyperactivation phenotype of pathogenic JH2 mutants such as V617F [78]. This clear association with human malignancies, combined with the documented ATP-mediated regulation of the pseudokinase domain, suggests that JH2 domains might be suitable small-molecule drug targets for the treatment of cancer and auto-immune diseases. Incidentally, ruxolitinib, an orally available tyrosine kinase inhibitor that targets the JAK1 and JAK2 JH1 canonical kinase domains, was the first US FDA approved inhibitor for the treatment of myelofibrosis [79], and has also been approved for patients with polycythaemia Vera to control thrombotic events that fail to respond to hydroxurea [80].

### 1.4.2 HER3

The clinically significant pseudokinase HER3 belongs to the EGFR family RTKs. The HER3 pseudokinase domain is classified as such as it lacks a canonical catalytic Asp [15]. In spite of this, much like JAK2, HER3 is able to tightly bind ATP in an atypical manner and also exhibits extremely weak kinase activity, although it is unclear how

significant this activity is for the biological function of HER3 [81]. Ligand-induced heterodimerisation of HER3 with EGFR or HER2 stimulates allosteric trans-activation of these kinases and modulates a myriad of cellular responses including downstream activation of the PI3K/AKT signalling pathway [82, 83]. HER3 overexpression and mutation has been associated with a multitude of human cancers including ovarian, prostate, colon, pancreas, stomach, oral cavity, and lung [83, 84] and is a potential diagnostic marker for breast cancer, where it is amplified in around 60% of cases [85].

One of the major consequences of aberrant HER3 activation is over stimulation of PI3K/AKT signalling which is a critical pro-survival pathway in cellular proliferation and has been linked to the development of multidrug resistance in certain cancers [86]. This is exemplified by the fact that dual-targeting of HER3 and EGFR has proven an effective method of overcoming acquired resistance against EGFR targeted therapeutics [87]. A study using primary human non–small cell lung carcinoma (NSCLC) H226 cells, resistant to both cetuximab and erlotinib, revealed that dual targeting of EGFR and HER3 with a monoclonal antibody, MEHD7945A, could inhibit tumour growth and cell-cycle progression in parallel with perturbed EGFR/HER3 signalling. Interestingly, several cancer-associated somatic mutations that confer a gain-of-function phenotype for HER3 have also been reported [84] [19]. A novel HER3 V855A somatic mutation was discovered in a clinical samples from a patient with advanced chemotherapy-resistant NSCLC. Val 855 is at the same position as L858 in EGFR, which frequently mutates to Arg to increase catalytic activity of EGFR in cases of acquired resistance to Type I ATP competitive inhibitors such as gefitinib and erlotinib. Co-expression of HER3 V855A and wild-type HER2 was shown to enhance ligand-induced transformation of murine and human cell lines. Immunoprecipitation experiments revealed that HER V855A has greater physical interactions with HER2, than WT, leading to enhanced PI3K pathway activation. The mechanisms of V855A HER3 induced activation of HER2 are not fully understood; future structural information might reveal a unique mechanism in HER3/HER2 catalytic functions.

### 1.4.3 STRADα

STRADα has a severely degraded kinase domain which is missing the canonical β3 Lysine, DFG motif and the HRD motif aspartate. STRADα cannot hydrolyse ATP but does, however, bind to ATP in an $Mg^{2+}$ independent manner [64]. Despite lacking

catalytic activity, structural and biochemical analysis has revealed that STRADα is an allosteric regulator of the tumour suppressor LKB1 (also known as STK11). Interestingly, its function is contingent on the adoption of an active conformation, which it assumes upon cooperative binding with both ATP and scaffolding partner, Calcium-binding protein 39 alpha (MO25α) [64]. Although the MO25α/β isoforms are not related to cyclins at the primary sequence level, the STRADα/MO25α complex somewhat resembles the interaction between CDK2 and cyclin A. Cyclin A binds to the αC-helix of CDK2 as well as the preceding loop. In the CDK2/cyclin A complex the cyclin molecule orients Glu51, from the CDK2 αC-helix, in order for it to form a salt bridge with the β3 Lys33 [30], thereby stabilising CDK2 in an active conformation. Comparatively, the position of MO25α in the STRADa/MO25a complex is centred on helix αC-helix and the loop preceding this helix [64]. The interaction between Glu118 from the αC-helix and Arg100 from the VAIK (VTVR in STRADα) motif (analogous to the Glu51-Lys33 interaction in CDK2) is maintained, via two water molecules [64].

Formation of the LKB1-STRADα-MO25α heterotrimeric tumour suppressor complex results in LKB1 dependent phosphorylation of AMP-activated protein kinase (AMPK) and the inhibition of cellular proliferation signalling pathway [88]. Affinity purified complexes of GST-tagged LKB1, FLAG-tagged STRADα and myc-tagged MO25α, expressed in HEK293 cells, activated AMPK-related kinases *in vitro* [88]. Several human cancers, and the rare inherited disease Peurtz-Jeghers syndrome, are the consequence of loss of function mutations in LKB1 that perturb binding to- and activation by STRADα and Mo25 [15]. Activation of LKB1 by anti-diabetes drugs, such as metformin, in PTEN deficient mice delayed tumour onset [89], which positions STRADα, a critical upstream modulator of LKB1 activity, as potential therapeutic target for the manipulation of downstream LKB1 effectors.

### 1.4.4 Kinase suppressor of Ras 1 and 2 (KSR1/2)

KSR 1 and 2 exert their roles as signalling proteins by forming scaffolds, which coordinate formation of the oncogenic Raf-MEK-ERK signalling complex [66]. They are also important regulators of immune function and metabolism [66]. Crystal structure analysis reveals that the kinase domain of human KSR2 binds to ATP and forms a complex with MEK1 by interactions that are mediated through their respective activation segments and C-lobe αG-helices. The mutual constriction of the active site

activation segments means that KSR2 is maintained in an inactive conformation. KSR1 and KSR2 both lack the canonical β3 Lys and despite this, however, they are proposed to have catalytic function towards MEK1 as a substrate [66]. Structural and biochemical analysis revealed that BRAF allosterically stimulates KSR2 catalytic activity, contingent on formation of a side-to-side KSR2–BRAF heterodimer. Additionally, this heterodimerization results in an increase of BRAF-induced MEK phosphorylation. Aberrant activation of Ras-Raf-MEK is an oncogenic driver for a large proportion of human cancer. As key regulators of MAPK signalling cascades, KSR proteins are a potential therapeutic target of Ras-driven tumours [66].

Disease associated mutations of KSR2 that disrupt KSR2 signalling through the Raf-MEK-ERK pathway have also been linked to obesity, insulin resistance and impaired cellular fuel oxidation [86]. In a cohort of 2,101 individuals with severe early-onset obesity and 1,536 controls, sequencing analysis revealed that multiple rare variants in KSR2 that disrupt signalling through the Raf-MEK-ERK pathway to impair cellular fatty acid oxidation and glucose oxidation in transfected HEK 293 cells [90]. Using available crystal structure information as a template, the KSR2 kinase domain modelled with the discovered mutations, which revealed that the P662L, E667V, and R684C mutations, which lie within the N-lobe of the kinase domain in a region involved in B-Raf binding, are directly involved in intermolecular interactions. Residue P662 was predicated to be involved in B-Raf interaction and residue R684 is predicated to form a salt bridge with Glu664 of B-Raf, which explains how mutation of these residues leads to reduced binding [90]. Other point mutations, located in the C-lobe of the catalytic domain, also lie close to the KSR2-MEK interface and are likely to disrupt KSR2-MEK interactions. In myocytes transfected with WT KSR2 palmitate-stimulated oxygen consumption increases. However, this effect was reduced for the KSR2 kinase domain mutants [90]. Studies using mouse embryonic fibroblasts (MEFs) from Ksr2−/− mice have suggested that the interaction between KSR2 and AMPK may contribute to their abnormal energy homeostasis and metabolism [91].

Merlin is a KSR1 binding partner in schwannomas cells, which suppresses KSR1 function by preventing its binding to c-Raf [92]. KSR1 overexpression has been suggested to be involved in many pathological phenotypes caused by Merlin loss, including multipolar morphology, enhanced cell-matrix adhesion, focal adhesion, increased proliferation and survival. Furthermore, proteomic analysis reveals that

KSR1 also interacts with several Merlin downstream effectors, including E3 Ubiquitin Ligase CRL4DCAF1 [92], suggesting that KSR1 is a potential therapeutic target for Merlin-deficient tumours.

### 1.4.5 Mixed lineage kinase domain like protein (MLKL)

MLKL possesses low micromolar, cation-independent affinity for ATP despite lacking a glycine rich loop and evolving a non-canonical HGK and GFE residues in place of the typical DFG and HRD motifs, but lacks the ability to catalyse the transfer of phosphate [93]. Structural analysis shows that MLKL retains the overall topology of a bilobial kinase domain. Analysis confirmed that MLKL was in an 'active' conformation, with the β3 lysine coordinating a conserved Glu residue in the αC-helix. The catalytic HGK motif (in place of HRD) Lys331 is located at the equivalent position normally occupied by the canonical catalytic Asp. A K331N mutation acutely reduced MLKL affinity for ATP, indicating that this Lys may be involved ATP coordination [65]. This could be reminiscent of WNK kinases, which do not possess a β3 Lys, but have evolved in an alternate compensatory Lys residue at the end of the glycine rich loop. MLKL cannot hydrolyse ATP (on account of other highly degraded remaining motifs) but ATP binding might be important for stabilising a functional 'active' conformation [65].

MLKL function is indispensable for tumour necrosis factor (TNF)-α induced necrosis, which proceeds via the obligate phosphorylation of two activation loop residues (T357 and S358) of MLKL by the canonical upstream kinase RIP3 [93]. Phosphorylation at these residues stabilises the active conformation of MLKL facilitating the release of the N-terminal domain four-helix bundle. This in turn permits MLKL1 oligomerization and membrane translocation and subsequent activation of necroptosis [93]. Under normal physiological conditions, necroptosis is triggered in response to physiological or pathophysiological stimuli, as part of an innate defence against pathogens that supress apoptosis [17]. Abrogated regulation of necroptosis, however, is a risk factor for a multitude of autoimmune and inflammatory diseases [94], highlighting MLKL as a novel therapeutic target. So far, only the biological functions of MLKL in relation to necroptosis are understood, but an E351K mutation in the non-canonical GFE sequence (which replaces the DFG motif) has also been described in human cancers

and this mutant exhibits an increased affinity for nucleotide binding, possibly resulting in hyperactivation of the pseudokinase [65].

### 1.4.6 With no lysine (WNK) kinases

WNK family of serine/threonine pseudokinases (comprising WNK1-4) [95] lack the conserved β3 lysine, which was long assumed to be indispensable for nucleotide binding and stabilisation of an active kinase conformation [63]. However, WNK kinases demonstrate phosphorylation-dependent regulation of a myriad of intracellular substrates and this has been made possible by the evolution a novel mechanism of catalysis; the terminal residue in the glycine rich loop (normally a Gly in active kinases) is a Lys residue in WNKs, which provides a compensatory charge for the binding of ATP [63]. Furthermore, it has been proposed that the site normally occupied by the β3 lysine functions as a chloride sensor by binding to halide ions and inhibiting WNK activation by autophosphorylation, thus facilitating a feedback mechanism for the regulation of $Cl^-$ levels [96]. In its active state, WNKs phosphorylate and activate SPAK and the oxidative stress response kinase (OSR1), which in turn modulate the downstream activities of Na+-driven, Cl−-importing NKCCs (Na+/K+/Cl− co-transporters) in order to modulate blood pressure and ion homoeostasis [95].

WNK kinase homologoues are differentially expressed in various tissues. Dysregulation of WNK kinases expressed in neuronal cells have been implicated in the aetiology of multiple disease, including hereditary neuropathy and glioma, marking them out as potential therapeutic targets [95]. Furthermore, mutations in WNK1 and WNK4 have been linked to hereditary hypertension [97]. WNK1 and WNK3 stimulate proliferative and invasive activity in glioma cells [98-100]. Conversely, WNK2 predominantly plays a role as a tumour suppressor and down-regulates cellular proliferation by increasing and decreasing activity of Rac1 and RhoA respectively [101].

## 1.5 Tribbles pseudokinases

Analysis of the tribbles 2 (TRIB2) pseudokinase is the main focus of this thesis and in this section I will discuss the diverse functions of tribbles proteins in cellular signalling and links to various diseases. The Tribbles (TRIB) pseudokinases control a broad array of eukaryotic cell biology by integrating a plethora of signalling networks and have evolved unique features distinguishing them from all other protein kinases. There are three human Tribbles homologues (TRIB1, TRIB2 and TRIB3), which are Ser/Thr pseudokinase members of the CAMK superfamily of kinases. A sequence alignment of full length human TRIBs reveal that they are characterised by an N-terminal PEST region, a pseudokinase domain with a MEK1 binding site and a C-terminal E3 ubiquitin ligase binding region (Figure 1.9). Sequence alignment analysis of the pseudokinase domains of human TRIBs with the canonical kinase domain of PKA reveals that TRIBs are defined by a unique SLE motif, instead of a DFG motif, which is conserved from fly trbl to human TRIBs (Figure 1.10). TRIB pseudokinases possess a canonical β3 Lys; the β3 motif of TRIB2 being LVCK. The only TRIB pseudokinase domain, including fly, that does not possess catalytic Arg and Asp residues is TRIB1, which has Gly and Asp residues instead.

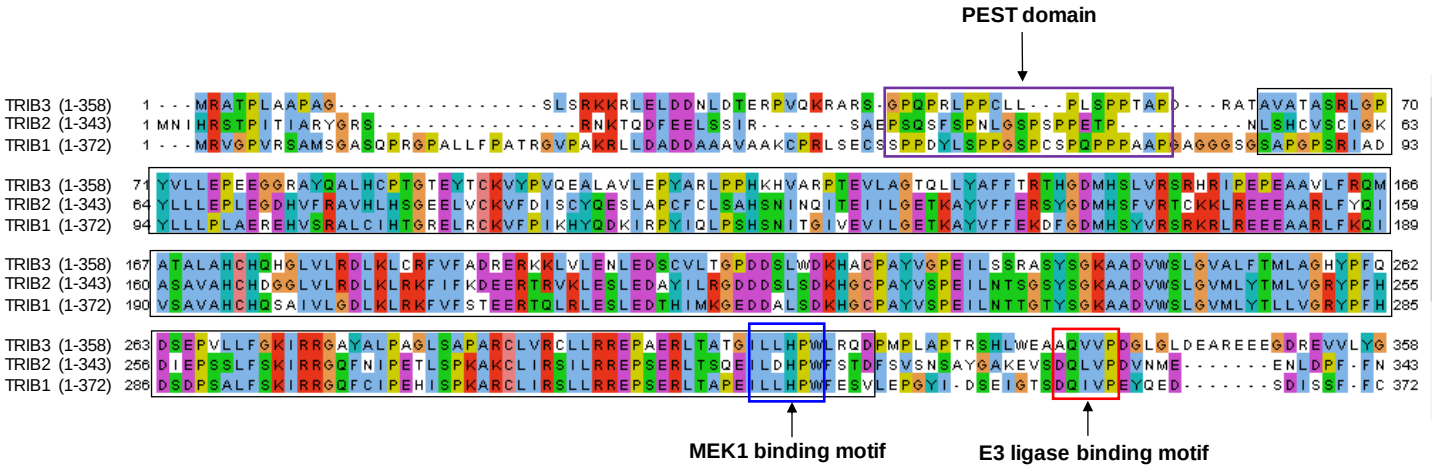


**Figure 1.9: Alignment of the full length human TRIB homologues.** The full length amino acid sequences of TRIB2 (1-343 Uniprot Q92519), TRIB1 (1-372 Uniprot Q96RU8) and TRIB3 (1-358, Uniprot Q96RU7) were aligned using the MUSCLE tool in and visualised in Jal view. The PEST region in the N-terminal domain is boxed in purple, the pseudokinase domain in black, the conserved MEK1 binding in blue and the E3 ligase binding site in red.

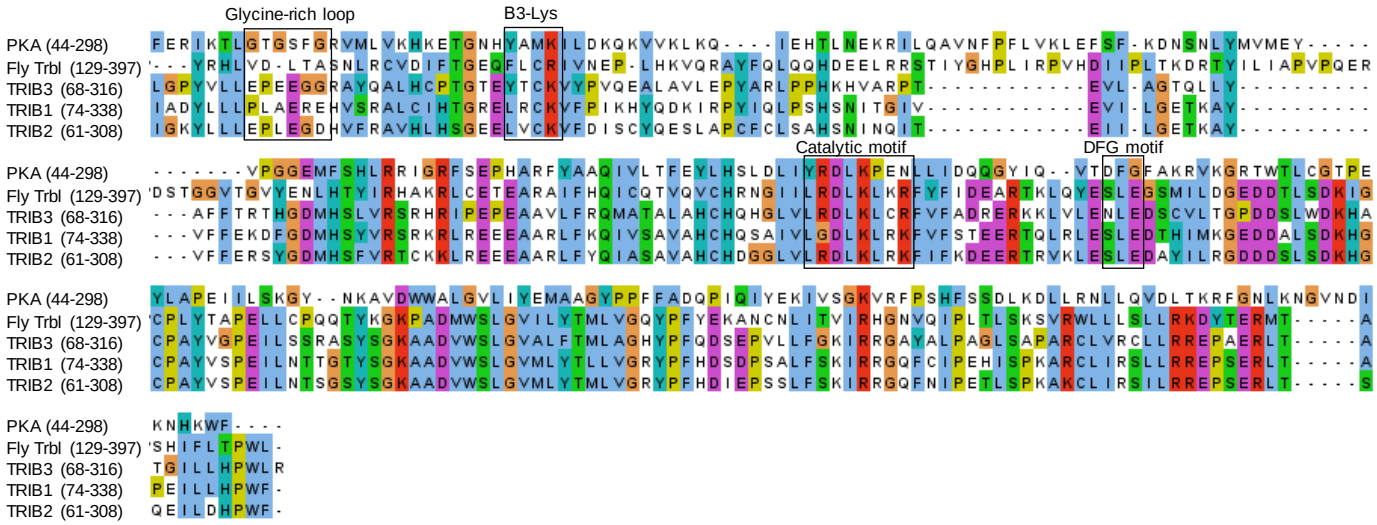


| Glycine rich loop | β3 Lys | Catalytic Asp and Asn | DFG Asp | Pseudo(kinase) |
|---|---|---|---|---|
| TLGTGSFG | YAMKI | YRDLKPEN | DFG | PKA |
| LLEPLEGD | LVCKV | LRDLKLRK | SLE | TRIB2 |
| LLPLAERE | LRCKV | LGDLKLRK | SLE | TRIB1 |
| LLEPEEGG | YTCKV | LRDLKLCR | NLE | TRIB3 |

**Figure 1.10: Sequence alignment of PKA and TRIB (pseudo)kinase domains.** Alignment of the PKA kinase domain with fly trbl and human TRIB1, TRIB2 and TRIB3 pseudokinase domains. The critical motifs for ATP binding and hydrolysis are highlighted. Only Fly Trbl does not possess a β3-lys, which has an arg instead. All TRIB pseudokinases have deviant glycine rich loops. All TRIB pseudokinases lack a canonical 'DFG' (metal-binding) motif. TRIB1 is the only TRIB pseudokinase that does not possess a catalytic Arg. (B) The critical motifs for PKA, TRIB2, TRIB1 and TRIB3 are highlighted in red.

Facilitating post-translational modifications allows proteins to control signalling though a combination of mechanisms. Indeed, both phosphorylation and ubiquitination are pivotal in cell signalling, with crosstalk important for controlling outputs. TRIB proteins appear to have evolved two main mechanisms of regulating cellular signalling. Firstly, the atypical pseudokinase domain retains a regulated binding platform for substrates,

which are ubiquitinated by context-specific E3 ligases (Figure 1.11A). Secondly, scaffolding functions of TRIB pseudokinases are utilised to integrate certain pathways and support the modulation of canonical MAPK and AKT modules (Figure 1.11 B and C).

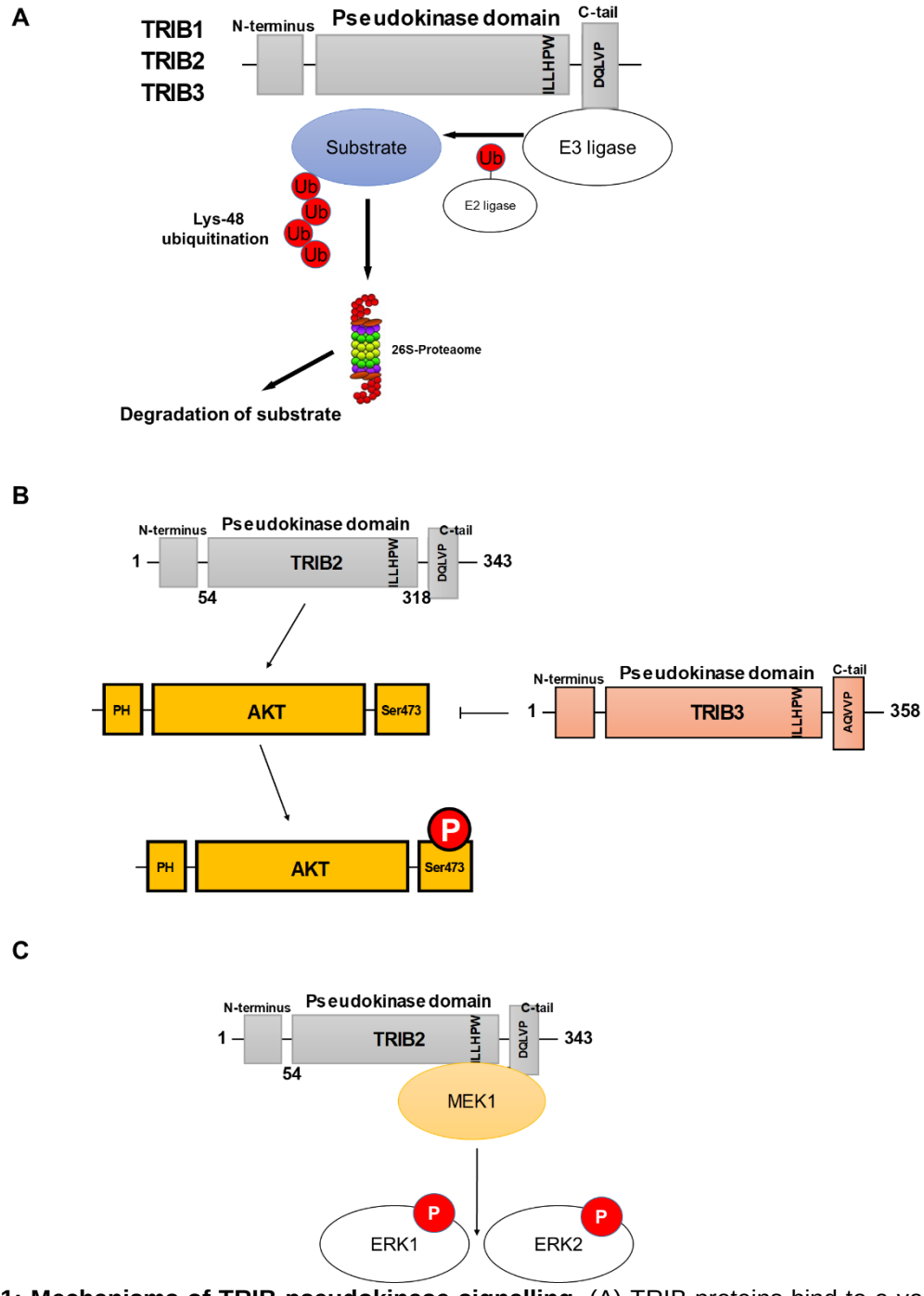


**Figure 1.11: Mechanisms of TRIB pseudokinase signalling.** (A) TRIB proteins bind to a variety of target protein substrates using the pseudokinase domain. Subsequently, distinct E3 ligases bind to the C-terminal DQLVP motif, which then recruits E2 ligases to polyubiquitinate the target substrate resulting finally in their proteasome-mediated degradation. (B) TRIB2 binds to AKT and induces phosphorylation at Ser473, whereas TRIB3 negatively regulates AKT activation. (C) The C-terminal HPW[F/L] motif

targets MAPKK/MEK family members, giving TRIBs the potential to regulate and/or integrate distinct stress and proliferative MAPK modules.

### 1.5.1 Origin and evolution of tribbles

TRIB proteins derive their name from the single metazoan fly gene ‘Tribbles’ (Trbl), which encodes a pseudokinase with developmental roles in this model genetic organism. The fly orthologue of the cell cycle regulating phosphatase M-phase inducer phosphatase (CDC25) is called string. String activates CDK1 by dephosphorylation, thereby regulating cell cycle progression after G2 phase. During morphogenesis, the gastrulating mesoderm cells highly express string, but they do not enter mitosis. 18 years ago Groβhans and Wieschaus surveyed data from genome-wide screens to identify novel regulators of string. There were two genes identified that were proposed to negatively regulate string, tribbles and frühstart. By microinjecting trbl mRNA into fly embryos, the authors revealed that tribbles inhibited mitosis. Trbl mutant cells exhibited premature mitosis, leading to defective gastrulation based on an inability to degrade target proteins. A recent study revealed that the human orthologue of trbl, TRIB2, is a modulator of CDC25 phosphatases, which it targets for degradation via the ubiquitin-proteasome system [102]. Fly trbl was also shown to regulate slbo, the mammalian orthologue of which is CCAAT enhancer-binding protein alpha (C/EBPα). Human TRIB1 and TRIB2 control hematopoietic differentiation by regulating C/EBPα stability through targeted ubiquitination. Fly trbl binds to and negatively regulates AKT. In human cells TRIB3 has been shown to directly bind to AKT and negatively regulate mTORC2-dependent activation. As AKT stability is not influenced upon binding to TRIB3, it is proposed that TRIB3 signalling functions, in this context, are contingent on TRIB scaffolding properties. In contrast to TRIB3, it has recently been demonstrated that TRIB2 can directly bind to and stimulate AKT phosphorylation of AKT at the C-terminal regulatory site Ser473, but not the activation loop Thr308 residue [103], which is dependent on the presence of an intact C-terminal tail (containing the E3 ligase binding motif).

Taxonomic analysis of TRIB related sequences reveals that they are almost exclusively restricted to metazoans; they are not present whatsoever in non-metazoan eukaryote kinomes, including fungi and plants [104]. Perhaps this is indicative of evolved functions equipped to utilise ubiquitin based regulatory mechanisms. Eyers and colleagues (2017) [104] recently proposed that the TRIB2 sequence is the most

ancestral. TRIB2 sequences can be detected in early metazoan kinomes, such as *Nematostella vectensis* and *Amphimedon queenslandica*, with TRIB1 and TRIB3 sequences occurring in more recently evolved metazoans, presumably as a result of genome-wide duplications. Orthologues of TRIB3 are confined to vertebrae metazoan lineages and it could be argued that the three homologous were specifically nominated, after genome-wide duplications, driven by evolutionary pressure unique to regulatory requirements in higher organisms. Furthermore, while most mammals possess at least a single copy of TRIB1, TRIB2 and TRIB3, some harbour multiple copies, suggestive of gene duplications that are functionally relevant.

### 1.5.2 Insights into TRIB structure and function

The C-terminal tail of TRIBs instigate protein–protein interactions *in cis* with the pseudokianse domain, which is readily identified as a distinguishing feature of TRIB pseudokinases. No detectable similarity is observed at this locus between TRIB primary sequences and any other evolutionarily related protein (pseudo)kinases, defining the tail as a statistically unique feature [104]. Although these motifs are not observed in the C-terminal tail of other protein kinases, they are predicted to engage with the TRIB pseudokinase domains in a manner analogous to canonical, well-studied AGC protein kinases, such as PKA and AKT.

Two recent studies, from the lab of Peter Mace (University of Otago), published crystal structures of TRIB1 [105, 106], revealing that TRIB1 undergoes conformational change relative to its substrate-free structure and to its C/EBPα substrate-bound structure. In the substrate-free state there is an intramolecular interaction between the E3 ligase binding region in the TRIB1 C-terminal tail and the αC-helix of the pseudokinase domain. Interestingly, substrate binding triggers an allosteric modulation that leads to release of the C-terminal tail from, and conformational rearrangement of, the pseudokianse domain to a closed ‘active’ like conformation. In accordance with molecular dynamics and biochemical studies, release of the C-terminal tail link substrate recruitment to Constitutive photomorphogenic protein 1 (COP1) [105].

Crystal structures of TRIB1 reveal a bilobal pseudokinase domain with a degraded ATP binding site and a Tyr134 residue protruding into the active site, which would occlude ATP binding [105]. Interestingly, the equivalent residue in TRIB2 is Cys104,

which would exert less steric hindrance and would perhaps explain why TRIB2 can very weakly bind to ATP in the absence of divalent metal cations. Moreover, without allosteric interactions from C/EBPα, rearrangement into a canonical SLE-in (canonical DFG-in) position is sterically prevented by the aC-helix Tyr134[105]. Tyr134 and Leu226 (of the SLE motif) rotate upon substrate binding, away from the active site, which is facilitated by 3.2 Å movement of Tyr134, causing it to pack on top of Leu226 (Figure 1.12). Consequently, Leu226 packs to complete the regulatory spine, thereby fulfilling a closed SLE-in conformation [105].

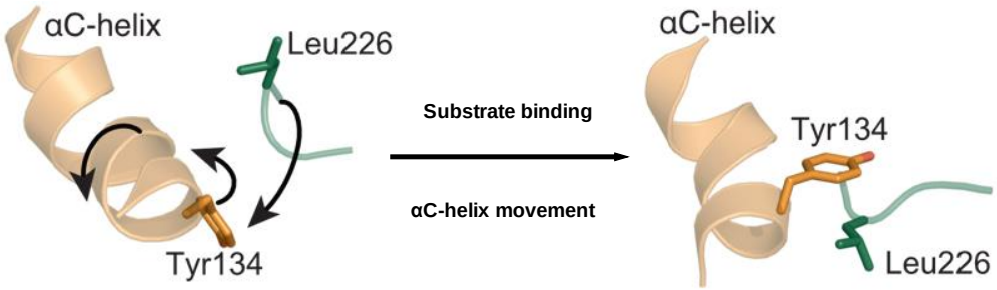


**Figure 1.12: Conformational change in the TRIB1 αC-helix.** Structural analysis of TRIB1 αC-helix and SLE motif regions showing relative organisation of Tyr134 and Leu226 between the substrate free SLE-out state (left) and substrate bound SLE-in state (right). Figure modified from [105].

TRIB1 and TRIB2 share ~72% sequence identity, decreasing to ~50% for TRIB3, with a high degree of homology in the C-terminal domain. Using the crystal structure of TRIB1 (PDB 5CEM) as a template (Figure 13A), a TRIB2 model was generated by automated homology modelling using Swiss Prot (Figure 1.13B). The quality estimate values for the TRIB2 model (with an overall QMEAN of -2.9) suggest an accurate representation of the potential TRIB2 structure. The αC-helices appear to be highly similar (green), which supports the interaction with the E3 ligase biding site in both TRIB1 and TRIB2 (blue). The C-lobes of the TRIB1 crystal and TRIB2 model exhibit similar structural features of active kinases PKA (Figure 1.13C). The close structural homology between TRIB1 and AMP-regulated kinases is interesting, given the fact that TRIB3 has been proposed to regulate the stability of AMPK effectors, including acetyl Coenzyme A carboxylase (ACC) [105, 107].

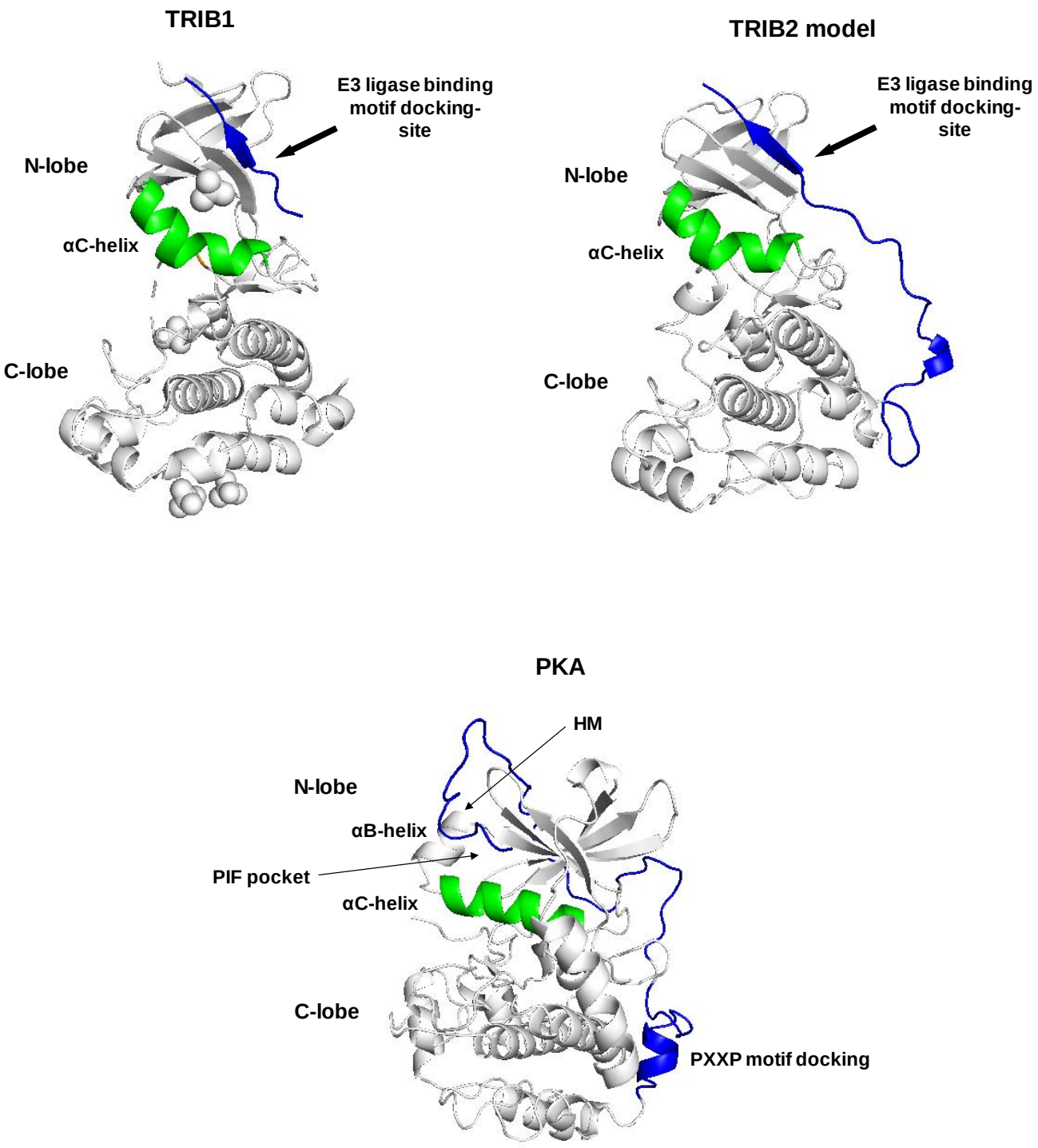


**Figure 1.13: C-terminal tail interaction with the (pseudo)kinase domain.** (A) Crystal structure of TRIB1 (5CEM) in the substrate free SLE-out confirmation with C-terminal tail (blue) interacting *in cis* with the αC-helix region (green). (B) Model of TRIB2 based on TRIB1. (C) Crystal structure of PKA (1ATP) showing C-terminal tail (blue) interactions with the kinase domain.

TRIB1 and TRIB2 are predicated to have an intact αF-helix that assembles to help form the catalytic and regulatory spines. The N-terminal lobes of TRIB1 and TRIB2 are more unusual. As well as having a truncated and distorted αC-helix, the glycine rich loop, which links the β1 and β2 strands, is shorter than usual and therefore restrictive [105]. Furthermore, the truncated C-helices of TRIB1 and TRIB2 are packed closer to the β3-strand, thereby decreasing plasticity of potential movement.

### 1.5.3 Biology of TRIB2

#### 1.5.3.1 TRIB2 mediated degradation of C/EBPα in AML

The C/EBP family of bZIP transcription factors are involved in a variety of physiological processes ranging from control of the cell cycle to cellular differentiation. Recent biochemical analysis revealed that TRIB1 binds to C/EBPα, β and γ homologous, with phosphorylation of C/EBPβ negatively regulating the interaction *in vitro* [105]. C/EBPα is an important transcription factor in myeloid cell differentiation and cell cycle regulation. It is able to achieve this through a variety of mechanisms, which include upregulation of the CDK inhibitor p21 and the inhibition of CDK2/CDK4 activity [108]. There are two isoforms of C/EBPα. C/EBPα p42 is the full length protein and contains a degron in the N-terminal domain, which is exploited by TRIB2, which targets it for ubiquitination and proteasome-mediated degradation [109]. Conversely, the truncated p30 isoform, resulting in gene splicing and the occur ace of an alternate start codon, is spared by TRIB2 [109]. The C-terminus of C/EBPα contains a series of regularly interspersed hydrophobic residues, which ultimately leads to the positioning of these residues on one particular side of an α-helix. As a result the C-termini of two bZIP monomers dimerize through intermolecular interactions [110]. The resulting scissor-like complex allows the charged basic regions of the C-terminus to make contact with the major groove of sequence-specific regions of DNA conforming to the consensus sequence RTTGCGYAAY [110]. Upon binding these regions, the C/EBP transcription factors are able to modulate the expression of their target genes [111]. As the p30 isoform is an N-terminal truncated protein, it can still bind to DNA and modulate transcription and is therefore oncogenic. Imbalance in levels of p30 and p42 C/EBPα leads to disturbed granulopoiesis and the onset of acute myeloid leukaemia (AML) [109].

TRIB2 overexpression alone drives fully penetrant and lethal AML in mice [109]. Conversely, TRIB3 expressing cell-transplants do not promote leukemogenesis, consistent with its inability to degrade C/EBPα Mice reconstituted with bone marrow cells, expressing TRIB2, displayed enlarged spleens and lymph nodes with an extensive involvement of myeloblasts and immature myelomonocytic cells, and due to the >20% proportion of blast cells, AML was the diagnosis. Flow cytometry confirmed the immature phrnotype [109]. In order to elucidate which regions of the TRIB2 were responsible for disturbed differentiation of granulocytes, a myeloid 32D cell line was engineered to express a variety of TRIB2 truncations and point mutants. Degradation of C/EBPα was negated by the deletion of either the COP-1 binding site or a mutation within the kinase domain, whereas an N-terminal mutant, which had a complete catalytic domain and total COP1 binding sequence integrity, could still reduce p42 C/EBPα protein levels [112]. Interestingly, mutation of the TRIB2 D326QLVP331 sequence to an AQLAA or mutation of the conserved Lys in the catalytic motif was unable to promote C/EBPα degradation [112].

Deregulation of the transcription factor E2F1 also occurs in AML, resulting in the perturbation of cell cycle and apoptosis. Keeshan and colleagues (2014) [113] discovered that E2F family members directly regulate TRIB2 expression in leukemic cells and identified a regulatory feedback loop. The p30 isoform of C/EBPα lacks the mitotic inhibitory, transactivation domain in the N-terminus, which is responsible for inhibition of the c-Myc promoter by E2F1. E2F1, 2, 3 and 4, but not E2F5, activate the TRIB2 promoter with overexpression of E2F1 leading to increased levels of TRIB2 mRNA [113]. Adjacent to the E2F1 binding sites in the TRIB2 promoter, there is a C/EBP binding site, where both isoforms of C/EBPα can bind [113]. There is an inverse correlation between TRIB2 promoter activity and the levels of C/EBPα p42 when co-transfected with E2F1. However, increasing amounts of C/EBPα p30 co-transfected with E2F1 increases TRIB2 expression [113]. From clinical AML samples, high TRIB2 expression correlated with high E2F1 expression levels [113].

#### 1.5.3.2 TRIB2 in acute lymphoblastic leukaemia (ALL)

There is currently no evidence available to implicate the involvement of TRIB1 and TRIB3 in ALL, in contrast there is growing evidence for a role of TRIB2 [109]. TRIB2 expression is highest in the lymphoid compartment of haematopoietic cells and

properly regulated expression is important for normal differentiation in B and T-cell lineages [114]. TRIB2 was first identified in a screen for downstream effectors of NOTCH1 signalling in ALL and activating NOTCH1 mutations were found to induce pathogenicity related to increased TRIB2 expression. Activating NOTCH1 mutations occur in 50% of all acute lymphoblastic leukaemias (T-ALL) [115]. TRIB2 is a NOTCH1 target gene. High TRIB2 expression is also associated with NOTCH1 acute lymphoblastic leukaemia (ALL) and is regulated by the transmembrane receptor NOTCH1 following proteolytic cleavage [115]. The levels of NOTCH1 protein are controlled by ubiquitination through FBXW7 [109, 115, 116] . Analysis of samples from 60 clinical paediatric ALL patients with either NOTCH1 or FBX7W mutations revealed that TRIB2 expression was increased, with the highest expression observed in patients that have a mutation to the PEST domain of NOTCH1, which regulates stability and proteasome-mediated turnover. Analysis of TRIB2 expression across 16 different subtypes of human leukaemia demonstrated that TRIB2 expression was higher in ALL phenotypes as compared to other phenotypes including AML, chronic lymphocytic leukaemia (CLL), myelodysplastic syndrome (MDS) and chronic myeloid leukaemia (CML) [115].

#### 1.5.3.3 Tumour suppressor role of TRIB2 in T-ALL

The thymus is a lymphoid organ where progenitors from the bone marrow (BM) commit to T-cell lineage development before differentiation into functional naive T cells, and subsequent export to the periphery as part of the adaptive immune system [114]. TRIB2 knock out mice do not display any obvious phonotypical changes. Furthermore, TRIB2 knock out does not affect the hierarchical organisation of the murine hematopoietic system and is thus dispensable for myeloid cell differentiation in steady state conditions [114]. TRIB2 expression is highest in the lymphoid compartment cells so it is not surprising that overexpression of TRIB2 in T-cells does not lead to malignancy. I fact, in models of T-ALL, TRIB2 plays an important tumour suppressor role and is essential for balanced proliferation of developing murine thymocytes [114]. TRIB2 knock out causes developing thymocytes to become highly proliferative but with heightened sensitivity to *in vivo* genotoxic drug treatment with the common chemotherapeutic agent 5-fluorouracil-induced. Furthermore, TRIB2 knock out, in NOTCH1-induced murine T-ALL, led to enhanced T-cell leukemic transformation associated with impaired MAPK signalling. In the human disease, low levels of TRIB2

expression correlate with a mature T-ALL phenotype and high levels of expression with an immature phenotype.

#### 1.5.3.4 TRIB2 in non-small cell lung cancer (NSCLC)

Proteasome-mediated degradation of C/EBPα due to TRIB2 overexpression has also been implicated in the development of NSCLC [117]. Cultured NCl-H1650 lung cancer cells injected into NOD/SCID mice had 76 fold higher TRIB2 expression due to a gene amplification that occurred in 12% of tumours that developed. However, knockdown of TRIB2 transformed the cells ability to be proliferate, suggesting that oncogenisity was driven through TRIB2 expression. Indeed, short hairpin RNA (shRNA) mediated knock down of TRIB2 in injected NOD/SCID mice did not result in tumour growth [117].

Subsequent analysis revealed that depletion of TRIB2 levels, by knock down, resulted in elevated quantities of C/EBPα; these cells matured into defined lineages. Conversely, TRIB2 expressing cells maintained an immature phenotype. Interestingly, although COP1 was expressed it was not found to be bound to TRIB2 [117]. The E3 ligase TRIM21 was in fact required for TRIB2 targeted degradation of C/EBPα in lung tissue [117]. This suggests that context and cell-specific expression E3-ligases are involved in TRIB2 mediated substrate regulation. When an independent lung cancer cell line, A549, as transfected with microRNAs that target the 3'UTR of TRIB2, levels of C/EBPα increased, causing the rate of proliferation to decrease. A459 cells transfected with the microRNA into mice developed smaller tumours compared to the TRIB2 expressing controls [118].

#### 1.5.3.5 Stability of TRIB2 are modulated by $SFC^{\beta\text{-}TRCP}$ and Smurf1

In liver cells, the stability and ubiquitination of exogenous TRIB2 is controlled by the ubiquitin E3 ligase $SCF^{\beta\text{-}TRCP}$ [119]. Knockdown of $SCF^{\beta\text{-}TRCP}$ resulted in increased levels of FLAG-tagged TRIB2 to be detected. Furthermore, in immunoprecipitations TRIB2 was bound to $SCF^{\beta\text{-}TRCP}$. $SCF^{\beta\text{-}TRCP}$ was found to regulate TRIB2 stability by binding to a region in the N-terminal domain termed the TRIB2 Degradation Domain (TDD) [119]. $SCF^{\beta\text{-}TRCP}$ binding is usually regulated by phosphorylation of its substrates. This includes the PERIOD, which contains a phosphodegron that has a phospho-Thr in the N-terminal domain in a TSGSYS motif. Interestingly, TRIB2 also possesses this motif, although it is not known if these Ser residues are phosphorylated on $SCF^{\beta\text{-}TRCP}$ binding. In another study, p70S6K was proposed to

phosphorylate TRIB2 at Ser83, which was required for ubiquitination and proteasome-mediated degradation of TRIB2 by Smurf1 [120]. Indeed, silencing of p70S6K, negated degradation of TRIB2.

#### 1.5.3.6 TRIB2 in liver cancer

TRIB2 protein is highly expressed in a subsets of hepatocellular carcinoma and its expression is closely correlated with β-Catenin cytoplasmic/nuclear accumulation in hepatocellular carcinoma tissue [121]. TRIB2 was found to have higher expression in βCatenin mutated HepG2 cells than βCatenin wild-type Huh7 and Hep3B cell lines, indicating that Wnt pathway activation correlates with TRIB2 expression [121]. Similar to AML and NSCLC subsets, TRIB2 also regulates degradation of C/EBPα in liver cancer cells. Levels of C/EBPα increase following TRIB2 knockdown in HepG2 cells [121]. The regulation of C/EBP was independent of TRCP and high C/EBPα levels prevented the YAP-TEAD interaction, which is important for YAP mediated transcriptional activation. In this context, TRIB2 functions as a signalling nexus to integrate the Wnt/βCatenin, Hippo/YAP and C/EBPα pathways in cancer cells [121].

#### 1.5.3.7 TRIB2 in malignant melanoma

FOXO transcription factors (forkhead/winged helix class O transcription factors) orchestrate gene expression programs known to control a variety of cellular processes such as cell cycle, apoptosis, DNA repair and protection from oxidative stress and abrogation is a key feature in many cancers [122]. Screening of an RNAi library against 7914 human genes identified TRIB2 as a regulator of FOXO activity [122]. TRIB2 mRNA levels are elevated in clinical samples of malignant melanoma. TRIB2 mRNA levels were significantly increased in 70% of malignant melanoma samples, compared to healthy samples. Interestingly, high TRIB2 mRNA transcription was not observed in samples from other skin tumour sources, including non-basal skin carcinoma [122]. Subsequent analysis revealed that TRIB2 mRNA levels were higher in stage III/IV lesions and immortalised lines derived from high grade skin malignancies. TRIB2 was found to negatively regulate FOXO target Bim, although the mechanism of inhibition is still unknown. In the melanoma cell line G-361, after knockdown of TRIB2 the cells were less invasive and growth was inhibited by cell-cell contact. Further to this, when G-361 were transplanted into SCID mice and TRIB2 knocked down, the tumours that formed were, on average, smaller [122].

The evidence that TRIB2 can both target cell context specific substrates for proteasome mediated degradadation and bind to key signalling proteins, facilitating their activation, in numerous types of hematopoetic and solid cancers, potentially marks TRIB2 out as an interesting, novel therapeutic target.

#### 1.5.3.8 TRIB2 induces phosphorylation of AKT at Ser473

The fundamental reason for failure of chemical therapy in patients with cancer is due to acquired resistance. Hill and colleagues (2015) [103] hypothesised that TRIB2 expression, in exogenous isogenic cell lines, contributed to resistance to PI3K and mTOR inhibitors (including the dual PI3K/mTOR inhibitor BEZ235). It was found that upon treatment with BAY439 (PI3K selective), BEZ235 (dual PI3K/mTOR) or BAY236 (RICTOR selective) in various cancer model cell lines (including U2OS, HEK293, G361 and SK-Mel28), overexpressing exogenous TRIB2, had increased resistance characterised by a significantly lower sub-G1 cell population and a reduction of caspase-3 cleavage [103]. Interestingly, treatment of AKT selective inhibitors, including BAY931 and AKT inh.VIII, were effective independent on whether or not TRIB2 was expressed. In the melanoma (SK-Mel28) and osteosarcoma (U2OS) cells with high TRIB2 expression, significantly higher levels of pSer473Ak were identified. Knock down of TRIB2 resulted in perturbed AKT phosphorylation at Ser473. This effect, however, was not observed for pThr308-AKT. It was subsequently discovered that TRIB2 directly interacted with AKT but not RICTOR in immunoprecipitations and PCAs. The TRIB2/AKT1 interaction was demonstrated to be as significant as the known AKT1/JIP1 interaction [103, 123].

To address whether or not over expression conferred resistance to PI3K or mTOR inhibitors *in vivo*, the established 293T cells were subcutaneously injected into the flanks of NOD/SCID mice. Tumours formed equally regardless of TRIB2 expression status. Oral administration of the PI3K/mTOR dual inhibitor BEZ235 to mice transplanted with 293T cells not expressing TRIB2, resulted in xenograft tumour regression along with a statistically significant increase in survival. However, 293T-TRIB2 tumours were highly resistant to BEZ235 treatment [103].

In order to assess whether or not TRIB2 expression status influenced prognosis under clinical circumstances, tumour tissue samples were collected from patients with melanoma, pancreatic and colon cancer prior to standard anti-cancer therapies (DTIC,

gemcitabine or paclitaxel). In comparison to samples from individuals with healthy tissue, TRIB2 mRNA and protein expression was significantly increased. Interestingly, no significant differences in TRIB1 and TRIB3 expression levels were detected between healthy and diseased tissues. Furthermore, increased TRIB2 expression correlated with increased pSer473 AKT and pSer253 FOXO3a protein levels. Indeed, of the clinical samples where TRIB2 expression levels were significantly higher, there was a correlation with poorer clinical outcome [103].

There is not yet any data to support a regulatory role of TRB1 in AKT activation. There is evidence, however, supporting the conjecture that TRIB3, in fact, negatively regulates AKT by preventing phosphorylation at both Thr308 and Ser473 residues [124]. Treatment of HEK293 cells with insulin-like growth factor (IGF1) for just 15 minutes induced detectable phosphorylation of AKT at Thr308 and Ser473. However, overexpression of exogenous FLAG-tagged TRIB3 inhibited AKT phosphorylation at both sites without effecting total amounts of AKT protein. It was subsequently revealed that overexpression of FLAG-TRIB3 reduced AKT activity *in vitro* by employing kinase assays, from HEK293 immunoprecipitates, and a peptide substrate corresponding to the consensus sequence recognised by AKT [124]. To determine whether the inhibitory action of TRIB3 on AKT was relevant under physiological circumstances, endogenous TRIB3 expression was disrupted in hepatocytes by RNAi. RNAi-mediated knockdown of TRIB3 in HepG2 cells potentiated AKT phosphorylation at Thr308 and Ser473 in response to IGF [124].

#### 1.5.3.9 Inhibition of MAPK signalling modules by TRIB2

TRIB2 has been proposed to be a novel regulator of interleukin-8 IL-8 induced inflammatory response driven through inhibition of MEK1, MEK4 and MKK7 [125]. THP-1 monocytes treated with acetylated low density lipoprotein (AcLDL), to induce MAPK mediated inflammatory response, had lower levels of TRIB2 expression [125]. By using ELISA and measuring TRIB2 RNA it was observed that knock down (with siRNA) of TRIB2 potentiated LPS-induced IL-8 production, which was due to enhanced activation of the extracellular signal regulated kinase JUN kinase MAPK pathways. Furthermore, the endogenous level of TRIB2 expression in primary human monocytes was inversely correlated to the cell's ability to produce IL-8. To confirm a physical interaction between MEK1, MEK4 and MKK7 in live monocytes a yellow

fluorescent protein (YFP)- based protein fragment complementation assay (PCA) was employed. This approach is based on the observation that the interaction of two fusion proteins coupled to the N or C-terminal of the proteins of interest will lead to re-folding and generate an active fluorophore, which can be observed by microscopy [126].

## 1.6 Targeting protein kinases and pseudokinases with small molecules

In 2001 imatinib, marketed by Novartis, was approved as a first line of treatment for CML patients with the hyperactive bcr-abl fusion gene and is on the World Health Organization's List of Essential Medicines. Non-coincidentally, after the approval of imatinib, there has been extensive research from all major pharmaceutical companies to develop kinase selective inhibitors to treat numerous cancerous and inflammatory diseases; to date there are nearly 40 FDA approved clinical kinase inhibitors. Most protein kinase inhibitors are reversible competitive ATP mimicking compounds that are broadly classified into two subgroups: type I inhibitors bind to the kinase active site and stabilise a DFG-in active conformation, whilst type II inhibitors (such as imatinib) stabilise the DFG-out inactive conformation. The latter compounds achieve this by occupying a hydrophobic groove adjacent to the ATP binding site that is accessible when the αC helix and DFG motif are in an outward orientation [127]. Due to the highly conserved nature of the kinase fold and specific mechanism of ATP binding and hydrolysis (section 1.1.2), finding selective ATP-competitive inhibitors for particular kinases has been extremely challenging. SB 203580 was an early example of a selective type I inhibitor that targets p38 MAPK α and β isoforms, but not the very closely related γ or δ isoforms. This specificity among MAP kinase isoforms arose due to the presence of a bulky ‘gatekeeper’ Met in the latter, which imparts steric hindrance to inhibitor binding [128]. Indeed, promiscuous inhibitors that target multiple dysregulated signalling pathways may be a pharmacological asset [127], however this could well increase the risk of adverse side effects such as vomiting, diarrhoea, muscle pain, headache, and rashes, which are commonly observed in the use of oncological kinase inhibitors. An ideal approach, especially in the treatment of non-cancer related diseases, is logical mechanistic targeting of a specific protein. In this way, targeting of

pseudokinases that are known to be dysregulated in certain diseases may be useful, in large due to the fact that these proteins have often evolved divergent mechanisms of regulation and possess atypical amino acid compositions and structural architecture, which could potentially be exploited for more exquisite selectivity [6]. Indeed, only ~25% of mammalian pseudokinase domains have been structurally characterized (Table 1). Many of the remaining pseudokinases, whose structures have not yet been elucidated (table 2), are implicated in the aetiology of many diseases and may yet be targetable by repurposing current kinase inhibitors.

| Pseudokinase | Crystal Structure of pseudokinase domain, amino acid residues and PDB ID | Function in humans | Diseases associated when deregulated | Refs |
|---|---|---|---|---|
| ADCK3 | Pseudokinase domain (256-647, PDB ID: 4PED) | UbiB family member with a putative protein kinase like fold that forms an electron-transferring membrane complex involved in isoprenoid lipid biosynthesis in the mitochondria. | Cerebellar ataxia<br>Estrogen receptor-positive breast tumours<br>Glioblastoma multiforme<br>Steroid-resistant nephrotic syndrome | [129] |
| CASK | CaM pseudokinase domain (1-337, PDB ID: 3MFT).<br>CaM pseudokinase domain (1-337) bound to 3'-AMP (PDB ID: 3C0G).<br>CaM pseudokinase domain (1-337) bound to ADP (PDB ID: 3C0H).<br>CaM pseudokinase domain (1-337) bound to ANP (PDB ID: 3MFR). | Contributes to neural development and regulation of gene expression. | Neurological diseases | [59, 130] |
| HER3 | Pseudokinase domain 698-1019 (PDB ID: 3KEX), 684-1020 ( PDB ID: 3LMG) pseudokinase domain bound to bosutinib<br>698-1020 (PDB ID: 4OTW)<br>EGFR/HER3 heterodimer (682-1022, 698-1020, PDB ID: 4RIW). | Binds to neuregulin 1, forms heterodimers with other HER family members and activates PI3K/AKT signalling. | Lung, melanoma, breast, pancreatic, prostate, ovarian, colon and gastric cancers | [81, 131-133] |
| ILK | Pseudokinase domain/alpha-parvin core complex (183-452, PDB ID: 3KMU) | Regulates actin polymerisation by linking integrins to the actin cytoskeleton. | Breast, prostate, brain, and colon cancers | [134] |
| JAK1 | JH2 domain (561-860, PDB ID: 4l00) | JH2 pseudokinase domain of JAK1 facilitates regulatory functions and is needed both for suppression and full activation of JH1 domain catalytic activity. | Gynecological tumours<br>Psoriasis<br>Rheumatoid arthritis, Crohn's disease | [135] |

| | | | | |
|---|---|---|---|---|
| | | | Multiple sclerosis<br>Myelofibrosis | |
| JAK2 | JH2 domain (536-812, PDB ID: 4FVP)<br>JH2 domain bound to Mg-ATP (536-812, PDB ID: 4FVQ)<br>V617F mutant JH2 domain bound to Mg-ATP (536-812, PDB ID: 4FVR)<br>E596A V617F mutant JH2 domain bound to Mg-ATP (535-812, PDB ID: 5I4N) | JH2 domain is catalytically active and phosphorylates two negative regulatory sites in JAK2<br>(Ser523 and Tyr570) to supress JAK-STAT signalling. The pathogenic V617F mutation promotes a confirmation in the JH2 α-C helix that enables stimulatory interactions with the JH1 domain. | Polycythemia vera<br>Acute myeloid leukemia<br>Somatic erythrocytosis | [136, 137] |
| KSR2 | Tyrosine pseudokinase domain (634-950) in complex with MEK1 (1-393) ( PDB ID: 2Y4I) | Scaffolding protein that coordinates the formation of the Raf-MEK-ERK signalling complex. Phosphorylates MEK1 upon interaction with BRAF. | Obesity<br>Type 2 diabetes<br>Tumour Cell transformation | [66] |
| MLKL | Pseudokinase domain (179-471, PDB ID: 4M67).<br>Pseudokinase domain (183-471, PDB ID: 4MWI). | Phosphorylated by RIP3 to mediate downstream necroptosis signalling. | Autoimmune diseases<br>Inflammatory bowel disease<br>Neoplastic diseases | [65, 138] |
| PAN3 | *Drosophila melanogaster* Pseudokinase domain bound to AMP phosphoramidate (349-790, PDB ID: 4BWP) | Forms a poly(A)-specific RNase complex with the exonuclease PAN2, which functions in mRNA deadenylation. | Unknown | [139] |
| ROR2 | Pseudokinase domain (464-751, PDB ID: 3ZZW), 452-753 ( PDB ID: 4GT4) | Modulates Wnt signalling upon receptor stimulation. | Osteosarcoma<br>Renal cell carcinoma<br>Melanoma<br>Colon cancer<br>Head and neck squamous cell carcinoma<br>Breast cancer | [140] |
| SGK 223 | Pseudokinase domain dimer (PDB ID: 5VE6) | Scaffold and an effector of Rnd2 GTPase. Stimulates RhoA activity to promote cancer cell invasion in a Src-dependent manner. | Pancreatic ductal adenocarcinoma<br>Breast cancer<br>Colon cancer | [141-144] |
| SGK 269 | Pseudokinase domain dimer (PDB ID: 6BHC) | Binds to Crk to assist recruitment of the Src/p130/Cas/Crk scaffold. | Breast cancer<br>Colon cancer | [145-147] |
| STRADα | MO25α in complex with the STRADα C terminus (59-431 PDB ID: 2WTK) and LKB1 | Binds to ATP and complexes with MO25 to allosterically stimulate LKB1 and other AMPKs. | Peutz Jeghers syndrome<br>Sporadic cancers | [148] |

| | | | | |
|---|---|---|---|---|
| TITIN | Pseudokinase domain 32172-32492 (PDB ID: 1TKI), 32172-32492 (PDB ID: 4JNW) | Regulator of muscle contraction | Human skeletal tibial muscular dystrophy Dilated cardiomyopathy Hypertrophic cardiomyopathy | [149-151] |
| TRIB1 | Pseudokinase domain (83-343, PDB ID: 5CEK), Pseudokinase and C-terminal domain (83-371, PDB ID: 5CEM) | Interacts with MKK proteins to modulate MAPK signalling. Binds E3 ubiquitin ligases to degrade target proteins via the proteasome | AML CML T-ALL Megakaryocytic leukaemia Fatty liver disease Coronary artery disease | [106] |
| TYK2 | JH2 domain bound to 5' ATP (556-871, PDB ID: 5C03). Pseudokinase domain bound to BMS-066 (575-869, PDB ID: 4WOV) | JH2 domain binds to ATP but is catalytically inactive, which is functionally important in JH1 domain regulation. | Autoimmune disorders including systemic lupus erythematosus (SLE) | [73, 152] |
| VRK3 | Pseudokinase domain (146-474, PDB ID: 2JII) | VRK3 negatively regulates MAP kinase signalling by promoting vaccinia H1-related (VHR) dependent inactivation of ERK in the nucleus. | Alzheimer's disease Parkinson's disease | [153] |
| WNK1 | Pseudokinase domain (210-482, PDB ID: 4PWN) | Stimulated the activities of $Na^+$ driven, $Cl^-$importing NKCCs ($Na^+/K^+/Cl^-$ co-transporters. | Hereditary neuropathy Glioma Hereditary hypertension | [96] |
| STK40 | Pseudokinase domain (PDB ID: 5L2Q) | Negative regulator of NF-kappa-B and p53. Potential modulator in TNFα signalling. | Elevated expression in certain cancers | [154] |

**Table 1: Publically available crystal structures of human pseudokinase domains**. All pseudokinses with solved crystal structures, along with functions and potential links to disease.

| Pseudokinse | Functions in humans | Diseases associated when deregulated | Refs |
|---|---|---|---|
| **EphA10** | The receptor domain binds to Ephrin-A ligand members but its functions in cell signalling are unclear. | Breast cancer Colon Caner Prostate cancer | [155, 156] |
| **EphB6** | Binds to Ephrin-B1, which induces EphB6 transphosphorylation by a catalytically active EphB partner to initiate signalling. | Triple-negative breast cancer B cell leukaemia Lung cancer Prostate cancer Melanoma Gastric cancer Neuroblastoma | [157, 158] |
| **GCN2** | Pseudokinase domain regulates function by interacting with GCN2 kinase domain. | Alzheimer's disease Xenograft tumour growth Liver, breast, lung and colon cancer | [159, 160] |
| **GUCY2C** | Tyrosine kinase activity in the active kinase domain facilitates the GC-C signalling pathway. The | Attention-deficit hyperactivity disorder (ADHS) Colon cancer | [161, 162] |

| | | | |
|---|---|---|---|
| | pseudokinase domain negatively regulates the catalytic GC domain. | Familial GUCY2C diarrhoea syndrome (FGDS)<br>Crohn's disease<br>Intestinal obstruction | |
| **GUCY2D** | Plays a role in the recovery phase of phototransduction. It is potentially involved in re-synthesis of cGMP. | Retinal dystrophy<br>Leber congenital amaurosis (LCA1) | [163] |
| **GUCY2F** | Catalyses the synthesis of cGMP. | Colon, lung, pancreatic and breast cancer | [164] |
| **IRAK2** | Associates with MyD88 and IRAK4 to upregulate NF-kappaB signalling. | Colorectal cancer | [165, 166] |
| **JAK3** | JH2 pseudokinase domain functions in both suppression and full activation of the JH1 domain which, modulates various biological processes including immune system regulation, haematopoiesis and metabolism. | Severe combined immunodeficiency (SCID)<br>Cancer | [68] |
| **KSR1** | Scaffolding protein that coordinates the formation of the Raf-MEK-ERK signalling complex, facilitating their phosphorylation and activation in regulation of immune function and metabolism | Inflammatory bowel disease | [167-170] |
| **NPR1** | Atrial natriuretic peptide (ANP) or brain natriuretic peptide (BNP) binds to the extracellular receptor domain to stimulate the intracellular guanylyl cyclase domain to hydrolyse GTP. | Hypertension, elevated blood pressure, salt-resistant hypertension, progressive cardiac hypertrophy<br>Obesity<br>Metabolic syndrome<br>Colon cancer | [171, 172] |
| **NPR2** | C-type natriuretic peptide (CNP) binds to the extracellular receptor domain to stimulate the intracellular guanylyl cyclase domain to hydrolyse GTP. | Achondroplasia<br>Endochondral ossification<br>Erectile dysfunction | [173-175] |
| **NRBP1** | Modulates Wnt signalling as a tumour suppressor | Breast cancer | [176] |
| **NRBP2** | Scaffold for the E3 component of the ubiquitin conjugation system responsible for substrate recognition. | Gliomas | [177, 178] |
| **PAN3** | Forms a poly(A)-specific RNase complex with the exonuclease PAN2, which functions in mRNA deadenylation. | Unknown | [179] |
| **Ptk7** | Binds to Fzd7 and Ror2 to stimulate Wnt5a signalling via Jnk. | Breast, colon, lung esophageal, gastric cancers<br>Liposarcoma<br>AML<br>T-ALL<br>ALL | [180, 181] |
| **RSKL1** | Binds sphingosine kinase 1 and peroxiredoxin 3, the implications of which are unclear. | Endometrial cancer | [182] |

| | | | |
|---|---|---|---|
| **RSKL2** | RSKL2 binds sphingosine kinase 1 and peroxiredoxin 3, the implications of which are unclear. | Unknown | [182] |
| **SCYL1** | Mediates transport of the KDEL endoplasmic reticulum protein retention receptor and regulates Golgi morphology. | Amyotrophic lateral sclerosis | [183] |
| **SCYL2** | C-terminal domain interacts with components of clathrin-AP1 complex to regulate clatherin-mediated endocytosis. | Unknown | [183] |
| **SCYL3** | Unknown | Unknown | |
| **Sgk 071** | Unknown | Unknown | |
| **Sgk 196** | Phosphorylates the 6-position of O-mannose required for dystroglycan function. | Congenital muscular dystrophy | [184] |
| **Sgk 424** | Unknown | Unknown | |
| **Slob** | Unknown | Unknown | |
| **STK31** | Localises to the centromeres during mitosis and promotes cell migration. | Cervical cancer<br>Colorectal cancer | [185, 186] |
| **Stradβ** | Allosteric stimulation of LKB1 in axon formation. | Unknown | [187] |
| **STYK1** | Binds to AKT to stimulate activity of GSK3β. | Cancer | [188-190] |
| **TBCK** | Rab GTPase activating protein that modulates the mTor signalling pathway. | Intellectual disability developmental delay, epilepsy, dysmorphism and hypotonia | [191-193] |
| **TEX14** | Recruited to kinetochores by PLK1 and regulates the maturation of the outer kinetochores and microtubule attachment. | cancer development and progression | [194, 195] |
| **TRIB2** | Interacts with MEK1, MKK7, AKT and p65/RelA to modulate signalling. Binds E3 ubiquitin ligases and drives degradation of target substrates via the proteasome. | AML<br>T-ALL<br>Liver cancer<br>Melanoma<br>NSCLC | [109, 121, 122, 196, 197] |
| **TRIB3** | Interacts with MEK1, MKK4, MKK7, AKT, MLK3 and PPARγ to modulate signalling. Binds E3 ubiquitin ligase to degrade target proteins via the proteasome. | Parkinson's Disease<br>Diabetes<br>Breast cancer<br>colorectal cancer | [197-199] |
| **TRRAP** | Acetyl histone transferase cofactor. | Glioblastoma<br>Breast cancer | [200, 201] |
| **ULK4** | Unknown | Ciliopathy<br>Neurodevelopmental, neuropsychiatric and neurodegenerative disorders | [202, 203] |
| **WNK2** | Stimulates the activities of Na+-driven, Cl−-importing NKCCs (Na+/K+/Cl− co-transporters) | Glioma | [95, 101] |
| **WNK3** | See WNK2 | Glioma | [95, 100] |
| **WNK4** | See WNK2 | Hereditary hypertension | [95, 97] |

**Table 2: Functions and links to disease of pseudokinases with no known structure.**

### 1.6.1 ATP competitive inhibitors

Pseudokinases whose biological functions are linked to ATP hydrolysis and direct substrate phosphorylation, such as WNK, are obvious targets for traditional ATP-competitive inhibitors. However, despite the fact that the majority of pseudokinases lack, or have very weak catalytic output, the binding of ATP competitive inhibitors to the pseudokinase domain can modulate their signalling output. The pseudokinase domain of MLKL can bind to but cannot hydrolyse ATP [58], which formed the rational to screen recombinant MLKL *in vitro* using DSF with the PKIS1. Compound 1 was found to bind to the pseudokinase domain of MLKL, which prevented its phosphorylation by upstream kinase RIPK3 and prevented necroptosis. KSR2 is a scaffold protein with and weak catalytic activity. It was discovered that pan kinase inhibitors such as ASC24, can reduce KSR2-dependent phosphorylation of MEK1 at non-BRAF phosphorylated Ser residues *in vitro* [204]. Suppression of JAK signalling could also be achieved indirectly with small molecules that promote JH2 auto-inhibition of JH1 kinase output, which has already been suggested mechanistically for TYK2. Crystal structure analysis of the JAK kinase TYK2 pseudokinase domain revealed that binding to an ATP competitive inhibitor stabilised the intra-domain auto-inhibitory interaction with the tyrosine kinase domain and blocked downstream signalling [152]. Bristol Myers Squibb have recently disclosed that a TYK2 JH2 domain inhibitor will proceed to Phase III clinical trials for the skin disease psoriasis. The TYK2 inhibitor BMS-986165 induces allosteric inactivation of the JH1 domain by binding to and stabilising the JH2 domain. Pfizer is also currently evaluating a TYK2/JAK1 pseudokinase domain inhibitor, PF-06700841, which is currently at mid stage studies for psoriasis, Crohn's disease and ulcerative colitis (UC).

There is a reduction in amino acid conservation in regions outside the ATP binding pocket, which become exposed when the kinase is maintained in a DFG-out state. Therefore Type II kinase inhibitors are potentially more selective. Moreover, there is also the greater conformational variability observed between kinases in their inactive states [205]. Imatinib is an example of a type II inhibitor, which binds to the active site of ABL and stabilises the DFG-out conformation [206]. Activity of pseudokinases may be regulated by conformational transitions, which are potentially targetable with small molecule inhibitors [207]. Crystal structure analysis of the RNas L pseudokinase domain (which is catalytically inactive) adopts an active-like DFG-in conformation

when bound to AMP–PNP, which is a non-hydrolyzable ATP analogue. In the absence of AMP-PNP the pseudokinase domain reverts to an inactive conformation. Homodimerization of the RNase domain only takes place when the pseudokinase domains are bound to AMP-PNP and maintained in an active conformation [208].

### 1.6.2 Allosteric targeting of kinases

Allosteric or type III inhibitors exploit alternate binding pockets outside the active site, which can be specific to particular kinases, thus the potential for exquisite selectivity can be enhanced. Binding of compounds distal to the ATP-binding pocket can drive conformational changes. In this regard type III can indirectly influence catalytic activity and indeed non-catalytic regulatory (such as scaffolding) functions [209]. For instance, the PIF-pocket, by the αC-helix of PDK1 has been targeted [210]. In AKT, the N-terminal PH domain binds intramolecularly with the kinase catalytic domain, stabilising the kinase in an inactive conformation (section 1.2.1.1). Similar to PDK1 allosteric inhibitors, AKT inhibitors, including MK2206 stabilise the inactive structure of the PIF-pocket by binding to the αC-helix, which locks the PH domain to the N-lobe of the kinase domain [211]. These inhibitors did not arise from the fruits of structure guided design, but rather the binding modes and mechanisms of inhibition were discovered serendipitously. Although no proof of concept for type III inhibition currently exists in the public domain for pseudokinases, the growing number of pseudokinases observed to undergo ‘kinase-like’ conformational changes to appropriate cellular signalling is a promising indication for the potential of this area in biomedical research.

### 1.6.3 Covalent inhibitors

The kinase-activating L858R EGFR mutation is highly responsive to first- generation EGFR inhibitors, including gefitinib and erlotinib. However, these patients often relapse due to a secondary, drug-resistant mutation in EGFR whereby the gatekeeper threonine is converted to methionine (T790M). This second mutation does not negate the binding of compounds gefitinib and erlotinib, but rather increases the kinase domains affinity for ATP, which means ATP competitive inhibitors are no longer effective [212]. Therefore, there has been a concerted effort to generate irreversible covalent inhibitors for EGFR in NSCLC. The majority of covalent compounds are adapted versions of previously established small molecule inhibitors. With the use of crystal structure analysis in tandem with *in sillico* structure-guided design, kinase

inhibitors have been modified by the addition of an electrophilic so called ‘warhead’ to enable targeting of specific nucleophilic thiol groups of Cys residues within the kinase domain [213]. For instance, analysis of the crystal structure of the quinazoline based ATP-competitive inhibitor gefitinib bound to EGFR (PDB: 3UG2), revealed that the thiol group of C797 is ~7 Å from the oxygen atom in the oxypropyl morpholine substituent, thus suggesting that an electrophilic ‘warhead’ at this position may be suitable for covalent bond formation. Indeed, this endeavour has resulted in the development of several type IV covalent kinase EGFR family kinase inhibitors, including afatinib and neratinib [213]. Crystal structure analysis confirmed covalent bonding of afatinib to EGFR while the non-covalent binding mode, typical of reversible binding by gefitinib, of hydrophobic and hydrogen bonding interactions were maintained [213].

Covalent inhibitors have various potential advantages over reversible inhibitors. Specificity may be enhanced via the targeting of a unique Cys residues in the target kinase. Secondly, the reactions are more energetically favourable, requiring lower inhibitor concentrations that achieve better efficacy. Furthermore, after covalent modification of the target terminal inhibition is usually achieved, meaning that new protein synthesis must occur in order to re-establish signalling activity. As targeted cysteine residues are not uniformly conserved amongst kinases and pseudokinases [207], they act as a specificity filter to limit inhibitor promiscuity. One downside is that irreversible inhibitors risk forming concentration dependent off-target adducts with reactive cysteines of unrelated proteins [207]. Indeed, proteome mapping has revealed that third generation covalent EGFR family kinase inhibitors have distinct off-targets. Patients often relapse due to a secondary, drug-resistant mutation in EGFR whereby the gatekeeper threonine is converted to methionine (T790M), which is where covalent inhibitors may become an effective therapeutic strategy. In particular, the FDA-approved drug osimertinib was found to covalently modify cathepsins in cell and animal models, which correlated with lysosomal accumulation of the compound [214]. Indeed, exploiting off targeting effects of covalent inhibitors could lend support to finding novel drug leads for pseudokinses [207].

The LUX-Lung trials are the first global, head-to-head trials comparing third- and first-generation EGFR-directed therapies (afatinib and erlotinib) for patients with EGFR mutation-positive NSCLC. The LUX-lung 8 phase III clinical trial compared the irreversible quinazoline based inhibitor afatinib with the quinazoline based type I ATP-

competitive inhibitor erlotinib, as second-line treatment for patients with advanced NSCLC. Progression free-survival was significantly longer with afatinib than with erlotinib (median 2.4 months compared to 1.9 months) [215]. The overall survival was also significantly improved with afatinib compared to erlotinib. The median overall survival for afatinib was 7.9 months and was 6.8 months for the erlotinib group. Resistance to afatinib inevitably arises due to a C797S kinase domain mutation. Interestingly, reversible compounds inhibit the C797S for which the reported third-generation EGFR candidates fail due to lack of potency from the formation of the covalent bond [213].

An advantage of analysing binding of covalent inhibitors is the prospect to detect covalent modification by mass spectrometry. Analysis by isothermal titration calorimetry (ITC), however, may be complicated when considering slower off-rates due to time dependent irreversible covalent binding. Mass spectrometry was used to confirm the covalent modification of HER3 by TX1-85-1. Addition of TX1-85-1 to recombinant HER3 followed by proteolysis trypsin and subsequent tandem mass spectrometry (MS2) analysis revealed unique modification of Cys721 [216].

## 1.7 Detecting small molecule interactions with pseudokinases

### 1.7.1 Screening

An effective method to screen canonical kinases with a known substrate would be to employ mobility shift assays, to observe percentage conversion of a fluorescent substrate peptide by the protein of interest, in the presence of candidate inhibitors. However, the majority of pseudokinases are poorly studied and specific targets are often unknown or ambiguous. Furthermore, most pseudokinases have very weak or no detectable catalytic output, which further limits the use of conventional assays. Employing *in vitro* kinase assays to assess pseudokinase activity faces various caveats, a major drawback being lack of sensitivity, especially when distinguishing the presence of potential minor quantities of contaminating kinases that may otherwise lead to incorrect conclusions. More effective avenues of screening, that many pseudokinase researchers have turned to, employ biophysical approaches. Biophysical tools are essential for the discovery, development, and characterisation of therapeutic proteins and drugs. Biophysical techniques are cheaper, less time

consuming and assay complexity is reduced while providing good information content data to bolster the efficiency of drug discovery campaigns.

It is currently estimated that ~40% of all pseudokinases possess detectable nucleotide binding activity, and this was established by means of a differential scanning fluorimetry (DSF) assay, which is a thermal shift assay (TSA) [58]. Importantly, the assay monitors the thermal denaturation of the major protein species, so any minor contaminants, including co-purified protein kinases, which would lead to misleading results in radiometric *in vitro* $^{32}$P kinase assays, do not contribute to the signal. With the recently solved TRIB1 crystal structure, efforts have been made to discover chemical ligands that modulate its important regulatory conformations. Inhibitors could serve as molecular probes and perhaps as potential therapeutic leads. TRIB1 was recently screened by DSF employing the protein kinase inhibitor set 1 (PKIS1). PKIS1 is a library of 367 ATP-competitive kinase inhibitors, covering ~30 chemotypes originally developed to target 24 distinct protein kinases. A subset of dual Angiopoietin-1 receptor (TIE-2) and vascular endothelial growth factor receptor (VEGF) benzimidazole based inhibitors were discovered to increase TRIB1 thermal stability. Interestingly, a thyophene based PLK inhibitor, GW804482X, reduced TRIB1 thermal stability, rather than stabilising the protein, which is potentially indicative of compound binding to alternate TRIB1 conformations. Additionally, MLKL was screened, using DSF, against the PKIS1. From this screen the previously discussed compound 1 was discovered [217].

### 1.7.2 Validation of potential ‘hits’

Choice of screening procedure is important and understanding the limitations of particular assays is vital. TSAs can be sensitive to different mechanisms of interference, such as from fluorescence from compounds that may disrupt readouts [218], redox cycling of compounds [219], compounds that induce protein aggregation [220], metal chelating compounds and metal contaminants [221]. The probability of misidentifying certain inhibitors as genuine hits is reduced by employing downstream confirmatory assays.

#### 1.7.2.1 Microscale thermophoresis (MST)

Thermophoresis is also known as the Ludwig–Soret effect and is defined as the movement of molecules through a temperature gradient [222]. The properties that determine the rate of movement are charge, size and hydration shell [223]. Any of these properties can change in a protein upon binding to a ligand. This measurement in change of thermophoresis can be used to calculate the affinity of the interaction between binding partners, be they protein–protein, antibody–antigen, protein–DNA, protein–RNA and protein compound [223]. The company NanoTemper have commercialised Monolith instruments to measure the thermophoresis of biomolecules, which uses an infrared laser to heat the sample loaded within a capillary. As the laser is focused it produces a localised microscopic temperature gradient with a heat range of 2–6 °C, and ligand–target protein complexes demonstrate a different movement velocity through the temperature gradient compared with unbound molecules. The movement induced by the laser is monitored via fluorescence of the target protein or from a label previously bound to the protein, such as attachment of a fluorescent dye coupled to nitrilotriacetate (NTA) to modify a 6His-tag [223].

The use of MST is increasingly being reported in fragment-based drug discovery for many kinases, such as p38α [224] and MEK1, [225] and bromodomain 9 (BRD9) [226]. In a study of MEK1 and BRD9, MST was used to confirm the binding of fragments identified first by surface plasmon resonance (SPR) and DSF. Interestingly, MST was able to identify additional hits not detected in the first line of screening.

#### 1.7.2.2 Isothermal titration calorimetry (ITC)

ITC is a reliable method to determine the K*d* of compound binding and is at present the gold standard for elucidating binding free energies (ΔG) into enthalpy (ΔH) and entropy (ΔS) contributions. Both the binding constant K*d*, and the stoichiometry can be calculated while ΔG and ΔS are then derived by calculation from the primarily measured properties [227]. However, for ITC analysis there is a requirement of a 10-15 fold excess of either one of the components (protein or compound). The vast majority of small molecule inhibitors are non-polar and thus very poorly soluble in conventional protein assay buffers), which usually means that very high μM concentrations of protein are required (<100 μM). Analysis by ITC would not be feasible if the protein of interest is unstable at high concentrations.

#### 1.7.2.3 Mass spectrometry (MS)

Ion mobility-mass spectrometry (IM-MS) can permit the detection of even low abundant species in complex samples. Proteins can retain their native folded structure in the gas phase and even if a protein ligand complex is maintained only by hydrophobic interactions, they can retain integrity [228]. Elucidation of the mass to charge ratio (m/z) provides information about stoichiometry, connectivity, and topology of protein interactions. At the same time, the charge state after electrospray ionization (ESI) can be analysed to give indications of protein shape 5. The affinity between a protein and compound can also be determined with results that are consistent with established solution-phase methods [229].

In IM-MS the protein-ligand complex is ionised by nano electrospray ionization (nESI), which results in the formation of an intact complex with few net charges [230]. Subsequently the ions are move through an ion mobility cell guided by a weak electric field filled with an inert gas (such as helium or nitrogen). Smaller ions experience fewer collisions with the gas and thus migrate within the cell at a higher velocity. Finally, the ionised sample enters a quadrupole and/or time-of-flight mass analyzer (ToF) followed by a detector. As a result, the investigated molecules are not only separated according to their m/z as in conventional MS but also according to their size and shape [231].

## 1.8 Aims of this thesis

The central hypothesis of my thesis is that TRIB2 can bind to small molecule kinase inhibitors which in turn may influence TRIB2 functions in cellular signalling. Chapter 3 discusses my exploration of TRIB2 biochemistry by analysing whether, like TRIB1, a regulatory interaction exists between the C-terminal tail region and TRIB2 pseudokinase domain. By employing a DSF assay, I deduce that TRIB2 can bind to certain small molecule kinase inhibitors. The remainder of chapter 3 is dedicated to validating the mechanisms of compound binding using a combination of techniques, including site-directed mutagenesis, MST, MS, molecular docking and molecular dynamic simulations. In chapter 4, I evaluate the effects of TRIB2 interacting small molecules in human cells, including an AML-derived cell line. In chapter 5, I discuss the conclusions of my work, and some potential future applications.

# Chapter 2: Materials and methods

## 2.1 Chemicals, reagents and antibodies

The pET Ek/LIC bacterial expression vectors were purchased from Novagen and pOPIN bacterial expression vectors from Addgene. The pGEx-6P-1 vector encoding C/EBPα was a gift from Dr Karen Keeshan (University of Glasgow, Great Britain). The pET Ek/LIC bacterial expression vectors encoding TRIB1 84-343 and TRIB1 84-372 were a gift from Peter Mace (University of Otago, New Zealand) The Flp-In T-REx system (for mammalian expression) including parental cells, pcDNA5/FRT/TO, and pOG44 plasmids were purchased from Invitrogen. Restriction enzymes were purchased from New England Biolabs (NEB). KOD polymerase was sourced from Novagen. All primers were purchased from Integrated DNA Technologies (IDT). All buffers were made using Milli-Q water unless otherwise indicated.

Tetracycline and doxycycline, MG132, AICAR and chloroquine were purchased from Sigma-Aldrich. Afatinib, neratinib, osimertinib, ibrutinib, erlotinib, lapatinib, TAK-285, BI2536, BI6727, gefitinib and bortezomib were purchased from LC laboratories or Selleck. Synthetic stapled C-terminal peptides were a gift from Dr Eileen Kennedy (University of Georgia, USA).

Total AKT, pSer 473 AKT, pThr 308 AKT, total ERK1/2, dual pThr 202/pTyr 204 ERK1/2, CDC25C, total acetyl coenzyme A carboxylase (ACC), pACC Ser79, cleaved Caspase 3 and α-tubulin antibodies were purchased from New England Biolabs. 6His-HRP and α-FLAG antibodies were purchased from Sigma-Aldrich, Glyceraldehyde 3-phosphate dehydrogenase (GAPDH) antibody was purchased from Proteintech and a polyclonal rabbit α-TRIB2 antibody was raised towards a unique N-terminal human TRIB2 sequence and affinity purified prior to evaluation with recombinant TRIB2 and a variety of human cellular extracts.

The PKIS chemical library (designated as SB, GSK or GW compounds) comprises 367 ATP-competitive kinase inhibitors, covering ~30 chemotypes (~70% with molecular mass <500 Da and clogP values <5) that were originally designed as ATP-competitive inhibitors of 24 distinct protein kinase targets [232]. Compounds were stored frozen as 10 mM stocks in dimethyl sulphoxide (DMSO) in 96-well plates.

## 2.2 Transformation of *E.coli* and plasmid purification

### 2.2.1 Generation of chemically competent *E. coli*

TOP10 and BL21(DE3)pLysS *E. coli* strains were streaked onto Luria-Bertani (LB) agar plates from a glycerol stock and grown for 18 hours in an incubator at 37 °C. From these plates, single colonies were grown in 50 mL of LB media for a further 18 hours in a shaker incubator (250 rpm) at 37 °C. From the 50 mL subcultures, 2 mL of bacteria in suspension were added to 200 mL of fresh LB media and grown to an $OD_{600}$ of 0.6. The cells were then centrifuged at 5000 **g** for 10 minutes, to pellet the cells. The LB media was decanted leaving the pelleted bacteria, which were re-suspended in buffer 1 (100 mM rubidium chloride, 50 mM manganese chloride, 30 mM potassium acetate, 10 mM calcium chloride and 15% (v/v) glycerol). The cell suspensions were incubated on ice for 5 minutes and subsequently centrifuged once again to pellet the bacteria. The supernatant was decanted and the bacteria was re-suspended in buffer 2 (10 mM MOPS, 10 mM rubidium chloride, 75 mM calcium chloride and 15% (v/v) glycerol) and incubated for a further hour on ice. The chemically competent bacteria were then aliquoted at a volume of 200 µL into sterile 1.5 mL ependorf tubes, flash frozen in liquid nitrogen and stored at -80°C.

### 2.2.2 Transformation protocol

Chemically competent TOP10 were transformed in order to amplify plasmid stocks for purification. Chemically competent BL21(DE3)pLysS was used for protein expression. In a 1.5 mL sterile ependorf tube, 20 ng of plasmid DNA was added to 50 µL of chemically competent *E. coli* and incubated on ice for 30 minutes. The mixture was subsequently transferred to a water bath, heated to a temperature of 42°C for 30 seconds in order to initiate bacterial heat shock. The bacteria were then placed on ice and left to cool for 2 minutes. 250 µL of SOC media (2% tryptone, 0.5% yeast extract, 10 mM NaCl, 2.5 mM KCl, 10 mM MgCl2, 10 mM MgSO4, 20 mM glucose) was added to the transformation mixture and incubated at 37°C for 1 hour in a shaker incubator. Lastly, 50 µL of bacterial suspension in SOC media was spread on an agar plate with, depending on the plasmid, appropriate antibiotic selection markers and incubated for 18 hours at 37°C.

### 2.2.3 Plasmid purification and sequencing

Chemically competent TOP10 *E. coli* were transformed with plasmids and grown on agar plates with specified antibiotics for selection. Single colonies were cultured in 5 mL of LB liquid media for 18 hours and then centrifuged for 5 minutes at 5000 **g** in order to pellet transformed cells. The supernatant was removed and these cells were treated sequentially by the constituents of the QIA Spin Miniprep kit, as described in the Manufacturer's instructions (Qiagen).

Once purified, the concentration of plasmid DNA was quantified by detecting UV absorbance at 260 nm, employing a NanoDrop 2000c system (Thermo Fisher Scientific). Subsequently 800 ng of plasmid DNA was mixed in a total reaction volume of 10 µL with 10 pmol/µL of appropriate sequencing primer (to generate between 500 and 1200 bp of readable sequence) before Automated Sanger Sequencing (GATC Biotech).

## 2.3 Mutagenesis

### 2.3.1 Site-directed mutagenesis

To specifically mutate a residue in TRIB2, primers were used that introduce designated mutation(s) into the coding sequence. Primers were designed to incorporate codons for the desired mutation(s), which were flanked either side by ~15 bp of coding DNA. The reverse primer was the exact reverse complement of the forward primer, so that the entire plasmid, encoding TRIB2, was amplified. The forward primers for Cys mutants were:

C96S:5'gtgtttgatatcagctcctaccaggaatccctg.
C104S:5'gaatccctggcaccgtcctttgcctgtctgct.
C104Y:5'gaatccctggcaccgtactttgcctgtctgct.

The general polymerase chain reaction (PCR) contained: 10 ng Plasmid template, 0.1-0.5 µM of forward/reverse primer (optimised case by case), 1 µL KOD hotstart DNA polymerase (NEB) (2000 U/ml), 5 µL 10x KOD Buffer (NEB), 10 mM $MgCl_2$ and 5 µL 10x dNTP mixture (Final concentration 50 µM of each) in final reaction volume of 50 µL (made up with nuclease free water). For the cycling parameters: Hot start at 95°C for 1 minute. Annealing temperature (1 °C bellow the specified primer melting temperature) for 30 seconds followed by amplification at 70°C for 16 minutes. These

parameters were cycled 30 times before a final hold at 70°C for 10 minutes. The PCR products were incubated with DpnI (20U) for 1hr at 37°C to eliminate the template (purine methylated) DNA. The PCR products were subsequently transformed into the TOP10 *E. coli* and expanded overnight in 3 mL of LB after single colony selection. After purification of plasmids by QIA miniprep QuickSpin Kit (Qiagen), successful mutagenesis was determined by Sanger Sequencing (GATC Biotech).

### 2.3.2 Truncation mutants

Primers were designed to flank the desired coding region of DNA for amplification, whilst incorporating the required sequences for LIC cloning. For the generation of pET30 encoding FLAG-His-TRIB2, the forward primer incorporated a sequence which codes for FLAG peptide (GACTACAAAGACGATGACGACAAG) after the start codon. PCR products were analysed by agarose gel electrophoresis, purified by gel extraction (Qiagen) and the DNA then quantified by UV absorbance detected employing a NanoDrop.

#### 2.3.2.1 Agarose gel electrophoresis and purification of cDNA fragments

After PCR amplification DNA products were isolated using electrophoresis in 1% (w/v) agarose gels. 1 g of agarose (Sigma-Aldrich) was added to 100 mL of Tris-acetate-EDTA (TAE) buffer and dissolved by heating in a microwave. After slight cooling the intercalating DNA stain ethidium bromide was added to a final concentration 5 µg/mL. The 1% agarose solution was added to a gel cast and left to solidify on cooling. The gel was placed in a tank containing 1% TAE buffer and the DNA was subsequently electrophoresed at a constant field strength of 6.7 Vcm-1 for ~45 min. A UV transilluminator was employed to visualise the migrated DNA with reference to a 1-10 kb DNA ladder, (New England Biolabs). The visualised DNA fragments were cut from the gel with a sterile scalpel and transferred to sterile 1.5 mL ependorf tubes. DNA was extracted and purified using the QIAquick Gel Extraction kit, as described in the manufacturer's protocol (Qiagen). The DNA content was then quantified by UV absorbance, employing a NanoDrop.

#### 2.3.2.2 Ligation-Independent Cloning (LIC)

The purified PCR products (0.2 pmol), flanked by the LIC overhangs, were incubated with 0.4 µL T4 DNA polymerase (3000 U/ml) with 2 µl 10X NEB buffer 2, 100 mM DTT,

0.5 µl dATP (100 mM) and 0.2 µL of 100X BSA stock solution with a final reaction volume of 20 µL for 30 minutes at ambient temperature. The reaction mixture was subsequently incubated for 20 minutes at 75°C in order to inactivate the polymerase.
The pET30 vector was linearized and treated with T4 polymerase, firstly by incubation with 5 µl 10X NEB buffer 3, 5 µg pET30/LIC vector DNA, 2.5 µL BsaI restriction enzyme (10U), and nuclease free water to a volume of 50 µL. The BsaI digested vector was resolved by agarose gel purification and purified using gel extraction (Qiagen). 600 ng BsaI-digested pET30 vector was then treated with T4 DNA polymerase as follows: 2 µL 10X NEB buffer, 600 ng BsaI-digested pET30, 0.5 µL dTTP (100 mM) 1 µL DTT (100 mM), 0.2 µL of 100X BSA and 0.4 µL of T4 DNA polymerase (3U) were incubated to a volume of 20 µL in nuclease free water for 30 minutes at ambient temperature. Then, to inactivate the polymerase, the reaction mixture was incubated for 20 minutes at 75°C.
In order to anneal the linearized vector and treated insert, they were mixed and incubated for 5 minutes at ambient temperature. Next 1 µl of EDTA (25 mM) was added followed by a further 5 minute incubation at ambient temperature. The plasmids were subseqntly transformed into TOP10 *E. coli* form amplification.

### 2.4 Recombinant protein expression

Bacterial expression vectors were transformed into) BL21(DE3)pLysS and streaked onto agar plates (with appropriate selection markers) and incubated for 18 hours at 37°C. All TRIB2 and TRIB1 proteins and PKA were encoded in pET30 vectors, which have resistance to kanamycin (50 µg/mL). The pGEx-6P-1 vector encoding C/EBPα carries resistance to ampicillin (50 µg/mL). BL21(DE3)pLysS possess an additional plasmid, which expresses T7 lysozyme and carries a resistance to chloramphenicol (34 µg/mL). For expression of each protein, a single colony from the agar plate was transferred to 100 mL of LB media (with antibiotics) and incubated for a further 18 hours at 37°C in a shaker incubator (250 rpm). The subcultures of *E. coli* were then transferred to larger volumes of LB media (10 mL of subculture per litre of LB media). For expression of each protein this was between 4 and 8 litres of culture medium. The flasks were incubated at 37°C in a shaker incubator until bacteria reached an $OD_{600}$ of 0.8 nm, at which point protein expression in was induced by the addition of sterile isopropyl-1-thio-β-D-galactosidase (IPTG) at a final concentration of 0.2 mM. The cultures were incubated at 18°C for 16 hours in a shaker incubator rotating at 250 rpm.

Subsequently the cultures were centrifuged at 5000 g for 10 minutes and the bacteria pellet was collected.

## 2.5 Recombinant protein purification

The bacterial pellets obtained (section 2.4) contained expressed protein, which were subsequently lysed. Proteins were then purified using a combination of techniques.

### 2.5.1 Lysis of *E. coli*

For purification of all TRIB2 proteins, from pET30 plasmids, *E.coli* was lysed in ice cold Bicine pH 9.0 lysis buffer (20 mM Bicine pH 9.0, 300 mM NaCl, 0.1% Triton X-100, 10 mM imidazole, 1 mM DTT, 10% glycerol and a cOmplete protease inhibitor cocktail tablet (Roche)). For purification of all other proteins *E coli* was lysed in 20 mM Tris-HCl pH 7.4 (with all other buffer components the same). The cells suspended in the lysis buffer were then sonicated for 30 second intervals on ice at an amplitude of 16 microns using a 3 mm exponential microprobe attached to a MSE Soniprep 150 plus motor unit. After sonication, the samples were centrifuged at 4°C for 1 hour at 5525 x g to pellet cellular debris. The supernatant of the cell lysate contained the expressed protein, which was subsequently purified by immobilised metal affinity chromatography (IMAC) or glutathione-S-transferase (GST) pull down. TRIB2, TRIB1 and PKA proteins all possessed 6His-tags and were therefore amenable to purification by IMAC. C/EBPα on the other hand possessed a GST tag.

### 2.5.2 IMAC of recombinant His tagged proteins

After centrifugation to remove cellular debris the cleared lysate was filtered and then applied to a 5 mL Ni Sepharose His Trap HP column (GE Healthcare), which had previously been equilibrated in 5 column volumes of filtered, degassed wash buffer (20 mM Bicine pH9.0/ 20 mM Tris-HCl pH 7.4, 500 mM NaCl, 20 mM imidazole, 1mM DTT) The column was subsequently washed with 5 further column volumes of wash buffer followed by elution of theHis-tagged protein with 10 mL of elution buffer (20 mM Bicine pH9.0 / 20 mM Tris-HCl pH 7.4, 100 mM NaCl, 300 mM imidazole, 1 mM DTT and 10% glycerol). Throughout the elution process 500 µL fractions were collected. Samples of the flowthrough were also collected. All fractions were immediately transferred to ice and 5 µL samples taken, which were analysed by SDS-PAGE (see section 2.8).

### 2.5.3 Purification of full length GST-p42 C/EBPα

Following cell lysis, instead of employing IMAC, GST-His-C/EBPα was purified by GST pull down. Glutathione Sepharose beads were incubated with the cleared lysate for 2 hours at 4°C under gentle agitation. The beads, with bound GST-His-C/EBPα, were pelleted by centrifugation at 1000 **g** followed by resuspension in 30 column volumes of wash buffer (20 mM Tris pH 7.4, 100 mM NaCl, 1 mM DTT and 10% glycerol). This process was repeated 3 times. GST-C/EBPα was subsequently eluted from the beads with the addition of 10 mM reduced glutathione in 20 mM Tris pH 7.4, 100 mM NaCl, 1 mM DTT and 10% glycerol in 3 500 µL fractions, which were analysed by by SDS-PAGE.

### 2.5.4 Size exclusion chromatography

After IMAC or GST pull-down proteins were further purified by size exclusion chromatography in order to isolate monomeric proteins and exchange from the IMAC/GST elution buffer to a buffer suitable for biochemical analysis. A Superdex 200 16/600 column (GE Healthcare) set up with an Äkta FPLC system (GE Healthcare) and a Frac-920 (GE Healthcare) was equilibrated with 2 column volumes of buffer (20 mM bicine pH 9.0 / 20 mM Tris-HCl pH 7.4, 100 mM NaCl, 1 mM DTT, 10% glycerol).The protein applied to the column at a flow rate of 0.5 mL/min. 1.5 mL fractions were collected and the elution volume was used to estimate the molecular weight of the eluted proteins by comparing their elution volume with reference to Molecular Weight standards (Chapter 3). 5 µL samples of the fractions, deduced to contain protein from UV absorbance, were analysed by SDS-PAGE.

## 2.6 SDS-PAGE

SDS-PAGE was performed in order to visualise the purity and molecular weight of purified proteins. SDS-PAGE was also performed prior to electrophoretic transfer to nitrocellulose during immunoblot analysis (section 2.9). Proteins were denatured in 5x SDS sample buffer (0.25 M Tris-HCl pH 6.8, 0.25% bromophenol blue, 500 mM DTT, 5% SDS and 50% glycerol) to a final concentration of 1% SDS and heated to 90°C for 2 minutes before being subjected to electrophoresis. To detect proteins bellow 32 kDa 12% polyacrylamide gels were used. To detect proteins predicted to be between 32 and 80 kDa 10% polyacrylamide gels were used. To detect proteins above 80 kDa, such as ACC, 8% gels were employed. Polyacrylamide gels resolved proteins for ~1

hour minutes (depending on the percentage) with an electric field strength of 20 Vcm-1 in running buffer (25mM Tris-HCl, 190mM glycine and 0.1% SDS). Subsequently, the resolving gel, containing the proteins, was immersed and incubated in Coomassie stain (0.2% Brilliant blue R-250, 7.5% acetic acid, 50% methanol) for ~1 hour with agitation. The stained gel was then washed for 16 hours using destain buffer ($H_20$, methanol and acetic acid 50/40/10 v/v/v).

## 2.7 Bradford assay

Bovine serum albumin (2mg/mL) (Thermo Scientific) was employed to produce protein standards and diluted to concentrations ranging between 0.1 and 0.6 mg/mL and used to generate a standard curve in a quantification assay. 200 µL of Coomassie Plus Protein Assay Reagent (Thermo Scientific), was mixed with 5 µL of sample. The absorbance at 595 nm was detected in a spectrophotometer in a 96-well plate. The absorbance of BSA standards were measured relative to a blank (BSA and buffer) and a standard curve was plotted (Figure 2.1) to allow estimation of protein concentration for unknown samples.

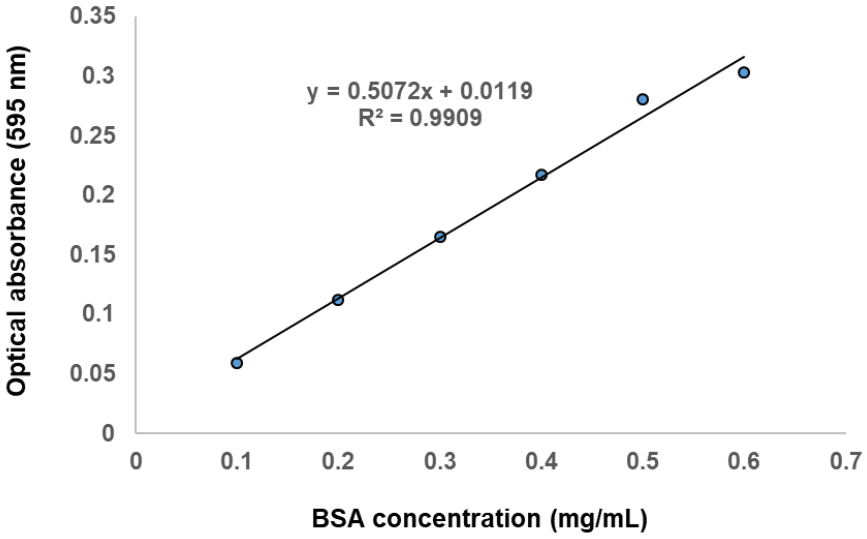


**Figure 2.1 Bradford Assay Standard Curve for determination of protein concentration.** Increasing concentrations of BSA were incubated with the Coomassie based reagent before reading the optical absorbance at 595 nm in a spectrophotometer. A standard curve was plotted in Excel.

## 2.8 Immunoblotting

The protein content of samples was quantified by Bradford assay prior to the addition of sample buffer and boiling. Samples were subjected to electrophoriesis by SDS-PAGE. The proteins within the resolving gel were then blotted onto a nitrocellulose membrane by electrophoretic transfer. To this end, the resolving gel and nitrocellulose membrane were sandwiched together with blotting pads within a cassette and placed into a tank containing chilled transfer buffer (25mM Tris, 190mM glycine, 0.1% SDS, 20% methanol). For transference the current was set to 0.28 amps. The membranes with bound proteins were incubated in 5% non-fat milk (Marvel) in Tris-buffered saline and 0.1% Tween 20 (TBS-T) for 30 minutes with agitation on a seesaw rocker. Subsequently the blocked membranes were incubated for 12 hours at 4°C with primary antibody at indicated dilutions in 5% non-fat milk in TBS-T on a rocker. The membranes were washed for 5 minutes 3 times in TBS-T and the secondary antibody, also diluted to a specific concentration in 5% non-fat milk TBS-T, was incubated with the membrane for a further 1 hour at room temperature. The membranes were again washed for 5 minutes 3 times in TBS-T before being placed into a developing cassette. ECL or ECL select (GE Healthcare) developing agent was added to the membranes in accordance with the manufacturer's protocol and films were exposed and developed for the indicated time periods. Immunoblots were quantified using ImageJ software.

## 2.9 Buffer exchange of recombinant proteins

Proteins were first concentrated to 2 mg/mL by centrifugation using a Vivaspin 2 (10 kDa molecular weight cut off) concentrator column (GE Healthcare). A HiTrap 5 mL desalting column (GE Healthcare) was then equilibrated with 5 column volumes of the indicated buffer and 2 mL of concentrated protein was loaded by means of a syringe. Subsequenty, buffer was passed through the column, employing an Äkta system and 500 µL fractions were collected. The fractions that corresponded to the peak on the elution profile (monitored by the absorbance at 280nm) were assessed by Bradford assay and those with sufficient amounts of protein (>0.2 mg/mL) were pooled. The proteins were then analysed by SDS-PAGE prior to biochemical assays.

## 2.10 TRIB2-C/EBPα interaction 'pull down' assays

A total of 20 µL of GST beads were equilibrated in 20 mM Tris-HCl pH 7.4, 100 mM NaCl and 1 mM DTT. Subsequently 10 µL of the beads were incubated with 10 µg of

GST-His-tagged C/EBPα, the other 10 µL of beads with 10 µg of recombinant GST and incubated at 4°C for 2 hours while mixing on a carousel. The GST beads that had been incubated with C/EBPα were washed 3 times with wash buffer (20 mM Tris-HCl pH 7.4 and 100 mM NaCl), to remove unbound protein, before being aliquoted into 2 separate ependorf tubes, each containing 5 µg of TRIB2 with a total reaction volume of 25 µL. The 10 µL of GST beads that had not been pre-incubated with recombinant GST were similarly divided into 2 eppendorf tubes, each containing 5 µg of TRIB2, with a total reaction volume equalling 25 µL. These mixtures were then incubated at 4°C for 2 hours under agitation on a carousel. Each reaction mixture was centrifuged for 1 minute at 1000 x **g** in order to separate out the GST beads. The supernatant was discarded and the beads were washed 3 times by re-suspension and centrifugation in wash buffer. After washing, 20 µL of elution buffer (20 mM Tris pH 7.4, 100 mM NaCl, 10 mM reduced glutathione and 1 mM DTT) was added to each reaction and mixed before being centrifuged once more at 1000 x **g**, after which the supernatants were collected and added to 5 x sample buffer prior to 5 minutes of boiling. Samples were electrophoresed by SDS-PAGE and then analysed by western blotting with an α-6His antibody conjugated to HRP, with chemiluminescence detected after the application of ECL reagent.

### 2.11 Differential scanning fluorimetry PKIS screening and analysis of compound binding

DSF experiments were performed using an Applied Biosystems StepOnePlus Real-Time PCR instrument using a standard DSF procedure previously developed and validated for the analysis of kinases [46, 48] and pseudokinases [47]. In order to generate a thermal melting profiles and assess the melting temperature of proteins (including WT TRIB2, all TRIB2 mutants and PKA), buffer exchanged proteins (in Tris-HCl pH 7.4, 100 mM NaCl, 1 mM DTT and 10% glycerol) were mixed with buffer (Tris-HCl pH 7.4, 100 mM NaCl, 1 mM DTT and 10% glycerol) and SYPRO Orange dye (Inivtrogen), which was used as the fluorescence probe. In each reaction the final volume was 25 µL, the concentration of protein was 5 µM, the dilution factor of SYPRO Orange dye was 1:5000. The 25 µL reaction mixtures were dispensed into individual wells of a MicroAmp Fast Optical 96-well reaction plate (Applied Biosystems). For every assay at least 2 reaction mixtures were made for each condition and the average $T_m$ taken. Mean $T_m$ values were derived from three independent assays. The plates

were sealed with optical adhesive covers and the reaction mixtures were vortexed. Subsequently the plate was centrifuged for 10 seconds at 500 x **g**. The plate was placed into a real time PCR machine (Applied Biosystems StepOne Plus). The machine was set to measure florescence emitted from the sample as the temperature was increased (at a rate of 0.3°C/minute) starting from 25°C and ending at 95°C. Fluorescence readings were made at 530 nm. Each assay was performed in triplicate unless stated otherwise. The data was collected by the StepOne Software v2.1 and using a combination of Microsoft Excel and GraphPad Prism 6, the detected fluorescence readings for each temperature increment were averaged and thermal denaturation curves generated. The thermal profiles were normalised so that the lowest value was assigned as 0% and the largest fluorescence reading as 100%. Only the melting curve generated by the protein was analysed; temperatures before and after the melting profile were disregarded. Linear regression analysis was employed by means of fitting the Boltzman sigmoidal equation to the melting curves, which allowed the $T_m$ to be deduced. The $T_m$ value determined, being the temperature at which 50% of the protein had become denatured.

In order to analyse the effects of ATP, EDTA and divalent cations on TRIB2, TRIB2 mutants and PKA stability, the DSF assay was employed to deduce the change in $T_m$ values between a buffer control and reaction mixture containing ATP/EDTA/divalent cations; this temperature change was referred to as the $\Delta T_m$. The reaction mixtures were at a final volume of 25 µL, comprising 5 µM of protein, 1:5000 Sypro Orange dye and the additions of ATP (10 mM) EDTA (1 mM) and/or $MgCl_2$ (1 mM). The 25 µL reaction mixtures were dispensed into individual wells of a MicroAmp Fast Optical 96-well reaction plate and the experiment was conducted as described above.

For initial screening, 20 µM of compounds were pre-incubated with 5 µM TRIB2 for 10 minutes and then subjected to DSF analysis, which was initiated by the addition of fluorescent SYPRO Orange. The final concentration of DMSO was 2% (v/v) in all conditions. For dose-dependent thermal-shift assays a compound range was prepared by serial dilution in DMSO, and added directly into the assay to the appropriate final concentration. All control experiments contained 2% (v/v) DMSO, which had essentially no effect on TRIB2 stability.

## 2.12 *In vitro* $^{32}$P kinase assays

Each reaction contained a final concentration of 5 µM of bacterially expressed His-tagged TRIB2 in 20 mM bicine pH 9.0, 100 mM NaCl, 1 mM DTT, 10% glycerol, which was incubated with 1 mM ATP (2.2 µCi $\gamma^{32}$P ATP) and either 10 mM of $MgCl_2$ or 1 mM EDTA in a total volume of 40 µL. Each condition was performed in duplicate.

The ATP was added prior to the start of the assays which were staggered to allow for termination at the stipulated time points. The assays were performed at 30°C whilst on a temperature-controlled Eppendorf shaking platform. The reactions were terminated by the addition of 5x SDS loading buffer and heated at 95°C for 5 minutes. 30 µL of sample of each terminated assay was loaded into 10% SDS PAGE gel and the resolved for 60 minutes at 20 $Vcm^{-1}$. TRIB2 was subsequently transferred to nitrocellulose membranes for western blotting and autoradiography analysis. The membranes were placed into a cassette that contained a reflector screen and an X-ray film was placed on top for analysis by autoradiography. The cassette was placed in a -80°C freezer and left for seven days. The films were then developed and fixed following standard procedures.

## 2.13 Microscale thermophoresis

A Monolith NT.115 instrument (NanoTemper Technologies GmbH) was employed for MST analysis. His-TRIB2 was firstly labelled with a NanoTemper labelling kit; the fluorescent red dye NT-647 was coupled via N-Hydroxysuccinimide NHS chemistry to the N-terminal His-tag, placing the fluorophore away from the pseudokinase domain. The labelled TRIB2 was diluted to 5 µM with 20 mM Bicine pH 9.0, 100 mM NaCl, 5% glycerol, 0.05% Tween-20 and 2 % (v/v) DMSO. The concentration of TRIB2 was kept constant in the assay, while the concetrations of compounds (afatinib and TAK-285) were titrated between 1 nM and 50 µM. Near-saturation of binding was achieved, allowing for an affinity to be estimated for the reversible interactions of afatinib and TAK-285 with the fluorescent labelled His-TRIB2.

## 2.14 Mass spectrometry

Intact mass spectrometry was first used to evaluate the interaction between afatinib and TRIB2. Recombinant His-TRIB2 was incubated with afatinib in a 1:10 molar ratio for 15 minutes at 20°C, followed by desalting using a C4 desalting trap (Waters

MassPREP™ Micro desalting column, 2.1 × 5 mm, 20 μ m particle size, 1000 Å pore size). TRIB2 was eluted with 50 % (v/v) MeCN, 0.1 % (v/v) formic acid. Intact TRIB2 mass analysis was performed using a Waters nano ACQUITY Ultra Performance liquid chromatography (UPLC) system coupled to a Waters SYNAPT G2. Samples were eluted from a C4 trap column at a flow rate of 10 µL/min using three repeated 0-100 % acetonitrile gradients. Data were collected between 400 and 3500 m/z and processed using MaxEnt1 (maximum entropy software, Waters Corporation).

In order to evaluate covalent binding of afatinib and neratinib to recombinant TRIB2 in vitro, MS2 analysis was employed. 50 µM of compounds were separately incubated with 5 µM of purified His-TRIB2 for 15 minutes at 20°C. The samples were then denatured denatured with 0.05 % (w/v) RapiGest SF (Waters, UK) and digested with chymotrypsin (1:20 protease:protein (w/w) ratio) for 16 h at 25 °C. The addition of triflouroacetic acid (TFA) up to 1 % (v/v) was employed to induce RapiGest hydrolysis, by incubation for 1 hour at 37 °C. Insoluble protein was cleared from the sample by centrifugation at 13, 000 x **g** for 20 minutes. The samples were then resolved using an UltiMate 3000 nano reversed-phase HPLC separation system (Dionex) coupled in-line with a Thermo Orbitrap Fusion Tribrid mass spectrometer (Thermo Scientific, Bremen, Germany). 500 fmol digested peptides were loaded onto the trapping column (PepMap100, C18, 300 µm × 5 mm), using partial loop injection, for 7 min at a flow rate of 9 µL/min with 2% (v/v) MeCN, 0.1% (v/v) TFA and then resolved on an analytical column (Easy-Spray C18 75 µm × 500 mm, 2 µm bead diameter column) using a gradient of 96.2% A (0.1% (v/v) formic acid (FA)): 3.8% B (80% (v/v) MeCN, 0.1% (v/v) FA) to 50% B over 35 min at a flow rate of 300 nL/min. MS1 spectra were acquired over m/z 400 – 1500 in the orbitrap (60 K resolution at 200 m/z). Data-dependent MS2 analysis was performed using a top speed approach (cycle time of 3 s), using higher-energy collisional dissociation (HCD) and electron-transfer and higher-energy collision dissociation (EThcD) for fragmentation, with product ions being detected in the ion trap (rapid mode). Data were processed using Thermo Proteome Discoverer (v. 1.4) and spectra were searched in MASCOT against the E. coli IPI database with the added sequence of full-length 6His-TRIB2 (1-343). Parameters were set as follows: MS1 tolerance of 10 ppm, MS/MS mass tolerance of 0.6 Da, oxidation of methionine and afatanib binding at cysteine as variable modifications. MS2 spectra were interrogated manually by Samantha Ferries.

## 2.15 Molecular modelling and docking studies

By using the TRIB1 crystal structure as a template (5CEM), SWISS-MODEL was used to generate a structural model of TRIB2 (UniProt ID: Q92519) containing the C-terminal tail (residues 42-343), which was visulised in PyMOL. For molecular docking studies the modeled TRIB2 structure was energy minimized using the Rosetta Relax protocol [233] and the model with the lowest energy score from 100 potential solutions was used for docking. Subsequently, the chemical structures of afatinib (CID 10184653) and neratinib (CID 9915743) were downloaded from PubChem and both compounds were docked using the PyMOL plug in AutoDock Vina [234] with an exhaustiveness of 1000, rigid body, and a full protein search space. A binding pocket formed between P-loop, αC-helix and the activation loop was the most frequently sampled site during blind docking. Compounds were docked to this putative docking site using the flexible side-chain covalent docking method implemented in Autodock [235]. The enamide group of each compound was covalently linked to the sulfhydryl group of Cys 96 and the rest of the compound was treated as a rigid side-chain to explore favourable binding poses, the vast majority of which converged on the same binding pocket. Each run generated 500 binding poses, which were visualized using PyMOL.

## 2.16 Maintenance of human cell lines

Adherent parental Flp-In T-REx-HeLa and parental Flp-In T-REx-HEK293 cells (Invitrogen) were cultured in Dulbecco's Modified Eagle medium (DMEM) supplemented with (filter sterilised) 4 mM L-glutamine, 10 % (v/v) Foetal Bovine Serum (FBS), Penicillin and Streptomycin (Gibco). Pre-transfection (parental) HeLa Flp-In T-REx cells were maintained in 4 µg/mL of Blasticidin (Melford), Zeocin 50 µg/mL (Invitrogen). HEK293 Flp-In T-REx cells were, however, cultured in 15 µg/mL Blasticidin and 100 µg/mL Zeocin. The cells were cultured at 37°C in a 5% CO2 atmosphere and were passaged approximately every 3 days in a lamina flow hood after trypsinising in trypsin/EDTA (Versene) (Gibco). Subsequent to transfection with pcDNA5/FRT/TO and pOG44 plasmids, to generate stable cell lines (section 2.19), Flp-In T-REx HeLa cells were maintained in 4 µg/mL of Blasticidin and 200 µg/mL Hygromycin B. Flp-In T-REx HEK293 cells were cultured in 15 µg/mL of Blasticidin and 150 µg/mL Hygromycin B at 37°C in a 5% CO2 atmosphere.

The U937 suspension cells were cultured in RPMI supplemented with 4 mM L-glutamine, 10 % (v/v) Foetal Bovine Serum (FBS), Penicillin and Streptomycin. Cells were maintained at 37°C and 5% $CO_2$. The cells were passaged when the concentration reached ~ 0.8 x$10^6$ cells/mL.

### 2.16.1 Generation of 'freeze down' mammalian cell stocks

For adherent cells, each cell line was grown in 6 separate 10 cm dishes to 90% confluence. Suspension cells were grown in 6 separate T-75 cell culture flasks with a volume of 20 mL of 90% confluent cells in each flask. Cells were harvested by trypsin/EDTA (Versine) treatment, washed in PBS and centrifuged for 5 minutes at 250 **g** and the cells were re-suspended in 6 mL of fully supplemented DMEM with 10% DMSO. Cells were aliquoted at a volume of 1 mL into sterile cryogenic storage vials and transferred to an isopropanol controlled rate freezing chamber (Mr. Frosty, Sigma-Aldrich) for 24 hours, before being moved to a -80°C freezer for storage.

## 2.17 Generation of stable tetracycline (TET) inducible HeLa and HEK293 cells

The Tetracycline repressor protein (TetR), from the *E. coli* tetracycline (TET) resistance operon, has been exploited in Flp-In T-REx to generate a regulatory system to express cDNA in mammalian cells. Before transfection, Zeocin selects for the pFRT/lacZeo vector that contains an integrated FRT (Flp recombination Target) site. Following cotransfection of a Flp recombinase (pOG44) and pcDNA5/FRT/TO vector containing the cDNA of interest, the pOG44 expresses the Flp Recombinase and homologously recombines the FRT sites in pFRT/lacZeo and pcDNA5/FRT/TO. Integration of cDNA to the FRT site causes a frame shift, whereby the cells no longer express the Zeocin resistance gene, but become resistant to Hygromycin B thanks to the resistance gene incorporated in pcDNA5/FRT/TO. The pcDNA6/TR, which encodes the Tet repressor gene, is selected for and maintained by the constant presence of Blasticidin. Therefore, after transfection, the TetR blocks initiation of transcription by binding to the Tet-operator (TO) in the promoter. However in the presence of TET, TetR binds to TET and dissociates from the TO, thereby allowing transcription to be initiated.

The human TRIB2 genes 1-343, 54-343, AQLAA, C96S and C96/104S, which had been previously cloned into pET30 were cloned by PCR. For cloning, the forward primers incorporated a BamHI restriction site (GGATCC) with 5' overhang (GCC)

followed by the sequence CCACCATGG, containing a start codon and then the first 20 bp of specified TRIB2 cDNA. Therefore, the forward primers were designed as follows GCC[GGATCC]CCACCATGG*TRIB2cDNA*. In the reverse primer, 5' overhang followed by a NotI (GCGGCCGC) recognition sequence were 3' to the insert. This was followed by the sequence TTATTATTATCA (containing a TCA stop codon), a sequence encoding the reverse complement of FLAG peptide (CTTGTCATCGTCGTCCTTGTAGTC) and finally reverse complement encoding the C-terminus of specified TRIB2 cDNA. Thus, the primers were designed as follows: GCC[GCGGCCGC]TTATTATTATCACTTGTCATCGTCGTCCTTGTAGTC*TRIB2*
After PCR, the TRIB2 inserts were resolved on agarose gel, purified and quantified by UV absorbance reading at 260 nm using a NanoDrop. TRIB2 inserts were BamHI and NotI digested and mixed with BamHI and NotI treated pcDNA5/FRT/TO vector, at a ratio of insert to vector 5:1. Ligation was initiated by the addition of 400U T4 DNA ligase (New England Biolabs). In order to confirm successful ligation, the products were treated with 10U BamHI and analysed by agarose gel electrophoresis. By analysis of the differences in migrated distance during electrophoresis it was possible to predict whether the ligation had occurred. Plasmids were Sanger Sequenced (GATC) and thentransformed into TOP10 E. coli for amplification and then purification (section 2.2.2).

HeLa or HEK Flp-In T-REx parental cells were cultured to 80-90% confluency in a 6-well plate. 1 µg pcDNA5/FRT/TOTRIB2 and 9 µg pOG44 were incubated in 250 µL of serum free media for 5 minutes at ambient temperature. 10 µL of lipofectamine 2000 was simultaneously incubated in 240 µL of serum free media for 5 minutes at ambient temperature. The DNA and lipofectaine aliquots were mixed together and incubated for 30 minutes at ambient temperature before being added to HeLa or HEK Flp-In T-REx parental cells (that had been washed in PBS and media replaced with fully supplemented DMEM). The cells were incubated for 24 hours at 37°C, 5% CO2. Fully supplemented DMEM was then replaced onto the cells without selection markers for a further 24 hours, at which point the appropriate concentrations of Blasticidin and Hygromycin were added to select for cells that had successfully integrated the specified TRIB2 transgene. Tetracycline (TET) (sterile-filtered stock solution was 1mg/ml in 70% EtOH) was added at a final concentration of 1 µg/ml to induce the expression of the recombinant protein in the stably transfected cells, and this was

confirmed by immunoblotting with an α-FLAG antibody. Cells were grown and 'freeze down' stocks were generated and stored at -80°C.

### 2.18 Transient transfections

For transient transfections, 40 µg pcDNA5/FRT/TO plasmid, encoding WT TRIB2 or indicated TRIB2 mutants, was incubated in 500 µL of serum free media containing 50 µL of lipofectamine 2000 (Invitrogen) for 30 minutes at ambient temperature. The DNA lipofectamine mixture was then added to a 10 cm dish of HeLa cells (~60% confluent) for 24 hours. The cells were then washed with PBS and fresh media containing 1 µg/mL was added. Cells were incubated for a further 16 hours before the addition of DMSO (0.1% v/v) or compounds for a further 4 hours prior to lysis and immunoblot analysis.

### 2.19 Incubation of compounds with human cells

Adherent HeLa cells were seeded at 2.2 x $10^6$ cells per 10 cm dish in 10 mL of fully supplemented DMEM cell culture media. After 24 hours, ± 1 µg/mL (from a 1 mg/mL stock) of Tet was added directly to media and the cells were incubated for a further 16 hours, at which point indicated compounds of specified concretions were added to cells. The DMSO concentration between treated and non-treated cells was kept constant at 0.1% (v/v).

U937 cells were incubated in fully supplemented RPMI media at a density of 0.2 x $10^6$ cells/mL for 24 hours. Cells were then incubated with specified compounds and the indicated concentrations for the indicated time period. The DMSO concentration between treated and non-treated cells was kept constant at 0.1% (v/v).

### 2.20 Human cell lysis

For adherent HeLa cells seeded into 10 cm dishes, the medium (with floating cells) was transferred to a 15 mL falcon tube. Subsequently, 10 mL of warm PBS was used to wash the cells. Once the PBS was removed, 1 mL of warm trypsin was added to the cells, which were incubated at 37 °C for 1 minute. The detached cells were re-suspended in the 10 mL of DMEM that was taken from the cells in the first step. Cells suspended in medium in 15 mL falcon tubes were centrifuged at 250 **g** for 5 minutes. The pelleted cells were re-suspended in PBS and centrifuged once again at 250 **g** for 5 minutes. This time, after removal of the PBS, 100 µL of RIPA lysis buffer (50 mM

Tris–HCl pH 7.4, 1 % (v/v) NP-40, 1 % (v/v) SDS, 100 mM NaCl, 100 nM Okadaic acid and a protease inhibitor tablet (Roche)) was added to the cellular pellet. The cells in lysis buffer were sonicated on ice for 3 seconds at an amplitude of 9. This process was repeated 3 times with brief cooling on ice in between each sonication. Following this, the lysate was centrifuged at 16,000 **g** for 20 minutes at 4°C. In order to quantify the protein concentrations, a sample of lysate was dilutes 1:20 with 20 mM Tris-HCl pH 7.4, 100 mM NaCl buffer prior to Bradford assay analysis.

U937 cells were grown 20 mL of RPMI in T-75 flasks (Corning). To collect the cells, the contents of the flask were centrifuged, in a 50 mL falcon tube, at 250 **g** for 5 minutes. The medium was removed and PBS was used to re-suspend the cells. The cells were centrifuged once again at 250 **g** for 5 minutes, prior to the removal of PBS and addition of 100 µL RIPA lysis buffer. From this point, the cells were subsequently lysed using the same protocol as HeLa cell lysis.

### 2.21 Serum block and release procedure

Stable HeLa cells were seeded with 2.2 x $10^6$ cells in 10 cm dishes for 24 hours (until ~60% confluent) in fully supplemented DMEM medium (with 10% FBS). Subsequently the cells were washed with 10 mL of PBS, and replaced with serum-free DMEM for 16 hours. The cells were again washed with 10 mL of PBS, which was replaced with fully supplemented DMEM (with 10% FBS) ± 1 µg/mL Tet for 16 hours, followed by addition of indicated inhibitor for a further 4 hours. Cells were then lysed, and whole cell extracts generated with modified RIPA buffer, followed by immunoblot analysis.

### 2.22 Immunoprecipitations

To set up immunoprecipitation experiments, 10 cm dishes were seeded with 2.2 x $10^6$ stable Hela Flp-In T-Rex cells for 24 hours. Half of the plates were then treated with 1 µg/mL of Tet to induce FLAG-TRIB2 expression, for 16 hours. Cells were then harvested by trypsinisation as previously described (section 2.20) except lysed in 500 µL of a modified 0.1% SDS and 0.1% NP-40 RIPA buffer (50 mM Tris–HCl pH 7.4, 0.1 % (v/v) NP-40, 0.1 % (v/v) SDS, 100 mM NaCl, 100 nM Okadaic acid and a protease inhibitor tablet (Roche)). The cleared lysates were incubated with 50 µL of FLAG M2 conjugated agarose beads (Sigma-Aldrich), which had been equilibrated in lysis buffer. The lysate and agarose bead mixture was aliquoted into 1.5 mL ependorf tubes and placed in a rotating carousel, for gentle agitation, in a 4 °C cold room for 2 hours.

The beads were then pelleted by centrifugation for 1 minute at 1000 g and washed 3 times with wash buffer (20 mM Tris-HCl pH 7.4 and 100 mM NaCl). Subsequently, 10 µL of 5 mg/mL 3xFLAG peptide (Sigma-Aldrich) was diluted in 150 µL of wash buffer, which was then added to the pelleted FLAG beads to elute the FLAG-TRIB2. The mixture was incubated on ice for 30 minutes with regular agitation. Both +/- Tet immunoprecipitations were then centrifuged and the eluate separated from the beads.

### 2.23 Cellular thermal shift assay (CETSA)

Whole cell CETSAs were performed according to a previously established protocol [236]. 2.2 x $10^6$ of Stable HeLa cells were seeded into 10 cm dishes (Corning) and incubated for 24 hours before being induced to express FLAG-TRIB2 by the addition of 10 µg/mL of Tet for 16 hours, at which point the cells were ~90% confluent. Subsequently, the Tet induced cells were incubated with either DMSO (0.1% v/v) or 100 µM of the specified compound for 1 hour. The intact cells were washed with 10 mL of PBS. Incubation with 1 mL of trypsin for 1 minute was used to detach adherent HeLa cells, which were then re-suspended in full supplemented DMEM medium, centrifuged at 250 **g** for 5 minutes and re-suspended in 5 mL of PBS (per plate). Cells suspended in PBS were then aliquoted into PCR tubes at a volume of 50 µL prior to heating at the indicated temperature in a PCR thermal cycler for 3 minutes. After heating the cells were immediately placed on ice for 2 minutes and then lysed by 3 short bursts of 3 second sonication at an amplitude of 9. The lysate was cleared by centrifugation at 16,000 x g for 20 minutes at 4°C and immediately added to 5 x sample buffer. The soluble lysate was analysed for the presence of FLAG-TRIB2 and α-tubulin by immunoblotting.

### 2.24 Lambda phosphatase (λPP assays)

Lambda phosphatase assays (λPP) were performed on whole cell HeLa lysates and on FLAG-peptide elutions from immunoprecipitation experiments. Purified, recombinant λ-phosphatase was provided by Dr Dominic Byrne (University of Liverpool). 40 µg of cellular extracts were incubated with 10 ng of λ-phosphatase at 37°C for 1 hour before being added to 5 x SDS sample buffer followed by immunoblot analysis.

## 2.25 Tryan blue cell viability assays

In order to test the effects of compounds on cell membrane integrity by means of deducing cellular viability a Trypan blue assay was employed. U937 cells were seeded in a 96 well plate at a concentration of 0.2 x 106 cells/mL 18 hours prior to compound addition. Various small molecule inhibitors were added (in triplicate) to a final concentrations ranging between 0.5 and 20 μM. After either 4 or 24 hours incubation cell samples were taken and diluted in 0.4% Trypan Blue dye solution at a 1:1 ratio. Non-viable cells were stained blue, with viable cells were unstained. These cell suspensions were incubated in a hemocytometer for 2 minutes at ambient temperature. The haemocytometer was then placed in a Countess automated cell counter, which was used to calculate the percentage of viable cells in the sample.

## 2.26 MTT cell cytotoxicity assays

To assess the cytotoxicity of kinase inhibitors in U937 cells, MTT assays were employed. U937 cells were seeded in a 96 well plate at a concentration of 0.2 x $10^6$ cells/mL, 18 hours prior to compound addition, which was performed in triplicate, with all experiments including a final concentration of 0.1% DMSO (v/v). Compounds were added to final concentrations between 10 nM and 20 μM. To quantify U937 cell viability, mitochondrial metabolic activity was assessed 72 hours subsequent to compound addition. Thiazolyl blue tetrazolium bromide was dissolved in PBS and added to cells at a final concentration of 0.25 mg/mL and incubated at 37 °C for 3 hours. In healthy mitochondria, this presence of NADH reduces the thiazolyl blue tetrazolium bromide resulting in the formation of insoluble formazan crystals. The reaction was stopped and crystals dissolved by the addition of 50 μL of acidified 10% SDS, followed by reading of absorbance at 570 nm. Viability was defined relative to DMSO-containing controls incubated for the same period of time.

# Chapter 3: Biochemical analysis and discovery of novel TRIB2 small molecule kinase inhibitors

## Introduction

Tribbles pseudokinases modulate many physiological signalling pathways and are potential therapeutic targets, due to overexpression and mutation, which implicates them in the aetiology of several human cancers, including leukeamias, melanoma, lung and liver cancer [109, 122, 237-239]. A recently reported crystal structure of TRIB1 shows a bilobal pseudokinase domain that cannot bind to ATP [106]. However, it was suggested that upon binding of the substrate C/EBPα the α-helix and 'SLE' motif (which replaces the normal DFG motif) undergo conformational rearrangement from an 'out' inactive-like to an 'SLE-in' active-like conformation [105]. In the absence of substrate, rearrangement into a 'SLE-in' position is sterically prevented by Tyr134 from the highly unusual TRIB1 αC-helix. The equivalent residue in TRIB2 is Cys104, which might therefore contribute to a different degree of freedom for conformational rearrangement. In support of this hypothesis, TRIB2 demonstrates a vestigial affinity for ATP and autophosphorylates very weakly *in vitro* in the absence of magnesium ions [60]. In addition, TRIB2 was shown to possess the ability to bind to 'bulky' ATP analogues upon mutation of the gatekeeper residue (Phe 190) to a small Gly or Ala side-chain [60]. These findings support the hypothesis that TRIB2 is 'druggable' with small molecules, which is one of the subjects of this chapter.

It is estimated that some 40% of pseudokinases retain the ability to interact with adenine-based nucleotides; these proteins are therefore likely to be targeted by ATP-competitive inhibitors [58, 240]. Capitalising on decades of intensive research, which has led to FDA approval of 43 kinase inhibitors to treat cancer and inflammatory diseases [241], it may therefore be possible to repurpose biologically active ligands to target pseudokinases in therapeutic settings [207].

Like TRIB2, the pseudokinase MLKL was shown to bind to ATP (though MLKL binding was much more robust) in the absence of divalent cations [58, 65]. Hilderbrand *et al* (2014) screened the protein kinase inhibitor set 1 (PKIS1) [242], using a recombinant mouse MLKL pseudokinase domain and a thermal shift assay (TSA) [217]. PKIS1 is

a validated library of 367 ATP-competitive kinase inhibitors, covering ~30 chemotypes that were originally developed to target 24 distinct protein kinases. From this screen, an inhibitor was discovered to bind to the MLKL pseudokinase domain and prevent its translocation to membranes, which in turn prevented necroptosis in an MDF cell model [217].

I hypothesised that by screening recombinant TRIB2 using PKIS1 and differential scanning fluorimetry (DSF), that ligands with the ability to modulate the thermal stability of recombinant TRIB2 *in vitro* could be discovered [242]. A counter-screen of potential TRIB2 ligands employed a K90M ATP binding-deficient TRIB2 mutant [60], the canonical active Ser/Thr kinase PKA and the closely related homologue TRIB1. Experiments were performed to evaluate selectivity and to try to support the use of small molecule inhibitors as potential chemical probes of TRIB2 cellular function.

Biochemical and crystallographic analysis suggests that adaptions in the pseudokinase fold of TRIB1, including the αC-helix, interact *in cis* with the C-terminal tail region that contains the conserved E3 ubiquitin ligase binding motif (nominally DQLVP) [106]. This interaction was proposed to stabilise TRIB1 *in vitro* and TSAs revealed that deletion of the C-terminal domain reduced TRIB1 thermal stability. I hypothesised that a similar mechanism also occurs in TRIB2. To this end a series of truncation mutants and a triple point mutant (DQLVP to AQLAA) were investigated to test the consequences on TRIB2 stability and relevance for compound binding.

Finally, I hypothesised that synthetic stapled TRIB2 C-terminal tail peptides, containing the COP1 and TRIB pseudokinase domain-binding DQLVP motif, might compete with the TRIB2 C-terminal tail for binding to the pseudokinase domain *in vitro*. Short peptide sequences are becoming of interest to target both protein-protein interactions and surfaces that are too large to be appropriately targeted by small molecule inhibitors [243]. The objectives of the work described in this chapter were:

1. Evaluate whether the TRIB2 C-terminal tail interacts with the pseudokinase domain.
2. Discover whether small molecule kinase inhibitors or other ligands interact with TRIB2.

3. Establish that the interaction between the TRIB2 C-terminal tail and pseudokinase domain can be targeted with small molecule inhibitors and stapled peptides.
4. Evaluate the molecular mechanism of small molecule interaction.

# RESULTS

## 3.1 Purification of stable His-tagged TRIB2

The purification of recombinant His-tagged TRIB2 has previously been optimised by Bailey and colleagues [60], where TRIB2 was purified sequentially by immobilised metal affinity chromatography (IMAC) and size exclusion chromatography (SEC) in 20 mM Bicine pH 9.0, 100 mM NaCl, 1 mM DTT and 10% (v/v) glycerol. This buffer was important to maintain protein stability during purification [60]. Here, full length (1-343) human TRIB2 (Figure 3.1A, top) with an N-terminal 6x His tag was expressed in BL21(DE3)pLysS *E. coli.* After centrifugation and cell lysis, IMAC was used to purify His-TRIB2 to near homogeneity (Figure 3.1A, bottom). After elution with 300 mM imidazole, the majority of His-TRIB2 eluted in the $2^{nd}$ to $5^{th}$ 0.5 mL fractions (Figure 3.1A). Molecular weight markers were resolved on an S200 gel filtration column to generate a standard curve (Figure 3.1B), in order to predict the relative molecular mass (M*r*) of TRIB2, calculated from the elution volume. Fractions from IMAC purifications containing the highest abundance of TRIB2 were pooled and analysed by SEC for the purpose of separation from high and low molecular mass impurities, prediction of M*r* and to permit buffer exchange into 20 mM Tris pH 7.4, 100 mM NaCl, 1 mM DTT and 10% (v/v) glycerol (Figure 3.1C) for DSF analysis. Subsequent to protein injection a peak appears at 20 mL, corresponding to the void volume where His-TRIB2 has presumably aggregated or multimerized. Following SEC analysis fractions corresponding to monodispersed His-TRIB2, eluting between 45 and 63 mL were analysed by SDS-PAGE (Figure 3.1D). At the elution volume 53.5 mL the calculated *Mr* of His-TRIB2 was 43.5 kDa, which is close to the theoretical molecular weight of 43.6 kDa. The average yield of protein was 2 mg of TRIB2 per litre of bacterial culture, calculated by Bradford assay. Purified protein was aliquoted into 1.5 mL ependorf tubes, snap frozen in liquid nitrogen and stored at -80˚C prior to analysis.

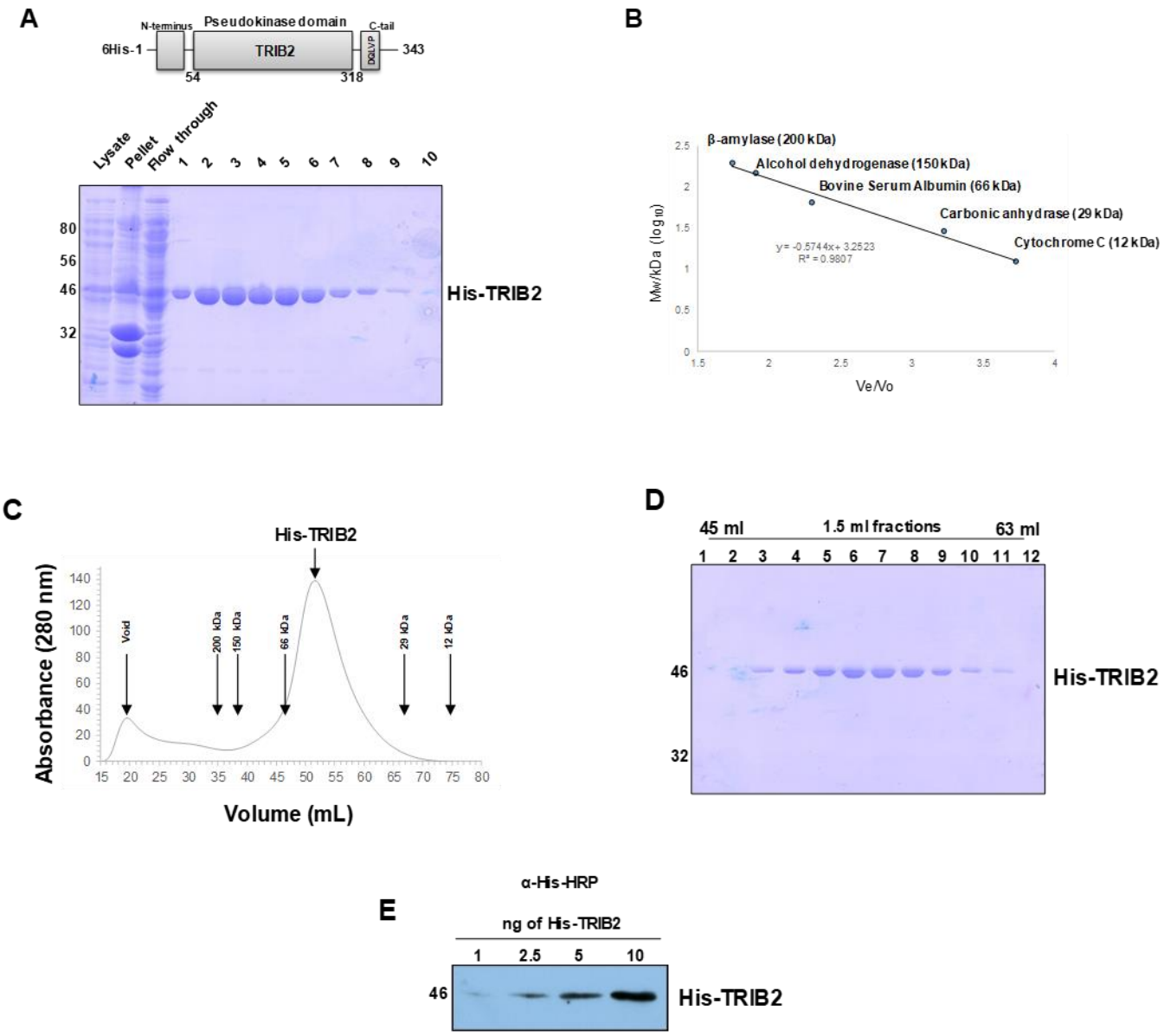


**Figure 3.1: Purification of His-tagged TRIB2 from BL21(DE3)pLysS.** Chemically competent *E. coli* transformed with pET30 encoding full length His-tagged WT TRIB2 were induced with IPTG for 16 hours at 18°C. Subsequent to lysis, (A) His-tagged TRIB2 from cleared bacterial lysate was bound to a Nickel column by IMAC and eluted with 300 mM imidazole. Fractions were collected at a volume of 0.5 ml. 5 µl of sample was boiled with 2 x SDS sample buffer and subjected to electrophoriesis on a 10% SDS poly acrylamide gel. Additionally a 5 µl sample of the cleared bacterial lysate, the cell pellet and the lysate collected post IMAC (flow through) were analysed alongside. The gel was stained with coomassie blue with His-TRIB2 visible at ~45 kDa. (B) Molecular weight standards of β-amylase, alcohol dehydrogenase, albumin from bovine serum, carbonic anhydrase and cytochrome C were resolved on an S200 column in order to obtain a standard comparison to purified proteins. (C) His-tagged TRIB2 was further purified by size exclusion chromatography. Fractions 1-8 of the IMAC purified His-TRIB2

were pooled and resolved on a S200/60 gel filtration column. Elution of His-TRIB2 apparent from UV absorbance at 280 nm. (D) Between the elution volume of 70 and 88 ml from the S200/60 column 1.5 ml fractions were collected and analysed by SDS PAGE. (E) Western blot of recombinant His-TRIB2: Varying amounts of His-TRIB2 that was purified from *E. coli* was resolved by electrophoresis on a 10% polyacrylamide gel. The protein was transferred to a nitrocellulose membrane and probed with an anti-His antibody conjugated to HRP and detected using ECL reagent.

Utilising an anti 6xHis HRP conjugated antibody a dose dependent response is seen when between 1 and 10 ng of purified protein was resolved by SDS-PAGE followed by immunoblot analysis (Figure 3.1E). The limit of detection in this experiment was 2.5 ng of His-TRIB2, with 1 ng being barely visible. Intact mass spectrometry (MS) analysis of the SEC purified His-TRIB2 revealed an ion of 43,587.09 Da with the predicted *Mr* of His-TRIB2 to be 43,587.22 kDa (Figure 3.2), supporting the identification of the purified protein.

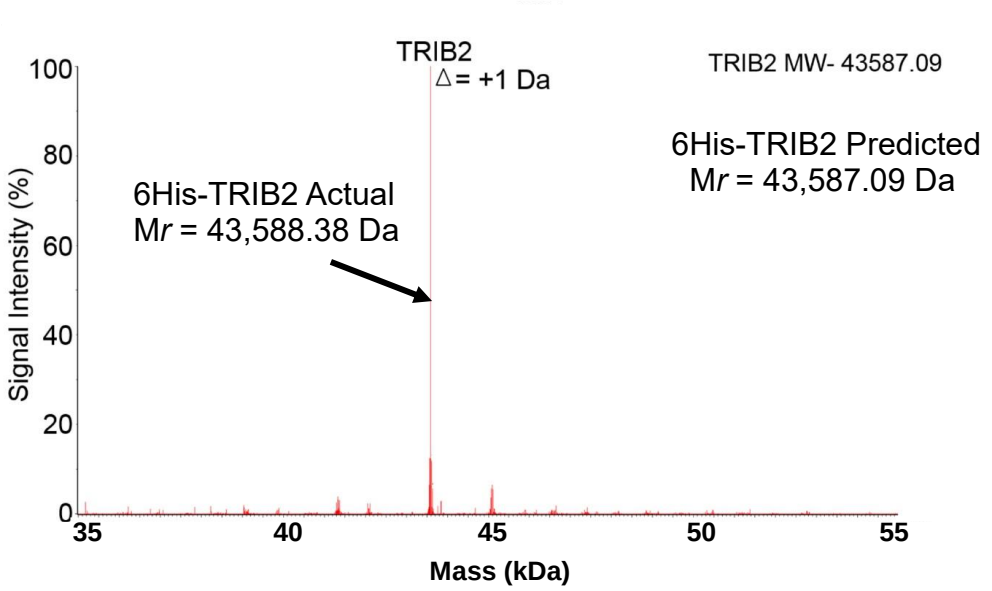


**Figure 3.2: Intact mass spectrum for purified His-TRIB2.** SEC purified TRIB2 was desalted into 0.1% formic acid and 50% acetonitrile and loaded onto a C4 trapping column before intact mass spectrometry (MS1) analysis. The Spectrum shows an ion with the molecular mass of 43,588.38 Da.

## 3.2 Effect of Tris, Hepes and Bicine on TRIB2 stability

In order to assess TRIB2 stability in various buffer conditions, a DSF thermal shift assay was used [244]. Purified protein was exchanged into various buffers using a desalting column. After buffer exchange, and if required, protein was concentrated using an Amicon® Ultra Centrifugal Filter to at least 0.5 mg/mL. The effects of different reducing agents present in the buffer was also tested. All buffers tested contained 100 mM NaCl plus or minus 1 mM DTT.

20 mM Bicine pH 9.0 was previously shown to be optimal for recombinant TRIB2 stability [60, 245], however, I was interested to evaluate TRIB2 behaviour at a physiological pH for *in vitro* biochemical analysis and using optimal buffers which have been used for the analysis of other pseudokinases [58]. The zwitterion bicine has ineffective buffering capacity below pH 8 [246]. TRIB1 (84-372) has previously been analysed in 10 mM Hepes at near physiological pH (pH 7.6) [106], so it was decided to assess this condition with recombinant His-TRIB2.

In accordance with previous studies TRIB2 is most stable in 20 mM Bicine pH 9.0 [60, 245] (Figure 3.3A) with a detected melting temperature of 40.8˚C ± 0.31. His-TRIB2 was less stable in 20 mM Tris pH 7.4 (38.4˚C), and far less stable in 10 mM Hepes pH 7.6 (36.6˚C). Bicine, with a pKa of 8.35 at 20°C, is a zwitterionic amino acid buffer that does not neutralise hydrogen ions at pH 7.4 [246]. Therefore, a buffer condition of 20 mM Tris pH 7.4 was chosen for future experiments despite slightly diminished TRIB2 stability compared to 20 mM bicene pH 9.0.

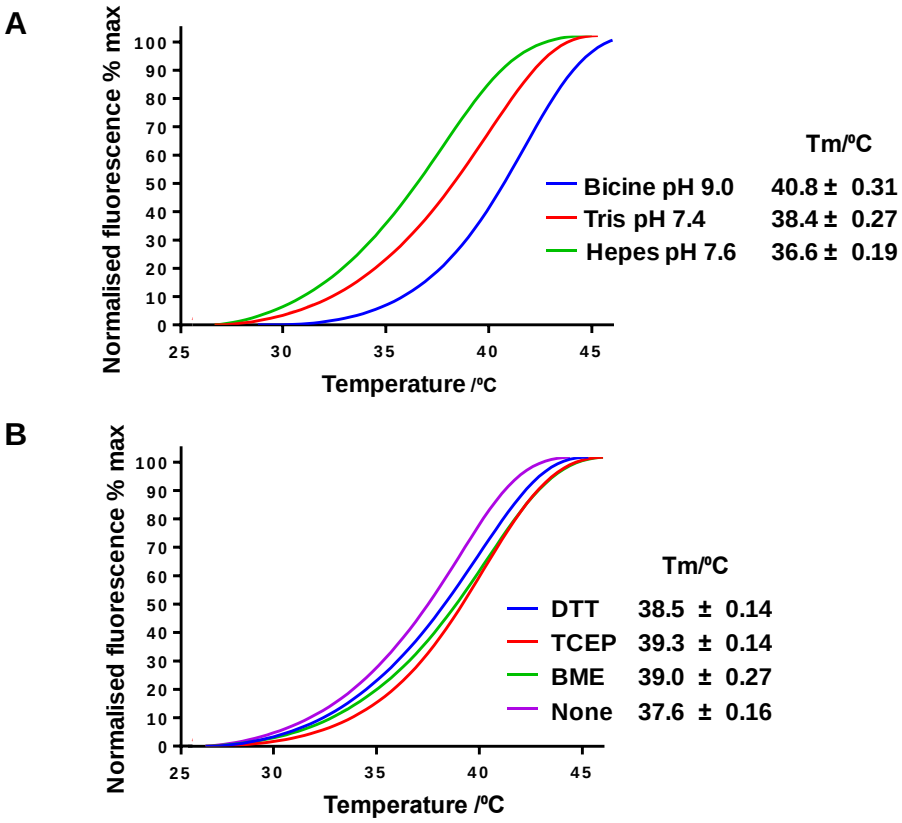


**Figure 3.3: Thermal denaturation profiles of recombinant His-TRIB2 in different buffers.** (A) Representative unfolding profiles are shown for 5 µM His-TRIB2 at different pH values (20 mM bicene pH 9.0, 20 mM Tris pH 7.4 and 10 mM Hepes pH 7.6). All buffers contained 100 mM NaCl and 1 mM DTT. (B) Thermal denaturation profiles of recombinant His-TRIB2 in 20 mM Tris pH 7.4 buffer with different reducing agents. Buffers contained either 1 mM DTT, 1 mM TCEP (tris(2-carboxyethyl)phosphine) or 1 mM BME (β-mecaptoethanol).

## 3.3 Analysis of the effect of reducing agent on TRIB2 stability

In 20 mM Tris pH 7.4, the effect of various established biochemical reducing agents, used in protein purification and enzyme assays were tested on His-TRIB2 by DSF (Figure 3.3B) [244]. Reducing agents such as dithiotreitol (DTT), tris(2-carboxyethyl)phosphine) (TCEP) or β-mecaptoethanol (BME) are required to disrupt disulphide bond formation by reducing sulphur-sulphur bonds to thiols in cytsteine residues to prevent aggregation [247]. When no reducing agent was present, His-TRIB2 had a lower melting temperature compared to His-TRIB2 in the presence of 1 mM DTT, TCEP or 2-mecaptoethanol BME. Due to the similarity between the melting temperatures of His-TRIB2 in all reducing agents tested, DTT was chosen for future

experiments, as it is more stable than BME, cheaper than TCEP and was employed in previous assays [60].

## 3.4 *In vitro* analysis of TRIB2 and C/EBPα interaction

In order to assess the ability of recombinant TRIB2 purified from *E. coli*, glutathione-S-transferase (GST) pull down assays were performed on His-TRIB2 and a previously established interaction partner, C/EBPα [105, 109]. The full length p42 isoform of C/EBPα, known to be targeted for degradation through binding to TRIB2 in human cells [109, 112, 196], was purified from *E.coli*. It was recently established that recombinant TRIB1 binds to recombinant C/EBPα by isothermal titration calorimetry (ITC) [106], in addition to a co-crystal structure in which C/EBPα binds at the interface where the DQLVP motif interacts with a binding pocket in the TRIB1 αC-helix [105].

### 3.4.1 Purification of GST-His-C/EBPα

Full length p42 C/EBPα with a GST N-terminal fusion tag was purified from bacteria. Bacteria were lysed in 20 mM Tris pH 7.4, 100 mM NaCl, 1 mM DTT and 10% (v/v) glycerol and soluble protein separated from cellular debris by centrifugation followed by glutathione-S-transferase (GST) 'pull-down'. After washing of GST-C/EBPα bound beads protein was eluted with 10 mM reduced glutathione. The flow through and first 3 elution fractions (1 mL each) were analysed by SDS-PAGE (Figure 3.4A). SEC analysis on an S200 column in 20 mM Tris pH 7.4, 100 mM NaCl, 1 mM DTT and 10% glycerol (Figure 3.4B) revealed that the majority of protein eluted at 40.0 mL. Samples from the corresponding peak observed at 40.0 mL were analysed by SDS-PAGE (Figure 3.4C). From SEC analysis the predicted *Mr* was 79.6 kDa, however the estimated *Mr* for GST-C/EBPα was 64.6 kDa. Indeed the visualised SDS-PAGE bands for C/EBPα (Figure 3.4C) appear to correspond to a molecular weight closer to 64.6 kDa. The GST-tag may have influenced the hydrodynamic volume of the protein and caused it to migrate through the column faster [248, 249]. Fractions containing GST-C/EBPα as established by SDS-PAGE were pooled, aliquoted into 1.5 mL eppendorf tubes, snap frozen in liquid nitrogen and stored at -80˚C for later analysis.

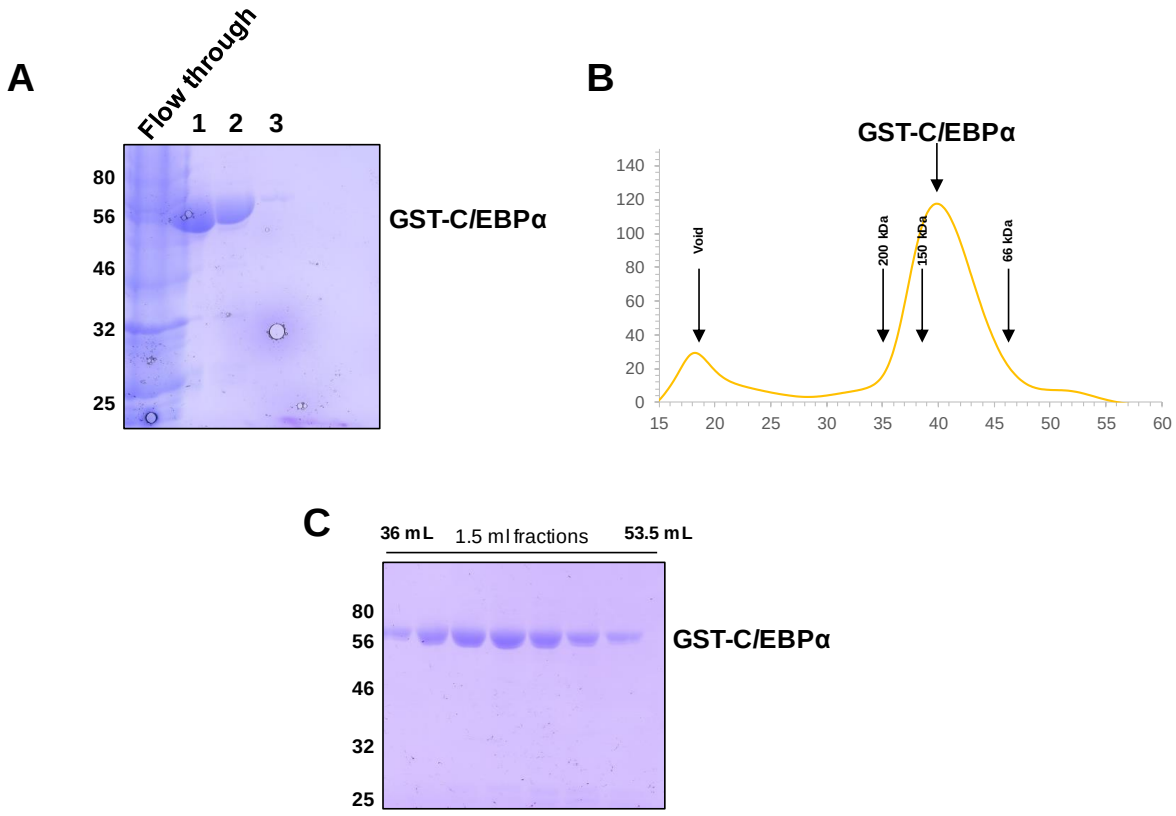


**Figure 3.4: Purification of GST-tagged C/EBPα.** (A) *E. coli* were induced to express GST-tagged C/EBPα for 16 hours at 18ºC. Subsequent to bacterial cell lysis, lysate was incubated with GST-sepharose for 4 hours at 4°C with gentle agitation. The beads were washed 3 times in 20 mM Tris pH 7.4, 100 mM NaCl followed by elution of protein with 10 mM reduced glutathione in 3 separate 1 mL fractions that were analysed by SDS-PAGE. (B) GST-C/EBPα was further purified by SEC, resolved on a S200/60 gel filtration column in 20 mM Tris pH 7.4, 100 mM NaCl, 1 mM DTT and 10% glycerol. (C) Samples from SEC corresponding to GST-C/EBPα elution, between the volumes of 36 and 44 mL, were analysed by SDS PAGE.

### 3.4.2 GST 'pull-down' of TRIB2 with C/EBPα

To provide evidence that recombinant TRIB2 is properly folded and binds to a known physiological target, 5 µg of recombinant GST-C/EBPα or 5 µg of recombinant GST (pre-bound to GSH-sepharose) were incubated with 5 µg of TRIB2 followed by pull down interaction experiments. Consistent with a functional interaction it was found that GST-tagged C/EBPα interacted with His-TRIB2 *in vitro* (Figure 3.5). GST displayed no detectable interaction with His-TRIB2, consistent with an interaction occurring between C/EBPα and TRIB2.

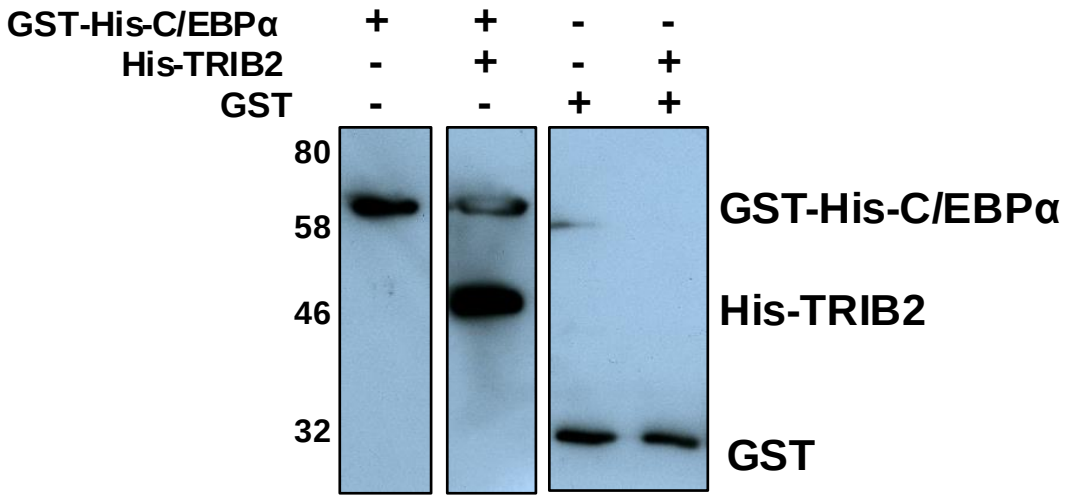


**Figure 3.5: Interaction of TRIB2 with C/EBPα.** The ability of His-TRIB2 to interact with GST-C/EBPα was assessed by GSH-sepharose pull-down followed by immunoblotting.

## 3.5 Analysis of His-TRIB2 ATP binding *in vitro*

TRIB2 has previously been shown to bind weakly to ATP, with a predicted $K_m$ [ATP] of 0.66 mM, and to autophosphorylate very weakly in the presence of ATP and absence of $Mg^{2+}$ ions [60]. The DSF assay was used to examine thermal stability of full-length (1-343) His-tagged TRIB2 protein in the presence of ATP, EDTA and $MgCl_2$. Autoradiography was also used to evaluate $^{32}P$-based autophosphorylation of His-TRIB2. His-TRIB2 ATP binding analysis was compared side by side with full-length His tagged cAMP-dependent protein kinase (His-PKAc), a C104Y TRIB2 mutant and TRIB1. Cys 104, within the αC-helix of TRIB2 is changed to Tyr 134 in TRIB1, and has been suggested to prevent rearrangement into a canonical DFG-in position in TRIB1 [106]. The equivalent Cys residue in TRIB2 may therefore allow for more freedom for rearrangement in the αC-helix to allow ATP binding.

### 3.5.1 TRIB2 binds to ATP and autophosphorylates in the absence of $Mg^{2+}$ ions

His-TRIB2 was not significantly stabilised by ATP alone, $Mg^{2+}$ alone, or in the presence of both ATP and $Mg^{2+}$ (Figure 3.6). EDTA however imparted a small stabilising effect ($\Delta T_m$ 1.4˚C). This stabilisation was further enhanced in the presence of ATP indicated by a statistically significant increase in $T_m$ of His-TRIB2 in the presence of both ATP and EDTA compared to EDTA alone (students t-test p=0.00930). EDTA-dependant

ATP binding activity was then assessed further by autoradiography (Figure 3.7) where there was around a 2 fold increase in His-TRIB2 autophosphorylation, as analysed by densitometry, in the presence of ATP and EDTA as compared to ATP and $Mg^{2+}$ (p=0.00110).

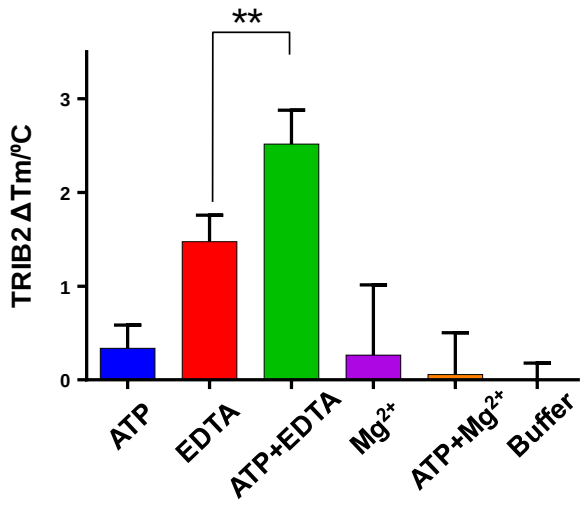


**Figure 3.6: Analysis of TRIB2 thermal stability in the presence of ATP and EDTA**. $\Delta T_m$ values from DSF analysis are shown for 5 µM His-TRIB2 incubated with 10 mM ATP,1 mM EDTA or 1 mM $MgCl_2$. Mean $\Delta T_m$ values (±SD) are with reference to a buffer control from 4 separate experiments are shown. Students t-test was used to reveal a statistically significant difference between the $\Delta T_m$ values of EDTA and ATP+EDTA (p = 0.00930).

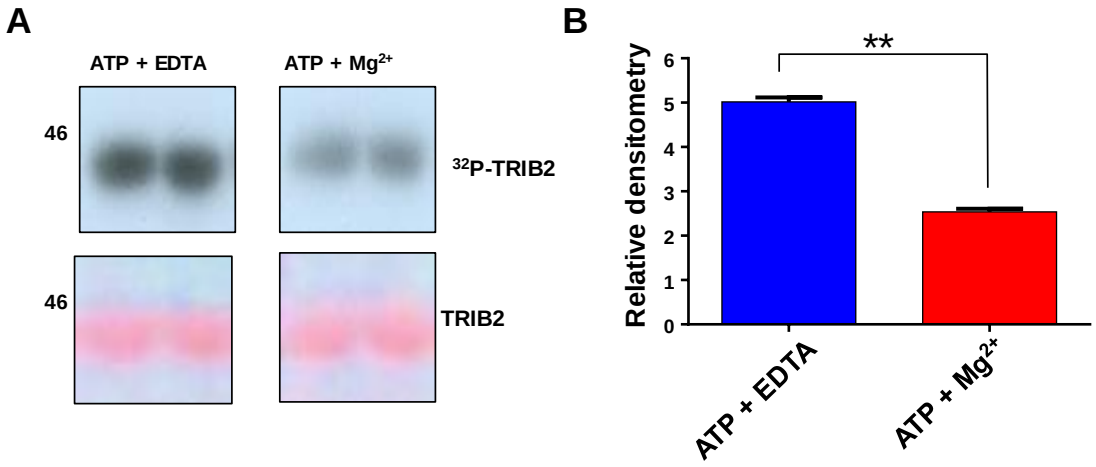


**Figure 3.7: His-TRIB2 autophosphorylates in the absence of Mg2+ ions.** (A) 6 µg of His-TRIB2 was assayed in duplicate for 30 minutes at 30°C in a shaking incubator with either 1 mM ATP (2.2 µCi γ-32P ATP) and 1 mM EDTA or 1 mM ATP with 1 mM $MgCl_2$. The reactions were stopped by the addition

of 5 x SDS loading buffer, protein resolved by SDS-PAGE and then transferred to a nitrocellulose membrane which was treated to autoradiography by exposure to x-ray film for 1 week. The nitrocellulose membrane was stained with ponceau to serve as a loading control. (B) Densitometry analysis of His-TRIB2 autophosphorylation by γ-$^{32}$P ATP incorporation. Band intensities were normalised to loading controls and a student's t-test was used to assess statistical difference between ATP + EDTA and ATP + $Mg^{2+}$ treated protein (p=0.00110).

### 3.5.2 Comparison of His-TRIB2 stability with His-PKA and a hyper-stable C104Y mutant

Thermal stability analysis was used to compare ATP binding properties of His-TRIB2 to the canonical kinase domain of PKA. His-TRIB2 ($T_m$ = 39.54°C) was much less thermostable than His-PKA ($T_m$ = 46.84°C) (Figure 3.8). In contrast to TRIB2, recombinant His-PKA was not stabilised by either ATP alone or ATP and EDTA together. His-PKA was instead stabilised by ATP in a $Mg^{2+}$ dependent manner ($\Delta T_m$ of 3.36˚C), as expected for a canonical Ser/Thr kinase domain [250].

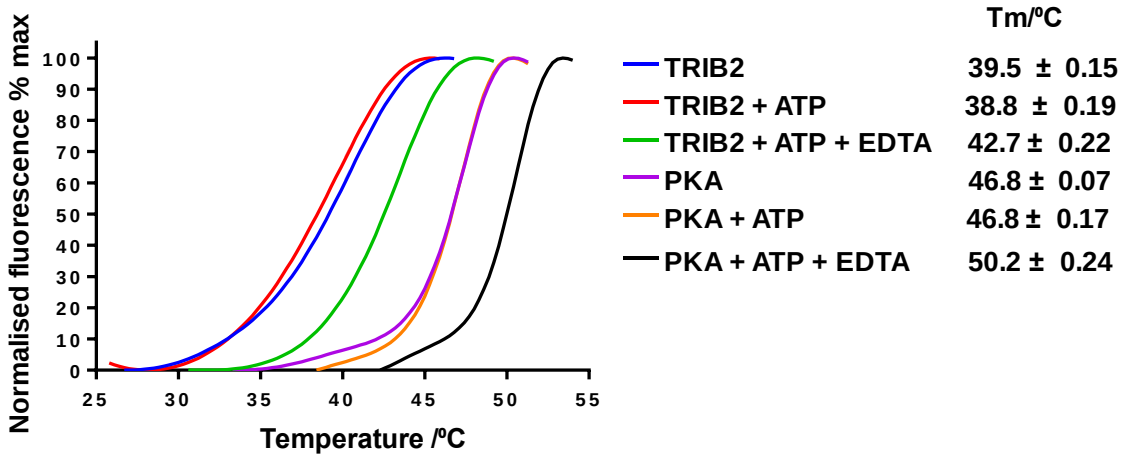


**Figure 3.8: Thermal denaturation profiles of recombinant His-TRIB2 and His-PKA ± ATP + EDTA/$Mg^{2+}$.** Representative unfolding profiles are shown for 5 µM His-TRIB2 incubated with/without 10 mM ATP or 10 mM ATP and 1 mM EDTA. 5 µM His-PKA was incubated with/without 10 mM ATP or 10 mM ATP and 1 mM $MgCl_2$. $T_m$ values (±SD) were obtained from 3 separate fluorescence profiles, each point assayed in duplicate.

It was previously reported that TRIB1 is sterically hindered from undergoing conformational rearrangement to an active like conformation and, therefore, unable to bind ATP [106]. This was in part due to the presence of a Tyr134 residue in the αC-

helix, the equivalent residue being Cys104 in TRIB2 [106]. WT TRIB2, C104Y TRIB2 and PKA were purified to homogeneity (Figure 3.9A, left). Sequence alignments of the TRIB1, TRIB2, TRIB3 and STK40 β3-Lys to αC-helix residues (Figure 3.9 right) reveals that Cys104 of TRIB2 is a Tyr residue in TRIB1 and TRIB3 and an Ile in the more distantly related STK40. The elution volumes from Superdex 200 were identical for purified WT and C104Y TRIB2, confirming that both proteins were stable and monomeric in solution (figure 3.9B), with an estimated Mr of 45.3 kDa. Thermal stability based on unfolding profiles were determined for each protein (Figure 3.9C). Remarkably, single substitution of Cys 104 with Tyr induced marked stabilisation of TRIB2, with the $T_m$ value increasing from 38.6°C for WT TRIB2 to 48.9°C for C104Y TRIB2. The increased thermal stability of C104Y TRIB2 is comparable to that observed to that of human TRIB1 ($T_m$ ~49˚C) in an independent study [106], suggesting an important structural role for this residue in both TRIB1 and TRIB2 (un)folding dynamics. As demonstrated earlier, TRIB2 did not bind to ATP alone or in the presence of $Mg^{2+}$ (Figure 3.9D), but was stabilised by ATP and EDTA. Interestingly C104Y TRIB2 was not stabilised by ATP alone, ATP with EDTA or ATP with $Mg^{2+}$. PKA was only stabilised in the presence of both ATP and $Mg^{2+}$.

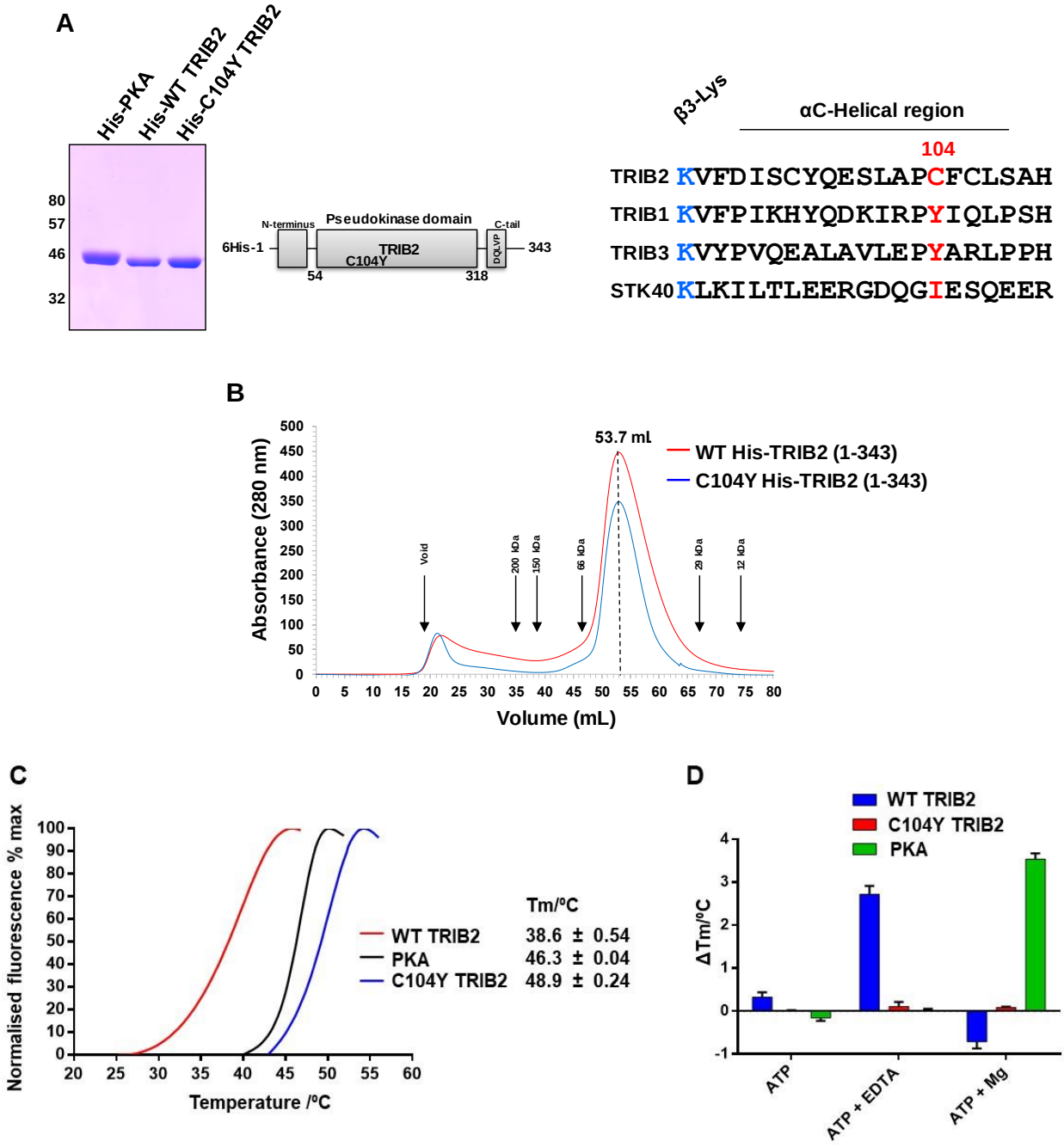


**Figure 3.9: Thermal stability and ATP binding analysis of a C104Y TRIB2 mutant by DSF.** (A) SDS-PAGE of recombinant proteins employed for *in vitro* analysis (left). Amino acid sequence alignment of the β3-Lys to the αC-helix region of TRIB2, TRIB1, TRIB3 and STK40 pseudokinases. (B) SEC analysis of WT and C104Y TRIB2 each purified from 4 litres of *E. coli*. (C) Thermal denaturation profiles of recombinant WT His-TRIB2, C104Y His-TRIB2 and His-PKA. (D) DSF analysis for 5 μM His-tagged WT TRIB2, C104Y TRIB2 and PKA incubated with/without 10 mM ATP or 10 mM ATP and 1 mM EDTA. 5 μM His-PKA incubated with/without 10 mM ATP or 10 mM ATP and 1 mM $MgCl_2$. $T_m$ values (±SD) were obtained from 3 separate fluorescence profiles, each point assayed in duplicate.

### 3.5.3 Comparison of TRIB2 stability with TRIB1

The thermal stability and ATP binding potential of His-tagged human TRIB1 was also analysed. TRIB1 lacking the N-terminal domain was expressed because residues 1-84 were predicted to be disordered and were absent in biochemical and crystallographic studies performed previously [106]. Two TRIB1 proteins were analysed, TRIB1 84-372, with an intact C-terminal tail and TRIB1 84-343, which lacked the C-terminal tail containing the COP1 binding site. The C-terminal tail was previously suggested to increase TRIB1 thermal stability by forming an *in cis* interaction with the pseudokianse domain [106].

TRIB1 proteins were purified by IMAC and SEC and buffer exchanged into 20 mM Tris pH 7.4, 100 mM NaCl and 1 mM DTT (Figure 3.10A). Interestingly TRIB1 84-343, the pseudokinase domain alone, eluted from the SEC column more quickly than TRIB1 84-372 with a calculated mw of 58.2 kDa suggesting dimerization (Figure 3.10B). For studies carried out previously [106] TRIB1 proteins were purified by SEC into Hepes pH 7.6, 300 mM NaCl, 2 mM DTT. Thus SEC analysis was performed by equilibrating an S200/60 gel filtration column with the same buffer before loading and resolving 2 mg of each TRIB1 protein and TRIB2 1-343 and 54-318 (Figure 3.9C). Interestingly in these buffer conditions TRIB1 84-343 no longer appeared to dimerize, the calculated *Mr* being 30.25 kDa.

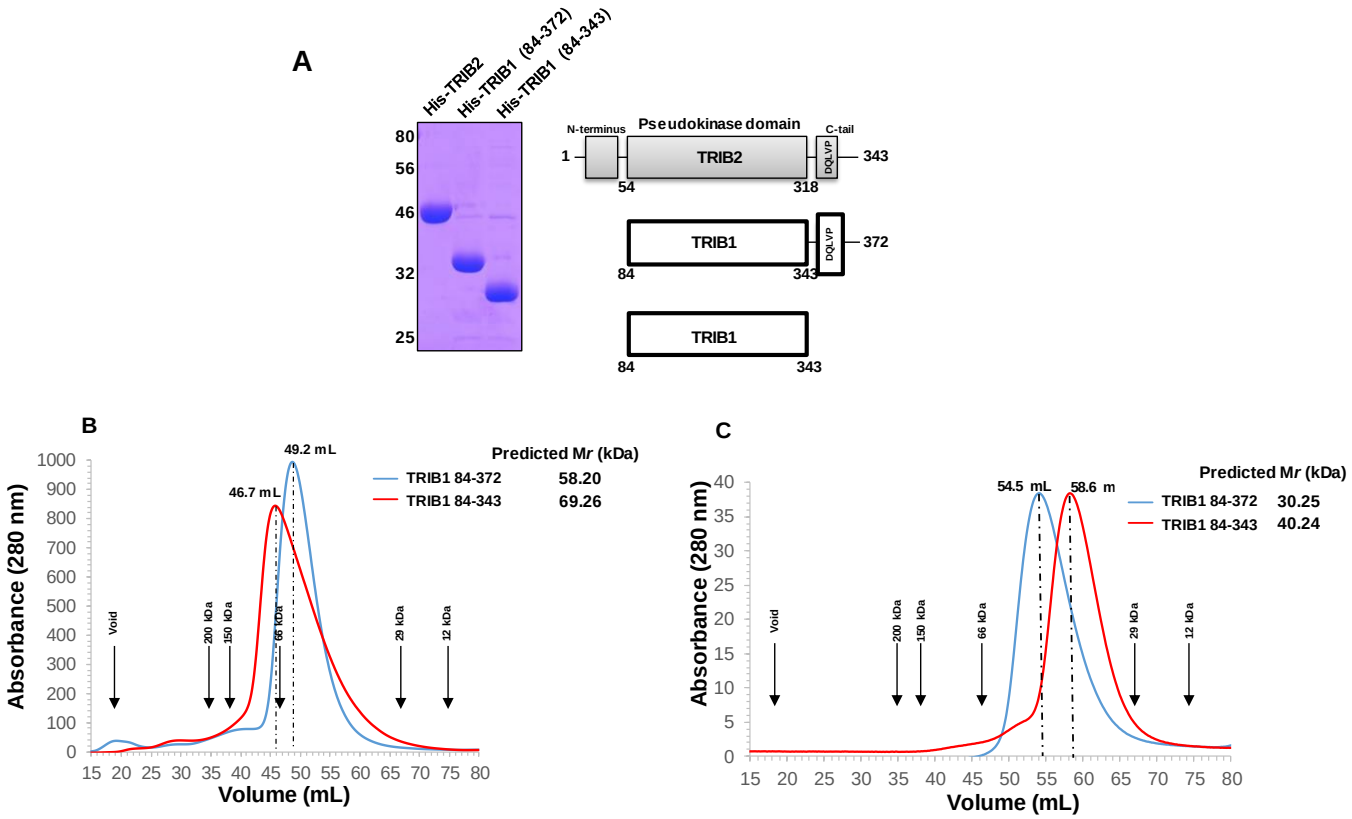


**Figure 3.10: Purification and SEC analysis of TRIB1 in Tris pH 7.4 and Hepes pH 7.6.** (A) SDS PAGE analysis of His-tagged TRIB2 1-343, TRIB1 84-372 and TRIB1 84-343 purified from *E. coli*. (B) SEC analysis TRIB1 84-372 (blue) and TRIB1 84-343 (red) resolved on an S200 column equilibrated in 20 mM Tris pH 7.4, 300 mM NaCl and 2 mM DTT. Predicated M*r* is shown. (C) 2 mg of each TRIB1 protein 84-372 (blue) and 84-343 (red), previously purified into Tris, were resolved on an S200 column equilibrated in 10 mM Hepes pH 7.6, 300 mM NaCl, 2 mM DTT. Predicted M*r* is shown.

Structural analysis of TRIB1 reveals an *in cis* self-assembly whereby the COP1 binding site of the C-terminal tail region (containing the conserved DQLVP motif) binds directly to the TRIB1 pseudokinase domain adjacent to the short αC-helix [106]. This hypothesis was supported by small angle X-ray scattering, DSF and *in vitro* competition assays [106]. Thermal melting curves (Figure 3.11A) reveal that both TRIB1 proteins have a greater thermal stability than TRIB2 1-343 and 54-318. However unexpectedly, TRIB1 84-372, with a $T_m$ of 41.9°C, was in fact less stable than the TRIB1 pseudocatalytic domain alone (84-343), which had a $T_m$ of 44.8°C. The TRIB1 DSF experiments were carried out in the same buffer (20 mM Tris pH 7.4, 100 mM NaCl and 1 mM DTT) as previously used [106]. Although in my experiments the

C-terminal tail did not stabilise TRIB1, the obtained $T_m$ values for both TRIB1 proteins were markedly different than previously reported [106]. Murphy *et al* (2015) obtained a $T_m$ ~49˚C for TRIB1 84-372 and a $T_m$ of ~47.5˚C for TRIB1 84-343. Consistently, neither TRIB1 protein was stabilised by ATP and EDTA (Figure 3.11B).

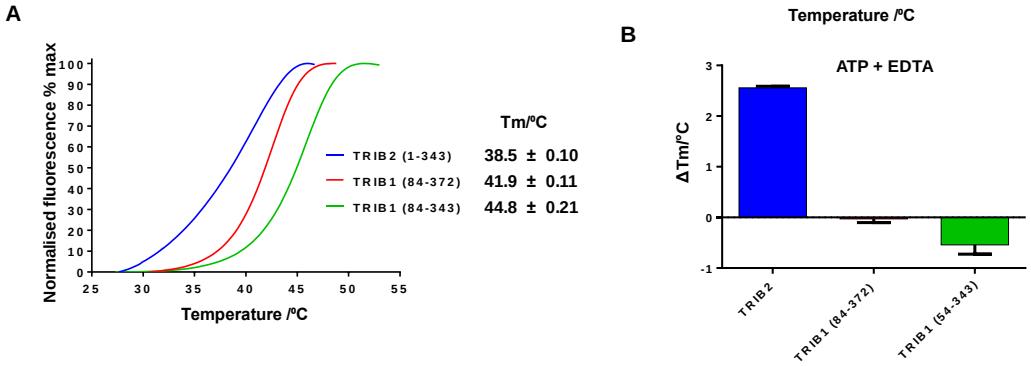


**Figure 3.11: Analysis of TRIB1 thermal stability in the presence of ATP**. (A) Thermal denaturation profiles of TRIB2 1-343 and TRIB1 proteins (84-372 and 84-343). Average melting temperatures are displayed with standard deviation. (B) Thermal shifts of TRIB2 and TRIB1 in the presence of 10 mM ATP and 1 mM EDTA.

### 3.5.4 Stability of TRIB1 in different buffer compositions

For subsequent analysis, purified TRIB1 proteins were buffer exchanged into either 20 mM Tris pH 7.4, 10 mM Hepes pH 7.6 or 20 mM bicene pH 9.0 ± 1 mM DTT. All buffers also contained 100 mM NaCl. TRIB2 was previously shown to be the most stable in Bicene pH.9.0 [60, 251]. In all buffers, Tris pH 7.4, Hepes pH 7.6 and Bicene pH 9.0, in the absence of DTT, $T_m$ values for TRIB1 84-372 were similar (40.6°C, 40.7°C and 41.1°C) (figure 12A). This was also observed for TRIB1 84-343, the $T_m$ values being similar in the absence of DTT regardless of buffer or pH (Figure 12B). However, TRIB1 84-343 $T_m$ values were comparatively greater than TRIB1 84-372 by ~2°C. DTT did not influence the stability of TRIB1 in the presence of Tris pH 7.4 or Hepes pH 7.6 however, surprisingly, did in the presence of Bicene pH 9.0 and 1 mM DTT. There was there a marked increase in the $T_m$ of both proteins. The $T_m$ for TRIB1 84-372 was 46.9°C and 47.0°C for TRIB1 84-343 in this condition, being relatively equal.

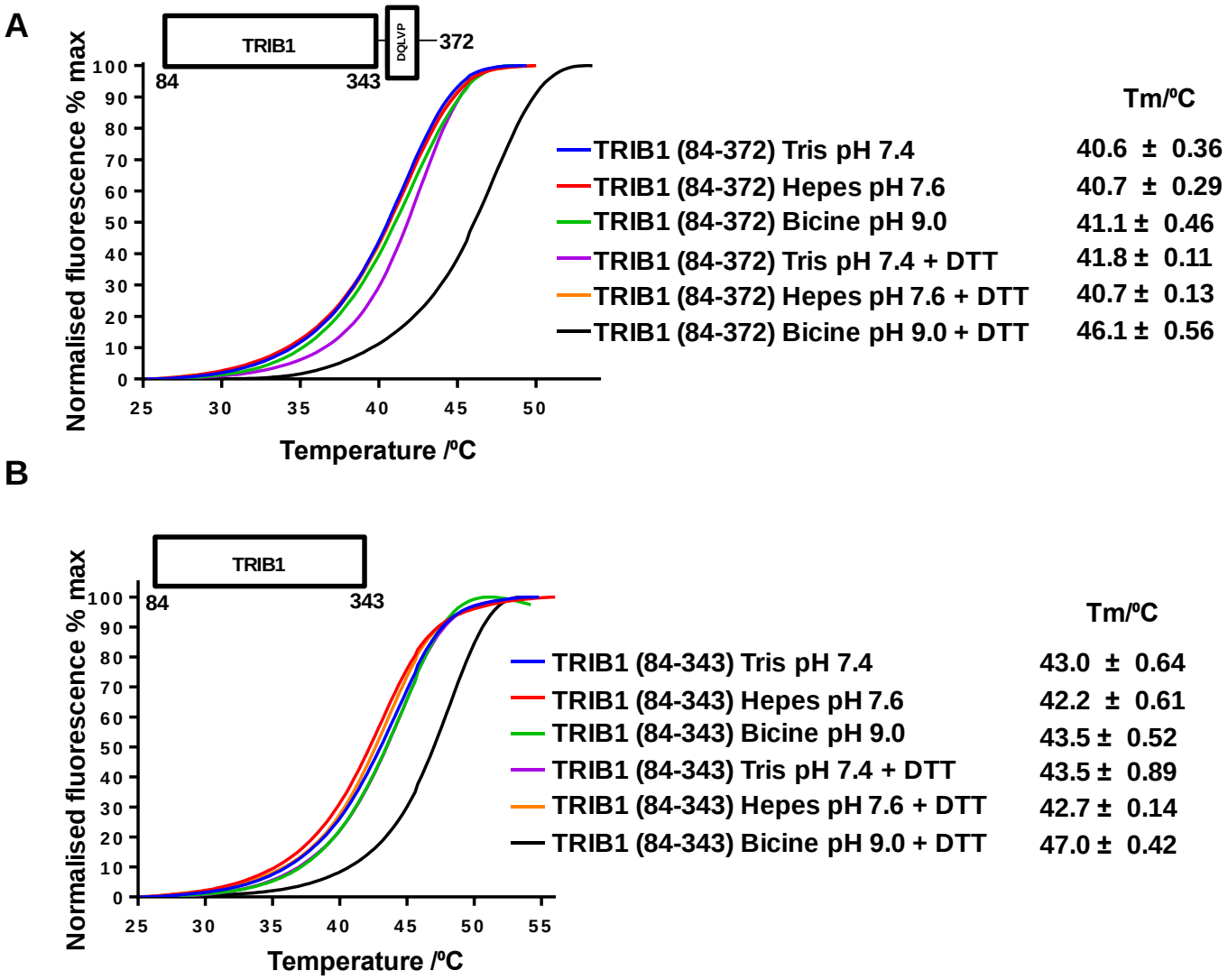


**Figure 3.12: Thermal denaturation profiles of recombinant His-TRIB1 in different buffer compositions**. (A) Representative unfolding profiles are shown for 5 µM His-TRIB1 (54-372) in buffers with differing pH (20 mM bicene pH 9.0, 20 mM Tris pH 7.4 and 20 mM Hepes pH 7.6). All buffers contained 150 mM NaCl and 1 mM DTT. (B) Same as for (A) but for the analysis of His-TRIB1 (84-343).

## 3.6 TRIB2 destabilisation in the absence of the C-terminal tail

### 3.6.1 Analysis of truncation mutants and a COP1 binding site mutant

To investigate whether the C-terminal tail region stabilises TRIB2, a series of point and truncation mutants were generated by PCR and recombinant protein expressed and purified. These proteins lacked either the N-terminal extension (54-343), predicted to be disordered by both I-TASSER [252] and VSL2 [253], the C-terminal tail (1-318)

or both regions (54-318). A COP1 binding site triple point DQLVP to AQLAA mutant was also generated (Figure 3.13A). SEC analysis from Figure 3.13B reveals that WT TRIB2 elutes in agreement to the predicted M*r*. However, SEC analysis indicated that TRIB2 54-318 (pseudokinase domain alone) eluted with a calculated M*r* of 56.2 kDa. The predicated molecular weight of TRIB2 54-318 is 32.0 kDa, which suggests that this truncation mutant formed a dimer or aggregated. Interestingly, AQLAA TRIB2 had a predicted molecular weight of 70.0 kDa, indicative of dimer formation (or potential aggregation).

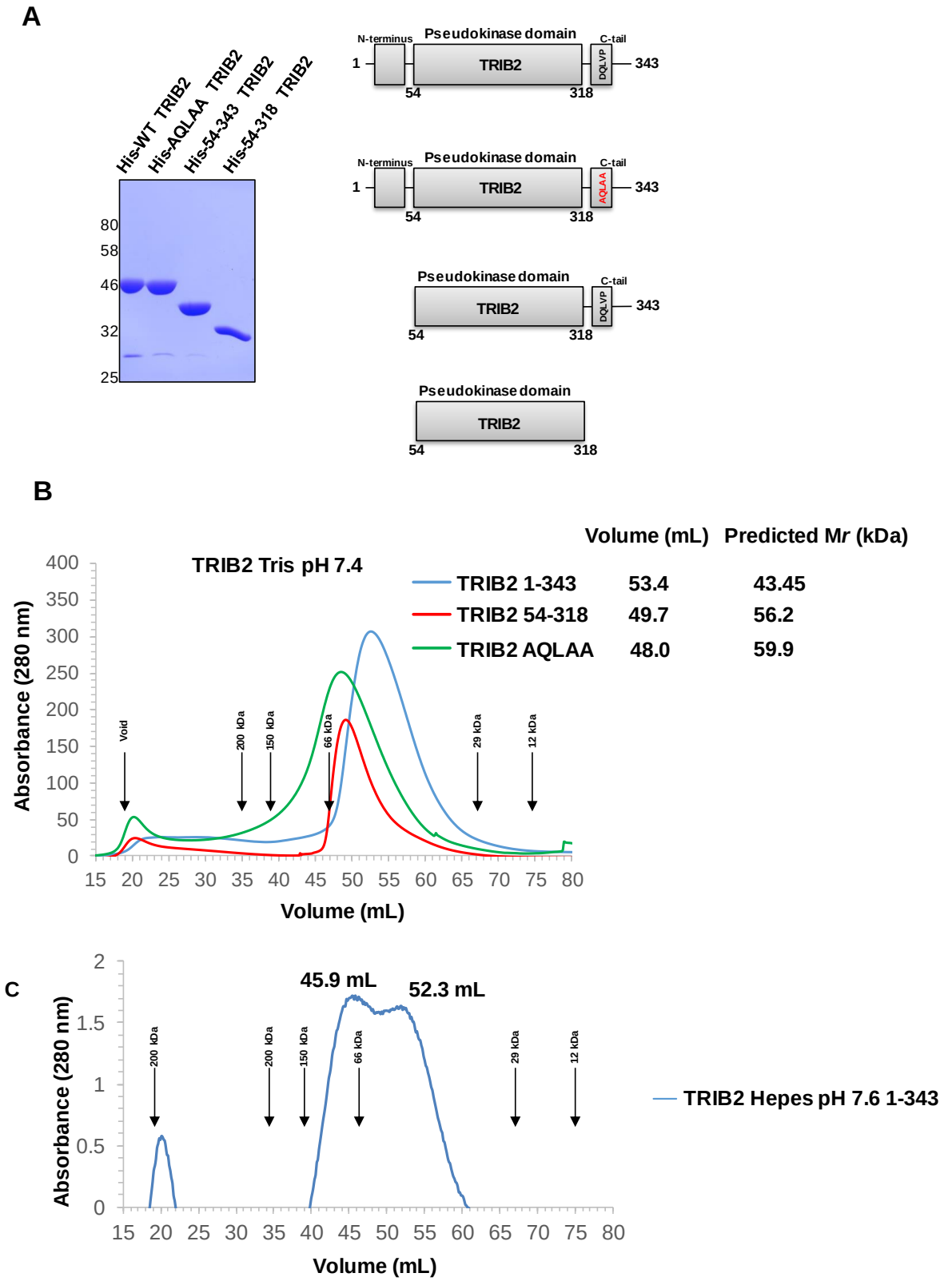


**Figure 3.15: Purification and SEC analysis of TRIB2 truncation and AQLAA mutants**. (A) SDS-PAGE analysis of TRIB2 proteins purified by IMAC and SEC. (B) SEC analysis of TRIB2 1-343, TRIB2 54-318 and AQLAA COP1 binding site mutant. (C) SEC analysis of TRIB2 1-343 in Hepes pH 7.6. TRIB2 54-318 was also loaded onto the column but no elution profile was detected.

It was described in Figure 3.10C that TRIB1 84-343 no longer formed a dimer in Hepes pH 7.6, 100 mM NaCl and 1 mM DTT as opposed to Tris pH 7.4, 100 mM NaCl and 1 mM DTT. Therefore TRIB2 was also analysed by SEC in this buffer Hepes pH 7.6. In Hepes pH 7.6 TRIB2 1-343 appeared to be unstable with peaks with very low signals appearing at calculated molecular weights of 46.9 and 73.23 kDa (Figure 3.13C). TRIB2 54-319 was completely unstable in this buffer and the absence of protein eluting in the void volume indicated that protein may have become blocked inside of the column.

In order to investigate these mutants further, DSF was exploited (Figure 3.14). Full-length (1-343) TRIB2 and TRIB2 lacking only the N-terminal domain (TRIB2 54-343) both exhibited similar $T_m$ values of 39-40°C (Figure 3.14). In contrast, deletion of the C-tail (residues 318-343), either in the absence (TRIB2 54-318) or presence (TRIB2 1-318) of the N-terminal region, markedly reduced TRIB2 thermal stability. This could be indicative of a destabilised conformation observed in TRIB1, as previously described [106]. Indeed, mutation of the DQLVP motif to AQLAA also caused TRIB2 thermal destabilisation, with a $T_m$ value of ~36°C (Figure 3.14).

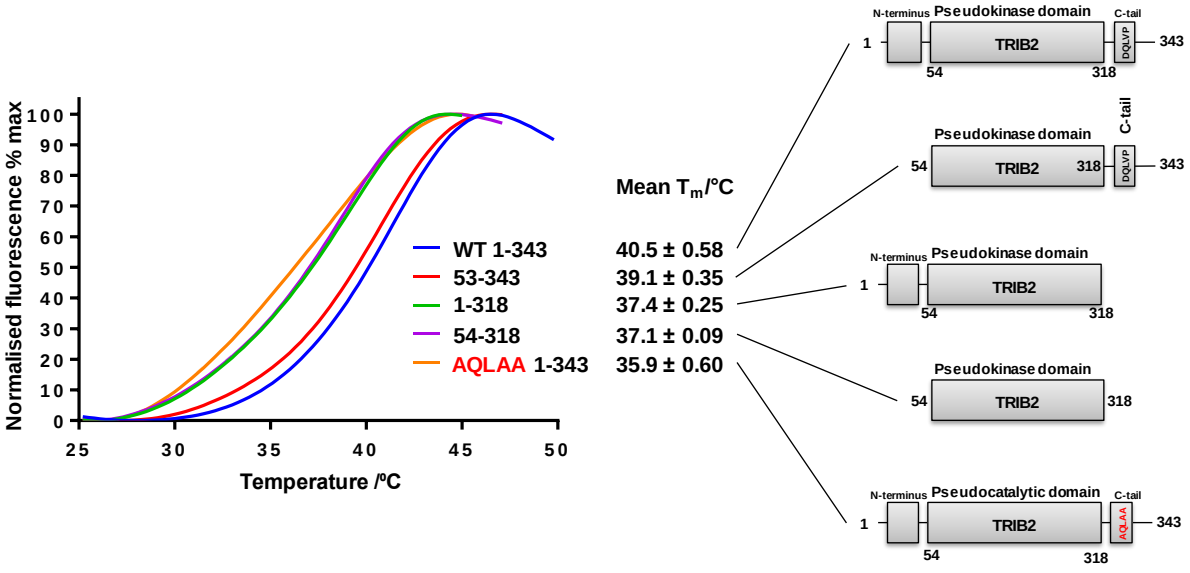


**Figure 3.14: Thermal stabilisation of TRIB2 by the C-terminal tail**. Thermal denaturation profiles of truncated TRIB2 proteins and a COP1 binding site DQLVP to AQLAA triple mutant with mean $T_m$ values ± standard deviation. Cartoon diagrams with domain boundaries illustrate TRIB2 proteins analysed.

### 3.6.2 DSF analysis with synthetic C-terminal TRIB2 peptides

Based on previous work in which the PKA regulatory subunit and AKAP binding were competed with using stapled peptides [24], I hypothesised that synthetic stapled C-terminal peptides (containing the DQLVP COP1 binding motif) could compete for binding with the TRIB2 C-terminal tail in TRIB2 pseudocatalytic domain, thus influencing TRIB2 thermal stability. Tribbles peptides were synthesised by Dr Eileen Kennedy (University of Georgia). A synthetic TRIB2 C-terminal peptide with the sequence YKAAYAKESDQLVPDK with a hydrocarbon staple between the residues highlighted in red (Figure 3.15A) and the COP1 binding DQLVP was synthesised. A control peptide, YKAAYAKEVSAQLVAAD with a mutated COP1 binding motif was also prepared and tested (Figure 3.15A). Lastly, a scrambled peptide was synthesised with the sequence YKAKSLAADQYDGPVE, which served as an additional negative control.

A

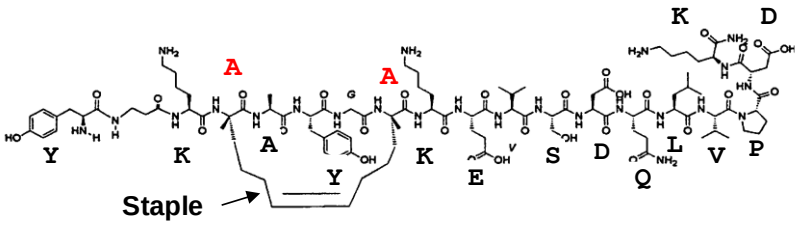


TRIB2 C-terminal peptide: **YKAAYAKESDQLVPDK**

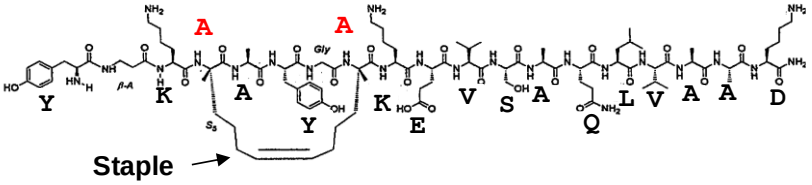


TRIB2 control peptide: **YKAAYAKEVSAQLVAAD**

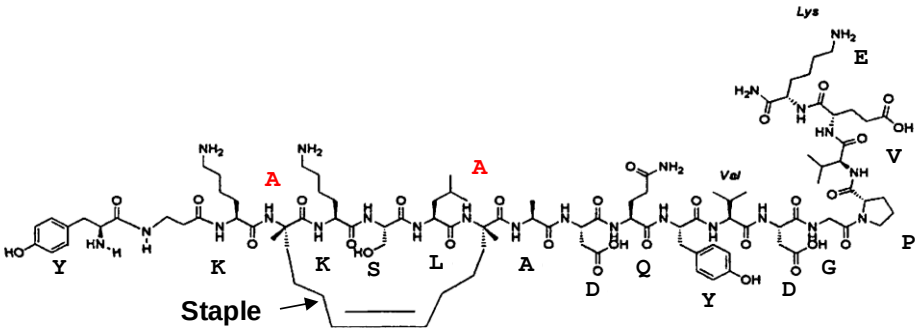


Scrambled peptide: **YKAKSLAADQYDGPVE**

B

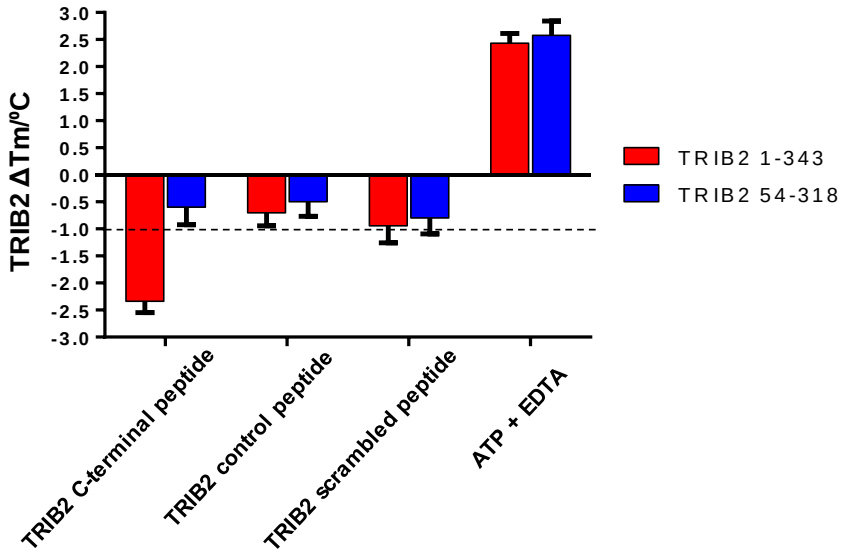

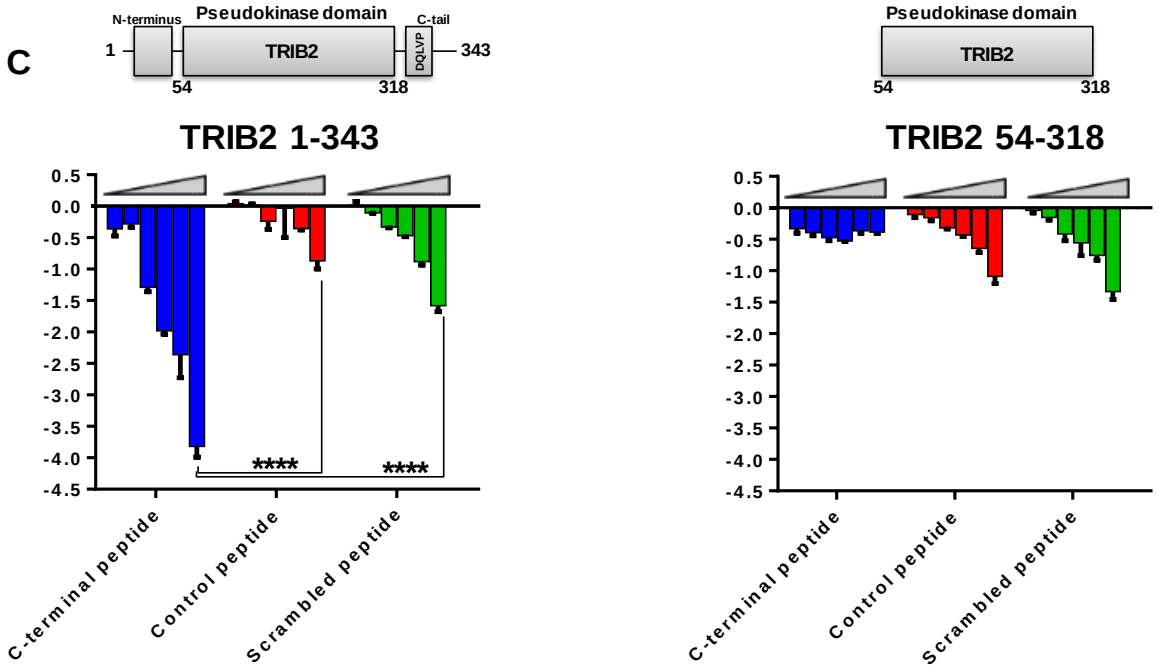


**Figure 3.15: DSF analysis of TRIB2 1-343 and 54-318 with stapled C-terminal tail peptides**. (A) Structures and sequences of TRIB2 C-terminal stapled peptide, containing the DQLVP motif, a control C-terminal peptide, with a divergent AQLVAA motif and a scrabbled peptide. (B) 5 µM of TRIB2 was assayed in the presence of 20 µM peptide and mean $\Delta T_m$ values are shown from 3 independent experiments. ATP + EDTA served as a control. (C) Dose response analysis of C-terminal peptides. 5, 10, 20, 40, 80 and 160 µM of peptides were analysed by DSF in the presence of 5 µM TRIB2 1-343 and TRIB2 54-318. The extent of destabilisation induced by the C-terminal peptide was significantly greater than that induced by both the control and scrambled peptide as measured by students t-test ($p<0.0001$).

DSF was used to assess the stability of full-length TRIB2 (1-343) and the pseudokinase domain alone (54-418) in the presence of the stapled TRIB2 synthetic stapled C-terminal peptide containing the DQLVP motif and the control peptide (Figure 3.15B). Excitingly the TRIB2 C-terminal peptide destabilised 1-343 ($\Delta T_m$ -2.3 °C) but not 54-318 TRIB2 ($\Delta T_m$ -0.6 °C). This $\Delta T_m$ for 54-318 TRIB2 could indicate the occurrence of a weak destabilising interaction in the pseudokianse domain. It is important to note that the C-terminal stapled peptide did not stabilise 54-318 TRIB2, supporting the hypothesis that the destabilisation induced in 1-343 TRIB2 was a result of C-terminal tail displacement. Furthermore, the destabilisation effect was reduced to -0.7˚C and -0.5 ˚C for 1-343 and 54-318 TRIB2 respectively in the presence of the

control peptide, which has a divergent AQLVA motif. Similarly, the destabilisation effect in the presence of the C-terminal scrambled peptide was markedly reduced compared to the TRIB2 C-terminal tail peptide, with $\Delta T_m$. values of -0.9 and -0.8 ˚C for 1-343 and 54-318 TRIB2 respectively. This suggests that the destabilising interaction by stapled peptides with full length TRIB2 (1-343) was sequence specific. ATP and EDTA stabilised both proteins to a similar extent (~2.7˚C).

The effect of destabilisation of full length (1-343) TRIB2 by the C-terminal stapled peptide was dose-dependent (Figure 3.15C), reaching a maximum $\Delta T_m$ of -3.9°C at a protein to peptide ratio of 1:32. Interestingly, there was a minor destabilisation effect on both 1-343 and 54-318 TRIB2 in the presence of the scrambled peptide, which was also dose-dependent, reaching a maximum $\Delta T_m$ of ~-1.5°C. This further evidenced that, to a lesser degree, non-specific interactions were instigated between the stapled peptides and the TRIB2 pseudokinase domain. Indeed, the more extensive destabilisation detected in 1-343 TRIB2 in the presence of the C-terminal tail stapled peptide was suggestive of a targeted interaction.

## 3.7 Small molecule analysis

It was previously suggested that the TRIB2 pseudokinase domain is ‘druggable’ [60]. Both the MLKL and TRIB1 pseudokinases have been screened by DSF using the 367 small molecule kinase inhibitors in the PKIS1 in order to discover novel drug leads [105, 217]. TRIB2 was analysed by DSF in the presence of known small molecule kinase inhibitors in order to find potential novel drug leads.

### 3.7.1 Staurosporine does not bind to His-TRIB2

Staurosporine binds to many protein kinases and pseudokinases through various binding modes [254, 255]. However, the thermal stability of His-TRIB2, in the presence of staurosporine, did not detectably change, even at concentrations as high as 100 µM (1:20 protein:inhibitor) (Figure 3.16B). His-PKA however was stabilised in a dose dependent manner, with 1 µM (5:1) giving no significant shift, 5 µM (1:1) a $\Delta T_m$ of ~3.5˚C and a $\Delta T_m$ obtained at 10 µM (1:2) of ~6.5˚C. In the presence of 100 µM staurosporine His-PKA was stabilised by ~6.5˚C.

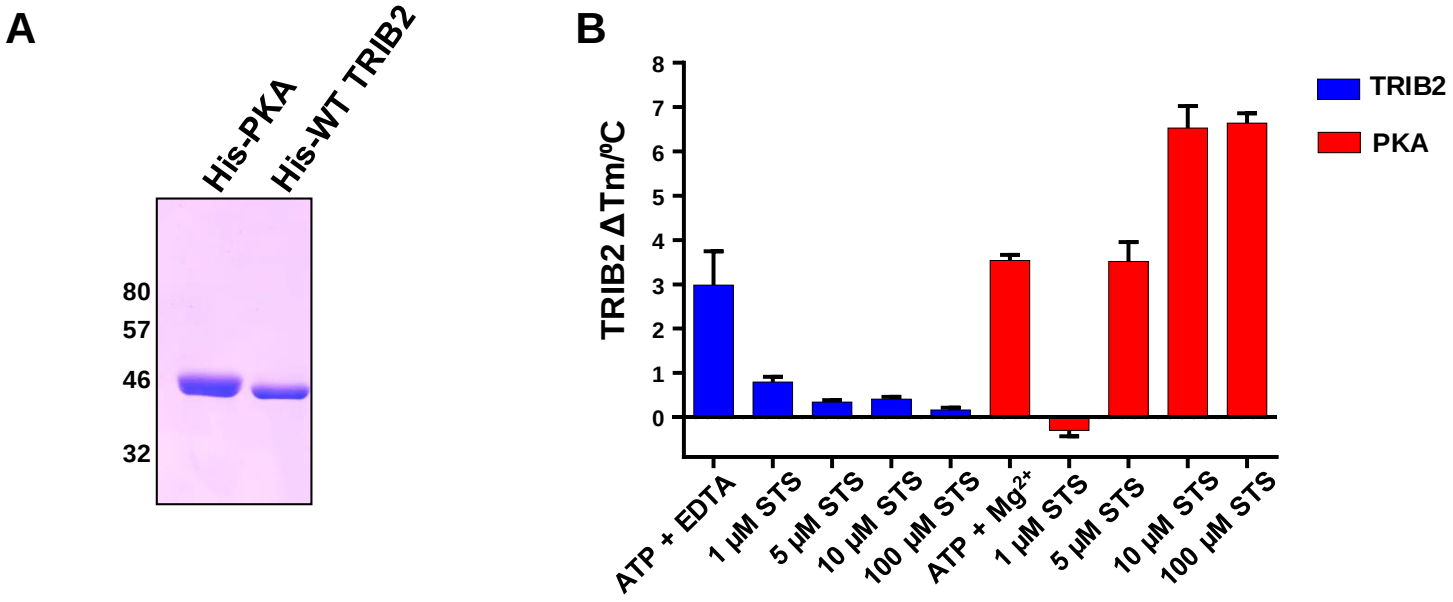


**Figure 3.16: His-TRIB2 is not stabilised by staurosporine**. (A) SDS-page analysis of recombinant His-TRIB2 and His-PKA used for DSF analysis. (B) Varying concentrations of staurosporine (STS) (1-100 µM) were incubated with 5 µM of either His-TRIB2 or His-PKA and analysed by DSF. ΔTm values were calculated with reference to a DMSO (2% v/v) buffer control.

### 3.7.2 A DSF screen for TRIB2 ligands

To discover potential ligands for TRIB2 I screened the PKIS1 against recombinant His-TRIB2 in a protein:compound ratio of 1:4 (Figure 3.17) [242]. Cut off values of $\Delta T_m$ = <-2°C and >+3.5°C were used to define 'hit' compounds that possessed the ability to either destabilise or stabilise TRIB2, respectively. The top 'stabilising' compound identified was GW693881A, a dual EGFR/HER2 thienopyrimdine inhibitor exhibiting a $\Delta T_m$ of 4.7°C. The top 'destabilising' compound was GW804482X, a thiophene polo-like kinase (PLK) inhibitor that induced a $\Delta T_m$ of - 3.4 °C (Figure 3.17, red symbols).

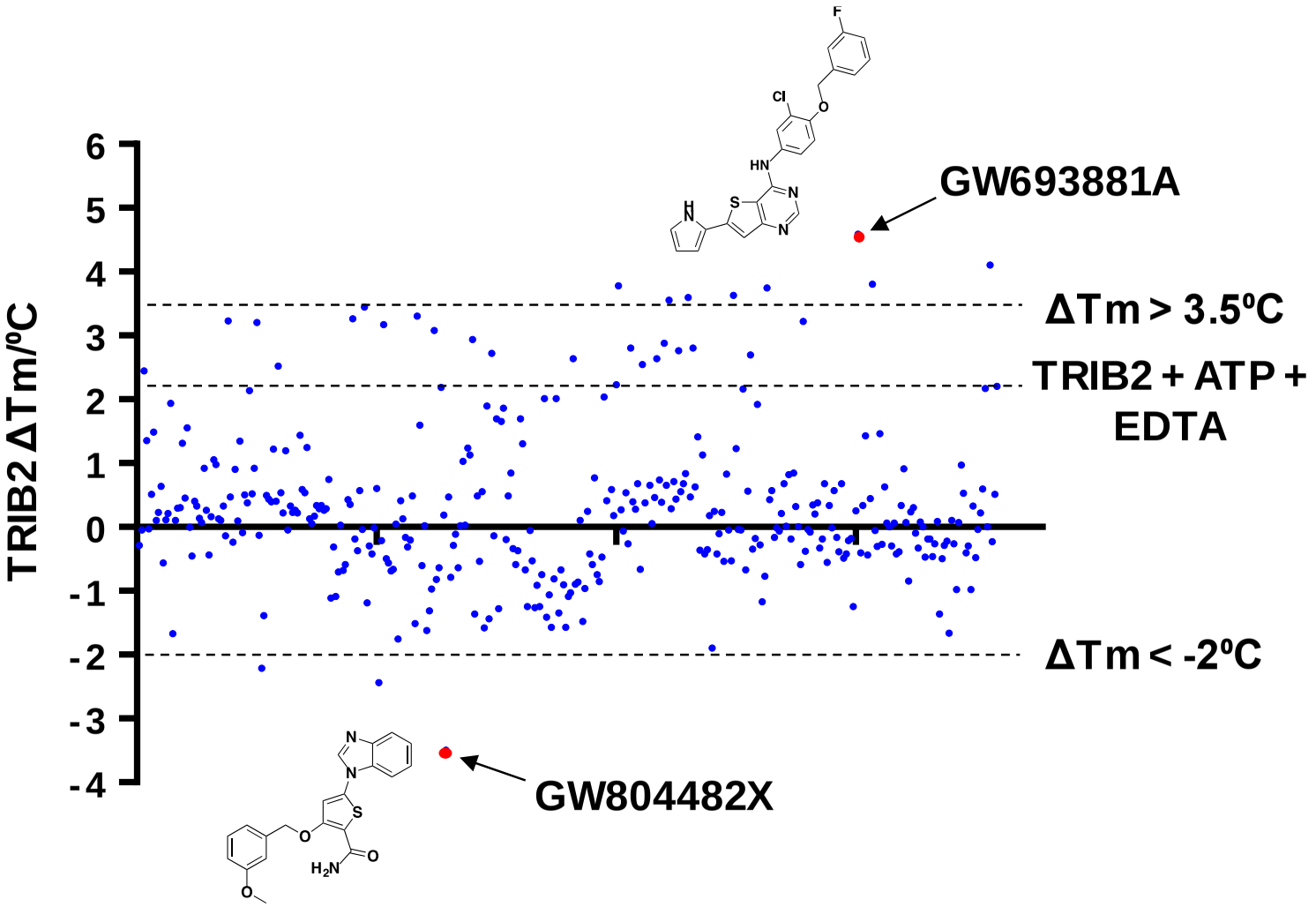


**Figure 3.17: TRIB2 DSF screen of PKIS1 compounds**. 5 µM His-TRIB2 and 20 µM of each compound was employed for DSF analysis. $\Delta T_m$ values were calculated for each compound. Scatter graph of data highlights a wide variety of compounds that either stabilise or destabilise TRIB2 *in vitro*. Cut off values of >3.5°C and < 2°C were used to designate 'hits'.

Examining the most stabilising hits (>2.5˚C) it was apparent that there was an abundance of thienopyrimidine based EGFR/HER2 and benzimidazole based TIE-2/VEGF2 dual inhibitors (Figure 3.18). The thiophene PLK inhibitor GW804482X was the most destabilising. Interestingly a structurally-related thiophene PLK inhibitor (GW853609X) also stabilised TRIB2 by 3.2˚C.

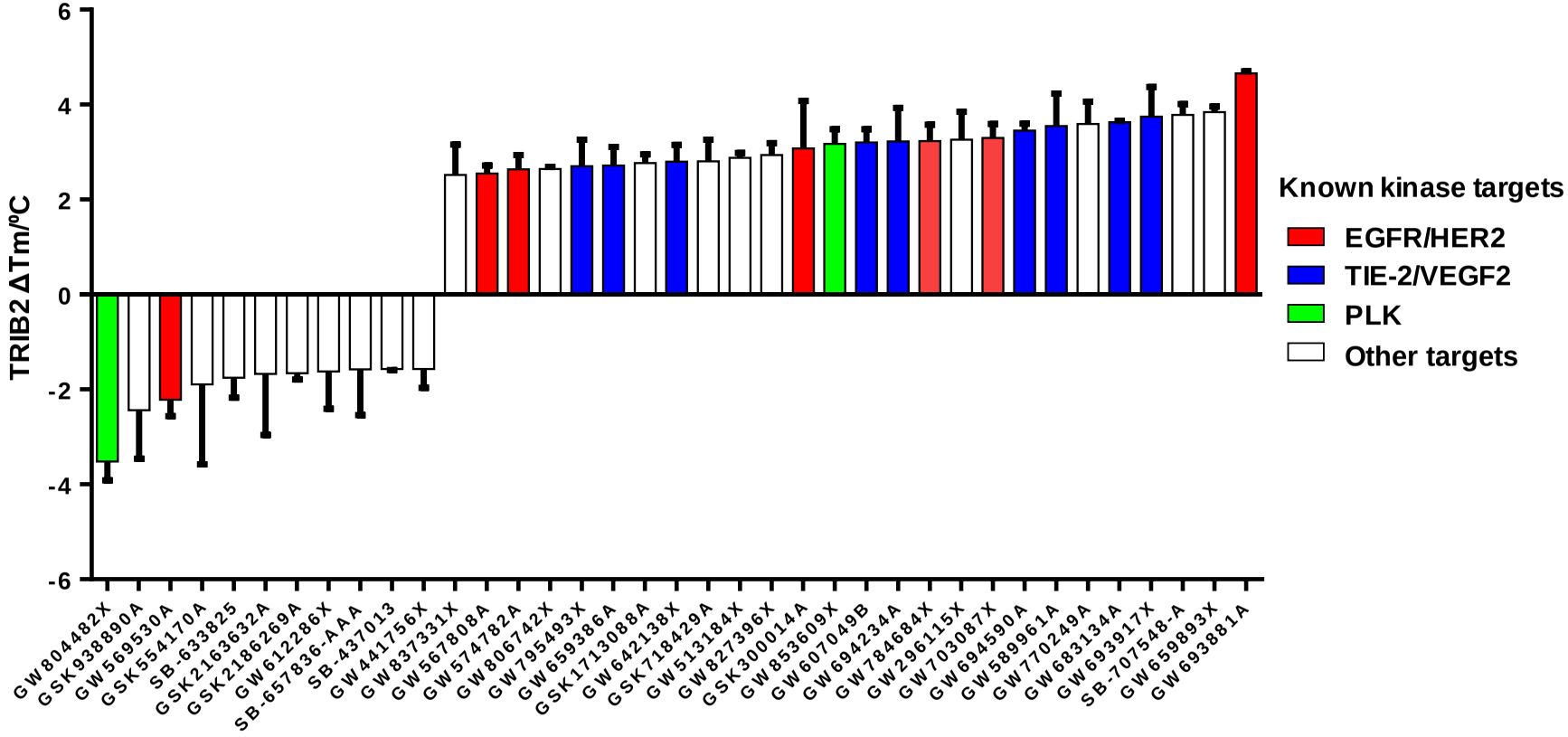


**Figure 3.18: DSF analysis of most stabilising and destabilising PKIS1 compounds**. 5 µM His-TRIB2 and 20 µM of each compound was employed for DSF analysis. $\Delta T_m$ cut off values of <-1.5°C for destabilisers and >2.5°C for stabilisers were employed.

As there were both stabilising and destabilising compounds belonging to known ATP-competitive thienopyrimidine EGFR/HER2 chemotypes (Figure 3.18) [256, 257], which suggested broad cross-reactivity between TRIB2 and EGFR/HER2, ligands from the PKIS 1 were selected and investigated by DSF. The most stabilising compound GW693881A ($\Delta T_m$ ~5°C) (Figure 3.19 top) is structurally similar to GSK969786A and GW68426B, which surprisingly did not modulate TRIB2 thermal stability (Figure 3.19 bottom). Both GSK969786A and GW68426B have a sulphur atom in a different position to GW693881A in the five membered ring of the thienopyrimidine scaffold (Figure 3.19 bottom Highlighted with red asterisks). In addition, a nitrogen is present at the β-position of the adjoining five membered ring in GW693881A, which are oxygen and sulphur atoms in GSK969786A and GW68426B (respectively), marked by blue asterisks in Figure 3.19 (bottom). Besides these rather subtle differences compounds GW693881A, GSK969786A and GW68426B are structurally identical. Some EGFR/HER2 dual inhibitors destabilised TRIB2. The second most potent destabiliser of TRIB2 in the PKIS1 was the EGFR/HER2 dual Thiazolylquinazoline inhibitor GW569530A (Figure 19).

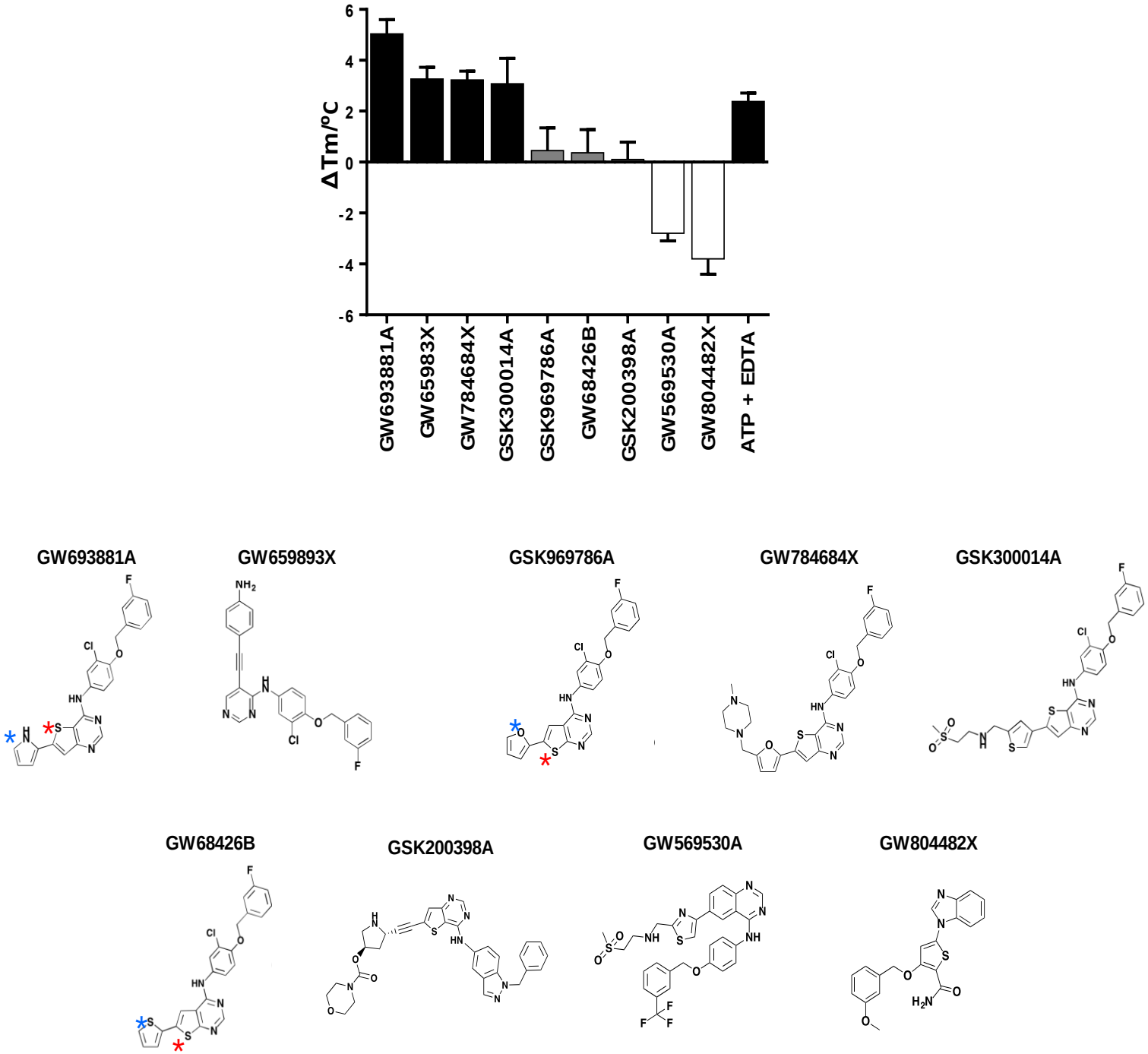


**Figure 3.19: Comparative DSF analysis of dual EGFR/HER2 PKIS inhibitors as potential TRIB2 ligands.** DSF analysis of selected compounds (TOP) and chemical structures of compounds (bottom).

### 3.7.3 Counter-screen with PKA and a TRIB2 β3 K90M mutant

The β-3 lysine (K90 in TRIB2) is pivotal for ATP binding in most canonical kinases, with mutation to an uncharged Met reducing ATP binding ability [58, 258]. Therefore His-TRIB2 K90M was purified sequentially by IMAC and SEC (Figure 3.20A). The yield of K90M TRIB2 was far lower than that of WT-TRIB2 (<0.1 mg per L of bacteria) and this decreased stability was reflected in the sharply reduced $T_m$ of purified K90M TRIB2 (30.2˚C) compared to WT TRIB2 (39.9˚C) (Figure 3.20B).

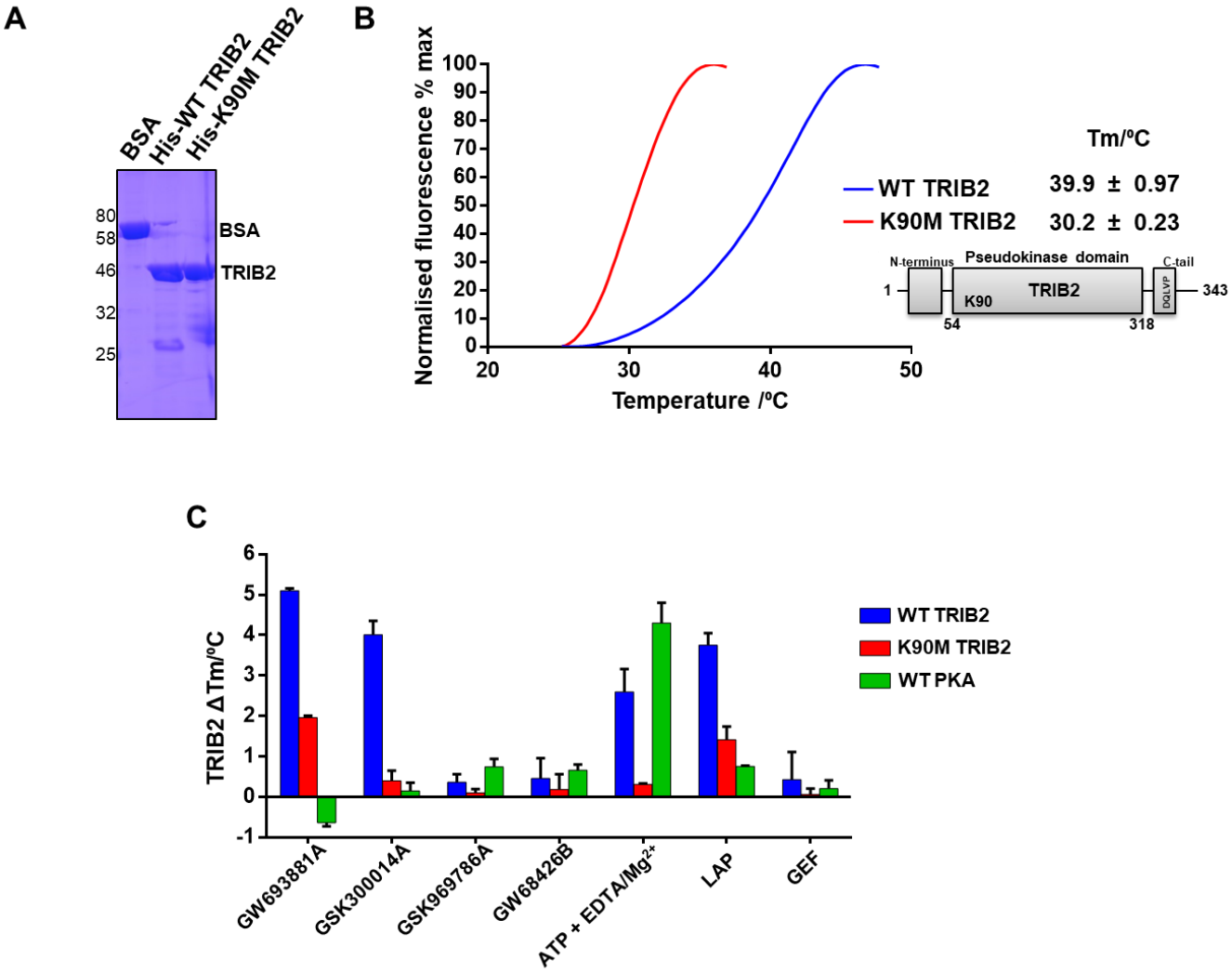


**Figure 3.20: Comparative DSF analysis between WT TRIB2, a β3 lysine K90M TRIB2 mutant and PKA**. (A) SDS PAGE analysis of purified WT and K90M His-TRIB2 (5 µg) electrophoresed side by side along with 5 µg of BSA. (B) Thermal denaturation profiles of WT and K90M TRIB2. (C) DSF analysis comparing binding of selected PKIS thienopyrimidine dual EGFR/HER2 inhibitors and clinical inhibitors lapatinib (LAP) (dual EGFR/HER2) and gefitinib (GEF) (EGFR) to WT TRIB2, K90M TRIB2 and PKA. ATP + EDTA served as the positive control WT TRIB2 and ATP + $Mg^{2+}$ served as the positive control for PKA.

To evaluate the relative specificity of PKIS 'hit' TRIB2-binding compounds, a counter-screen was performed employing PKA and K90M TRIB2 using two of the most highly stabilising EGFR/HER2 ligands (GW69388A and GSK300014A) and two non-stabilising EGFR/HER2 ligands (GSK969786A and GW68426B) (Figure 3.20C). ATP and EDTA were used as the positive control for TRIB2 and ATP and $Mg^{2+}$ was used as the positive control for PKA. The clinically approved dual EGFR/HER2 inhibitor lapatinib as well as the clinically approved EGFR inhibitor gefitinib were also tested. GW69388A strongly stabilised TRIB2 by ~5˚C the effect of which was acutely reduced to ~2˚C for K90M TRIB2. On the other hand, GSK300014A induced a $\Delta T_m$ of ~4˚C for WT TRIB2 but did not promote any significant stabilisation of K90M TRIB2. PKA exhibited no response to either of these compounds or the two EGFR/HER2 non-stabilisers (GSK969786A and GW68426B). The clinically approved and commercially available thienopyrimidine based dual EGFR/HER2 inhibitor lapatinib did in fact stabilise WT TRIB2 ($\Delta T_m$ 4˚C). The 1.5˚C shift exhibited by K90M TRIB2 indicated a reduced affinity for lapatinib. Interestingly, the clinical monovalent EGFR inhibitor gefitinib afforded no significant thermal stabilisation or destabilisation for any of the proteins tested and would hence forth serve as a negative control for TRIB2.

## 3.8 DSF screen for TRIB2 interaction with clinically approved kinase inhibitors

In order to build upon the finding that some compounds originally developed to bind to the catalytic domain of EGFR, HER2 and PLK tyrosine kinases also influenced TRIB2 thermal stability, it was hypothesised that the cross reactivity observed could be exploited to repurpose clinical inhibitors to target TRIB2. To this end a panel of commercially available inhibitors were analysed for their ability to modulate recombinant TRIB2 stability by DSF.

### 3.8.1 Screen of EGFR, EGFR/HER2 and PLK inhibitors

Screening a panel of commercial EGFR/HER2 and PLK inhibitors revealed that the clinical type I EGFR/HER2 inhibitors TAK-285 and lapatinib potently stabilised TRIB2 to a greater extent than ATP and EDTA (Figure 3.21A). In addition, the Type IV irreversible EGFR/HER2 inhibitors afatinib, neratinib, osimertinib, dacomitinib and

canertinib were also tested. The type IV irreversible inhibitor of Bruton's Tyrosine Kinase (BTK) ibrutinib [259] was also tested. EGFR/HER2 type IV inhibitors contain a strategically positioned highly electrophilic acrylamide group designed to covalently bind to specific thiol functional groups found in target cysteines, such as Cys 797 in EGFR, Cys805 in HER2 and Cys803 in HER4 [207]. Remarkably, afatinib, neratinib and osimertinib induced a thermal shift in TRIB2 through destabilisation. The extent of which was comparable to the most potent destabilising hit from the principal screen (PLK1 inhibitor GW804482X), inducing $\Delta T_m$ values of -3.0˚C, -2.5˚C and -2.3˚C for afatinib, neratinib and osimertinib respectfully. Surprisingly, the closely related type IV EGFR/HER2 inhibitors dacomitinib and canertinib had no effect on TRIB2 stability. Afatinib, neratinib, osimertinib and canertinib share a quinazoline-based scaffold (Figure 3.21B) developed from gefitinib [213]. Differential binding properties based on compounds with subtle differences in the positions of functional groups were highlighted in section 3.7.2 (Figure 3.19).

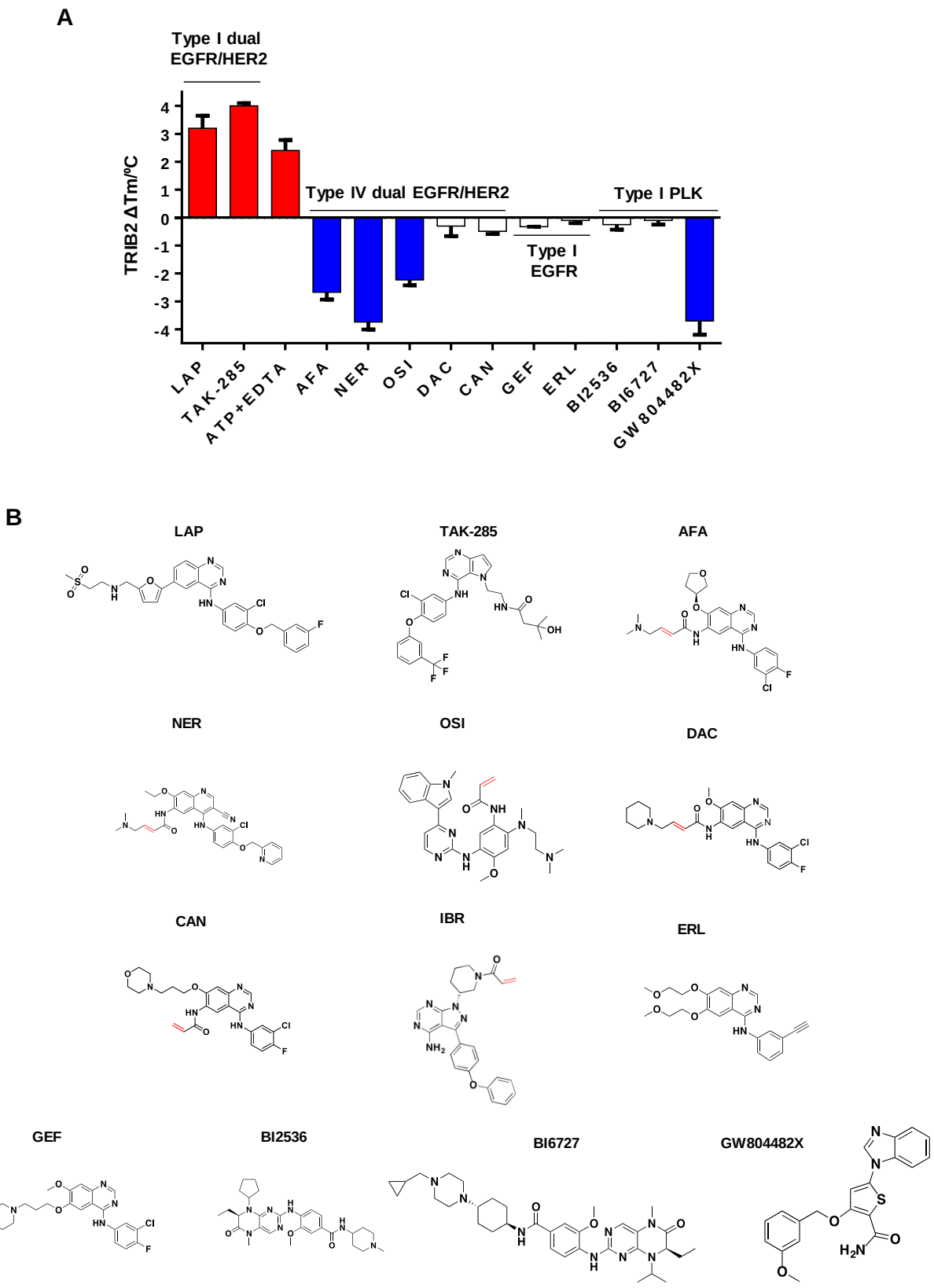


**Figure 3.21: Comparative DSF analysis of clinical and preclinical kinase inhibitors as potential TRIB2 ligands**. (A) DSF of TRIB2 with selected clinical and preclinical kinase inhibitors**:** lapatinib (LAP),

TAK-285 (TAK), afatinib (AFA), neratinib (NER), osimertinib (OSI), ibrutinib (IBR), erlotinib (ERL), and gefitinib (GEF). (B) Structures of listed small molecule kinase inhibitors.

Ibrutinib, the covalent BTK inhibitor, afforded no thermal stabilisation or destabilisation for TRIB2 in the DSF assay as did both type 1 clinically approved EGFR inhibitors gefitinib and erlotinib (Figure 3.21A). PLK type 1 inhibitors BI2536 and BI6727, are dihydropteridinone derivatives which contain 2-aminopyrimidine (Figure 3.21B). Only thiophene based PLK inhibitors appear to modulate TRIB2 stability; GW804482X induced a thermal destabilisation of -3.9˚C (Figure 3.21A) and GW853609X a thermal stabilisation of +3.2 (Figure 3.18).

By employing PKA, afatinib, neratinib, osimertinib, erlotinib and lapatinib were counter-screened at the highest inhibitor to protein ratio (1:32) tested in Figure 3.22. The purpose was to elucidate the potential presence of non-specific interactions at high inhibitor concentrations. The promiscuous kinase inhibitor Dasatinib, which has previously been shown to induce a strong thermal shift for PKA in the DSF assay [250], was used as a positive control and gave a $\Delta T_m$ of 11.08˚C (Figure 3.22). Afatinib, neratinib, osimertinib, erlotinib and lapatinib did not result in any discernible thermal shift when 5 µM of PKA was analysed with 160 µM compound demonstrating no non-specific binding.

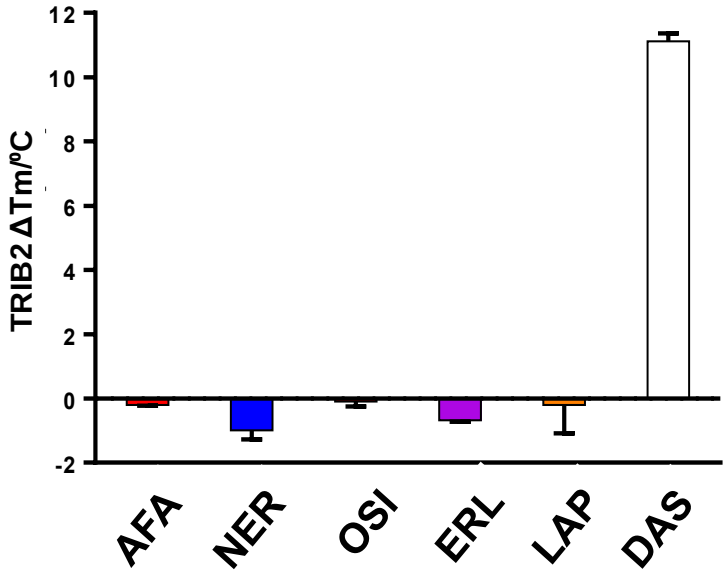


**Figure 3.22: Screen of EGFR/HER2 inhibitors with PKA**. 5 µM His-PKAc thermal shifts were analysed in the presence of a panel of dual EGFR/HER2 or EGFR inhibitors (final concentration 160

μM), confirming a lack of binding. The PKA-stabilizing compound dasatinib (160 μM) was employed as a positive control. Data from N=2 experiments (± SD) for triplicate assays are shown.

To determine that the extent of TRIB2 thermal stabilisation/destabilisation was dependent on kinase inhibitor concentration, a dose-response experiment was conducted (Figure 3.23A). At 5 μM (1:1 protein:compound), lapatinib began to induce detectable TRIB2 stabilisation ($\Delta T_m$ 1.6˚C ± 0.04). At 10 μM (2:1) lapatinib induced a thermal stabilisation comparable to 10 mM of ATP ($\Delta T_m$ 2.40˚C ± 0.02). By 20 μM (4:1) maximal stabilisation afforded by lapatinib was reached with a $\Delta T_m$ 3.25˚C, with a similar thermal shift observed at 160 μM inhibitor concentration. Destabilisation of TRIB2 by all three covalent EGFR/HER2 inhibitors, occurred in a dose-dependent manner. Neratinib appeared to have the strongest affect, inducing marked destabilisation at 5μM ($\Delta T_m$ 2.58˚C) and a maximal destabilisation at 160 μM inducing a thermal shift of 6.18˚C. Afatinib was the second most potent of the type IV inhibitors, influencing TRIB2 stability in a dose dependent manner with a maximal destabilisation of 4.57˚C at 160 μM compound concentration. Osimertinib, whilst inducing destabilisation in a dose dependent manner (maximal $\Delta T_m$ of -2.98˚C exhibited at 80 μM), was least effective. Consistent with our previous findings erlotinib at all concentrations tested did not produce a detectable thermal shift in TRIB2.Denaturation profiles (Figure 3.23B) show that inhibitors in relation to DMSO (black) induce typical thermal shifts.

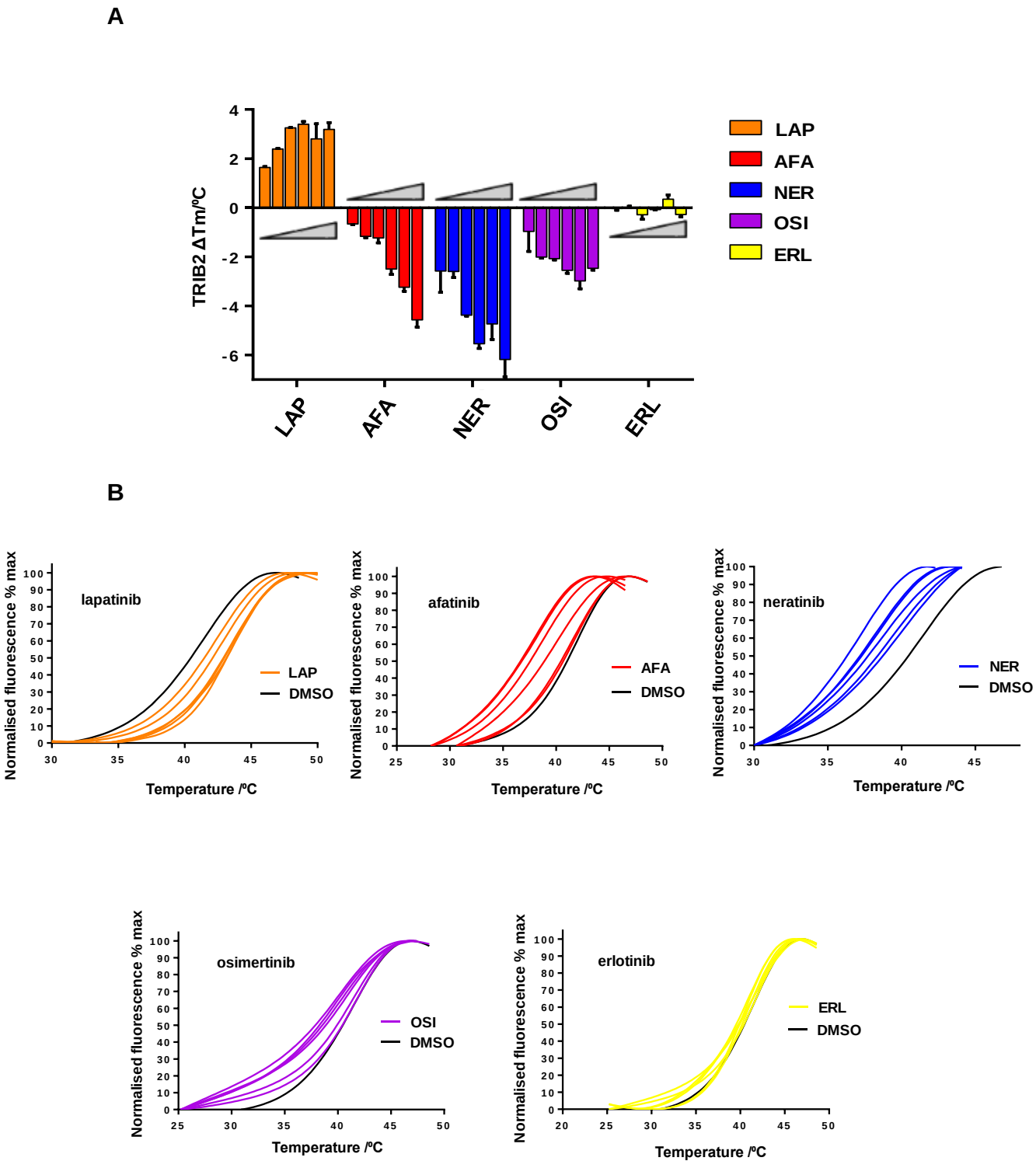


**Figure 3.23: Dose-dependent analysis of thermal shifts induced by clinical TRIB2 ligands**. (A) Thermal shifts of 5 μM TRIB2 in the presence of compounds tested at 5, 10, 20, 40, 80 and 160 μM. (B) Thermal denaturation profiles of TRIB2 in the presence of increasing concentrations of inhibitor.

### 3.8.2 Binding analysis of TRIB2 using Microscale Thermophoresis (MST)

To further evaluate compound interactions with TRIB2, Microscale Thermophoresis (MST), a biophysical technique that detects the motion of fluorescent labelled proteins along a microscopic temperature gradient in a capillary, was used [260]. By exploiting the 6xHis tag, WT TRIB2 was labelled with nitrilotriacetic acid (NTA) conjugated to a fluorescent tag. 0.001-100 µM of compounds were titrated into 5µM of labelled TRIB2. Due to poor solubility of compounds in Tris pH 7.4, 100 mM NaCl and 1 mM DTT accurate data past 100 µM compound concentration could not be obtained. An interaction between afatinib and fluorescent NTA-coupled His-TRIB2 was detected, which could be fitted to a reversible binding event with a K*d* value of ~16 µM (Figure 3.24A). As MST is designed to evaluate saturated, reversible binding of small molecules to proteins, it can be argued that this value reflected the initial (reversible) binding before covalent modification [261]. To lend further support to this idea, the reversible EGFR/HER2 inhibitor TAK-285 was also tested, resulting in a predicted K*d* of ~20 µM (Figure 3.24B). For a positive control Myeloid cell leukemia 1 (Mcl-1), a pro-survival member of the Bcl-2 family (regulators of apoptosis) was assayed by MST in the presence of a selective inhibitor, A1210477. A sub-micromolar interaction of 740 nM between MCL-1 and A1210477 was observed (Figure 3.24C) [262]. Previous TR-FRET binding affinity assays for MCL-1 and A1210477 revealed a K*d* of 430 nM [263].

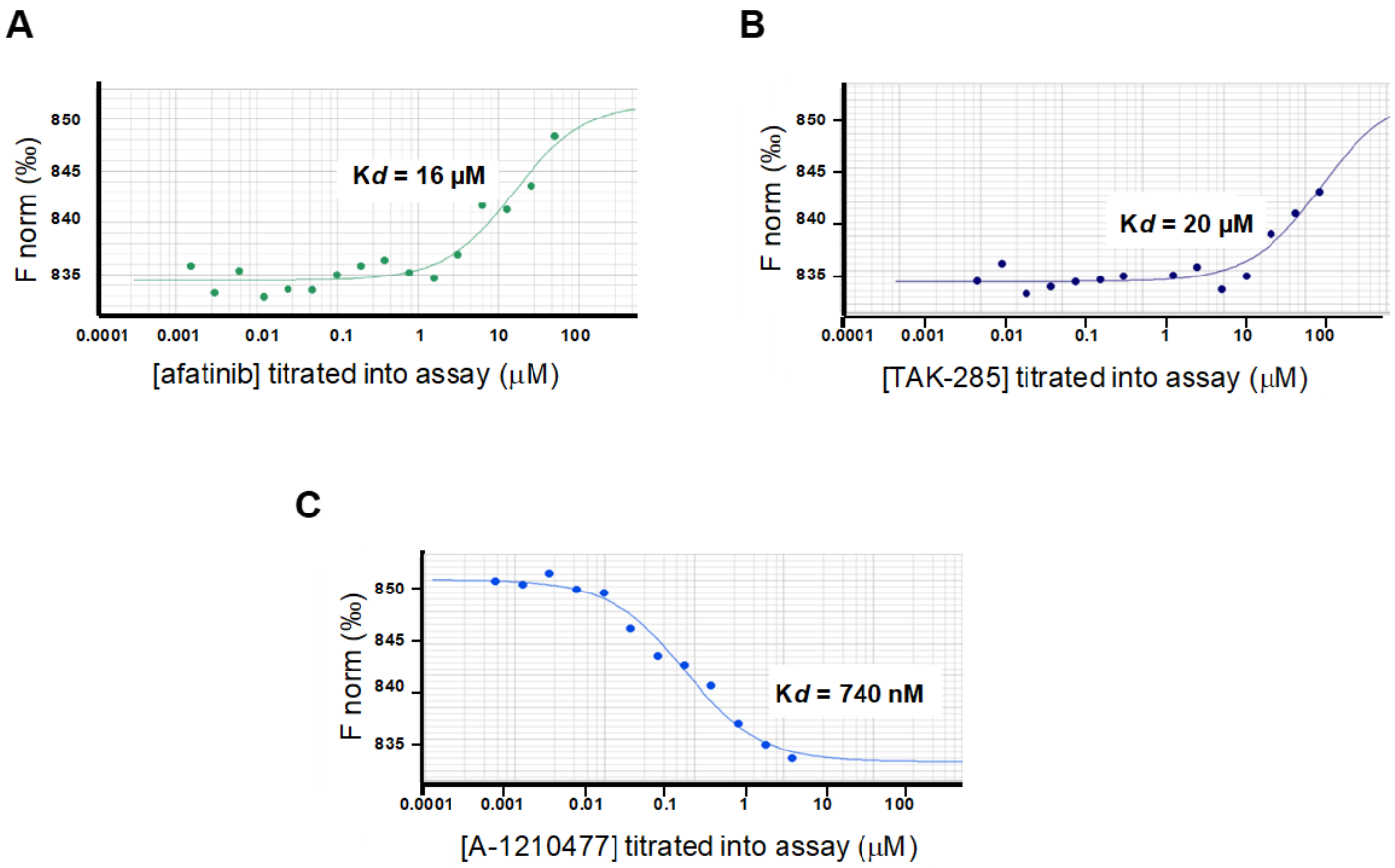


**Figure 3.24: Microscale Thermophoresis (MST) analysis of compound binding**. (A) MST analysis of reversible binding of afatinib to fluorescently labelled TRIB2. (B) MST analysis of reversible binding of TAK-285 to TRIB2. (C) Positve control of high-affinity (sub-micromolar) binding of A-1210477 to MCL-1. Data for duplicate experiments were plotted.

### 3.8.3 Counterscreen employing TRIB1 and C104Y TRIB2

In order to test the mechanism and selectivity of the TRIB2 ligands discovered from DSF screening, TRIB1 84-372, TRIB1 84-343 and the 'TRIB1-like' C104Y TRIB2 mutant were counter-screened. The αC-helix region of TRIB2 possesses distinct Cys residues at positions 96, 104 and 106, that are not present in TRIB1, TRIB3 or STK40 (Figure 3.25B). As TRIB1 and C104Y TRIB2 are not destabilised by afatinib, neratinib or osimertinib, these distinct Cys residues could potentially be sites of covalent modification by type IV inhibitors.

As controls, the type IV inhibitors afatinib, neratinib and osimertinib destabilised TRIB2 ($\Delta T_m$ -2.9, -3.3 and -2.1°C) (Figure 3.25A). Afatinib, neratinib and osimertinib did not destabilise either of the TRIB1 proteins analysed. TRIB1 84-372 in fact showed

a consistently positive $\Delta T_m$ of ~1°C in the presence of both afatinib and osimertinib. Remarkably, upon mutation of Cys104 to Tyr in TRIB2, neratinib induced a positive thermal shift of 2.6˚C, confirming the importance of this TRIB2 residue in compound binding. Importantly, the type I PLK inhibitor GW804482X also destabilised C104Y TRIB2 and both TRIB1 proteins (Figure 3.25A). Consistently, lapatinib and TAK-285 strongly stabilised WT-TRIB2 and C104Y TRIB2. Both TRIB1 proteins displayed a modest increase in melting temperature in the presence of lapatinib ($\Delta T_m$ 1.68°C and 1.54°C respectively) but not TAK-285. The established TRIB2 negative control EGFR type I inhibitor gefitinib did not induce a thermal shift in any of the proteins assayed. Finally, ATP did not induce a thermal shift in C104Y TRIB2 or either TRIB1 proteins, consistent with the TRIB1 crystal structure, which revealed an active site that occludes ATP binding due to the Tyr134 (Cys104 in TRIB2) causing the αC-helix and 'SLE' motif to adopt an inward orientation. The Leu226 residue of the SLE motif in TRIB1 is directed towards a binding pocket overlapping with the position usually occupied by the gatekeeper residue (Phe160), which is instead displaced towards the hinge region of the N- and C-terminal lobes [106]. In this 'SLE-out' conformation Leu226 of TRIB1 stabilises the activation loop which obstructs the ATP binding pocket. The 'SLE-in' conformation, associated with conformational rearrangement upon C/EBPα substrate binding, in TRIB1 opens the a binding pocket that can bind to small molecule ATP mimicking inhibitors but not ATP [105].

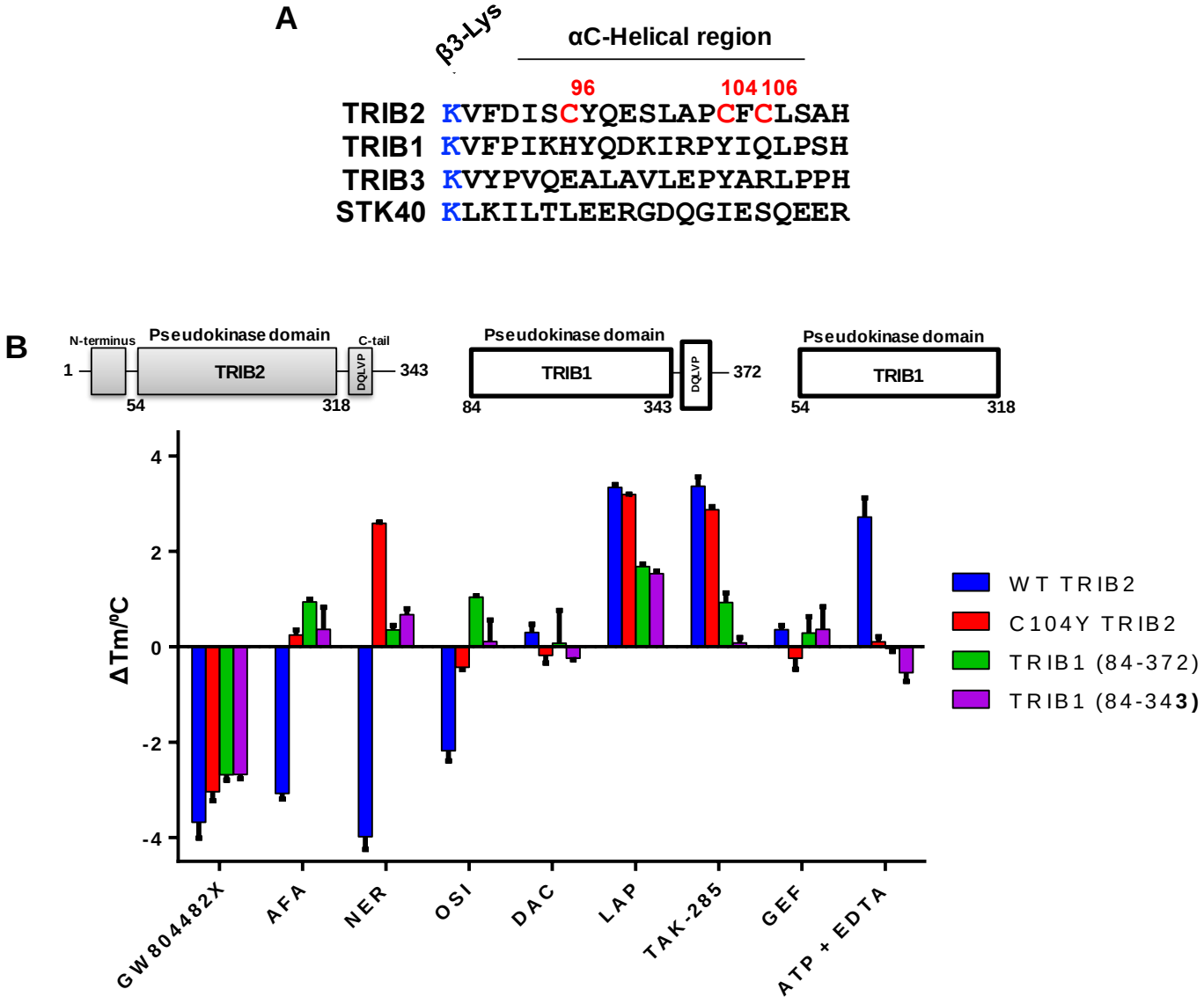


**Figure 3.25: Counter-screen of TRIB2 with a TRIB2 C104Y mutant and TRIB1**. (A) DSF analysis of WT TRIB2, C104Y TRIB2, TRIB1 84-372 and TRIB1 84-343 in the presence of selected compounds. (B) Sequence alignment of the TRIB2, TRIB1, TRIB3 and STK40 β3-Lys and 'αC-Helix' revealing unique perhaps targetable Cys residues in TRIB2.

## 3.9 Mechanistic analysis of destabilisation

As it was shown in section 3.6 that TRIB2 is stabilised by the C-terminal tail, it was next hypothesised that destabilisation of TRIB2 upon binding of type IV EGFR/HER2 inhibitors resulted in displacement of the TRIB2 C-terminal tail.

The thermal stability of the previously described TRIB2 truncation and AQLAA mutants (Figure 3.14) was assessed in the presence of selected kinase inhibitors, in order to interrogate the nature of TRIB2 stabilisation/destabilisation in the context of compound binding (Figure 3.26). As observed before, Full-length (1-343) TRIB2 was destabilised by covalent type IV EGFR/HER2 inhibitors afatinib and neratinib and the reversible type I PLK inhibitor GW804482X. Accordingly, the type I EGFR/HER2 inhibitors lapatinib and TAK-285 stabilised TRIB2. Consistently, the EGFR-specific inhibitor erlotinib had no discernible effect (Figure 3.26). The N-terminal deletion mutant of TRIB2 (54-343) displayed similar behaviour to WT when assayed by DSF; the TRIB2 N-terminus had no effect on $\Delta T_m$ values induced by any of the compounds. Conversely, in all proteins where the C-terminal tail was deleted (1-318 and 54-318) or mutated (AQLAA) afatinib and neratinib induced destabilisation was prevented. Interestingly, the C-Terminal deletion had negligible effect on GW804482X binding, supporting the hypothesis that type I compound binding modulates TRIB2 stability through an alternate mechanism.

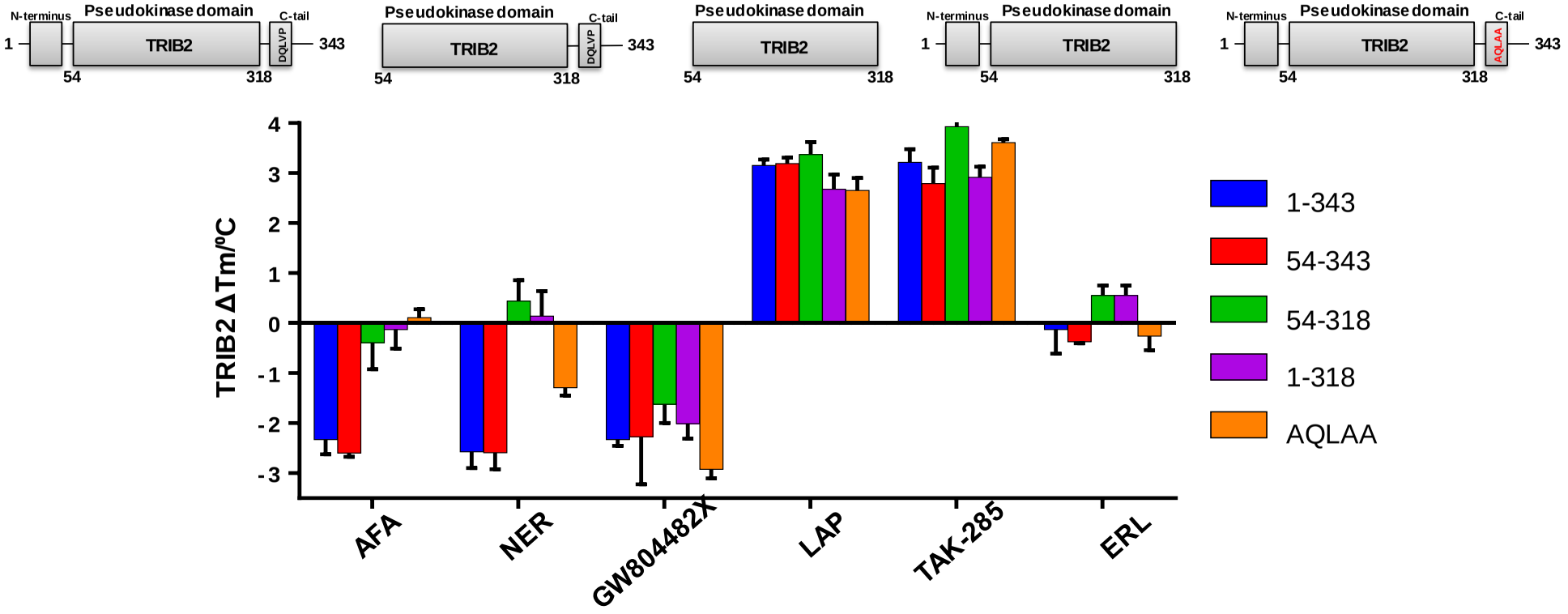


**Figure 3.26: DSF thermal shift analysis of truncated and AQLAA TRIB2**. Change in thermal stability of TRIB2 proteins (5 μM) measured in the presence of a panel of compounds (20 μM), with reference to buffer, 2% (v/v) DMSO controls.

Destabilisation by afatinib was also completely prevented in the AQLAA triple mutant, whereas neratinib effects were reduced by >50% (Figure 3.26). Furthermore, the destabilisation/stabilisation effect of GW804482X and lapatinib/TAK-285 was analogous to that observed in full-length TRIB2 (1-343).

Previous ITC studies showed that a fusion protein, containing the C/EBPα recognition sequence, had reduced affinity for the pseudocatalytic domain in the presence of the C-terminus (K*d* 7.2 μM) compared to the C-terminal deletion mutant (K*d* 11 μM) [106]. This difference in affinity suggested competition between C/EBPα and C-terminal peptide binding. Following this, it can be proposed that an equilibrium exists between C-terminal peptide binding and dissociation resulting in ‘stabilised/closed’ and ‘destabilised/open’ states, the latter potentiated by type IV inhibitor binding in TRIB2.

## 3.10 Investigating covalent binding of type IV clinical inhibitors to TRIB2

Cysteines are ideal for targeting ‘drug-resistant’ EGFR kinases, because the reactive thiol side-chain potentially represent an irreversible covalent target, depending on redox state [261], within the ATP-binding site for covalent type IV inhibitors [264, 265]. Afatinib, neratinib, osimertinib, dacomitinib and canertinib are type IV inhibitors of EGFR and HER2 tyrosine kinases [264], and function by first reversibly binding to the catalytic domain of their targets (Cys797, Cys805, or Cys803 for EGFR, HER2, and HER4, respectively). The conformational changes associated with initially reversible binding to the catalytic domain potentially brings the cysteine residue closer to the β-carbon of the enamide functional group. Subsequently the sulfhydryl of the Cys residue becomes deprotonated by a base and performs an electrophilic attack on the β-carbon of the enamide moiety in a Michael 1,4 addition reaction to form a covalent adduct [265] (Figure 3.27). This mechanism is hypothesised to instigate covalent binding of afatinib and neratinb to distinct cysteines of TRIB2.

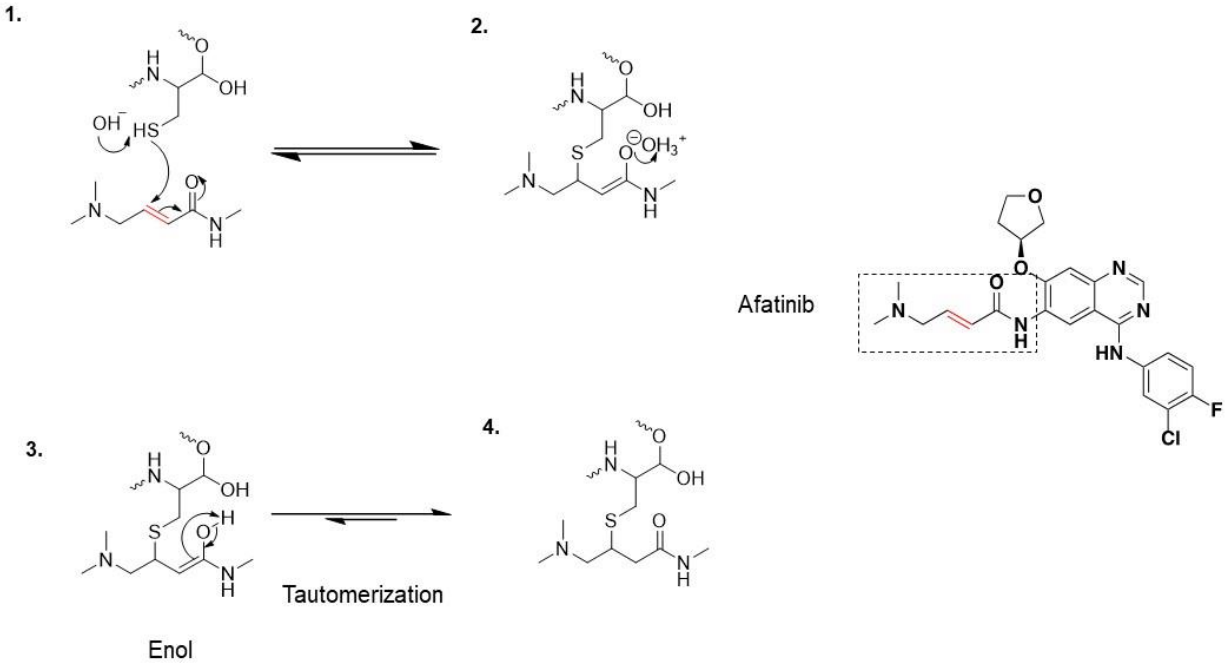


**Figure 3.27: Proposed chemical mechanism of covalent inhibitor binding to cysteine residues by a Michael 1-4 addition**. 1. The sulphur in the thiol of a cysteine in a polypeptide becomes deprotonated by a base and performs electrophilic attack on the β-carbon, which causes an electron rearrangement and formation of an enolate. 2. The enolate becomes protonated to form an enol. 3. The enol tautomerizes to a more energetically favourable state through bond rearrangement.

### 3.10.1 Covalent binding of AFA and NER to TRIB2

In order to confirm whether afatinib and/or neratinib covalently interact with TRIB2, mass spectrometry (MS) analysis was performed (Figure 3.28A). As these inhibitors possess an electrophilic 'warhead' designed to covalently modify target cysteine residues, it was hypothesised that afatinib and neratinib covalently bind to TRIB2 at a certain solvent exposed cysteine residue(s). As shown in Figure 3.28A the intact mass spectrometry (MS1) of 5 µM TRIB2 1-343, incubated with 25 µM of afatinib for 15 minutes, revealed peaks corresponding to His-tagged TRIB2 1-343 with the added mass of either 1 or 2 afatinib molecules. Subsequently a chymotryptic digest and Higher-energy collisional dissociation (HCD) mass spectrometry (MS2) revealed a product ion representing the TRIB2-derived DISC96Y:afatinib peptide adduct at m/z 543.2 (Figure 3.28B). Unequivocal evidence that the modification of TRIB2 at Cys96 was due to afatinib came from the characteristic nature of the measured:theoretical isotopic ratio of the $^{35}Cl$ or $^{37}Cl$-containing peptide ions (Figure 3.27C). Evidence of a

second site of covalent modification arose from MS2 analysis of 5 μM TRIB2 incubated with 25 μM neratinib for 15 minutes. A reducing chemotrypsin digest identified a distinct peptide which included Cys96 plus the molecular weight of neratinib (Figure 3.28D). In addition, another peptide containing Cys104 of TRIB2 was found to be modified by neratinib (Figure 3.28E). The MS evidence suggests that afatinib and neratinib can bind to TRIB2 and modify Cys residues 96 and 104 located within the TRIB2 αC-helix (figure 3.25B).

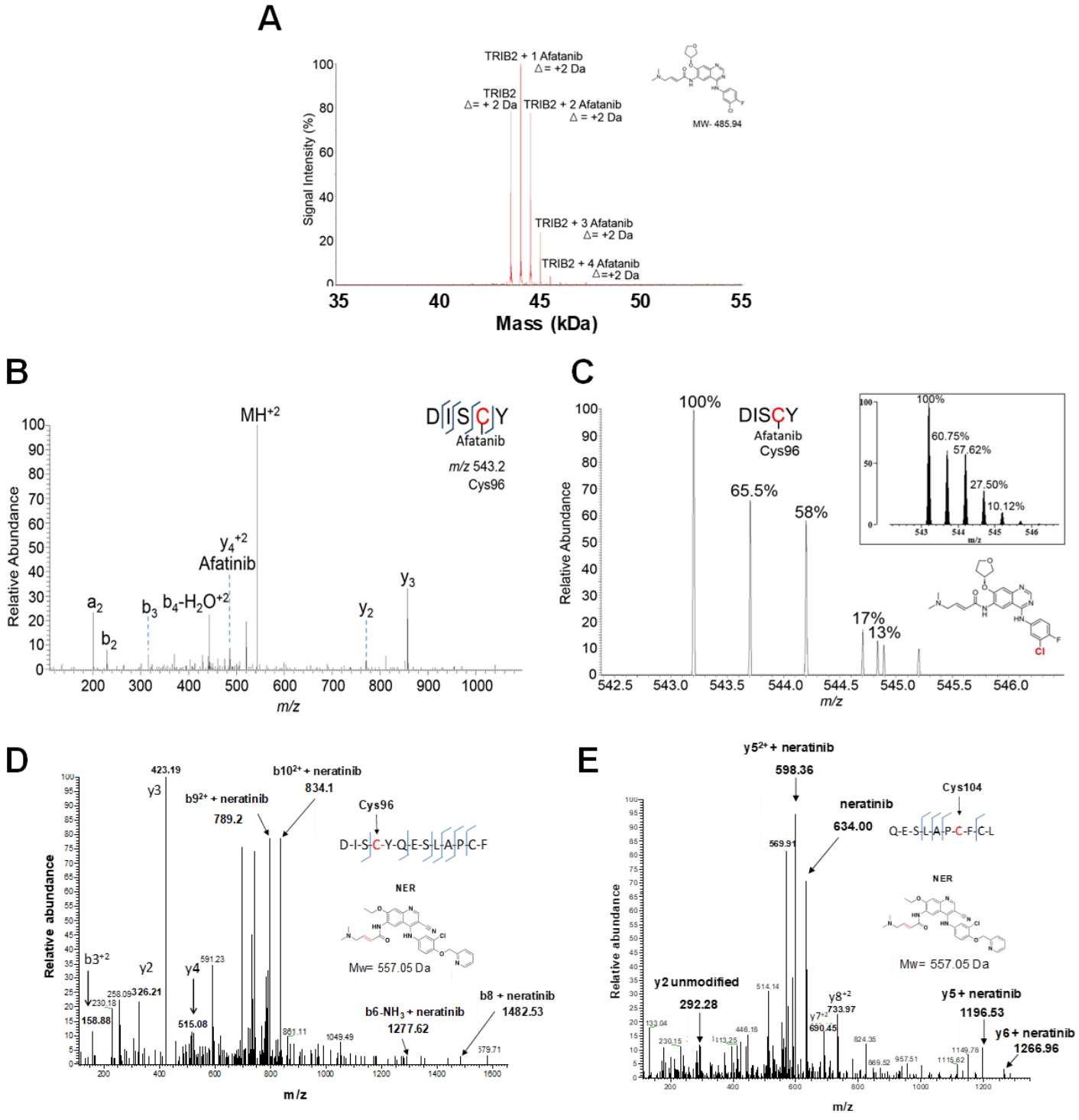


**Figure 3.28: Mass spectrometry (MS) analysis of TRIB2 bound to afatinib and neratinib.** (A) Intact mass spectrum (MS1) for purified TRIB2 pre-incubated with afatinib for 15 minutes at 20°C. (B) MS2 spectra generated by Higher-energy collisional dissociation (HCD) of chymotryptic peptides derived from 5 μM full length His-tagged TRIB2 1-343 incubated with 20 μM afatinib for 15 minutes The doubly charged ion at *m/z* 543.2 confirms covalent binding of afatinb to Cys96 in the diagnostic Asp-Ile-Ser-Cys96-Tyr tetrapeptide derived from chymotrypsin digestion. (C) The isotopic distribution for the 543.2 m/z ion precisely matches the theoretical isotopic distribution for an ion containing chlorine isotopes $^{35}Cl$ and $^{37}Cl$, which are present in the spectrum due to the chlorofluro-benzyl moiety present in afatinib.

(D) Binding of neratinib to Cys96 and (E) Cys104 of TRIB2. 5 µM of His-TRIB2 was incubated with 25 µM of neratinib for 15 minutes at 20 °C before reducing chymotrypsin digest and HCD MS2 analysis. Product ion mass spectra revealed two TRIB2 peptides modified with neratinib at Cys96 and 104. MS was performed by Samantha Ferries.

### 3.10.2 Analysis of TRIB2 Cys mutations

MS analysis had revealed covalent interactions of afatinib and neratinib with αC-helix Cys residues 96 and 104. To evaluate this binding mode further, recombinant His-TRIB2 C96S, C104S and C96/104S were generated by site directed mutagenesis and purified from bacteria. Proteins were purified by IMAC and SEC to homogeneity (Figure 3.29A). In contrast to the previously described Cys104 to Tyr mutant (Figure 3.9B), mutation of either one or both Cys96 and 104 residues to the closely related amino acid serine did not alter the thermal stability of TRIB2 (Figure 3.29B). DSF assays were then used to assess the thermal stability of the Cys mutant TRIB2 proteins in the presence of selected inhibitors. As demonstrated previously, afatinib and neratinib destabilise TRIB2 by 3.1 and -2.7°C respectively (Figure 3.29C). Interestingly, mutation of either Cys residues, 96 or 104, was sufficient to preclude destabilisation, apparent from the observation of no discernible thermal shift for C96S, C104S or C96/104S TRIB2 in the presence of afatinib and neratinib.

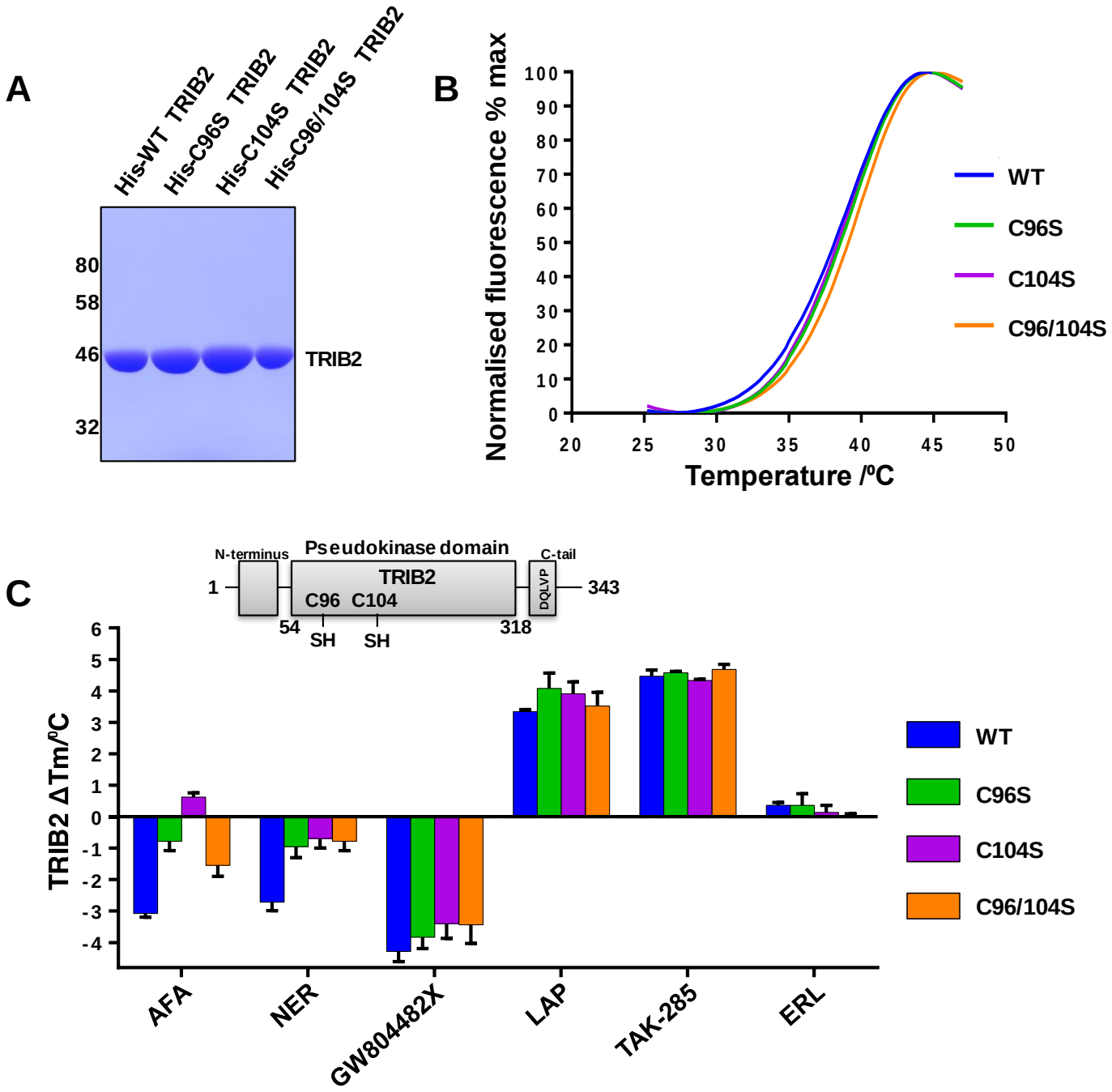


**Figure 3.29: TRIB2 Cys 96 and 104 mutants are not destabilised by type IV EGFR/HER2 inhibitors**. (A) Recombinant TRIB2 cysteine mutant proteins employed for in vitro analysis. 5 µg of the indicated purified proteins were resolved by SDS-PAGE. (B) Thermal denaturation profiles of recombinant proteins. (C) Comparative DSF thermal shift analysis of TRIB2 Cys-mutated proteins measured in the presence of a panel of compounds (20 µM).

The reversible type I PLK inhibitor GW804482X (Figure 3.29C), which was shown previously to destabilise WT TRIB2, has a similar destabilising effect on all TRIB2 Cys mutants, indicative of an alternative (currently unknown) binding mechanism. As

TRIB2 destabilisation was prevented when the Cys residues involved in covalent binding (elucidated by MS) are mutated, it can be hypothesised that the irreversible targeting of these distinct Cys residues induced the destabilisation effect on TRIB2.

Lapatinib, TAK-285 and ATP+EDTA did indeed stabilise WT TRIB2 and all three cysteine mutants. This lends credence to the idea that mutation of residues 96 and 104 to serine was not detrimental to global protein integrity, as the binding of ATP competitive ligands and ATP was not impacted.

### 3.10.3 Computation model of afatinib and neratinib binding to TRIB2

To examine the potential interaction of afatinib and neratinib with the TRIB2 pseudokinase and C-terminal domain (41-343) *in silico*, a model was generated by Dr Natarajan Kannan (University of Georgia), using the crystal structure of TRIB1 as a template in PyMOL. The AutoDock Vina plugin was used in studies to assess compound binding *in silico* [266]. An unbiased search of TRIB2 (41-343) revealed putative binding-pockets close to Cys96 and the potential binding modes for afatinib and neratinib using a covalent docking approach were assessed [267]. Figure 30 shows that the compounds were flexibly docked to the protein by covalently linking the electrophilic enamide to the sulfhydryl Cys. Docking of covalent inhibitors revealed a putative binding pocket formed by residues from the vestigial TRIB2 C-helix, including Cys96, the P-loop and the activation loop.

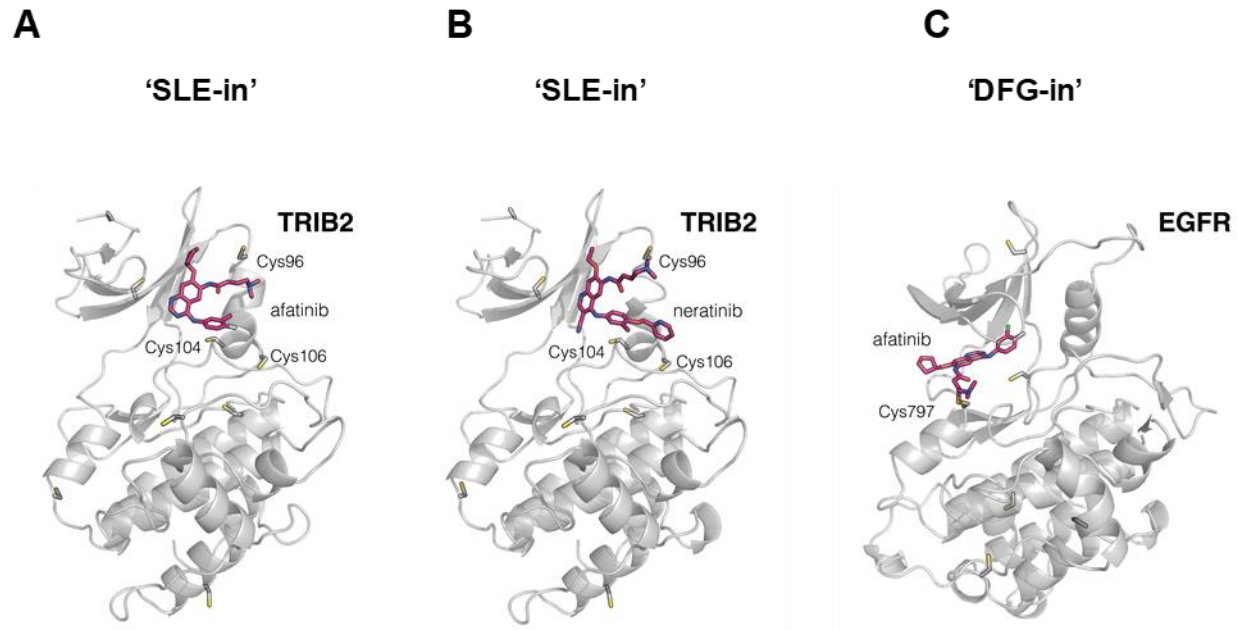


**Figure 3.30: Molecular model of TRIB2 bound to afatinib (A) and neratinib (B)**. The TRIB2 pseudokinase domain was modelled based on an 'SLE-in' TRIB1 crystallographic conformation and subjected to energy minimization followed by docking of compounds revealing the enamine moiety situated next to Cys96. Distinct solvent exposed Cys residues 104 and 106 are also highlighted. (C) Analysis of afatinib binding to the EGFR hinge region (PDB ID: 4G5J) with the tyrosine kinase domain in an active 'DFG-in' conformation. The enamine moiety was revealed to be in close proximity to Cys797 of EGFR. Computational analysis was performed by Safal Shrestha (University of Georgia, USA).

In contrast to the known structure of EGFR bound to afatinib, it was revealed that TRIB2 adopts a unique binding mode that is both structurally and energetically-feasible. In a molecular dynamics simulation (Figure 3.31) both afatinib and neratinib remained stably bound to TRIB2 for ~17 ns. Interestingly a similar time for afatinib and EGFR interaction was reported, giving confidence in this model of TRIB2 covalent modifications. Additionally the enamide β-carbon remained within 3-5 Å of the Cys96 sulphur atom during the simulation, which is a viable distance for covalent adduct formation [213].

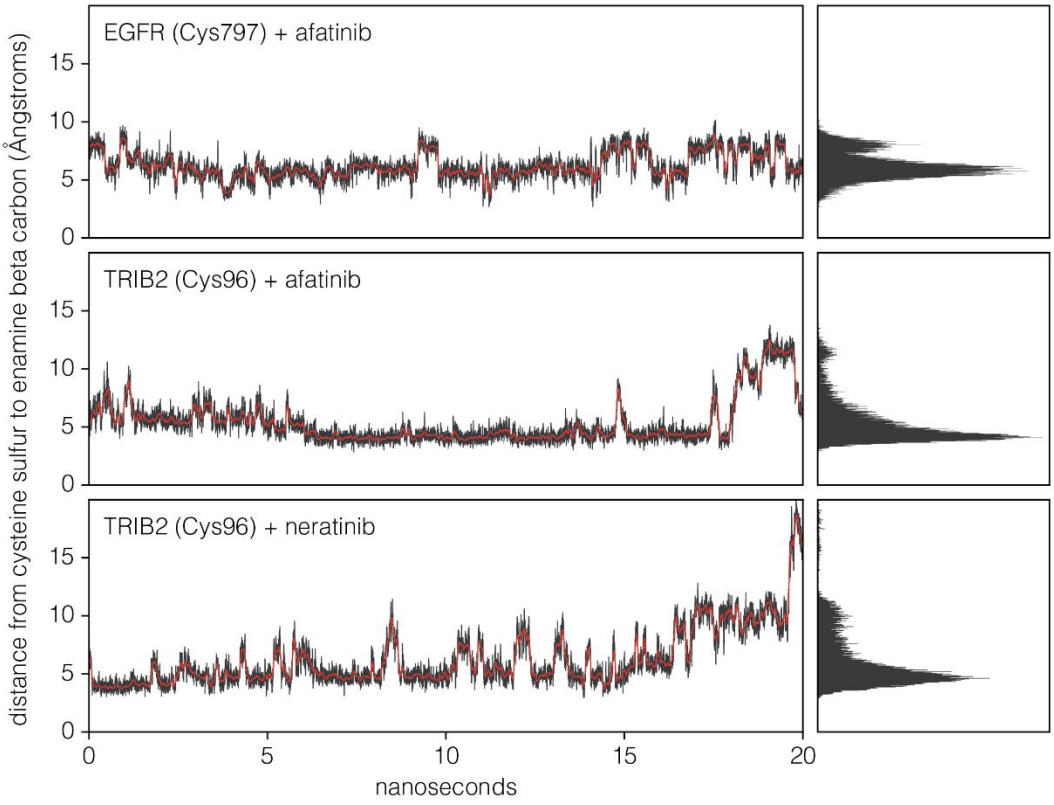


**Figure 3.31: Molecular dynamics simulation of afatinib and neratinib binding to TRIB2 and EGFR**. A 20 nanoseconds (ns) molecular dynamics simulation was employed to analyse binding of afatinib and neratinib in the binding modes modelled in figure 3.30. Interactions of afatinib and neratinib adjacent to EGFR Cys797 and TRIB2 Cys96 were stable for ~17 ns with predicted distance of the sulphur atom to the enamide β-carbon in Å. Analysis was performed by Safal Shrestha (University of Georgia, USA).

The binding surface for the TRIB1 C-terminal tail forms when the activation loop folds away from the αC-helix and the pseudokinase domain is sustained in an 'SLE-out conformation' [105], blocking the putative ATP-binding pocket. Upon substrate binding, and speculatively for TRIB2 upon covalent kinase inhibitor binding (Figure 3.32), the activation loop becomes fully ordered and folds between the N and C lobes of the pseudokinase domain and movement of the αC-helix completes the regulatory spine. Thus, compound binding is proposed to induce an open 'destabilised' conformation in TRIB2 (Figure 3.32).

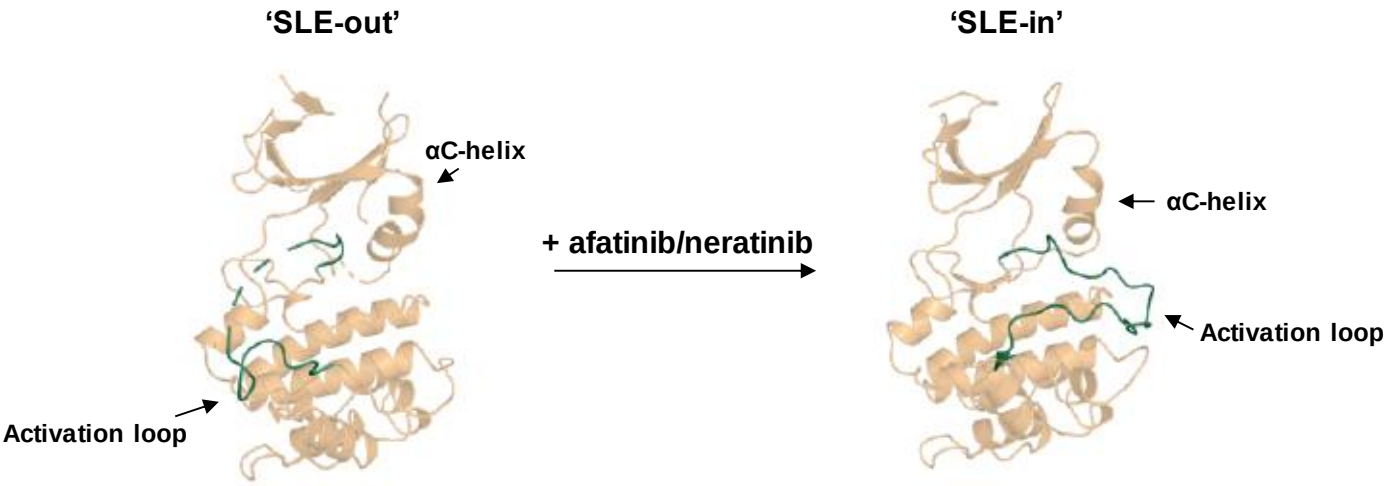


**Figure 3.32: Proposed modulation of TRIB2 conformation upon compound binding**. The crystal structures of TRIB1 in the SLE-in and SLE-out conformation were used to illustrate the proposed conformational change that occurs in TRIB2 upon binding of covalent inhibitors afatinib and neratinib. Data was obtained from Jamieson and colleagues (2018) [105].

## 3.11 Discussion

### 3.11.1 Biochemical characterisation of recombinant TRIB proteins

The aim of the studies carried out in this chapter was to discover novel small molecule ligands that bind to TRIB2 using an unbiased TSA [58, 60]. To this end, functional and folded monomeric recombinant His-tagged human TRIB2, expressed in *E. coli* was purified into a buffer composed of 20 mM Tris pH 7.4, 100 mM NaCl, 1 mM DTT and 10% glycerol. The presence of TRIB2 was confirmed using a combination of SDS-PAGE, MS and immunoblotting. Recombinant TRIB2 had the propensity to aggregate if at a concentration over 5 mg/mL (>100 μM). The instability of monomeric soluble TRIB2 is perhaps a primary factor as to why there is yet no structural information available. Consistent with previous findings TRIB2 was more stable in Bicine pH 9.0 [60] than Tris pH 7.4 and least stable in Hepes pH 7.6, which was incidentally the optimal buffer for TRIB1 purification reported previously [106]. Although TRIB2 was more stable in the presence of reducing agent there was no significant difference between 3 reducing agents tested (TCEP, DTT and BME) (Figure 3.3). Importantly, with DTT as the reducing agent in Tris pH 7.4 buffer, TRIB2 was found to bind to a physiological target, C/EBPα p42 *in vitro* (Figure 3.5).

In agreement with previous findings [60] TRIB2 was thermally stabilised by ATP and EDTA. In contrast to the canonical kinase PKA [250], binding was inhibited in the presence of magnesium ions. Indeed, TRIB2 did autophosphorylate weakly in the presence of ATP and EDTA, but not ATP and magnesium, the canonical co-factor complex in most kinases. Due to the apparent thermal stabilisation in the presence of EDTA alone, and no destabilisation in the presence of magnesium ions alone, it seems logical that EDTA was not only acting as a metal ion chelator but also interacting with TRIB2 (Figure 3.6). Conceivably this interaction allowed TRIB2 to take on a conformation more amenable to ATP binding. As hyper-stable C104Y TRIB2 was not stabilised by either EDTA or ATP (Figure 3.9C), nor was TRIB1 (Figure 3.11B), it is plausible that these proteins were stabilised in an 'SLE-out' conformation. Structural analysis of TRIB1 and TRIB1 co-crystallised with C/EBPα [105, 106], reveals a Tyr residue in the αC-helix at the equivalent (134) position causing TRIB1 to adopt an inactive conformation, consistent with my findings.

Chromatography analysis suggested that the pseudokinase domains of TRIB1 (Figure 3.10) and TRIB2 and the TRIB2 COP1 binding site AQLAA mutant can dimerize (Figure 3.13). This could be indicative of a yet unknown regulatory function of tribbles upon uncoupling of the C-terminal tail. Where TRIB2 was more thermally stable in the presence of the C-terminal tail (Figure 3.14), suggestive of a functional interaction between the C-terminal tail and pseudocatalytic domain, TRIB1 was not (Figure 3.11A). This was surprising since this was not reported previously [106], although this could be explained by an apparent decreased TRIB1 stability with buffer exchange and the protein concentration steps employed. Purified and buffer exchanged TRIB1 84-372 $T_m$ was measured at 41.9˚C (Figure 3.11A). However previous studies reported a TRIB1 84-372 $T_m$ of 49˚C [106]. Strikingly the thermal stability of both the TRIB1 catalytic domain alone (84-343) and with the C-terminal tail (84-372) had a considerably increased melting temperature (~5˚C) in alkaline Bicine pH 9.0 only in the presence of reducing agent (DTT) (Figure 3.12). Understanding potential structural changes in the presence of different buffers would be interesting to elucidate in future experiments.

### 3.11.2 Can the TRIB2 C-tail be uncoupled with stapled peptides?

Previous studies revealed an interaction between C/EBPα and the TRIB1 αC-helix [105, 106], and that competition for binding with the TRIB1 C-terminal tail can take place. Compounds and peptides that compete for binding in the unusual αC-helix region of TRIB2 could modulate binding and signalling outputs of known TRIB2 interactors, for instance C/EBPα, CDC25C and AKT [102, 103, 109]. TRIB2 is involved in a plethora of signalling pathways so, therefore, it may be difficult to decipher TRIB2 outputs with repurposed small molecule inhibitors. In this chapter it was also discovered that a synthetic stapled TRIB2 C-terminal peptide also had the ability to destabilise TRIB2 *in vitro* (Figure 3.15), in a manner that was dependent on the C-terminal region, but did not occur with a scrambled peptide. The TRIB2 catalytic domain alone (54-318) was not as potently destabilised by the TRIB2 C-terminal stapled peptide, indicating that destabilisation results from uncoupling of the TRIB2 C-terminal tail. In contrast, and in a dose-dependent manner, full length TRIB2 was destabilised by such peptides, indicating that peptides can be used to target this unique feature tribbles pseudokinases.

Cell-permeable TRIB2 ‘specific' stapled peptides might therefore be used to investigate signalling *in cellulo*, potentially reducing complication of factoring-in targeted (and off targeted) effects of kinase inhibitors that appear inevitable.

Stapled peptides based on a helix from the Ras exchange factor Son of Sevenless (SOS) have been used to target KRAS [268]. Although successfully inhibiting ERK-MAP kinase phosphosignalling the Ras-binding peptides described by Leshchiner *et al* (2015) are not selective for the GTP-bound form of the Ras protein [268]. In fact, Thomas *et al* (2016) were able to target GTP-bound Ral with a single helix stapled peptide, providing proof-of-principle for the maturation to therapeutically useful antagonists of Ras signalling [269]. Targeting scaffolding functions of TRIB2 with stapled peptides might also modulate interactions with C/EBPα or AKT [103, 109] and have consequences on downstream signalling. The hypothesis that stapled peptides could abrogate PPIs is also supported by studies carried out by Fulton *et al* (2018) who showed that targeting the H-helix of EGFR could prevent dimerization, inhibit phosphorylation and downstream signalling in MDA-MB-231 cell based assays [270].

### 3.11.3 ATP binding and targeting with ATP-competitive inhibitors

The majority of kinase inhibitors are reversible and ATP-competitive, and interact with the ATP binding site in a stereotypical fashion [207, 271]. The mechanism by which most canonical kinases bind and hydrolyse ATP is also highly conserved, therefore, achieving selectivity with small molecules has proven extremely challenging [271]. However, the promiscuity of such inhibitors may be exploited to discover new drug targets, and indeed, targeting of multiple kinase family members in some therapeutic circumstances could be beneficial. Dasatinib, a highly promiscuous type I inhibitor, is approved for the treatment of imatinib-resistant chronic myeloid leukaemia (CML). Kinome wide profiling shows that dasatinib inhibits all nine members of the Src family of kinases (and numerous other kinases) [271, 272]. Despite this lack of selectivity, dasatinib exhibits a more favourable side effect profile than conventional cytotoxic chemotherapy. Indeed compounds have the potential to not only be repurposed as selective TRIB2 ligands, but be used for polypharmacological therapy where TRIB2 is a driver of disease or drug resistance [103, 104, 109]. This, together with previous studies suggesting that TRIB2 is 'druggable' [60], formed the rational to screen TRIB2 using PKIS1 [273].

From screening a library of known small molecule kinase inhibitors (PKIS1) it was discovered that distinct classes of ATP-competitive dual EGFR/HER2 ligands, including thienopyrimidines [257] and thiazolylquianazolines [256] modulated TRIB2 stability when analysed by DSF (Figure 3.17). Several EGFR/HER2 inhibitors are commercially available and a panel was created to analyse alongside TRIB2 by DSF (Figure 3.21). It was discovered that lapatinib and the pyrrolo[3,2-d]pyrimidine EGFR/HER compound TAK-285 strongly stabilised TRIB2. TRIB2 stabilisation could be informative of conformational changes upon inhibitor binding as lapatinib and TAK-285 both bind to HER2 in an active 'DFG in' conformation. In the absence of a high-resolution TRIB2 pseudokinase crystal structure, conformation(s) relevant for small molecule interaction are not yet known. However, there is ~71% sequence similarity between TRIB2 and TRIB1. Critically, TRIB1 can adopt two conformations, 'SLE-in' and 'SLE-out', the former vulnerable to small molecule compounds [105]. Therefore, it is conceivable that an 'SLE-in' conformation in TRIB2 is targeted by small molecule inhibitors. Analysis of a β3 lysine mutant, which suggested that compound binding was in the atypical TRIB2 nucleotide-binding site, offers further support to this conclusion

[258]. Binding of lapatinib was abolished upon mutation of the TRIB2 β3 lysine. This Lys is not only important for interaction with the α and β ATP phosphates, but can also form a salt bridge with a conserved Glu residue in the αC-helix which maintains the kinase domain in an active conformation [37]. However, the melting temperature of TRIB2 K90M was reduced compared to WT (Figure 3.20), suggesting an important role for this residue in global protein stability. Therefore, it is difficult to definitively conclude that these inhibitors are stabilising TRIB2 by binding to the active site or inducing an 'SLE-in' conformation, as K90M may be too dissimilar to WT to glean mechanistic information. The TRIB2 'SLE-out' conformer may also be amenable to inhibitor targeting that bind in an allosteric mode. In an inactive conformation, the positioning of the αC-helix results in exposure of a targetable allosteric binding pocket present in kinases such as ERK1/2, which are targeted by inhibitors including SCH772984 [274].

As well as thienoyrimidine base EGFR/HER2 dual inhibitors, an abundance of benzimidazole based inhibitors, originally designed to target both TIE-2 and VEGFR-2 kinase domains, were discovered. However, due to the availability of various clinical inhibitors with well characterised mechanisms of binding, attention was focused towards EGFR/HER2 clinical type inhibitors. These included type IV irreversible inhibitors afatinib, neratinib and osimertinib, which although initially unexpected, induced a decrease in TRIB2 thermal stability *in vitro* (Figure 3.21).

### 3.11.4 Targeting TRIB2 with type IV EGFR/HER2 inhibitors

Type IV 'third generation' EGFR inhibitors contain well-established kinase inhibitor chemotypes that have been modified to include an electrophilic 'warhead' to react with nucleophilic thiol groups of cysteine residues found in their targets. Structure guided design of type IV from type I inhibitors owes fruition to the availability of high resolution crystal structures. Afatinib, neratinib, osimertinib, dacomitinib and canertinib all possess the same quinazoline-based scaffold as gefitinib with a strategically positioned enamide moiety [213]. Co-crystal structures of gefitinib and afatinib in complex with EGFR confirmed formation of the non-covalent instigated through interaction of nitrogen, on the quinazoline ring in the hinge binding motif, which is required to stabilise compound orientation and give sufficient time for covalent bond formation [213].

Irreversible binding poses serval distinct advantages, including enhanced selectivity, long-lasting cellular inhibition and lower concentrations required at site of action [207, 213]. As it was demonstrated from the PKIS1 DSF screen that EGFR/HER2 dual type I inhibitors seemed to have broad cross reactivity with TRIB2, type IV EGFR/HER2 inhibitors were also tested. Despite being developed from gefitinib, which had no effect on TRIB2 thermal stability, TRIB2 thermal stability was in fact decreased in the presence of afatinib, neratinib and osimertinib but not dacomitinib or canertinib. Interestingly, afatinib, neratinib and osimertinib destabilised TRIB2 but not TRIB1 or C104Y TRIB2 (Figure 3.25) in a dose dependent-manner (Figure 3.23). Although like TRIB2, destabilisation of TRIB1 was evident in the presence of GW804482X, which is perhaps indicative of an alternative targetable conformation in both these Tribbles pseudokinases.

Using MS, it was possible to detect covalent binding of afatinib and neratinib to TRIB2 at residues Cys 96 and 104 (Figure 3.28), mutation of which to Ser residues abolished destabilisation detected by DSF (Figure 3.29). Moreover, these Cys residues are absent in TRIB1, TRIB3 and STK40, which may lead to selectivity to evaluate TRIB2 signalling in cellular contexts. Consistent with this hypothesis, only WT TRIB2 was destabilised by afatinib, neratinib or osimertinib (Figure 3.25) when analysed by DSF. Targeting pseudokinase domains with covalent compounds to investigate signalling builds upon Xie *et al* (2014) who found that the ligand TX1-85-1 was able to covalently bind to HER3 at Cys721 in the roof of the ATP binding pocket, leading to HER3 degradation in cells and in turn inhibited HER3-mediated signalling [62].

In EGFR, binding of afatinib to HER2 induces repositioning of the αC-helix bringing the enamide moiety closer to Cys797. Afatinib and neratinib covalently bind to EGFR, HER2 and HER4 (at Cys 797 in EGFR, Cys805 in HER2 and Cys803 in HER4) [213]. The equivalent residue in HER3 is Ser794, which results in reversible binding of afatinib and conformational change giving rise to an active state with low catalytic activity [131]. The kinetics of reversible interactions of type IV covalent inhibitors were explored by Schwartz *et al* (2014), using nonreactive compound analogues and biochemically by analysing recombinant EGFR with sulfinylated and glutathiolated cysteine residues [261]. MST was used to measure reversible binding of afatinib to TRIB2 with a K*d* of 16 μM (Figure 3.23). Molecular modelling and simulation suggest that the enamide of both afatinib and neratinib and the sulfhydryl of Cys96 in TRIB2

remain ~5 Å apart for ~17 ns, which is thought to be sufficient for covalent bond formation [267].

When the key TRIB2 cysteine residues involved in covalent binding of afatinib and neratinib were mutated, there was no longer any destabilisation (Figure 3.29), supporting the hypothesis that destabilisation results from covalent binding. Presumably there was transient reversible binding event, which did not result in a change in TRIB2 thermal stability. Further biophysical analysis of compound binding to TRIB2 Cys mutants should be considered using ITC and NMR, although poor compound solubility and low protein stability thus far has limited such studies.

### 3.11.5 Mechanistic analysis of TRIB2 destabilisation with covalent compounds

Similar to effects previously observed for TRIB1 [265], when the C-terminal tail (containing the DQLVP motif) of TRIB2 (1-318 and 54-318) was deleted or mutated (AQLAA), protein stability was reduced. These data supports the hypothesis that pseudokinase-domain docking to the C-terminal tail generates a thermally-stable conformation TRIB2. The functional divergence of C-tail interactions, *in-cis,* within the kinase domain has also been observed in AGC kinases PKA, PKB and PKC [24]. The C-terminal tail of AGC kinases possess three separate regions that interact with the kinase domain: the N-lobe tether (NLT), the active-site tether (AST), and the C-lobe tether (CLT). Conservation of the C-tail was also found in AGC kinase family members across diverse organisms, suggesting an evolutionary mode of regulation. The conservation of residues within the kinase domain of AGC kinases that directly interact with the C-tail suggests that the catalytic core may have coevolved with the C-tail [24]. In Tribbles pseudokinases, TRIB2 being the ancestor [104], co-evolution of the pseudokinase domain and regulatory interaction with the C-terminal tail is also apparent. Interestingly, certain TRIB2 orthologues (for instance in the pathogenic thread worm) lack both sequence similarity in the C-terminal tail COP1 binding site and the normally complementary docking region for the tail in the pseudokinase N-lobe [104].

When assayed in the presence of compounds, destabilisation of TRIB2, induced by covalent inhibitors afatinib and neratinib, occurred only in the presence of an intact C-terminal tail (Figure 3.26). This indicated that compound-induced destabilisation resulted from the TRIB2 pseudokinase domain becoming uncoupled from the C-tail.

The orientation of the ‘SLE’ motif which creates a binding pocket for the E3 ubiquitin ligase binding motif (DQLVP) in the C-terminal tail could be a unique feature of Tribbles pseudokinases [105, 106]. The dynamic interaction between the TRIB2 C-terminal tail and pseudokianse domain could potentially be targeted with small molecule inhibitors.

In Chapter 4 I address the use of small molecules to target exogenous and endogenous TRIB2 in human cells. By using mutagenesis and cellular thermal shift assays (CETSAs) as validation approaches, and by analysing TRIB2 signalling outputs in intact cells, I have begun to elucidate targeted interactions of compounds with TRIB2. Such an initial analysis is important to determine whether or not small molecule kinase inhibitors can be used as chemical probes to evaluate cellular functions of TRIB2 and to furnish the first potential therapeutic leads for evaluation of diseases associated with TRIB2 (over)expression [275].

# Chapter 4: Investigating TRIB2 with small molecule kinase inhibitors in human cells

## Introduction

In chapter 3, I demonstrated that TRIB2 pseudokinase-domain intramolecular docking to the C-terminal tail generated a thermally-stable conformation in TRIB2, and that covalent binding of several type IV (covalent) dual EGFR/HER2 inhibitors disturbed this interaction, causing TRIB2 to adopt a destabilised conformation. In this chapter I address whether small molecules that bind to TRIB2 *in vitro* can be used to interrogate the functions of exogenous and endogenous TRIB2 in human cells.

TRIB and STK40 proteins are thought to exert their cellular signalling roles by acting as scaffolds to bridge (and regulate) components of AKT signalling networks or functioning as adaptors that recruit ubiquitin E3 ligases, such as COP1, resulting in ubiquitination and subsequent proteasome-mediated degradation of substrates, such as C/EBPα, CDC25C and Acetyl Coenzyme A carboxylase (ACC) [276-278]. Tribbles family members are differentially expressed in numerous tissues where they have been reported to have context specific roles [279]. For instance, TRIB3 has been shown to negatively regulate AKT in the liver [124], TRIB1 and TRIB2 are proposed to serve scaffolding roles to modulate MAPK kinase signalling [279, 280] and recently TRIB2 overexpression has been shown to induce AKT phosphorylation at Ser473, contributing to clinical resistance to inhibitors of the PI3K signalling network [103].

In order to better understand the roles of TRIB2 in cellular signalling, the effects of the repurposed EGFR/HER2 ligands, described in the previous chapter, were analysed in exogenous TRIB2 expressing stable cell models and in a leukaemia cell model, where endogenous TRIB2 overexpression is linked to pathogenicity. It was hypothesised that if selected reversible and irreversible EGFR/HER2 inhibitors could bind to TRIB2 in cells, then it may be possible to probe and gain insights into TRIB2 functions in cellular signalling. If small molecule kinase inhibitors can modulate TRIB2 activity in cells, they may provide a foundation for the development of therapeutic strategies where TRIB2 overexpression or mutation is a contributor to disease aetiology. The objectives of the work described in this chapter were to:

1. Generate tetracycline (TET) inducible isogenic stable human cell lines and evaluate cellular expression of (exogenous) TRIB2.
2. Discover whether or not small molecule kinase inhibitors can modulate the stability of TRIB2 in stable human cells, with targeted validation approaches such as cellular thermal shift assays (CETSAs) and mutational analysis.
3. Analyse the effects of TRIB2 expression on cellular signalling with the application of potential repurposed inhibitors.
4. Discover whether or not 'repurposed' inhibitors can be used to interrogate endogenous TRIB2 functions in a human leukaemia cell model.

# Results

## 4.1 Detection of FLAG-tagged TRIB2 in transfected HeLa cells and development of inducible TRIB2 expressing stable cell line

### 4.1.1 Transient transfection of HeLa cells for FLAG-TRIB2 expression

In order to generate a positive control for immunoblotting with an anti-FLAG antibody, recombinant TRIB2 with an N-terminal 6His tag followed by a single FLAG peptide sequence (DYKDDDDK) was purified from *E. coli* (Figure 4.1A). As well as serving as a control, varying amounts of *E. coli* purified His-FLAG-TRIB2 were analysed by immunoblotting to generate a standard curve to estimate levels of FLAG-TRIB2 expression in HeLa cells [281, 282] (Figure 4.1B). Immunoblot analysis utilising a commercial anti-FLAG (Sigma Aldrich) antibody revealed that 50 ng of recombinant His-FLAG-TRIB2 could be detected after a short exposure of 10 seconds using ECL reagent (Figure 4.1B). Up to 500 ng of recombinant FLAG-TRIB2 could be detected before signal saturation. In the final lane (Figure 4.1B left) whole cell lysate obtained from TET induced transiently transfected HeLa Flp-In T-Rex (with pcDNA5/FRT/TO encoding FLAG-TRIB2) was analysed. FLAG-TRIB2 was only observed in the presence of TET, levels of which were calculated by plotting a standard curve of the relative densitometry values (ImageJ software) from recombinant FLAG-TRIB2 signal (Figure 4.1B right). The predicted amount of FLAG-TRIB2 expressed in HeLa cells was ~7.5 ng FLAG-TRIB2 per µg of whole cell lysate.

To optimise lysate loading for immunoblot analysis increasing amounts (between 10-160 µg) of lysate from TET induced transiently transfected HeLa cells were analysed by immunoblotting with anti-FLAG and anti-Histone H3 (loading control) (Figure 4.1C). Detection of Histone H3 also provided evidence that the nuclear components of the HeLa cells were obtained during lysis [283]. Detection of FLAG-TRIB2 was clear in 40, but not, 20 µg lysate at an exposure of 10 seconds, although a longer exposure was not tested. Incomplete transfer of lysate proteins from SDS-PAGE gels to nitrocellulose was observed when 160 µg of lysate was subjected to electrophoresis, with a substantial amount of protein still visible in the coomassie-stained gel post transfer (data not shown). Therefore, 40 µg of whole cell lysate, which was well within the limit of linear detection for TRIB2, was used for immunoblot analysis.

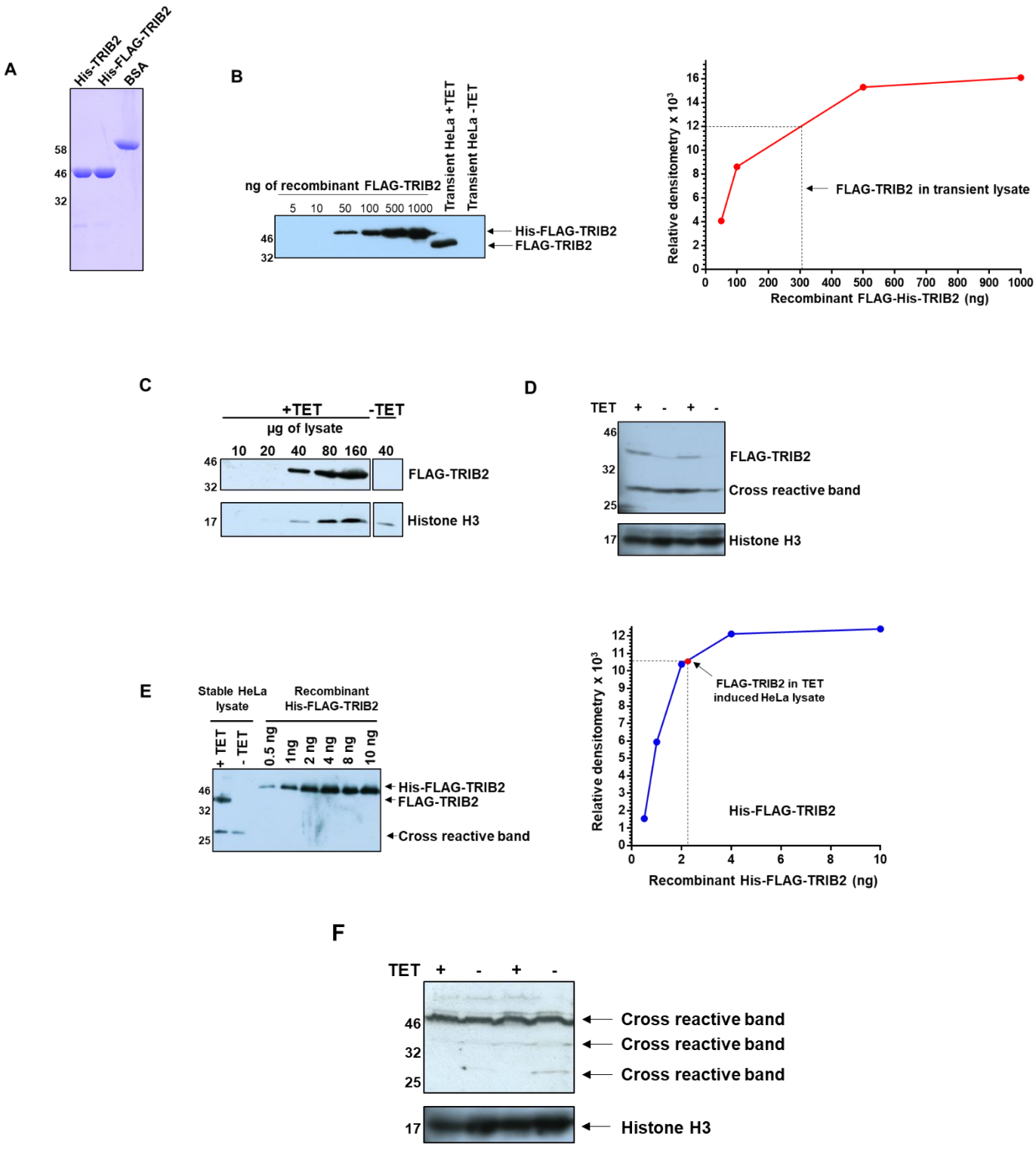


**Figure 4.1: Detection of recombinant FLAG-TRIB2 and comparison of expression levels in stable and transient HeLa Flp-In T-Rex cells**. (A) SDS-PAGE analysis of 5 µg IMAC and SEC purified His-TRIB2 and His-FLAG-TRIB2.(B) Western blot of increasing amounts of recombinant His-FLAG-TRIB2 and by 40 µg of whole cell lysate from pcDNA5/FRT/TO FLAG-TRIB2 lipofectamine transiently transfected TET induced parental HeLa Flp-In T-Rex cells. Normal ECL reagent was used for a

detection time of 10 seconds (left). Densitometry analysis of recombinant FLAG-His-TRIB2 standards and estimated amount of FLAG-TRIB2 observed in 40 µg of transient whole cell lysate (right). (C) Flp-In T-REx-HeLa cells were transiently transfected and induced with TET to express FLAG-TRIB2. Varying quantities of lysate were subjected to electrophoresis and analysed by immunoblotting. (D) Establishment of stably expressing FLAG-TRIB2 HeLa cells and optimisation of loading. Stable Flp-In T-REx-HeLa cells that expressed FLAG-TRIB2 upon incubation with tetracycline (TET) were incubated with 1 µg/mL of TET for 16 hours. Whole cell extracts were then obtained and the indicated amount of loaded into lanes on an SDS-PAGE gel followed by immunoblotting to detect FLAG-TRIB2. Histone H3 served as the loading control. ECL select reagent with an exposure time of 15 seconds. (E) Western blot of TET induced and non-induced lysates from a WT FLAG-tagged TRIB2 stably expressing HeLa cell line followed by increasing amounts of recombinant His-FLAG-tagged TRIB2 standards. ECL select reagent was used for a detection time of 15 seconds (left). Densitometry analysis of recombinant His-FLAG-TRIB2 standards and estimated amount of FLAG-TRIB2 observed in 40 µg of stable whole cell lysate (right). (F) Stable FLAG-TRIB2 Flp-In T-REx-HEK293 cells were generated. Transfected FLAG-TRIB2 Flp-In T-REx-HEK293 cells were seeded in 10 cm dishes at a density 2.2 x $10^6$ for 24 hours then incubated +/- 1 µg/ml of tetracycline (TET) for 16 hours. Whole cell lysates were prepared followed by western blot analysis using ECL select reagent for detection. An exposure time exposure time of 20 minutes was used to attempt detection of FLAG-TRIB2.

### 4.1.2 Establishment of an inducible FLAG-TRIB2 expressing stable HeLa cell line

In order to generate stable FLAG-TRIB2 expressing cell lines, parental HeLa Flp-In T-Rex cells had been co-transfected with pcDNA5/FRT/TO (encoding FLAG-TRIB2) and pOG44 plasmids to insert the FLAG-TRIB2 gene into the FLP-recombinase site, which was under control of a tetracycline-regulated CMV/TetO2 promoter [284]. Cell that had successfully integrated the TRIB2 transgene were selected using 200 µg/mL of hygromycin (chapter 2, section 2.19).

Stable isogenic HeLa cells were cultured in 10 cm dishes to ~70% confluence, 1 µg/mL of TET added directly to the medium and the cells incubated for a further 16 hours. Whole cell lysates were obtained by lysis of cells (after washing) in RIPA buffer, followed by SDS-PAGE and immunoblot analysis with an anti-FLAG antibody (Figure 4.1D). Histone H3 served as the loading control [283]. The more potent detection reagent ECL select (Amersham) had to be utilised to observe FLAG-TRIB2 in stable HeLa lysate, consistent with the lower levels of expression. TET induced HeLa cells (Figure 4.1D) had detectable levels of FLAG-TRIB2 with little to no detectable protein

at this molecular weight in the absence of TET. In lane 2 (-TET) there was a faint band that corresponded to the FLAG-TRIB2 molecular weight, which could have been due to either the α-FLAG antibody binding to cross reactive protein(s) or to low levels of leaked expression. In the repeat experiment (Figure 4.1D lane 3 and 4) had no detectable protein at this molecular weight. Consistently, another potential non-specific band was observed between the molecular weights of 25 and 32 kDa throughout all experiments regardless of whether or not cells had been incubated with TET.

In order to estimate the amount of FLAG-TRIB2 present, 40 µg of whole cell lysate, from both induced (+TET) and non-induced (-TET) isogenic HeLa cells along with varying amounts (between 0.5 and 10 ng) of purified recombinant His-FLAG-TRIB2 were western blotted with an α-FLAG antibody (Figure 4.1E, left). The more potent ECL select regent was again used for a detection time of 10 seconds to observe FLAG-TRIB2. Recombinant His-FLAG-TRIB2 signal increased in linear proportion between 0.5 and 2 ng, evident from densitometry analysis (Figure 4.1E, right). Based on the signal output, it was estimated that there was ~60 pg of FLAG-TRIB2 present in 1 µg of whole cell lysate from isogenic TET induced HeLa cells, far lower than the amount of FLAG-TRIB2 expressed in transiently transfected parental HeLa cells (~7.5 ng).

### 4.1.3 FLAG-TRIB2 was not detected in stable HEK293 cells

In order to analyse FLAG-TRIB2 in an independent stable cell line, Flp-In T-Rex HEK 293 cells were generated as previously described for HeLa cells. However, no FLAG-TRIB2 was detected in these cells on induction with TET (Figure 4.1F), perhaps due to expression levels that were below the limits of detection. ECL select reagent was used for 10 minutes in order to maximise detection of FLAG-TRIB2. Very faint bands corresponding to the expected molecular weight of FLAG-TRIB2 were observed across all lysates regardless of TET exposure, therefore indicating the presence of a cross reactive band. In addition, there was a strong contaminant observed just above 46 kDa as well as various other more faint non-specific bands. It was therefore decided that future experiments would proceed using only the isogenic HeLa cells.

## 4.2 Analysis of cellular FLAG-TRIB2 stability and potential phosphorylation

### 4.2.1 TRIB2 is degraded by the proteasome in HeLa cells

As TRIB2 turnover was previously established to be regulated by the ubiquitin proteasome system [113, 285], FLAG-TRIB2 expression in stable HeLa cells was assessed in the presence of the proteasome inhibitor MG132. Consistent with this finding, FLAG-TRIB2 was shown to be stabilised in the presence of proteasome inhibitor MG132 (Figure 4.2). A brief 4-hour exposure of TRIB2-expressing cells to the proteasome inhibitor MG132 led to an increase in TRIB2 protein expression (Figure 4.2A). A titration of increasing concentrations of MG132 revealed that 10 µM was sufficient to observe maximal increase in exogenous TRIB2 levels for 4 hours exposure (Figure 4.2B).

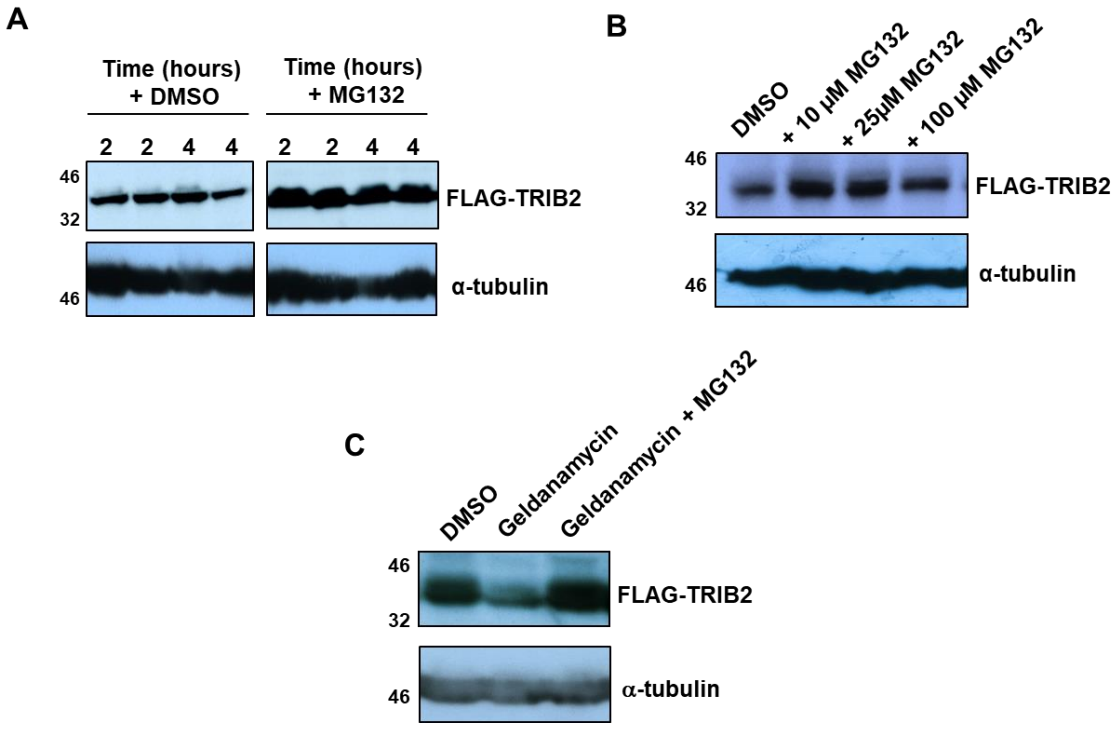


**Figure 4.2: FLAG-TRIB2 is stabilised by MG132 and destabilised by geldanamycin**. (A) Stable isogenic HeLa cells were induced to express FLAG-tagged TRIB2 with TET for 16 hours and then incubated with DMSO (0.1% v/v) or 10 µM of MG132 for the indicated number of hours before lysis and immunoblotting with an anti-FLAG antibody. α-tubulin served as the loading control. (B) HeLa cells were induced to express FLAG-tagged TRIB2 with TET for 16 hours and then incubated with DMSO (0.1% v/v), 10, 25 or 100 µM of MG132 for 4 hours prior to lysis and immunoblot analysis. (C) HeLa cells were induced to express FLAG-tagged TRIB2 with TET for 16 hours and then incubated with DMSO (0.1%

v/v), 10 μM geldanamycin or 10 μM of both geldanamycin and MG132 for 4 hours prior to lysis and immunoblot analysis.

To provide further evidence that FLAG-TRIB2 was regulated by proteasome turnover, expression was assessed in the presence of heat shock protein 90 (HSP90) inhibitor geldanamycin. HSP90 is a molecular chaperone that contributes to folding and regulation of many cytosolic proteins [286]. Ubiquitination of human Hsp90 has been reported to induce degradation of several client proteins, including p53, CDK4 (cyclin-dependent kinase 4), PLK1 (Polo-like kinase 1) and AKT1 via the proteasome [287, 288]. After only 4 hours of incubating TET-induced HeLa cells with geldanamycin, there was a marked decrease in the amount of TRIB2 detected (Figure 4.2C). Remarkably co-incubation of geldanamycin with MG132 completely reversed this effect, with levels of TRIB2 even greater than DMSO exposed cells. As well as confirming that TRIB2 turnover is regulated partially by the proteasome this finding suggests that heat shock proteins are important for TRIB2 stability.

### 4.2.2 FLAG TRIB2 is phosphorylated in stable HeLa cells

It was intriguing to observe that there was a fainter and smeared second band above the band corresponding to FLAG-TRIB2 in cell extracts. Interestingly, this band became intensified in the presence of MG132 (Figure 4.2). The higher band corresponding to TRIB2, with a lower electrophoretic mobility, was potentially a phospho-form. To investigate this specifically, a lambda phosphatase (λPP) assay was developed [289]. Accordingly, 40 μg of lysate from TET induced HeLa cells that had been incubated with 10 μM MG132 for 1 and 16 hours were incubated with 10 ng of λPP for 30 minutes at 37˚C. Without λPP a faint smeared band was observed above the dominant FLAG-TRIB2 corresponding band (Figure 4.3A). As hypothesised, the smeared bands above FLAG-TRIB2 were no longer present upon incubation with λPP (Figure 4.3A). In order to offer further support to this assertion, a FLAG-immunoprecipitation was performed to enrich and isolate FLAG-TRIB2 from the HeLa extract (Figure 4.3B). Two separate elutions, using FLAG peptide, were obtained and incubated for 30 minutes at 37˚C ± λPP. The samples were resolved by electrophoresis for an extended period in order to further resolve the proteins. After immunoblot analysis with anti-FLAG antibody, it was observed that the upper FLAG-TRIB2 bands had disappeared, suggesting dephosphorylation by λPP. Moreover, in

the absence of λPP various other faint smeared bands became visible, potentially indicating the presence of multiple TRIB2 phosphosites.

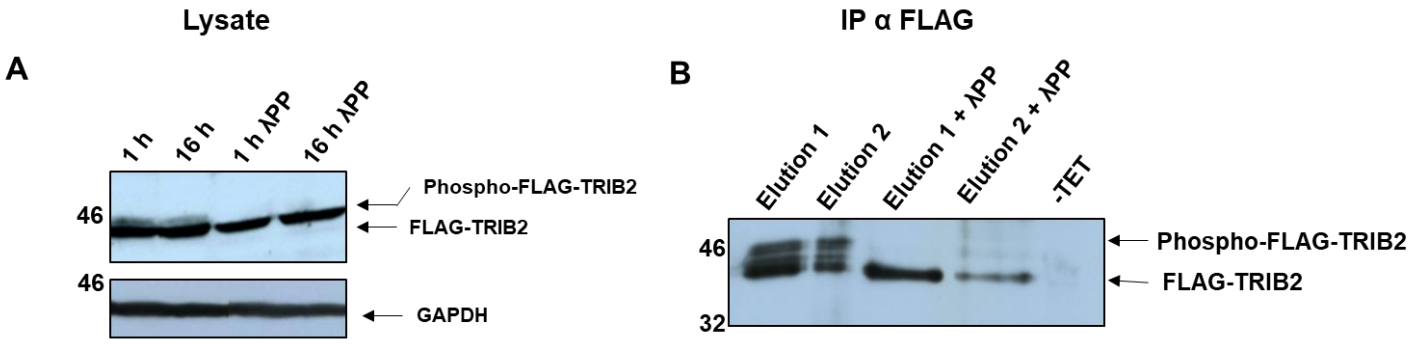


**Figure 4.3: FLAG-TRIB2 is phosphorylated in HeLa cells.** (A) Stable isogenic HeLa cells were induced to express FLAG-TRIB2 by addition of TET for 16 hours at which point whole cell lysates were obtained. 40 µg of whole cell lysate was incubated +/- 10 ng of λ phosphatase (λPP) at 37˚C for 1 hour prior to western blot analysis. (B) TET induced HeLa cells was lysed followed by FLAG immunoprecipitation. Bound FLAG-TRIB2 was eluted with FLAG peptide. 500 ng of each elution (1 and 2) were incubated +/- 10 ng of λ phosphatase (λPP) at 37˚C for 1 hour prior to western blot analysis.

## 4.3 Validation of novel TRIB2 antibodies and detection of endogenous TRIB2 in U937 cells

U937 cells are widely used as an *in vitro* model to analyse haematological malignancy and were isolated from a 37 year old male with histiocytic lymphoma [290]. The regulation of TRIB2 expression and its various roles in pathogenesis, through targeted degradation of substrate proteins (including the p42 isoform of C/EBPα) in U937 cells has previously been well-characterised [109, 113]. To evaluate and compare endogenous TRIB2 expression in U937 cells to exogenous FLAG-TRIB2 expression in stable HeLa, three novel polyclonal TRIB2 antibodies and a commercial TRIB2 antibody was tested by immunoblotting cellular lysates.

### 4.3.1 Comparison of novel and commercial TRIB2 antibodies

In order to support the assertion that FLAG-TRIB2 was indeed being expressed and detected in stable HeLa cells, and to analyse endogenous TRIB2 in U937 cells, three polyclonal TRIB2 antibodies were generated in rabbits (Figure 4.4A). Lysate from TET

induced and non-induced HeLa cells were assessed alongside 10 ng His-FLAG-TRIB2 purified from *E. coli*. Immunoblot analysis α-TRIB2 1 produced a crisp signal with very little background noise. TRIB2 antibodies were generated from 3 separate immunised rabbits. The α-TRIB2 1 and the commercial anti-FLAG antibodies appeared to be equally effective at recognising cellular FLAG-TRIB2 and recombinant His-FLAG-TRIB2. The α-TRIB2 2 and 3 antibodies were able to detect cellular FLAG-TRIB2 and bacterial His-FLAG-TRIB2 but with an increased abundance of cross reactive bands and background noise. Analysis with the CST commercial TRIB2 antibody resulted in high levels of background noise and signals from cross reactive bands. Furthermore, immunoreactive bands appeared at the predicted molecular weight of FLAG-TRIB2 in the absence of TET, which could potentially lead to a 'false-positive' detection of TRIB2. The clear signal using α-TRIB2 1 and indecisive results achieved with the commercially available TRIB2 antibody highlights the importance in taking careful measures to collaboratively share reagents to support new research into TRIB2 cellular signalling. Interestingly, the levels of endogenous TRIB2 in HeLa Flp-In T-REx were too low to be detected with any of the TRIB2 antibodies, indicated by no TRIB2 signal in the absence of TET. This finding explains the need for inducible HeLa cells to mechanistically analyse TRIB2, as it would be expected that the extremely low background levels of endogenous TRIB2 might not significantly contribute to signalling outputs. It was further demonstrated that the α-TRIB2 1 antibody could detect recombinant His-FLAG-TRIB2 purified from *E. coli* in a dose dependent manner and detect FLAG-TRIB2 expressed in transiently transfected HeLa cells (Figure 4.2B). The commercial α-FLAG and novel α-TRIB2 1 antibodies appeared to be equally effective at detecting FLAG-TRIB2, which supports the idea for their use to comparatively analyse both endogenous and exogenous TRIB2 expression in different cell lines.

### 4.3.2 Comparison of exogenous and endogenous TRIB2 in HeLa and U937 cells

U937 cells were a gift from Karen Keeshan (University of Glasgow). In order to compare TRIB2 expression in TET induced HeLa and U937 cells, 40 µg of lysate from each cell line was analysed side by side (Figure 4.4C). Exogenous FLAG-TRIB2 from HeLa cells was observed to be at a similar level to endogenous TRIB2 in U937 cells, both with ~60 pg of TRIB2 per µg of cellular lysate. This finding supports the idea that stable HeLa cells, with similar expression levels of TRIB2 to U937, is a reasonable exogenous TRIB2 expressing model to comparatively analyse TRIB2 related

signalling outputs. It was also established that TRIB2 in U937 cells was stabilised after 4 hours incubation with MG132 (Figure 4.4D), consistent with protein turnover by the proteasome [113].

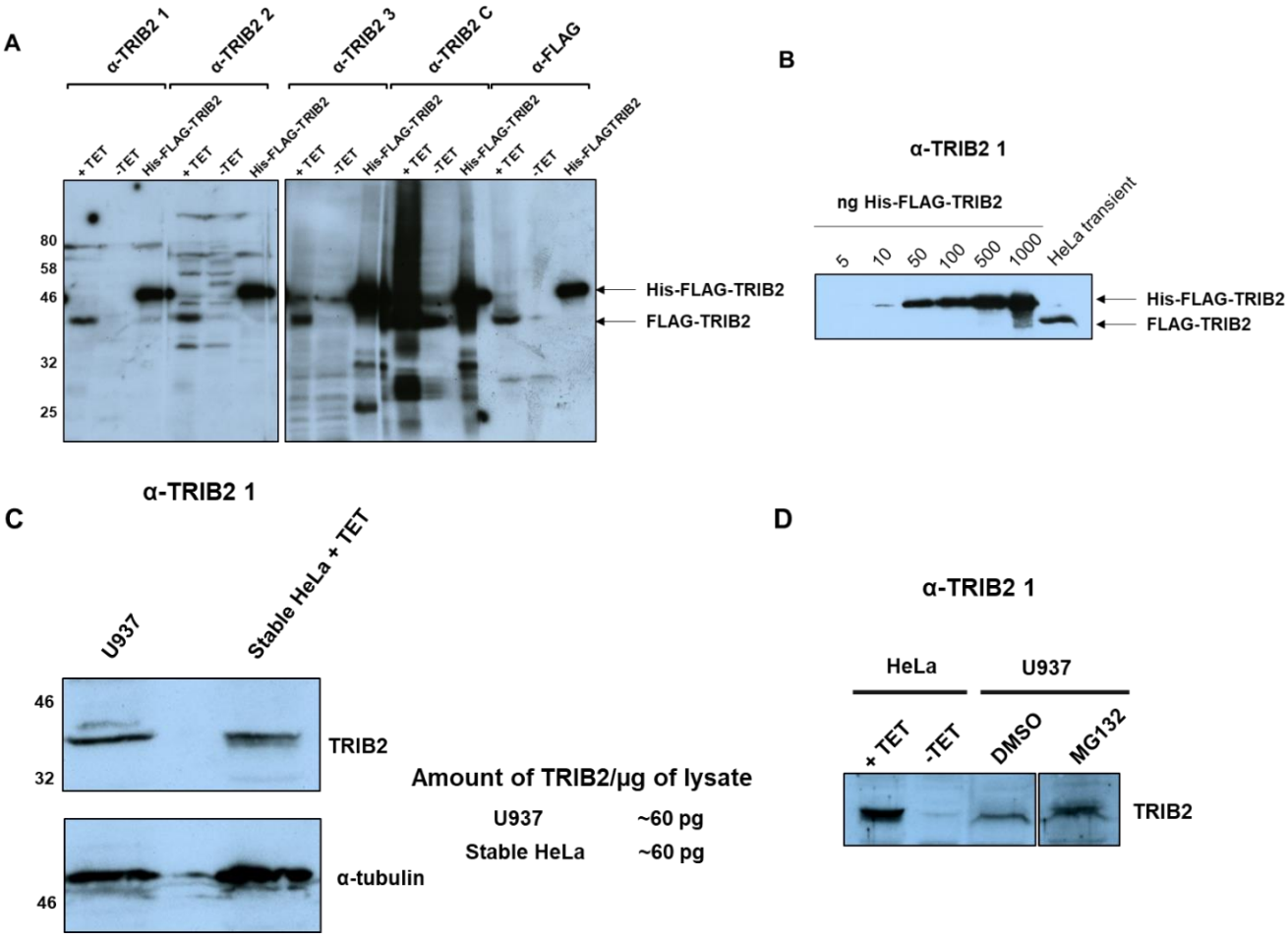


**Figure 4.4: Comparison of novel polyclonal and commercial TRIB2 antibodies**. Three novel polyclonal rabbit α-TRIB2 antibodies (α-TRIB2 1, 2 and 3) were raised towards a unique N-terminal TRIB2 sequence in human TRIB2, affinity purified, and used to immunoblot for FLAG-TRIB2 (in stable isogenic TET induced HeLa cells) and 10 ng of recombinant His-FLAG-TRIB2 protein. These antibodies were compared alongside a commercial TRIB2 antibody (α-TRIB2 C) and a commercial α-FLAG antibody. ECL select reagent was used for an exposure time of 15 seconds. (B) Detection of His-FLAG-TRIB2 standards and exogenous FLAG-TRIB2 in transiently transfected HeLa cells: Increasing amounts of recombinant His-FLAG-TRIB2 and 40 µg of whole lysate from transiently transfected HeLa cells were analysed by immunoblotting with the α-TRIB2 1 antibody. Normal ECL regent was used for an exposure time of 15 seconds. (C) Analysis of endogenous TRIB2 expression in U937 cells and exogenous FLAG-TRIB2 in stable HeLa cells. Whole lysates were obtained for U937 cells and TET induced stable FLAG-TRIB2 expressing HeLa cells. 40 µg of protein was loaded and resolved by SDS-

PAGE before western blot analysis with α-TRIB2 1 and α-tubulin. (D) Endogenous TRIB2 in U937 cells is stabilised by MG132. U937 cells were incubated for 4 hours with either DMSO or 10 μM MG132.

## 4.4 Evaluation of small molecule inhibitors in stable HeLa cells

In Chapter 3, it was discussed that covalent EGFR/HER2 dual inhibitors had the ability to both stabilise and destabilise recombinant TRIB2 *in vitro*. I wished to investigate whether these compounds interact with FLAG-TRIB2 in the inducible HeLa model discussed above. As proof of concept, covalent binding of the hydrophobic compound TX2-121-1 to HER3 at Cys721 [291], causes proteasomal mediated degradation of the HER3 pseudokinase [62]. It was hypothesised that repurposed EGFR/HER2 ligands could bind to intracellular TRIB2 and modulate its stability, which could be evaluated by immunoblot analysis.

### 4.4.1 Analysis of EGFR/HER2 inhibitors in HeLa cells

ERK western blots were initially optimised in the absence of TRIB2. Varying amounts of un-induced HeLa lysate were analysed by immunoblotting for total ERK1/2 and activated pERK1/2 (phosphorylated at Thr202 and Tyr204) (Figure 4.5A). At 40 μg both non-phosphorylated ERK1 and ERK2 isoforms could be detected. However, pERK1 was barely visible, with pERK2 not detectable whatsoever. The signal for pERK1 was far stronger when 80 μg of total HeLa lysate was analysed, although still the presence of pERK2 was not apparent. Only when 160 or 320 μg of lysate was resolved by electrophoresis could both phosphorylated isoforms of ERK be detected.

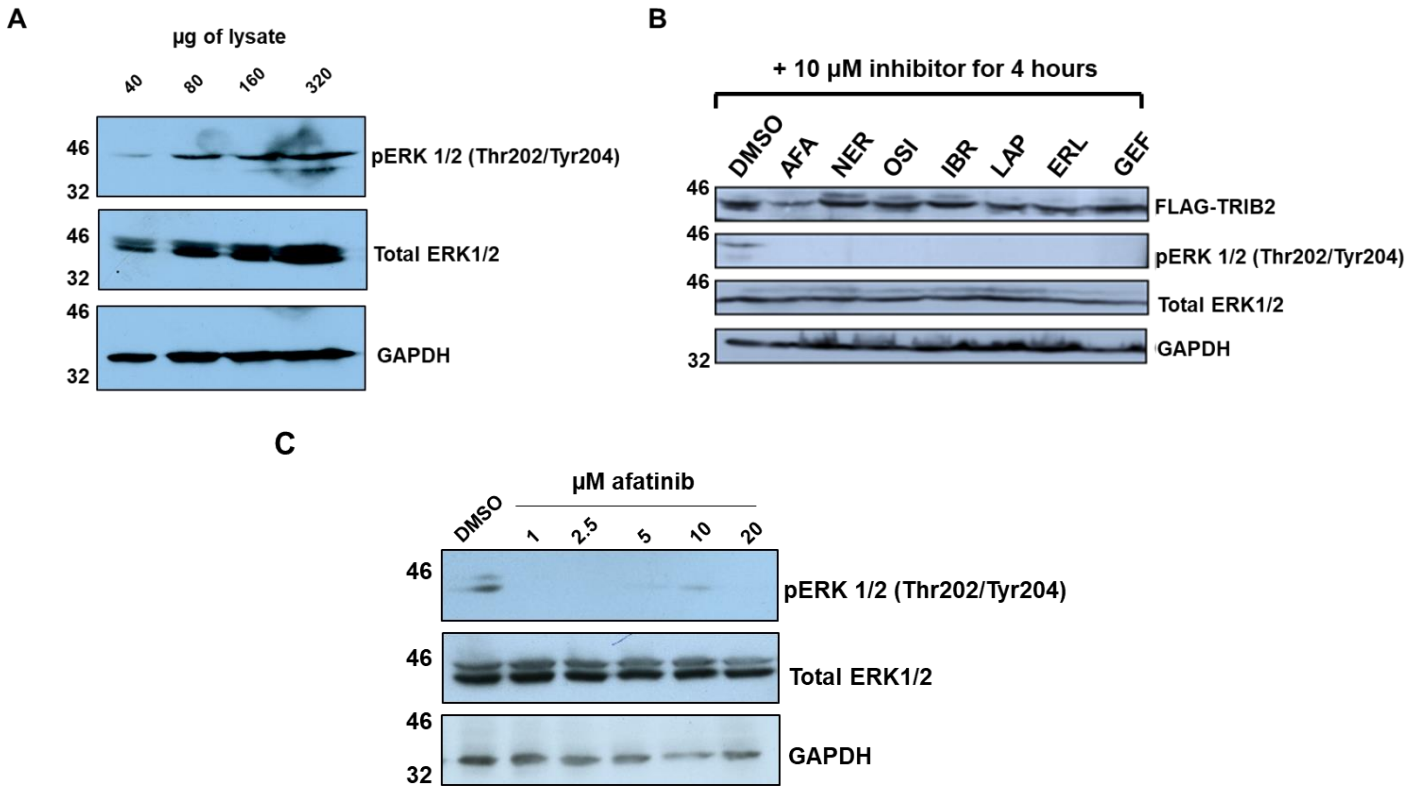


**Figure 4.5: Analysis of EGFR/HER2 clinical inhibitors in HeLa cells and effect on exogenous FLAG-TRIB2**. (A) Optimisation of pERK detection. Parental HeLa cells were grown to 70% confluence at which point whole cell lysates were obtained. Increasing amounts of lysate were resolved by SDS-PAGE before western blot detection of total ERK1/2 and phosphorylated ERK1/2 (pERK) at Thr202 and Tyr204. GAPDH served as a loading control. (B) A screen of clinically approved EGFR/HER2 inhibitors in FLAG-tagged TRIB2 expressing stable HeLa cells. HeLa cells were induced to express FLAG-tagged TRIB2 with tetracycline for 16 hours and then incubated with DMSO (0.1% v/v) or 10 µM of inhibitor for 4 hours prior to lysis and western blot analysis. AFA (afatinib), NER (neratinib), OSI (osimertinib), IBR (ibrutinib), LAP (lapatinib), ERL (erlotinib), GEF (gefitinib). (C) Parental HeLa cells were incubated with 0.1% DMSO (v/v) or the indicated concentration of afatinib for 4 hours prior to immunoblot analysis of total ERK1/2 and phosphorylated ERK1/2 (pERK) at Thr202 and Tyr204. GAPDH served as a loading control.

The ability of a panel of EGFR/HER2 inhibitors to inhibit ERK phosphorylation was assessed in FLAG-TRIB2 expressing (TET induced) HeLa cells. The effects of these compounds on FLAG-TRIB2 expression was also analysed. In the presence of DMSO both ERK1 and 2 were phosphorylated. Interestingly, there was a greater abundance

of ERK2 but higher levels of ERK1 phosphorylation in the un-induced HeLa cells treated with DMSO (Figure 4.5B). Upon incubation with 10 µM inhibitor total ERK1/2 levels remained constant but ERK phosphorylation was completely inhibited, for all EGFR/HER2 inhibitors tested, confirming inhibition of their canonical (EGFR-family) targets. The Type IV dual EGFR/HER2 small molecule kinase inhibitors afatinib, neratinib and osimertinib were shown in Chapter 3 (section 3.8.1) to destabilise TRIB2 *in vitro*. The dual EGFR/HER2 inhibitor lapatinib stabilised TRIB2 with monovalent EGFR inhibitors gefitinib and erlotinib having no discernible effect. The type IV BTK inhibitor ibrutinib that did not affect TRIB2 stability *in vitro,* was also assessed as a control alongside gefitinib and erlotinib. Interestingly, levels of FLAG-TRIB2 decreased in the presence of afatinib (Figure 4.5B). However, in this experiment, neratinib and osimertinib did not appear to have any major effect on TRIB2 levels. The *in vitro* TRIB2 stabilising ligand lapatinib did not appear to have any effect on TRIB2 protein levels in HeLa cells at this concentration, and neither did the EGFR inhibitors gefitinib or erlotinib.

A dose response experiment was performed using afatinib in un-induced (undetectable TRIB2) HeLa cells to analyse concentration dependent inhibition of pERK. Varying concentrations of afatinib (between 1 and 20 µM) were incubated with un-induced HeLa cells for 4 hours prior to immunoblot analysis. In DMSO treated and for all concentrations of afatinib tested the total amount of ERK remained constant. However, pERK was only detected in lysate from cells exposed to DMSO, indicated by total inhibition of pERK at 1 µM afatinib, the lowest concentration tested. This information was important as subsequent experiments evaluated the effects of inhibitors within this concentration range with unique effects of drugs on TRIB2 therefore likely to be ‘off-target’ to EGFR/HER2.

### 4.4.2 Analysing the effect of EGFR/HER2 inhibitors on TRIB2 in stable HeLa cells

To understand the effect of TRIB2 destabilisation in the presence of afatinib, a dose response experiment was performed on TET induced isogenic HeLa cells (Figure 4.6A). The amount of TRIB2 was markedly reduced at the concentration of 10 µM, with a maximum observed affect at 15 µM. This finding supports the hypothesis that levels of TRIB2 were directly responsive to afatinib in a dose-dependent manner.

Gefitinib at a concentration of 10 µM was employed as a negative control and did not have an observable effect on the amount of TRIB2 detected.

Although it was previously demonstrated that 10 µM of the covalent inhibitor neratinib had no observable effect on TRIB2 after 4 hours (Figure 4.5B), a dose response experiment revealed that, as for afatinib, TRIB2 was destabilised in a dose-dependent manner after an extended incubation (Figure 4.6B). 5 µM of the type IV EGFR/HER2 kinase inhibitor neratinib was insufficient to induce a convincing TRIB2 destabilisation effect in HeLa cells. However, TRIB2 was clearly destabilised in the presence of 10 µM neratinib, albeit not as extensively as in the presence of 10 µM afatinib (the positive control). Finally, at a concentration of 20 µM neratinib, the extent of TRIB2 destabilisation was essentially complete (Figure 4.6B).

As lapatinib was previously shown by DSF to stabilise TRIB2 (section 3.8.1), it was hypothesised that intracellular lapatinib binding might result in increased levels of TRIB2 in stable TET-induced HeLa cells. Varying concentrations of lapatinib (between 2-20 µM) were incubated with TET induced HeLa cells for 4 hours, however no effect on TRIB2 stability was observed (Figure 4.6C), which suggested that either lapatinib did not engage TRIB2 in the HeLa cells, or binding of lapatinib could not confer an effect on TRIB2 protein levels.

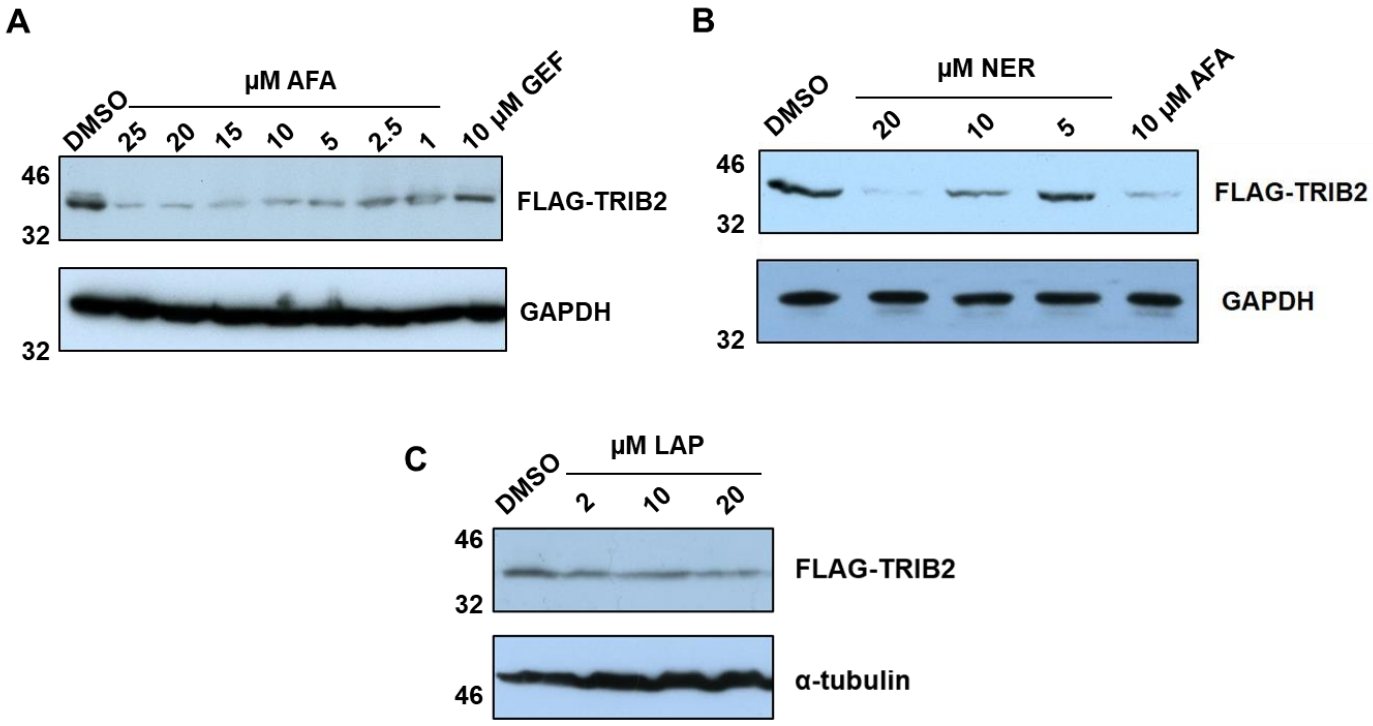

**Figure 4.6: Dose dependent analysis of EGFR/HER2 clinical inhibitors in FLAG-TRIB2 expressing stable HeLa cells**. (A) Stable HeLa flp-in TRIB2 cells, induced for 16 hours with TET, were incubated with DMSO (0.1% v/v), increasing concentrations of AFA or 10 μM gefitinib for 4 hours followed by whole cell lysis and immunoblot analysis. (B) Stable HeLa flp-in TRIB2 cells, induced for 16 hours with TET, were incubated with DMSO (0.1% v/v), increasing concentrations of neratinib (NER) or 10 μM afatinib for 4 hours followed by whole cell lysis and immunoblot analysis. (C) Stable HeLa flp-in TRIB2 cells, induced for 16 hours with TET, were incubated with DMSO (0.1% v/v) or increasing concentrations of lapatinib for 4 hours followed by whole cell lysis and immunoblot analysis.

## 4.5 Investigating the mechanism of TRIB2 destabilisation in the presence of afatinib

### 4.5.1 Time dependent destabilisation of TRIB2 by afatinib

In order to elucidate the time at which afatinib begins to induce TRIB2 destabilisation, TET induced HeLa cells were incubated with afatinb for varying lengths of time. A rapid time-dependent elimination of TRIB2 protein was evident (Figure 4.7B), in contrast to DMSO controls in which TRIB2 levels remained observably stable throughout the experiment (Figure 4.7A). In the presence of afatinib, after only a 2 hour incubation, there was substantial loss of TRIB2 and the maximal effect of destabilisation was observed by 4 hours. Incubation with the proteasome inhibitor MG132 induced stabilisation of TRIB2 (Figure 4.7C), consistent with previous findings that TRIB2 turnover is proteasome-dependent [113]. In the presence of both afatinib and MG132, TRIB2 levels remained stable for a longer period of time than in the presence of afatinib alone (Figure 4.7D). However, TRIB2 was eventually destabilised, indicating that perhaps the proteasome was not completely inhibited. By employing λPP assays it was again shown that TRIB2 is potentially phosphorylated in HeLa cells.

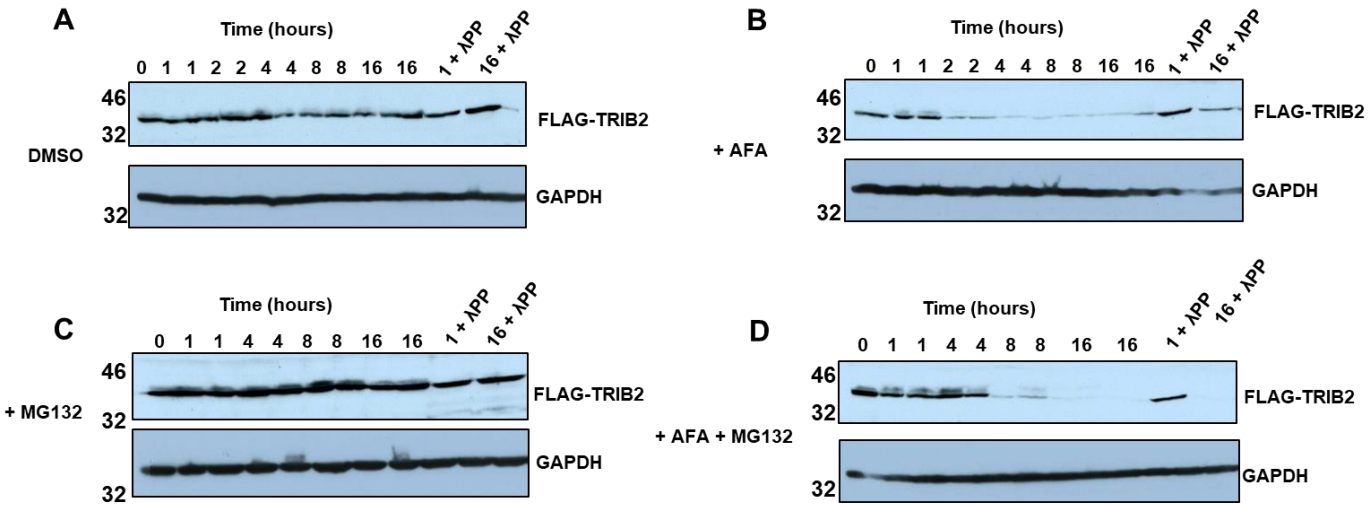


**Figure 4.7: Afatinib induces FLAG-TRIB2 degradation in a time-dependent manner in HeLa cells**. (A) HeLa cells were induced to express FLAG-TRIB2 for 16 hours with TET, incubated with either 0.1% (v/v) DMSO (A), 10 µM afatinib (B), 10 µM MG132 (C) or both 10 µM afatinib and 10 µM MG132 (D) and then lysed at the indicated time points prior to immunoblot analysis. A λPP was performed on 40 µg of lysate from time points 1 and 16 hours for each condition.

### 4.5.2 Proteasome inhibition in the presence of afatinib

After a 4-hour incubation, TRIB2 levels were acutely decreased in the presence of afatinib and stabilised by proteasome inhibition with MG132. Incubation of TET induced stable HeLa cells with both afatinib and MG132 reversed TRIB2 degradation (Figure 4.8A). However, the total amount of TRIB2 in the MG132 treated cells exceeded the total amount of TRIB2 in the cells that had been treated with afatinib and MG132. This indicated that either degradation of TRIB2 in the presence of afatinib was not solely dependent on the proteasome, or the proteasome was not completely inhibited.

Subsequently, TET-induced HeLa cells were incubated with afatinib, MG132 or both afatinib and MG132 together for 1 and 16 hours to observe effects on TRIB2 levels. In the presence of DMSO, between 1 and 16 hours, TRIB2 levels remained constant (Figure 4.8B). After 1 hour incubation with afatinib, TRIB2 levels were similar to the amount observed in the presence of MG132 over the same time, suggesting that changes to TRIB2 levels were gradual. After 16 hours, however, in the presence of afatinib, TRIB2 levels were markedly reduced.

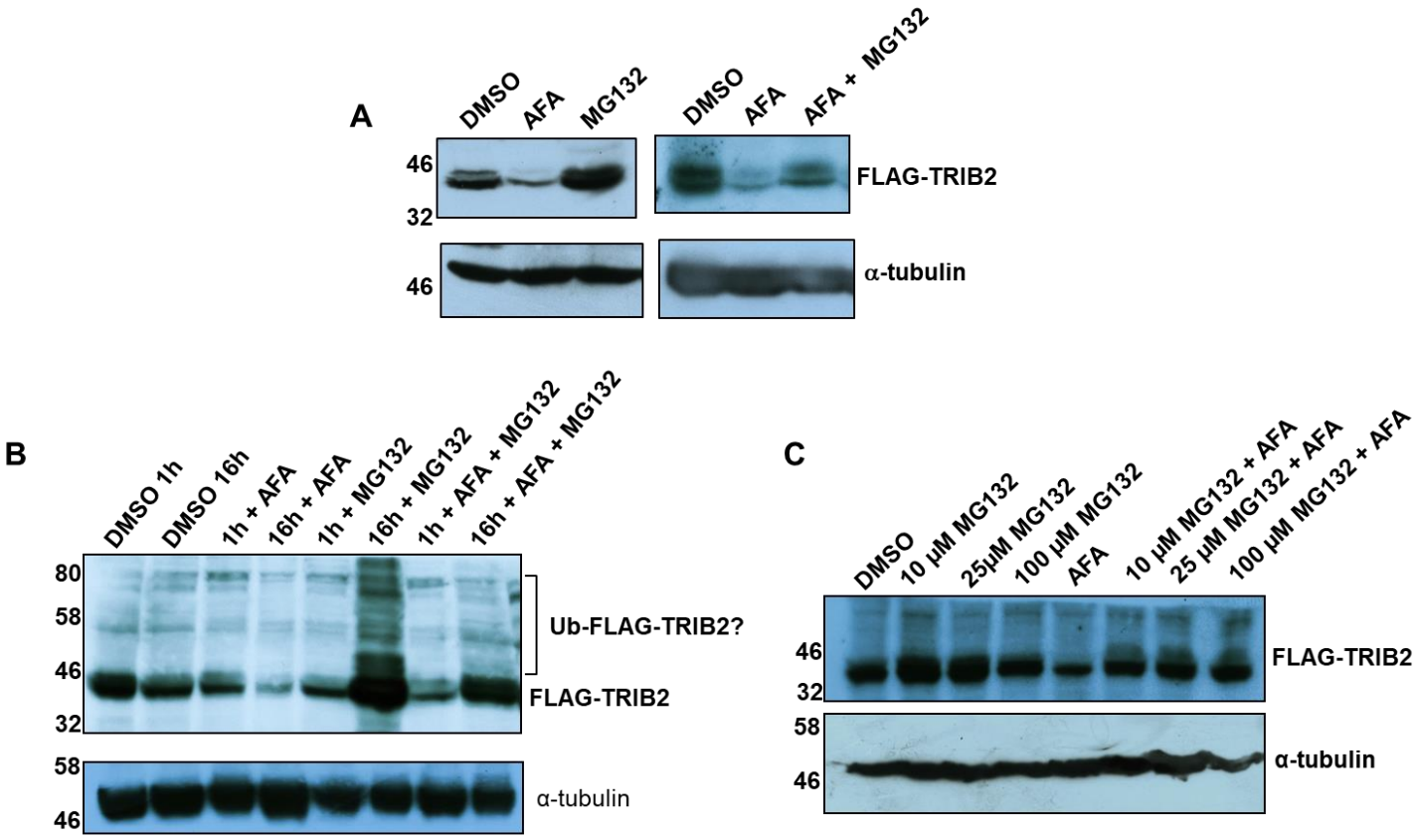


**Figure 4.8: FLAG-TRIB2 is degraded partially by the proteasome in the presence of afatinib**. (A) Stable HeLa cells induced for 16 hours with TET were incubated with DMSO (0.1% v/v) 10 μM afatinib or 10 μM afatinib and 10 μM MG1312. (B) Stable HeLa cells induced for 16 hours with TET then treated for either 1 or 16 hours with 10 μM afatinib, 10 μM MG132 or both 10 μM AFA and MG132 followed by lysis and immunoblot analysis. (C) Stable HeLa cells induced for 16 hours with TET then incubated with increasing concentrations of MG132 ± 10 μM AFA for 4 hours.

Interestingly, there was an apparent 'laddering effect' of higher molecular weight bands, which potentially corresponded to (poly)ubiquitinated TRIB2 (Figure 4.8B). After 16 hours incubation with MG132 alone there was substantial TRIB2 stabilisation along with extensive laddering. Between 1 and 16 hours treatment with both afatinib and MG123 there was a substantial increase in the amount of observed TRIB2 (Figure 4.8B), which was also accompanied by increased levels of laddering. Although, again the amount of TRIB2 in the presence of both MG132 and afatinib was less than in the presence of MG132 alone. It could have been that either afatinib induced a rapid

proteasome-mediated turnover of TRIB2 prior to complete inhibition of the proteasome by MG132, or an alternate degradation pathway was also involved.

In order to investigate whether or not the decrease in TRIB2 levels in the presence of both afatinib and MG132 (relative to MG132 treatment alone) was due to only partial inhibition of the proteasome, TET induced HeLa cells were incubated with increasing concentrations of MG132 in the presence of afatinib (Figure 4.8C). In the presence of MG132 alone the amount of TRIB2 was increased to similar extents, regardless of MG132 concentration. As expected, TRIB2 was destabilised by afatinib but was rescued in the presence of MG132 to an extent similar to MG132 alone, when the MG132 concentration was increased to 100 μM. This result suggested that MG132 concentrations of 100 μM were required to sufficiently inhibit the proteasome and prevent degradation of TRIB2 in the presence of afatinib.

### 4.5.3 Analysis of lysosome inhibitors in the presence of afatinib

In order to determine whether TRIB2 was exclusively degraded via the proteasome upon incubation with afatinib, the levels of TRIB2 were also assessed in the presence of autophagy and autophagy/lysosomal inhibitors AICAR and chloroquine. AICAR and chloroquine had no effect on TRIB2 stability (Figure 4.9A), in contrast to MG132 which stabilised TRIB2. In comparison to afatinib treatment, stabilisation was apparent when MG132 and afatinib were used in combination. When AICAR or chloroquine were incubated together with afatinib, there was no detectable rescue of TRIB2 destabilisation. Autophagy, lysosomal and proteasome inhibitors where then pre-incubated for 1 hour with TET induced HeLa cells prior to the addition of afatinib (Figure 4.9B). Consistently, TRIB2 decrease in the presence of afatinib was not mitigated in the presence of AICAR or chloroquine. Employing another proteasome inhibitor bortezomib (Figure 4.9C), it was shown that there is a clear rescue of TRIB2 degradation when afatinib exposed HeLa cells were incubated with either MG132 or bortezomib.

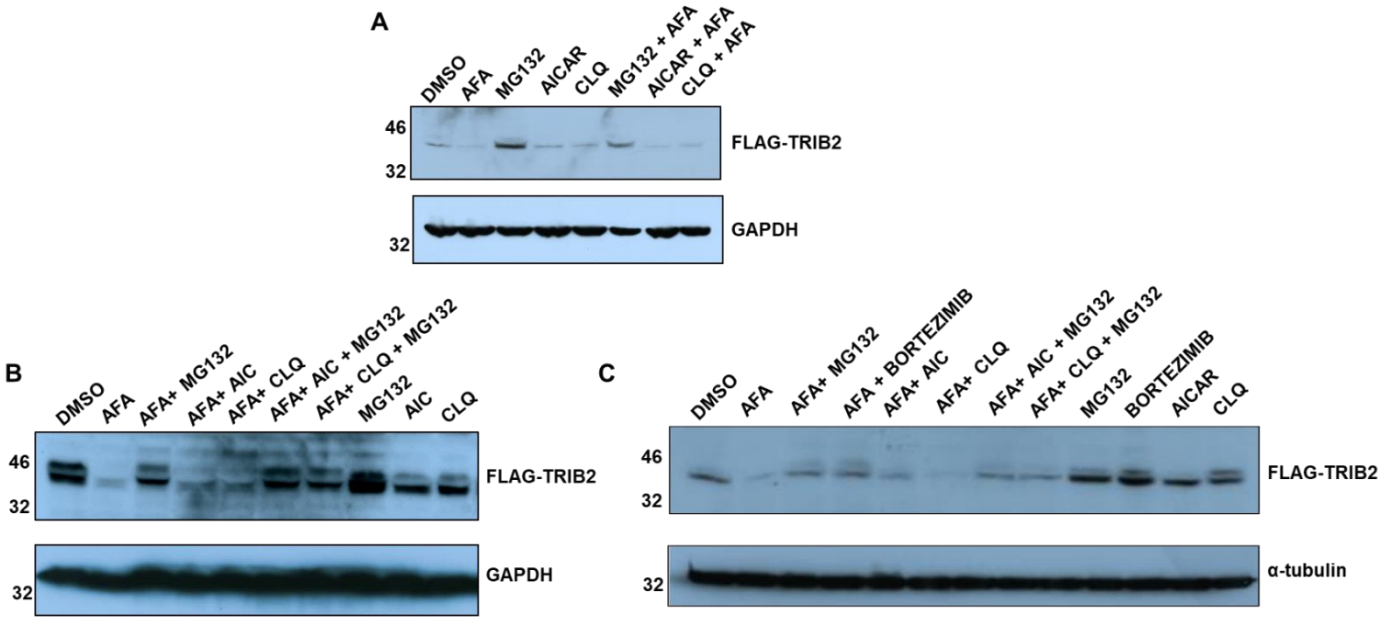


**Figure 4.9: Analysis of FLAG-TRIB2 stability in the presence of AFA with proteasome and lysosome inhibitors**. (A) TET induced HeLa cells were incubated with 10 µM MG132 and lysosome inhibitors 1 mM ACAR (AIC) and/or 50 µM chloroquine (CLQ) ± 10 µM afatinib for 4 hours followed by western blot analysis. (B) FLAG-TRIB2 expressing stable cells were incubated with 10 µM MG132, 1 mM AIC and/or 50 µM CLQ for 1 hour prior to 4 hour incubation ± 10 µM afatinib followed by western blot analysis. (C) HeLa cells were induced to express FLAG-tagged TRIB2 with TET for 16 hours and then for 1 hour with10 µM MG132, 10 µM bortezomib, 1 mM AIC and/or 50 µM CLQ. Subsequently 10 µM or 0.1% (v/v) DMSO was added for a further 4 hours prior to western blot analysis.

### 4.5.4 Analysis of COP1 binding site and N-terminal truncation TRIB2 mutants

In chapter 3 it was established that afatinib binding to TRIB2 induced a thermally-destabilised conformation, in which the C-terminal tail likely became uncoupled from the pseudokinase domain. Here, I show that afatinib induces degradation of TRIB2 in isogenic HeLa cells via the proteasome. In order to investigate whether or not TRIB2 degradation, in the presence of afatinib, occurred through the C-terminal tail, a HeLa cell line expressing FLAG-TRIB2 with a COP1-binding motif mutation (DQLVP to AQLAA) was generated. As the N-terminus (residues 1-54) were predicted to be disordered (section 3.6.1) and contain a PEST region, which might regulate TRIB2 turnover [104], a HeLa cell line expressing an N-terminal truncation (54-343) FLAG-TRIB2 mutant was also generated.

Stable HeLa cell lines were generated to express FLAG-tagged TRIB2 lacking the N-terminal domain (54-343) and a full length (1-343) C-terminal tail AQLAA TRIB2 mutant on induction with tetracycline (Figure 4.10A). After 4 hours incubation with afatinib all TRIB2 proteins were destabilised (Figure 4.10B), indicating that degradation of TRIB2 was independent of the N-terminus and an intact E3 ubiquitin ligase binding motif in the C-terminal tail. Moreover, after 4 hours treatment of TET induced HeLa cells with MG132, there was a marked increase of all TRIB2 proteins, suggesting that neither the N-terminal domain nor the DQLVP E3 ligase binding motif are required for TRIB2 turnover by the proteasome.

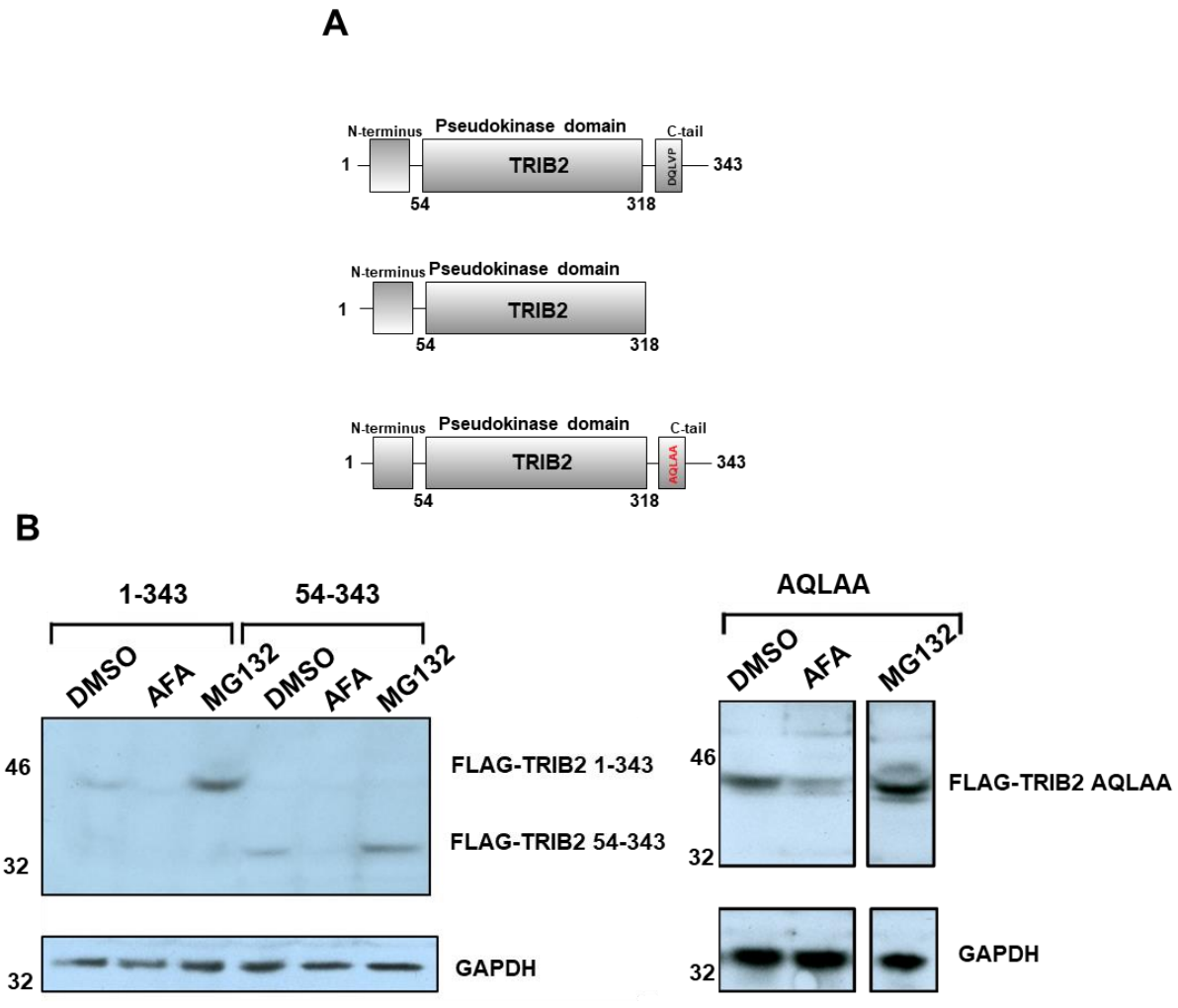


**Figure 4.10: Degradation of FLAG-TRIB2 through in the presence of the pseudokinase domain**. (A) Cartoon representation of FLAG-TRIB2 proteins; full length TRIB2 (residues 1-343) (top), the N-terminus with pseudokinase domain (residues 1-318) (middle) and full length TRIB2 with a COP1 binding site DQLVP to AQLAA mutation (bottom). (B) (Left) Immunoblot analysis of stable HeLa cell lines expressing full length FLAG-TRIB2 and a truncation mutant lacking the N-terminal domain (1-53)

incubated with either 0.1% DMSO (v/v), 10 µM afatinib or 10 µM MG132 for 4 hours. (Right) Immunoblot analysis of stable HeLa cells expressing full length FLAG-TRIB2 with a C-tail AQLAA mutation incubated with 0.1% DMSO (v/v), 10 µM afatinib or 10 µM MG132 for 4 hours.

## 4.6 Investigating targeted interactions of TRIB2 ligands using CETSA

To investigate whether or not small molecule inhibitors that bound to TRIB2 *in vitro* had intracellular engagement with exogenous TRIB2 expressed in HeLa cells, cellular thermal shift assays (CETSAs) were employed [292, 293]. Biophysical ligand-induced changes in protein thermal stability can be detected by treatment of cells with compounds that bind to and modulate thermal stability of target proteins [293]. Engagement of compounds can either increase or decrease the melting temperature of the target protein, causing protein aggregation which can be separated from the soluble lysate. TRIB2 expressing HeLa cells were incubated with compounds for 1 hour followed by aliquoting, heating to different temperatures for 3 minutes, lysis by sonication, centrifugation and finally immunoblot analysis for FLAG-TRIB2. The cellular lysate was centrifuged to separate soluble proteins from precipitated proteins.

### 4.6.1 Establishing the melting temperature of FLAG-TRIB2 in HeLa cells

Before analysing TRIB2 thermal stability in the presence of compounds the melting temperature of FLAG-TRIB2 in HeLa cells had to be elucidated. This was completed in order to establish the temperature range at which exogenous TRIB2 becomes aggregated with no compound present [294]. Firstly, a narrow temperature range, between 38 °C and 46 °C, was employed, however FLAG-TRIB2 remained stable under these conditions and did not become denatured (Figure 4.11A). Thus an extended temperature range up to 70°C was investigated (Figure 4.11B). TRIB2 expressed in stable HeLa cells remained stable until cells were heated to a temperature of 50°C, at which point levels of TRIB2 began to decrease, probably marking the onset of protein aggregation. At 60°C the majority of FLAG-TRIB2 had become insoluble and by 70°C TRIB2 protein was no longer detectable in the soluble fraction of the cellular lysate. The loading control α-tubulin was observed to be destabilised steadily throughout the experiment, demonstrating aggregation as a function of temperature increase.

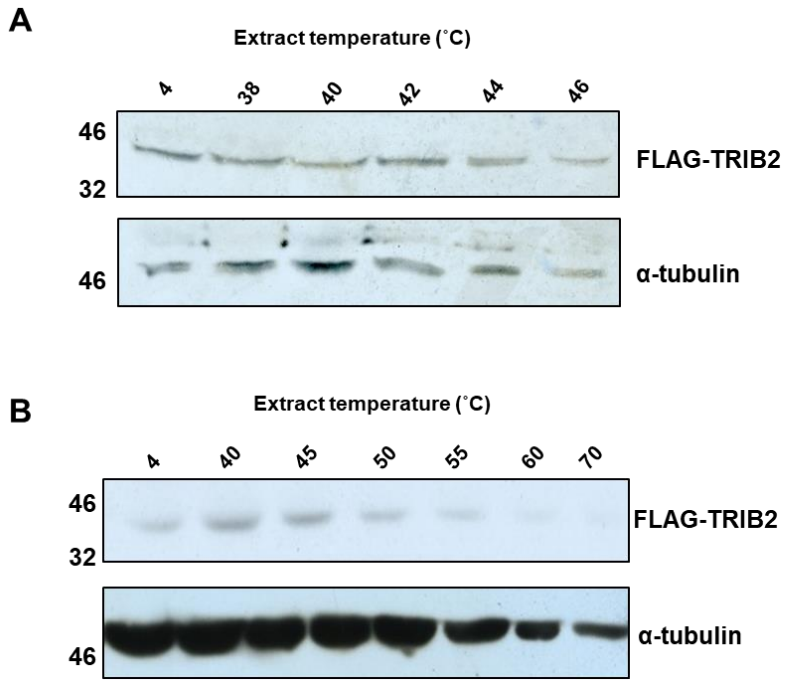


**Figure 4.11: Optimisation of whole cell cellular thermal shift assay (CETSA)**. (A) Stable isogenic HeLa cells were induced to express FLAG-TRIB2 with TET for 16 hours with cells reaching 90% confluence. Cells were thereafter incubated with 0.1% (v/v) DMSO for 1 h and subsequently collected and re-suspended in PBS. The re-suspended cells were sub-aliquoted into PCR tubes and heated in a series of 2ºC increments between 38 and 46ºC. The cells were subsequently lysed by sonication, centrifuged for 20 minutes at 18,000 g and analysed by western blot for FLAG-TRIB2 and alpha tubulin. (B) Same as for (A) but with an extended temperature range of 5 ºC increments between 40ºC and 60ºC with a final temperature of 70ºC.

### 4.6.2 Analysing the effect of small molecule inhibitors on cellular TRIB2 thermal stability

Lapatinib was previously shown to increase the thermal stability of recombinant TRIB2 *in vitro* by DSF (section 3.8.1). Although, lapatinib did not induce detectable changes in the amounts of TRIB2 in HeLa cells incubated with lapatinib (Figure 4.6B). It is still possible, however, that lapatinib bound to cellular TRIB2 without changing the total amount protein present. To test this hypothesis CETSAs were performed employing lapatinib with DMSO as a control (Figure 4.12A). Consistently, in the presence of DMSO TRIB2 was thermally stable up to 50 °C before beginning to aggregate, indicated by a decrease in total TRIB2 protein at 56 °C. Interestingly, after 1 hour

incubation of lapatinib with TET induced stable HeLa cells, TRIB2 became less affected by temperature increase and remained soluble at a heating temperature of 58 °C. In addition, overall TRIB2 signal intensity was greater for lapatinib treated cells, as opposed to DMSO treated, across the temperatures range of 50-58 °C, the onset of TRIB2 aggregation (Figure 4.12B). By employing densitometry analysis (Figure 4.12B), it was elucidated that the $T_m$ of TRIB2 in the presence of DMSO was ~49 °C and ~51 °C in the presence of lapatinib.

Next the effects of lapatinib, afatinib and erlotinib on intracellular TRIB2 thermal stability were tested (Figure 4.13A). TRIB2 in HeLa cells that had been exposed to lapatinib as opposed to DMSO was again more stable. Remarkably, when HeLa cells were exposed to afatinib TRIB2 was less thermally stable with no TRIB2 being detected at a temperature of 45 °C, giving an estimated $T_m$ of ~40 °C (Figure 4.13B). This result provided evidence of a direct intracellular interaction between afatinib and TRIB2 and furthermore, consistent with DSF analysis (section 3.8.1), TRIB2 had a lower melting temperature in the presence of afatinib. Erlotinib, which had no detectable interaction with TRIB2 when assayed by DSF, did not have any influence on intracellular TRIB2 thermal stability compared to DMSO (Figure 4.13A).

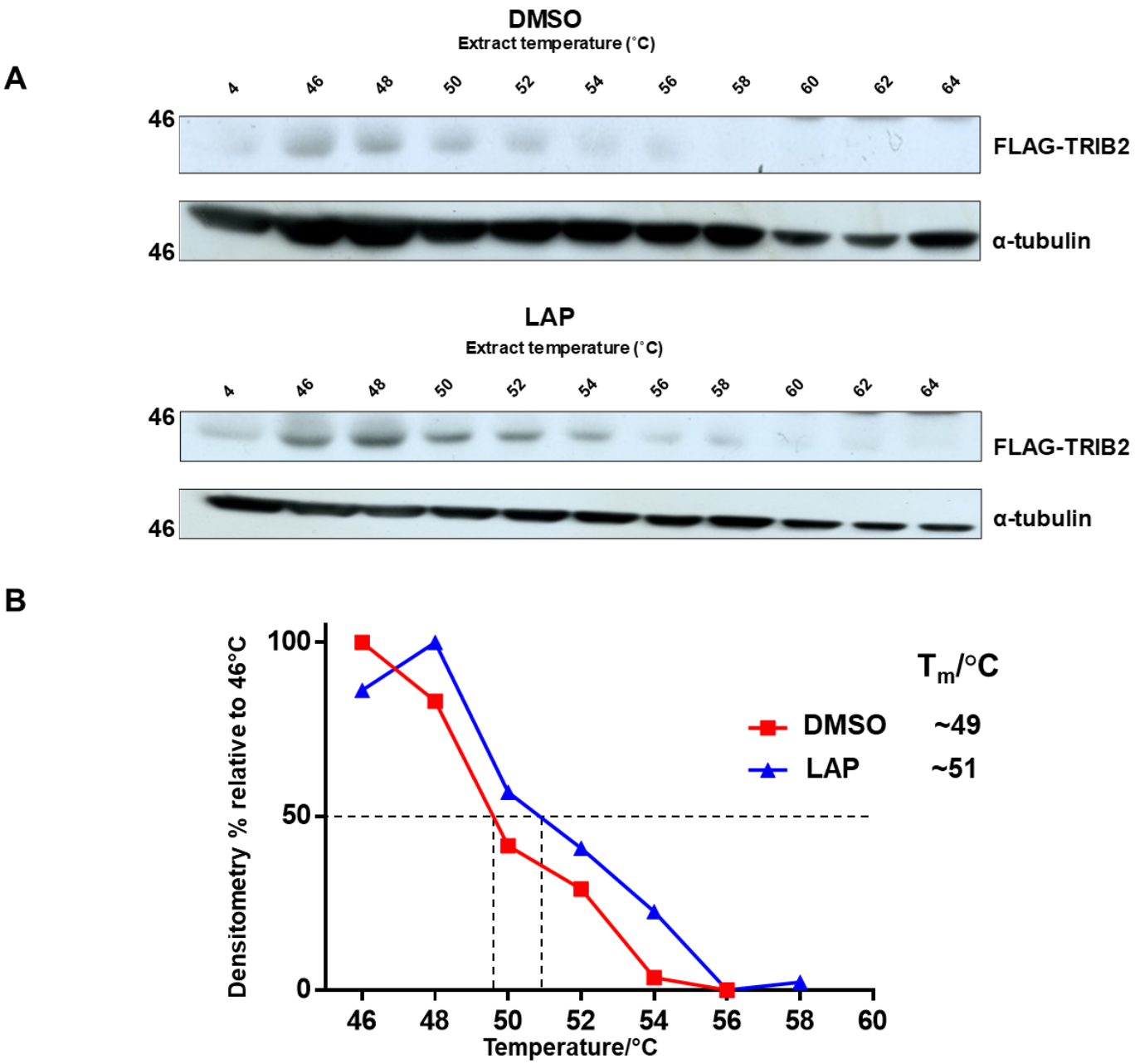


**Figure 4.12: CETSA analysis of lapatinib in FLAG-TRIB2 expressing HeLa cells**. (A) Stable isogenic HeLa cells were induced to express FLAG-TRIB2 with TET for 16 hours with cells reaching 90% confluence at which point they were incubated with 0.1% (v/v) DMSO or 100 µM lapatinib for 1 h. Cells were subsequently trypsinised and re-suspended in PBS. The re-suspended cells were sub-aliquoted into PCR tubes and heated in a series of 2ºC increments between 46 and 64ºC. The cells were subsequently lysed by sonication, centrifuged for 20 minutes at 18,000 g and analysed by western blot for FLAG-TRIB2 and α-tubulin. (B) Densitometry analysis data from (A). Percentage is relative to the densitometry value obtained at 46°C.

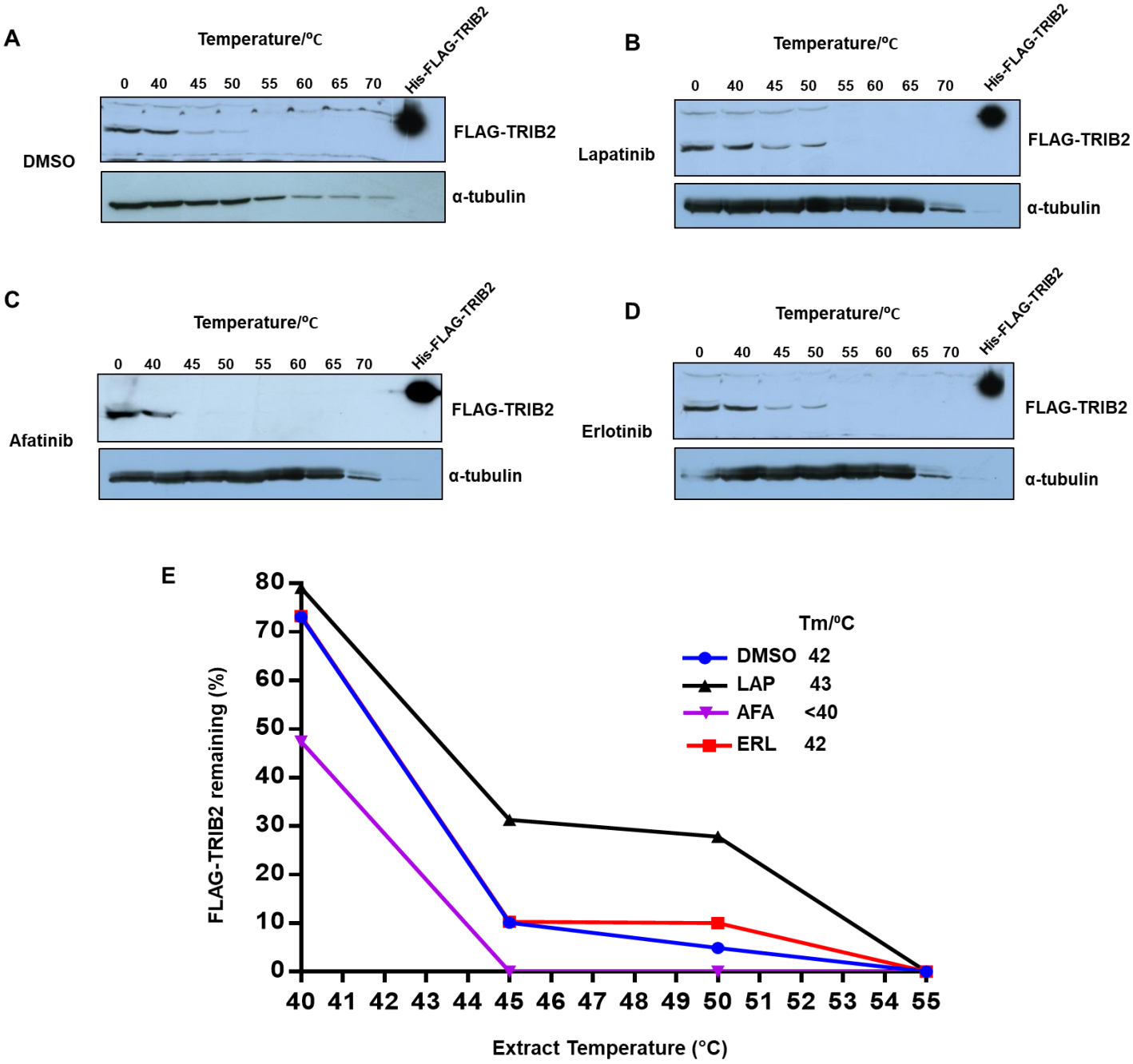


**Figure 4.13: CETSA suggests intracellular engagement of afatinib and Lapatinib**. TET induced HeLa cells were gown to 90% confluence and treated with either (A) DMSO or 100 µM of (B) lapatinib, (C) afatinib or (D) erlotinib for 1 hour. Cells were subsequently collected and re-suspended in PBS. The re-suspended cells were aliquoted into PCR tubes and heated at 5 ºC increments from 40 to 70ºC followed by lysis by sonication, centrifugation for 20 minutes at 18,000 **g** and immunoblot analysis. (E) Densitometry analysis of CETSA. Bands were normalised relative to the DMSO control.

## 4.7 Compound binding analysis with TRIB2 cysteine mutants

In Chapter 3 mass spectrometry was used to demonstrate that afatinib covalently bound to TRIB2 at two distinct cysteine residues in the αC-helix, Cys96 and Cys104. CETSA analysis revealed that afatinib binding reduced TRIB2 thermal stability. Destabilisation of TRIB2 in HeLa cells could have been driven through similar mechanisms of covalent binding identified by *in vitro* analysis (section 3.10.2, Figure 3.29). It was hypothesised that afatinib covalently bound to cellular TRIB2, in turn inducing destabilisation. For this reason, HeLa cells lines expressing Cys 96 and Cys 104 Ser residues, were generated.

### 4.7.1 Stability of WT, C96S and C96/104S-TRIB2 in the presence of EGFR/HER2 kinase inhibitors

PCR was performed to introduce C96S and double cysteine to serine C96/104S mutants into TRIB2 encoded within the pcDNA5/FRT/TO plasmid. Parental HeLa Flp-In T-Rex were transfected, as previously described, generate stable TRIB2 Cys mutant expressing cell lines. On TET induction all full length TRIB2 proteins (WT, C96S, C96/104S and AQLAA) were expressed to similar levels (Figure 4.14) and total TRIB2 levels were increased after 4 hours incubation with MG132. In the absence of TET there appeared to be either a faint cross-reactive band or a slight degree of expression leakage, which was consistent regardless of the cell line.

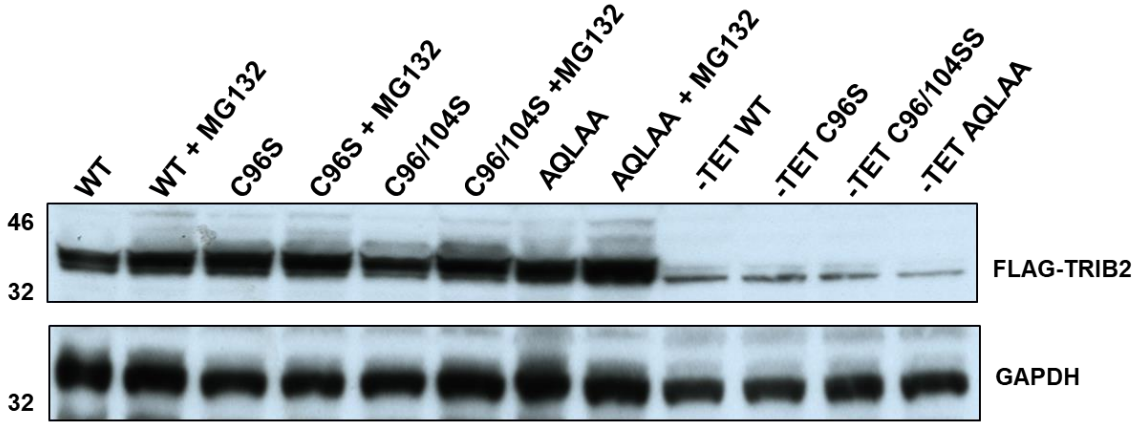


**Figure 4.14: FLAG-TRIB2 cysteine mutants and COP1 binding site AQLAA mutants express at similar levels to WT TRIB2**. Stable HeLa cell lines were induced with TET for 16 hours to express either WT, C96S, C96/104S or AQLAA FLAG-TRIB2 followed by incubation with either 0.1% DMSO (v/v) or 10 µM MG132 for 4 hours prior to lysis and immunoblot analysis.

Firstly, with comparison to WT TRIB2, the effect of selected EGFR/HER2 inhibitors on cellular C96S TRIB2 was assessed in TET induced HeLa cells. As expected, after 4 hours incubation, afatinib induced extensive destabilisation of WT TRIB2 (Figure 4.15). Excitingly, the destabilisation effect was diminished for C96S TRIB2. Neratinib induced partial degradation of WT TRIB2 but C96S TRIB2 remained more stable. In this experiment, there was less WT TRIB2 in the presence of lapatinib, but this was not seen consistently and such a decrease in TRIB2 expression in the presence of lapatinib was not apparent in previous or subsequent experiments. Moreover, levels of C96S TRIB2 did not seem to be influenced by lapatinib. Lapatinib gave an identical stabilising thermal shift profile for both WT and C96S TRIB2 when recombinant proteins were assayed *in vitro* by DSF (section 3.10.2, Figure 3.29). In chapter 3 it was also demonstrated that the thienopyrimidine EGFR/HER2 dual type I inhibitor TAK-285 also stabilised recombinant WT and C96S TRIB2 when assayed by DSF. However, in TET induced HeLa cells, TAK-285 did not appear to have a significant effect on WT or C96S-TRIB2 stability. Erlotinib, as expected, did not observably affect the amount of WT or C96S-TRIB2.

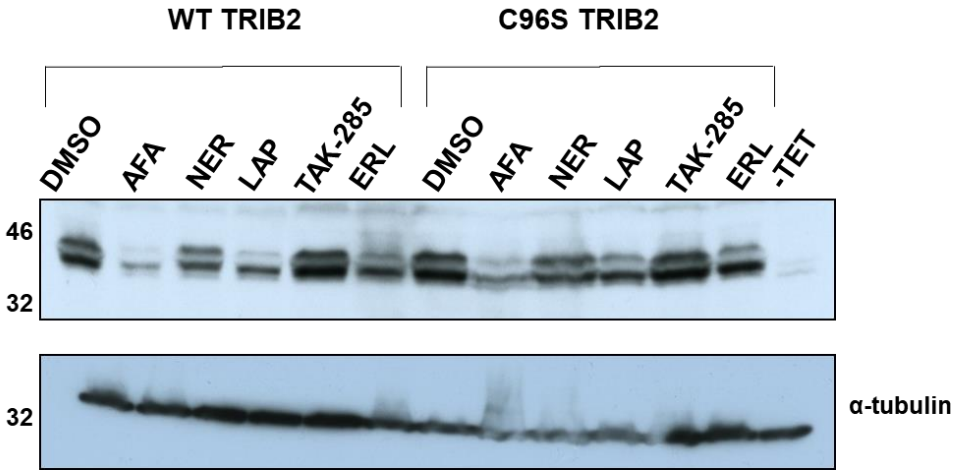


**Figure 4.15. Comparison of WT and C96S TRIB2 in HeLa cells in the presence of EGFR/HER2 inhibitors**. HeLa flp-in cells expressing either WT or C96S full length FLAG-tagged TRIB2 were induced with TET for 16 hours. Cells were subsequently treated with either DMSO, 10 μM afatinib, neratinib, lapatinib, TAK-285 or erlotinib for 4 hours. Whole cell extracts were obtained followed by immunoblot analysis.

Next the effect of inhibitors were tested on the double C96/104S mutant in inducible HeLa cells. Erlotinib had no discernible effect on WT or C96/104S TRIB2 (Figure 4.16).

It was interesting to observe that, unlike WT, C96/104S was only partially destabilised in the presence of afatinib and almost completely resistant to degradation in the presence of neratinib (Figure 4.16). As demonstrated from my previous DSF TRIB2 analysis (Chapter 3), both C96S and C96/104S TRIB2 were resistant to destabilisation to the covalent EGFR inhibitors afatinib and neratinib. However, as deduced from cellular analysis, the double Cys TRIB2 mutant was the most resistant to destabilisation induced by afatinib and neratnib in HeLa cells.

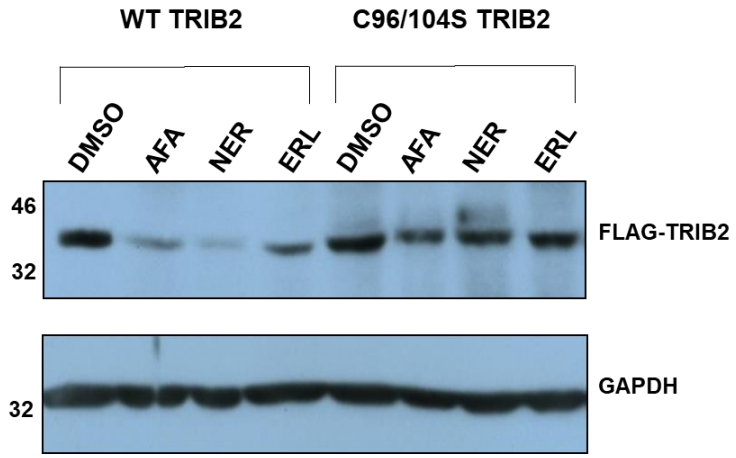


**Figure 4.16: Comparison of WT and C96/104S TRIB2 in HeLa cells in the presence of EGFR/HER2 inhibitors.** HeLa flp-in cells expressing either WT or C96/104S full length FLAG-tagged TRIB2 were induced with TET for 16 hours. Cells were subsequently treated with either DMSO, 10 μM afatinib, neratinib or erlotinib for 4 hours. Whole cell extracts were obtained followed by immunoblot analysis.

### 4.7.2 Afatinib dose response analysis of C96S and C96/104S-TRIB2 mutants in HeLa cells

TET-inducible WT, C96S or C96/104S TRIB2 mutant stable cell lines were evaluated in the presence of varying concentrations of afatinib. To determine the effect on exogenous TRIB2 stability, immunoblotting and densitometry analysis was employed. Afatinib induced dose-dependent loss of TRIB2 in WT-TRIB2 cells, which was partially prevented for C96S, and completely abolished in C96/104S TRIB2-expressing cells (Figure 4.17A). Densitometry analysis from three separate dose response experiments confirmed that differences in WT-TRIB2 and Cys mutant TRIB2 levels were statistically significant (Figure4.17B). Interestingly, for WT TRIB2 the greatest degree of destabilisation took place between concentrations of 10 and 20 μM of

afatinib. A K*d,* between afatinib and WT TRIB2 previously measured at 16 µM (section 3.8.2, Figure 3.24) is in agreement with these results and supports the hypothesis that there is a direct interaction between afatinib and TRIB2 in HeLa cells, with subsequent covalent modification of TRIB2 by afatinib leading to TRIB2 degradation.

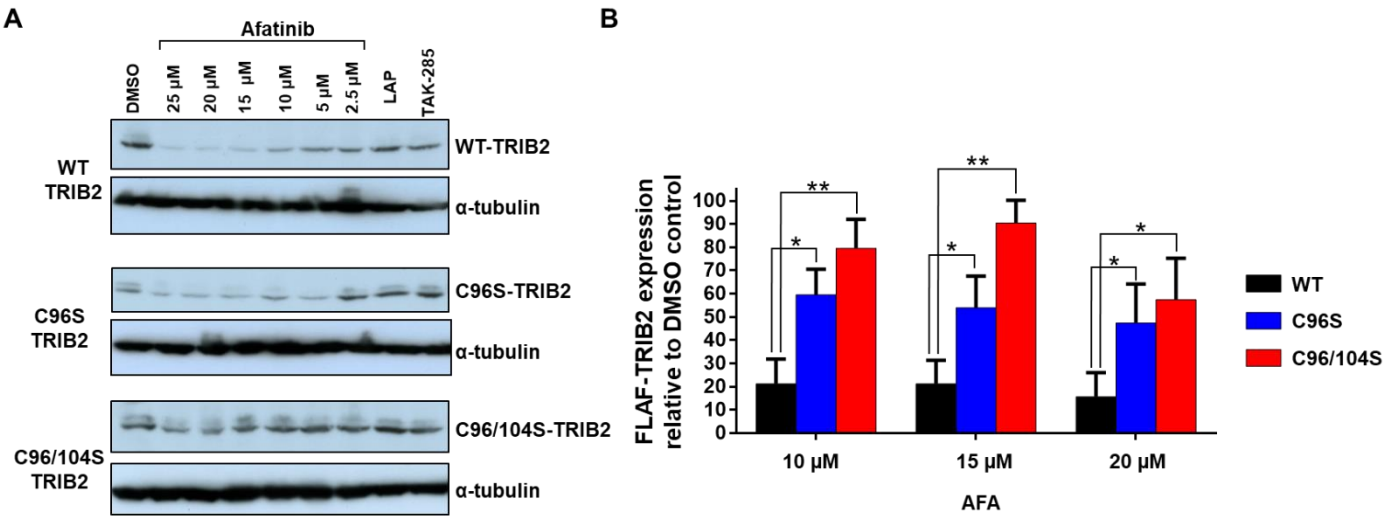


**Figure 4.17: Dose response of afatinib versus WT, C96S and C96/104S**. (A) The indicated concentration of afatinib, 10 µM lapatinib or 10 µM TAK-285 were incubated for 4 hours with isogenic stable HeLa cells expressing WT-TRIB2, C96S or C96/104S TRIB2 (induced by TET exposure for 16h). After lysis, whole cell extracts were immunblotted with the indicated antibodies. (B) FLAG-TRIB2 levels were quantified after exposure to 10, 15 and 20 µM afatinib relative to DMSO controls using densitometry, with a representative experiment shown (significance assessed using data from three independent experiments and students t-tests $p < 0.05$* and $p=0.01$ **).

### 4.7.3 Analysis of AQLAA-TRIB2 destabilisation in the presence of afatinib

From *in vitro* DSF analysis, it was suggested that binding of afatinib to TRIB2 caused the C-terminal tail to uncouple from the pseudokinse domain. To explore and better understand what effect this might have on cellular TRIB2, an afatinib dose response analysis of WT and AQLAA TRIB2 was carried out in HeLa cells. The C-terminal tail AQLAA-TRIB2 mutant was indeed destabilised in a dose dependent manner (Figure 4.18). In side by side analysis, AQLAA-TRIB2 was more sensitive to afatinib mediated degradation than WT-TRIB2 (Figure 4.18A). WT-TRIB2 had greater stability than AQLAA-TRIB2 at afatinib concentrations of 2.5 and 5 µM. In a repeat experiment it

was clear that AQLAA was pointedly destabilised at an afatinib concentration as low as 2.5 µM (Figure 4.18B). Previous thermal profiling analysis (section 3.6.1, Figure 3.14) along with biochemical and crystal structure analysis of TRIB1 [105, 106], suggested that absence of an *in-cis* interaction between the E3 ligase binding motif (DQLVP) and binding pocket in the αC-helix causes TRIB1 and TRIB2 to adopt an open 'destabilised' conformation. It could be hypothesised that this open conformation predisposes AQLAA-TRIB2 to afatinib binding and subsequent degradation. As AQLAA-TRIB2 was expressed at similar levels to WT-TRIB2 and was degraded in the presence of afatinib, it can be argued that AQLAA-TRIB2, in the open 'destabilised' conformation, is not degraded until covalently modified by afatinib.

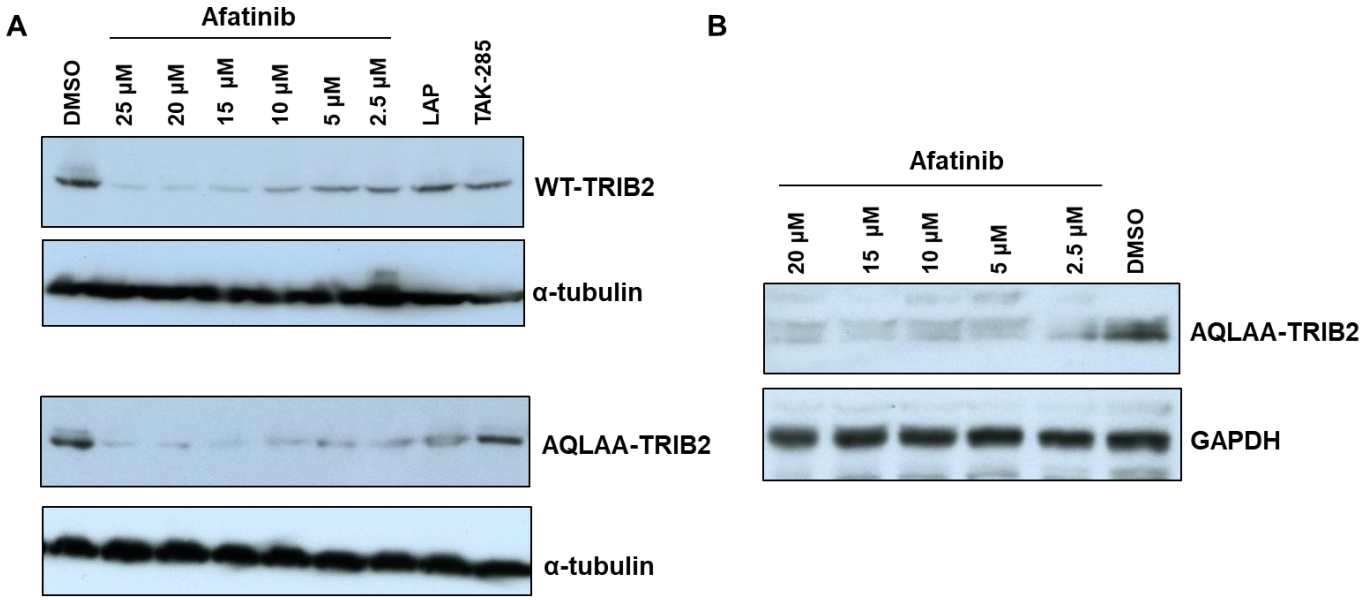


**Figure 4.18: AQLAA TRIB2 is more sensitive to afatinib mediated degradation**. (A) The indicated concentration of afatinib, 10 µM lapatinib or 10 µM TAK-285 were incubated for 4 hours with isogenic stable HeLa cells expressing WT-TRIB2 (top) or AQLAA-TRIB2 (bottom). After lysis, whole cell extracts were immunoblotted with the indicated antibodies. (B) The indicated concentration of afatinib was incubated for 4 hours with isogenic stable HeLa cells expressing AQLAA-TRIB2 prior to immunoblot analysis.

## 4.8 Effects of TRIB2 signalling in transiently transfected HeLa cells

In order to investigate the effects of TRIB2 overexpression on certain signalling pathways, previously established to be influenced by TRIB2 expression, transiently transfected HeLa cells were TET induced and analysed by western blotting. As shown

in section 4.1.1, transiently transfected HeLa Flp-In T-Rex cells expressed ~7.5 ng per µg of lysate after 16 hours induction with TET. With high expression it was expected that effects of TRIB2 on various signalling pathways associated with normal TRIB2 function would be amplified.

### 4.8.1 Investigating TRIB2 dependent regulation of AKT, CDC25C and ACC in transiently transfected HeLa

A previous study found that TRIB2 could directly interact with AKT leading to AKT phosphorylation, through an unknown mechanism, at Ser473 but not Thr308 [103]. The effects of high FLAG-TRIB2 expression on cell signalling outputs was assessed (Figure 4.19). In the absence of TET There was no detectable TRIB2 expression and a very faint band corresponding to phosphorylated AKT at Ser473. When TRIB2 expression was induced with TET there was an unequivocal increase in AKT phosphorylation at Ser473. This result was consistent with previous findings [103], whereby transfection and expression of TRIB2 in HeLa cells induced phosphorylation of AKT at Ser473 but not Thr308. AKT phosphorylated at Thr308 was not detected in HeLa Flp-In T-Rex cells (data not shown).

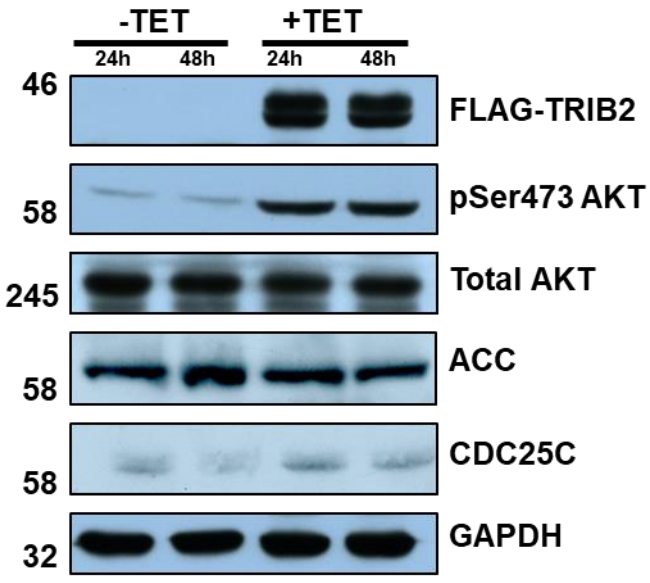


**Figure 4.19: Activation of AKT in transiently transfected parental HeLa cells**. (A) HeLa parental cells were transiently transfected with pcDNA5/FRT/TO encoding the full length WT human TRIB2 gene with a C-terminal FLAG-tag using lipofectamine. Cells were then incubated with TET for 16 hours followed by whole cell lysis and immunoblotting with the indicated antibodies.

CDC25C is an established effector of TRIB2, which becomes targeted for ubiquitination and subsequently degraded via the proteasome [102]. TRIB3 targets acetyl Coenzyme A carboxylase (ACC) for proteasome mediated degradation, via association with the E3 ligase COP1, in adipocytes [107]. To examine the effects of TRIB2 expression on levels of CDC25C and ACC in HeLa cells, immunoblot analysis was performed on lysates from TET induced transiently transfected HeLa cells (Figure 4.19). It was hypothesised that expression of TRIB2 in HeLa cells would result in a decreased observable amounts by immunoblotting due to ubiquitination and degradation of these target proteins. On the contrary, levels of ACC in transiently transfected HeLa cells did not perceivably change (Figure 4.19). CDC25C levels did not decrease in the presence of TRIB2 either.

### 4.8.2 Analysis of the effect of hyper stable C104Y TRIB2 mutant on AKT signalling

The TRIB2 C104Y mutant was established to have a thermal stability far greater than WT-TRIB2 when analysed by DSF (Figure 4.20A). The cartoon diagrams represent the amino acid Tyr for Cys substitution. Steric hindrance due to the Tyr134 in TRIB1 (Cys104 in TRIB2) is proposed to reduce freedom of movement in the αC-helix and thus maintain TRIB1 in the SLE-out 'stabilised' conformation [105, 106]. Consistent with this finding, upon mutation of Cys104 to a Tyr, TRIB2 had the same $T_m$ (~49 °C) as previously observed for TRIB1 by Murphy and colleagues (2015) [106], suggesting that TRIB2 was stabilised in the SLE-out conformation. Remarkably, this increased thermal stability resulted in greater expression levels of C104Y compared to WT-TRIB2 in HeLa cells (Figure 4.20B). Furthermore this increase in TRIB2 correlated with enhanced levels of AKT phosphorylation at Ser473.

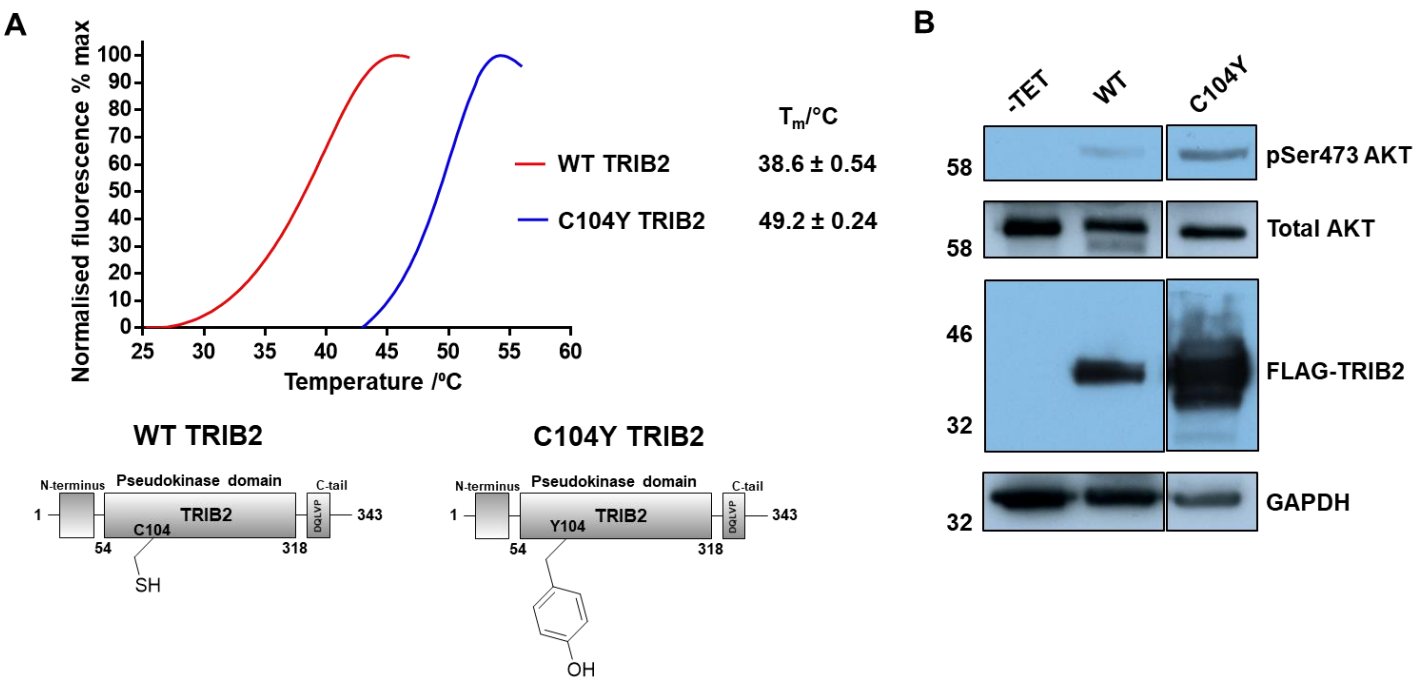


**Figure 4.20: C104Y FLAG-TRIB2 is more stable than WT in HeLa cells**. (A) Thermal melting profiles of WT and C104Y TRIB2 analysed by DSF. (B) HeLa parental cells were transiently transfected with pcDNA5/FRT/TO encoding either WT or C104Y FLAG-TRIB2 using lipofectamine. Cells were TET induced for 16 hours followed by immunoblotting with the indicated antibodies.

### 4.8.3 Analysing the effect of afatinib on TRIB2 and AKT in transiently transfected HeLa cells

Overexpression of TRIB2 activated pSer473 AKT. Afatinib was proposed to covalently bind to TRIB2, exploiting the thiol functional group of Cys96 and Cys104, resulting in conformational rearrangement towards an SLE-in ‘destabilised’ state (section 3.10.3, Figure 3.32) before cellular degradation. I therefore hypothesised that exposure of afatinib to transiently transfected TET induced TRIB2 expressing HeLa cells would destabilise TRIB2 in turn leading to abrogated AKT phosphorylation at Ser473. Consistently, TET induced transiently transfected HeLa cells with WT-TRIB2 and C96/104S-TRIB2 had a higher levels of detectable pSer473 AKT in the presence of DMSO, as opposed to un-induced transfected HeLa (Figure 4.21). This finding demonstrated that mutation of both Cys96 and 104 residues to Ser did not block the ability of TRIB2 to induce Ser473 phosphorylation in AKT. After 4 hours incubation

with afatinib, however, the amount of observable WT, but not C96/104S-TRIB2, decreased. Remarkably, the destabilisation of WT-TRIB2 accorded with less pSer473 AKT. Conversely, AKT phosphorylation at Ser473 in the presence of C96/104S-TRIB2 and afatinib remained consistent relative to DMSO exposed HeLa cells. This finding supports the hypothesis that TRIB2 is targeted by afatinib, which directly influences AKT phosphorylation at Ser473. Although in the presence of afatinib WT-TRIB2 was destabilised in transiently transfected HeLa cells, this was not tantamount to the extent TRIB2 destabilisation in stable HeLa cells. An explanation could be that the greater quantity of TRIB2 expressed in transiently transfected HeLa cells (~7.5 ng/µg) relative to stable HeLa cells (0.06 ng/ µg) was not fully destabilised within the 4 hours of afatinib incubation. Therefore the effects of TRIB2 cellular signalling were assessed in stable HeLa cell lines.

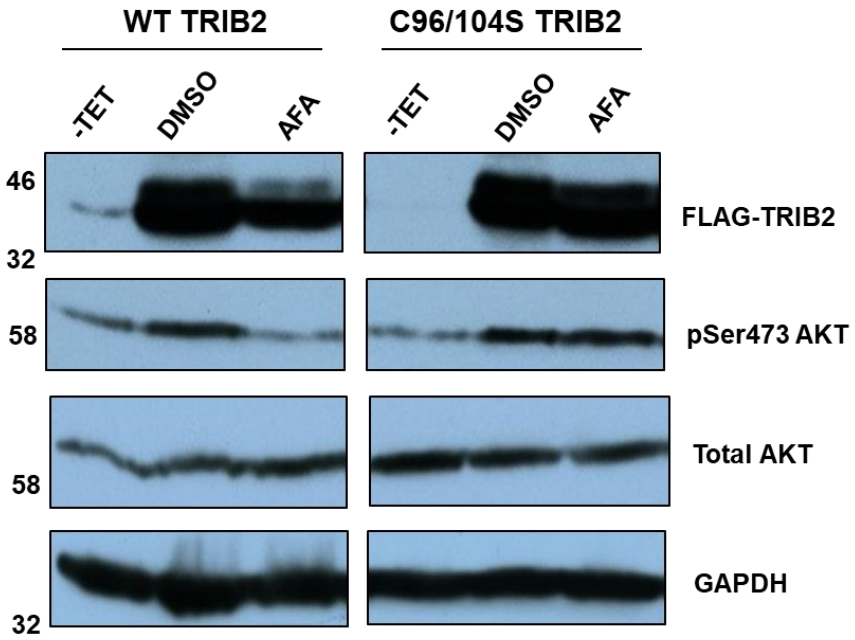


**Figure 4.21: Partial degradation of WT FLAG-TRIB2 followed by decreased AKT activation in transiently transfected parental HeLa cells**. (A) HeLa parental cells were transiently transfected with pcDNA5/FRT/TO encoding the full length WT or C96/104S FLAG-TRIB2 using lipofectamine. Cells were TET induced for 16 hours followed by incubation with either DMSO (0.1% v/v) or 10 µM afatinib prior to lysis and immunoblotting with the indicated antibodies.

## 4.9 Analysis of TRIB2 signalling using kinase inhibitors in stable HeLa cells

I was interested to explore the effects of kinase inhibitors on TRIB2 stability and AKT signalling in the stable TRIB2 expressing HeLa cell lines, because levels of TRIB2 expression were deduced to be closer to those of the disease U937 cell model. The high degree of TRIB2 overexpression in transient HeLa cells (~7.5 ng/µg) is likely not reflective of physiological TRIB2 signalling nor of pathological TRIB2 expression in U937 cells. Moreover, the destabilisation of WT-TRIB2 in transiently transfected HeLa cells by afatinib was not equivalent to that observed in stable induced HeLa, with a significant amount of TRIB2 still remaining after afatinib incubation (Figure 4.21). The effects of TRIB2 expression in stable HeLa cells on levels of total and phosphorylated ACC and CDC25C were also investigated. The main aim of this section was establish whether or not a targeted interaction between WT-TRIB2 and afatinib leads to diminished AKT phosphorylation by analysing the afatinib resistant C96/104-TRIB2 mutant and by employing a panel of various other EGFR/HER2 kinase inhibitors as controls.

### 4.9.1 Effect of TRIB2 expression on levels ACC and CDC25C in stable HeLa cells

In TET induced stable HeLa cells, as opposed to transiently transfected HeLa, there was a decrease in the total amount of ACC observed, compared to un-induced HeLa (Figure 4.22). Interestingly, phospho ACC was detected in un-induced cells but not when TRIB2 was expressed. This finding suggest that phosphorylation might have a role in regulating targeted ACC degradation in the presence of TRIB2. Upon incubation of TET induced stable HeLa with afatinib TRIB2 was destabilised and levels of both total and phosphorylated ACC increased. The increased signal was, however, far greater than from those from the un-induced HeLa cell lysate, suggesting that afatinib influenced ACC and phospho ACC levels through off targeted compound induced effects. Therefore it would not be possible to come to any conclusions about the effect of TRIB2 on ACC, in the presence of afatinib.

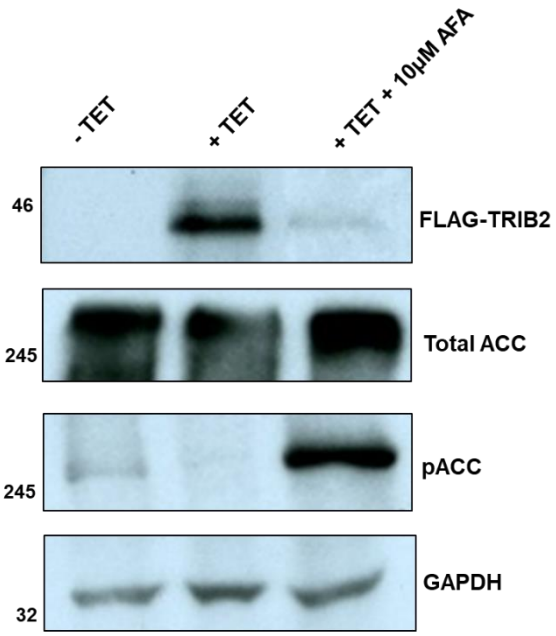


**Figure 4.22: Expression of FLAG-TRIB2 correlates with decreased levels of acetyl Coenzyme A carboxylase (ACC) in stable HeLa cells.** (A) Stable HeLa cells were incubated ± TET for 16 hours followed by a further 4 hour incubation with DMSO (0.1% v/v) or 10 μM afatinib prior to whole cell lysis and immunoblot analysis.

Despite the fact that TRIB2 expression led to a decrease in the quantity of total ACC and abolition of phospho ACC, matters were complicated by the presence of afatinib, which appeared to induce a sharp rise in both total and phospho ACC levels (Figure 4.22). Therefore, as a potential alternative, TRIB2 mediated effects on CDC25C were explored. Although afatinib and neratinib destabilised TRIB2 in TET induced stable HeLa cells, there was no apparent change in the quantity of CDC25C observed (Figure 4.23). The employed EGFR and dual EGFR/HER2 kinase inhibitor controls geftinib and lapatinib, previously demonstrated to not influence TRIB2 stability in the stable HeLa cell model, did not modulate the amount of CDC25C observed either. Hence CDC25C levels did not appear to be modulated by the potential off target effects of the EGFR/HER2 inhibitors tested, however, targeted degradation of CDC25C in the presence of TRIB2 could not be evidenced in this experiment.

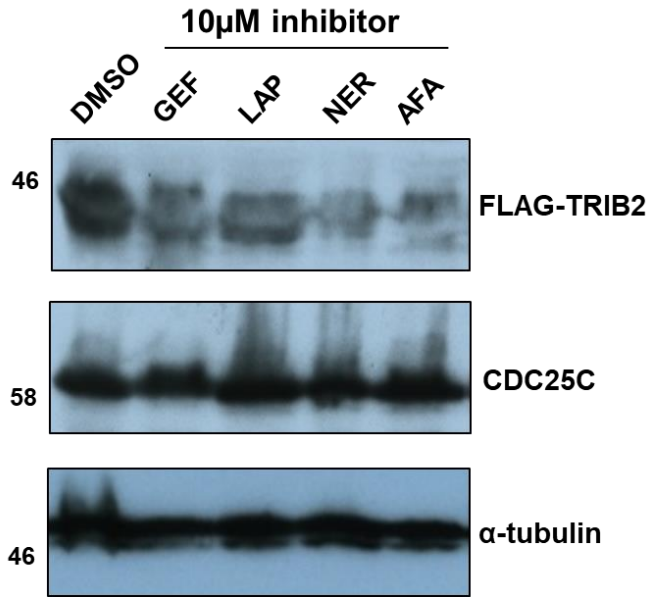


**Figure 4.23: Expression of FLAG-TRIB2 does not affect CDC25C levels in stable HeLa cells**. (A) Stable HeLa cells were incubated ± TET for 16 hours followed by a further 4 hour incubation with DMSO (0.1% v/v) or 10 μM of indicated inhibitor prior to whole cell lysis and immunoblot analysis.

### 4.9.2 Development of a serum block and release procedure to observe the effect of TRIB2 expression and degradation on AKT activation

Unfortunately, no AKT pSer473 could be detected in induced or un-induced stable HeLa cells under standard cellular conditions (data not shown). This was presumably due to low levels of AKT activation, which were below the limits of detection by immunoblotting. However, by utilising a serum block and release procedure, pSer473 AKT levels became much more readily detectable (Figure 4.24). After serum starvation for 16 hours, stable HeLa cells were incubated ± TET. Interestingly, in the absence of TET, AKT became phosphorylated at Ser473 at 4 hours after serum addition and remained phosphorylated for the next 4 hours before being totally undetectable once again. Excitingly at 4 hours, in the presence of TRIB2, AKT phosphorylation was evident and lasted for 24 hours. After 48 hours, with subsided TRIB2 expression, phospho AKT signal was no longer detected. This experiment showed that the presence of TRIB2 could stimulate AKT phosphorylation. In a stable HeLa cell line, at 24 hours there was clear phosphorylation of AKT in the TET induced HeLa cells; this

would provide a time framework from which to investigate the effects of repurposed kinase inhibitors on TRIB2 signalling in stable HeLa cells.

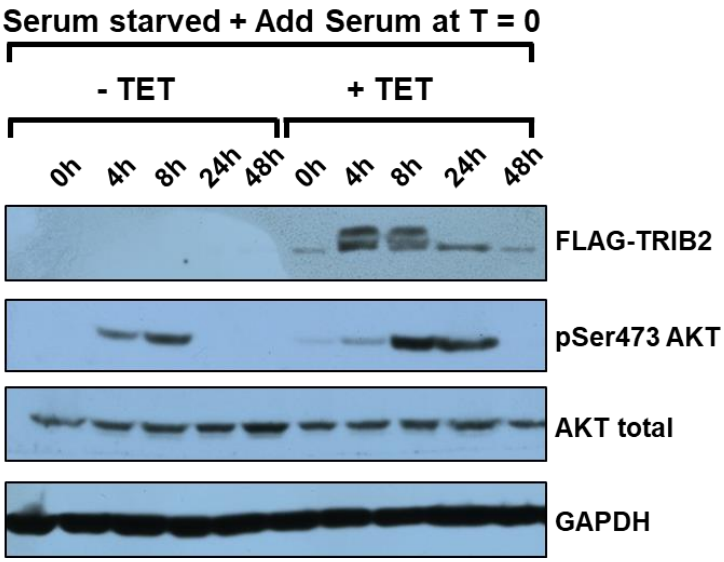


**Figure 4.24: TRIB2 induces AKT phosphorylation in stable HeLa cells after serum block and release**. Uninduced (-Tet) or Tetracycline-induced (+Tet) FLAG-TRIB2 stable HeLa cells were serum starved for 12 h prior to the addition of serum, and lysed at the indicated times. Whole cell extracts were blotted with FLAG antibody to detect TRIB2, pSer 473 AKT antibody or total AKT and total GAPDH as loading controls.

### 4.9.3 Analysing the effect of inhibitors on WT and C96/104S-TRIB2 and AKT signalling in stable HeLa cells

HeLa cells were serum starved for 16 hours prior to the addition of TET and fully supplemented medium for 20 hours. Thereupon selected EGFR/HER2 inhibitors were added for a further 4 hours before lysis and immunoblotting (Figure 4.25). In the presence of afatinib WT-TRIB2 was completely destabilised, which in turn resulted in a large decrease in AKT phosphorylation. In support of this assertion, C96/104S-TRIB2, as before, was completely resistant to degradation in the presence of afatinib, which caused levels of Ser473 phosphorylated AKT to be unaffected. The important controls TAK-285 (EGFR/HER2 dual type I inhibitor) and erlotinib (monovalent EGFR type I inhibitor) had no effect on TRIB2 expression or AKT phosphorylation, but both completely abolished ERK phosphorylation. Importantly, all of the EGFR or

EGFR/HER2 signalling pathway inhibitors consistently blocked ERK phosphorylation (Figure 4.25); any unique effects of drugs amongst this panel are therefore likely to be 'off-target' to EGFR/HER2.

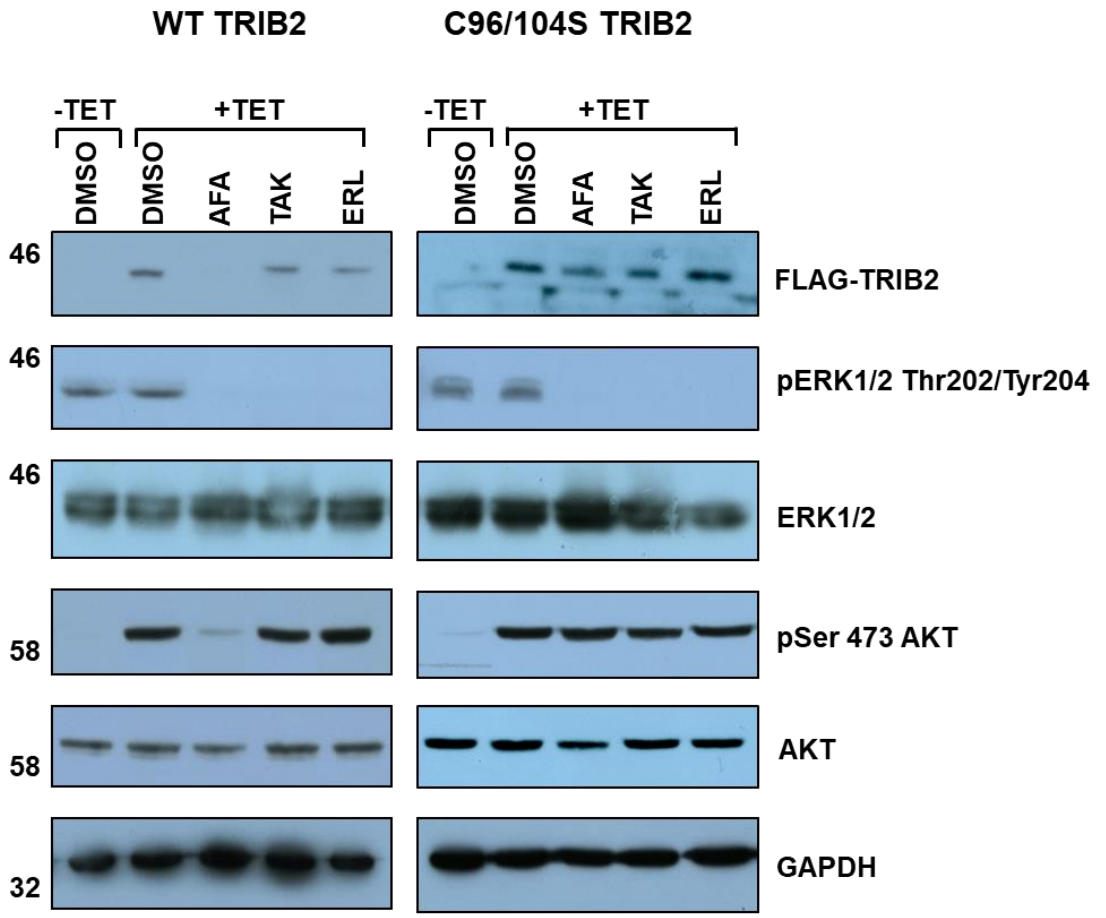


**Figure 4.25: C96/104S TRIB2 is resistant to afatinib mediated degradation and maintains AKT phosphorylation at Ser473.** WT and C96/104S stable HeLa cell lines were subjected to a serum block-and-release protocol (materials and methods). Subsequently, the indicated compounds (10 μM) were added for 4 h prior to cell lysis and immunoblotting with the indicated antibodies.

## 4.10 Analysis of novel TRIB2 inhibitors in U937 cells

TRIB2 expression has only previously been analysed in a few cell types, in large part due to a lack of reliable TRIB2 reagents. Using the previously described novel in-house TRIB2 antibody (Figure 4.4), the effects of endogenous TRIB2 stability and signalling outputs in U937 cells were explored in the presence of kinase inhibitors.

High levels of TRIB2 expression drive AML *in vivo* by inhibiting myeloid differentiation and promoting proliferation [109, 112]. TRIB2 expression is required for U937 survival, with loss of viability after knockdown of TRIB2 with siRNA [113].I therefore hypothesised that kinase inhibitors that induced degradation of endogenous TRIB2 would have enhanced cytotoxicity in U937. To this end Trypan blue and MTT cell viability assays were carried out on U937 cells in the presence of selected small molecule kinase inhibitors.

### 4.10.1 Investigating endogenous TRIB2 stability and AKT signalling in U937 cells using EGFR/HER2 kinase inhibitors

Incubation of afatinib with U937 cells for 4 hours induced destabilisation of endogenous TRIB2 (Figure 4.26). Erlotinib, as previously shown in HeLa cells, had no effect on levels of TRIB2. MG132 induced an increase in TRIB2 levels, consistent with previous findings that describe the regulation of TRIB2 turnover through the ubiquitin-proteasome system and my observations in HeLa cells.

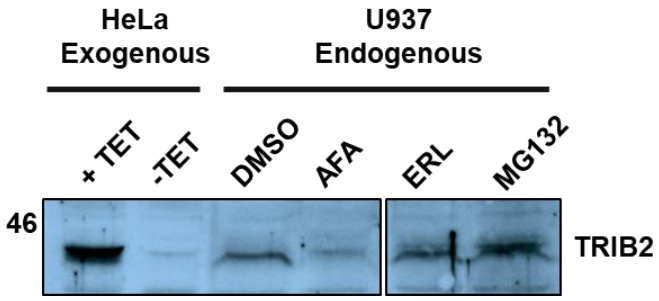


**Figure 4.26: Analysis of endogenous TRIB2 expression U937 cells**. Stable isogenic HeLa cells were incubated +/- TET for 16 hours followed by a 4 hour incubation with DMSO (0.1% v/v) then immunoblotted with α-TRIB2 antibody. U937 cells incubated with either DMSO (0.1% v/v) or 10 μM of afatinib, afatinib with MG132, erlotinib or MG132 alone followed by immunoblotting with α-TRIB2.

Following on from this promising result, varying concentrations of afatinib were incubated with U937 cells for 4 and 24 hours (Figure 4.27A) to observe the effects on endogenous TRIB2 expression and AKT signalling. Endogenous TRIB2 was eliminated in U937 cells in a dose dependent manner. The quantity of detectable TRIB2 was acutely diminished at 10 μM and completely abolished at 20 μM afatinib, which was consistent with that observed for exogenous TRIB2 levels in HeLa cells in

the presence of afatinib (Figure 4.6A). Remarkably, this decrease in endogenous TRIB2 correlated with a decrease in AKT phosphorylation at Ser473, with none being detected at afatinib concentrations where TRIB2 had been extensively destabilised. ERK phosphorylation was totally inhibited at the lowest concentration of afatinib tested (0.5 µM). Therefore, it is likely that the reduction in pSer473 AKT, at the increased afatinib concentrations, was not due to a targeted inhibition of EGFR and HER2. Furthermore, lapatinib and erlotinib did not influence TRIB2 stability or modulate AKT phosphorylation but did inhibit pERK (Figure 4.27A). Cleavage of caspase-3 marks the onset of apoptosis and is an indicator of cell viability and was detected in the presence of compounds. At high concentrations of afatinib, when TRIB2 was extensively destabilised and AKT phosphorylation was inhibited, the cleavage products of caspase-3 could be observed (Figure 4.27A), the intensity of which rose with increasing afatinb concentration and TRIB2 elimination. The protesomal inhibitor bortezomib is a clinical agent in the treatment of some haematological malignancies and is highly cytotoxic to U937 cells [278]. Bortezomib was therefore employed as the positive control, which induced caspase-3 cleavage in U937 cells (Figure 4.27A).

An extended period of 24 hours incubation with compounds was next used to explore the effects on endogenous TRIB2, pSer473 AKT and caspase-3 cleavage (Figure 4.27B). Interestingly, with 24 hours exposure to afatinib, endogenous TRIB2 was cleared from U937 cells at lower concentrations than observed for 4 hours incubation. It was again observed that phosphorylation of AKT at Ser473 concomitantly decreased with TRIB2 degradation, which correlated with caspase-3 cleavage. Both lapatinib and erlotinib had no effect on pSer473 AKT phosphorylation during the 4 hour incubation. However, lapatinib, but not erlotinib caused a decrease in pSer473 AKT levels after 24 hours incubation, but this led to a very slight increase in caspase-3 cleavage.

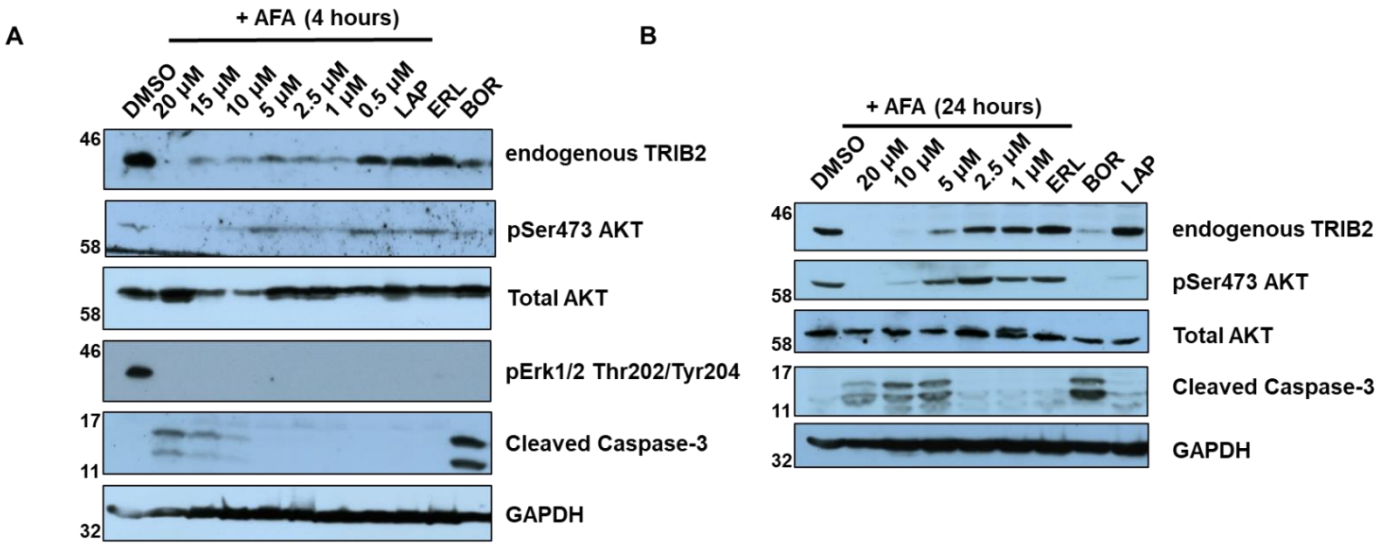


**Figure 4.27: Afatinib destabilises endogenous TRIB2 and induces caspase-3 cleavage in U937 cells.** (A) U937 cells were incubated with either DMSO (0.1% v/v), varying concentrations of afatinib or 10 μM of lapatinib, erlotinib or bortezomib for 4 hours prior to lysis and western blot analysis of endogenous TRIB2, AKT, ERK and cleaved caspase 3. GAPDH served as a loading control. (B) U937 cells were incubated with either DMSO (0.1% v/v), varying concentrations of afatinib or 10 μM of erlotinib or bortezomib for 24 hours prior to lysis and western blot analysis of endogenous TRIB2, ATK and cleaved caspase 3. GAPDH served as a loading control.

### 4.10.2 Exploring the effects of repurposed EGFR/HER2 inhibitors on U937 cell viability

To determine the impact of afatinib treatment on U937 cell viability, cellular cytotoxicity after 4 and 24 hour exposure was measured by employing a Trypan blue assay (Figure 4.28). The untreated cells (DMSO) were calculated to be ~90% viable. After brief 4 hour exposure to varying concentrations of afatinib (between 0.5 and 20 μM), cell viability seemed unaffected (Figure 4.28A). Lapatinib and erlotinib had no effect during this time period and neither did the clinical proteasome inhibitor bortezomib, which was utilised as a positive control for a later exposure (see below). This result could suggest that the destabilisation of TRIB2 and inactivation of pSer473 AKT in the presence of afatinib (Figure 4.27A) at this time point (4 hours) reflected an acute response to compound binding prior to cell death. After 24 hours incubation with compounds cell viability, as measured by Trypan blue, was proportionally affected as a function of increasing afatinib concentration (Figure 4.28B). At an afatinib

concentration of 2.5 µM the percentage of viable cells had decreased slightly from 90% to 77%. After 24 hour incubation with 5 µM afatinib, at which point there was considerable caspase-3 cleavage (Figure 4.27B), cell viability had decreased to 69% (Figure 4.28B). In the presence of 10 µM afatinib cell viability was calculated to be 41%. Bortezomib had enhanced cytotoxicity in U937 cells (26% cell viability) when incubated with the same concentration for 24 hours. The dose dependent effect of afatinib on U937 cell viability was consistent right up to the final concentration tested (20 µM) at which point only 6% of cells were deduced to be viable by Trypan blue assay. Consistent with no apparent caspase-3 cleavage (Figure 4.27), erlotinib had no discernible effect on U937 cell viability after 24 hours (Figure 4.28B). Despite have no apparent cytotoxic effect, as measured by Trypan blue, lapatinib induced small degree of caspase-3 cleavage.

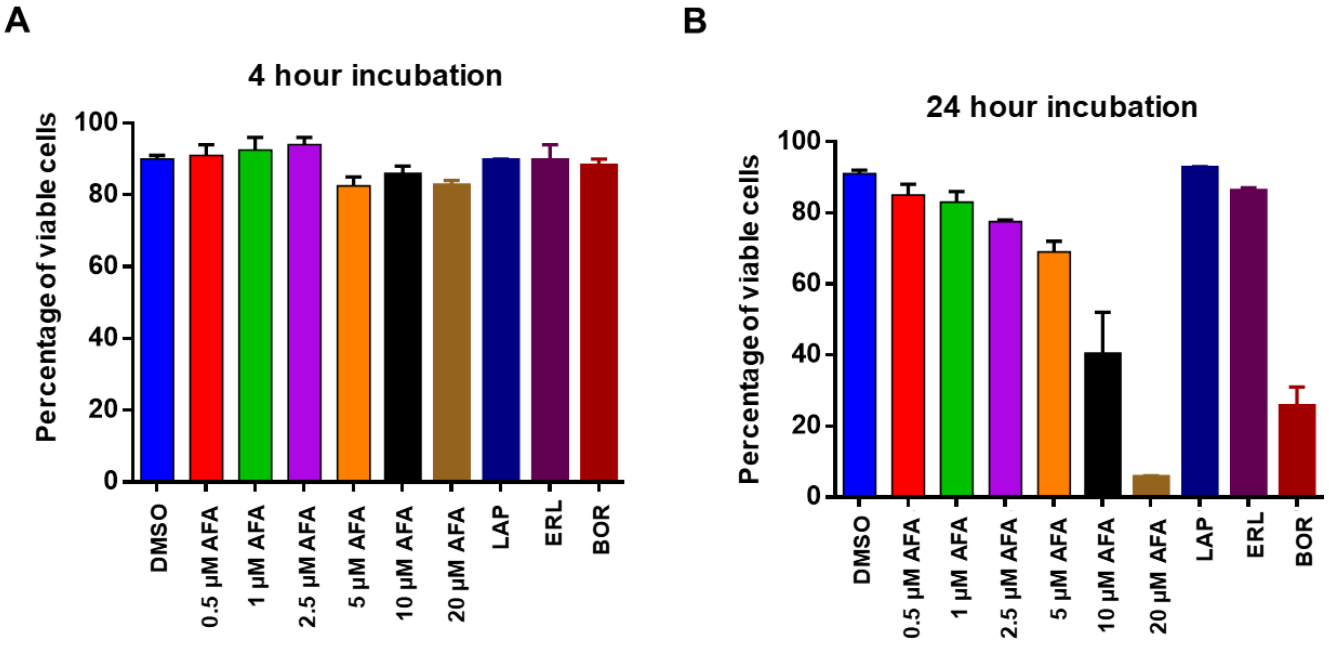


**Figure 4.28: AFA reduces U937 cell viability after 24 hours**. (A) U937 cells were incubated with DMSO (0.1% v/v), the indicated concentration of afatinib or 10 µM of either erlotinib, lapatinib or bortezomib for 4 hours. Cells were then assayed with Trypan blue to assess viability. (B) Same as in (A) except compounds were incubated for 24 hours prior to Trypan blue assay and immunoblot analysis.

Trypan blue analysis revealed that even in the short window of 24 hours, albeit with high inhibitor concentration, there was a marked effect on U937 viability. Interestingly the concentrations at which afatinib began to be cytotoxic (5-20 µM) were the

concentrations that caused TRIB2 destabilisation. It is also fascinating that these concentrations are proximate to the previously reported K*d* for reversible binding (prior to covalent modification) of afatinib to TRIB2, which was 16 µM (section 3.8.2, Figure 3.24A).

To further understand the cytotoxicity of EGFR/HER2 kinase inhibitors in U937 cells and to obtain reliable $IC_{50}$ values (with reference to the positive control bortezomib), MTT assays were completed after incubation with compounds for 72 hours. Afatinib and neratinib reduced cell viability with sub-micromolar $IC_{50}$ values, whereas EGFR inhibitors erlotinib and gefitinib and the dual EGFR/HER2 inhibitor TAK-285, were 10-20 fold less effective when compared side-by-side (Figure 4.29). As these compounds did not induce cellular TRIB2 destabilisation, AKT activation or caspase-3 cleavage, this data suggests that the TRIB2-destabilising ligands afatinib and neratinib possess an enhanced ability to kill AML-derived cells [103]. Interestingly lapatinib, whilst still having a far greater $IC_{50}$ than afatinib and neratinib, was still more potent than gefitinib, erlotinib and TAK-285. It could be hypothesised that lapatinib influenced TRIB2 function and in turn cell viability through a binding mode that did not modulate TRIB2 stability.

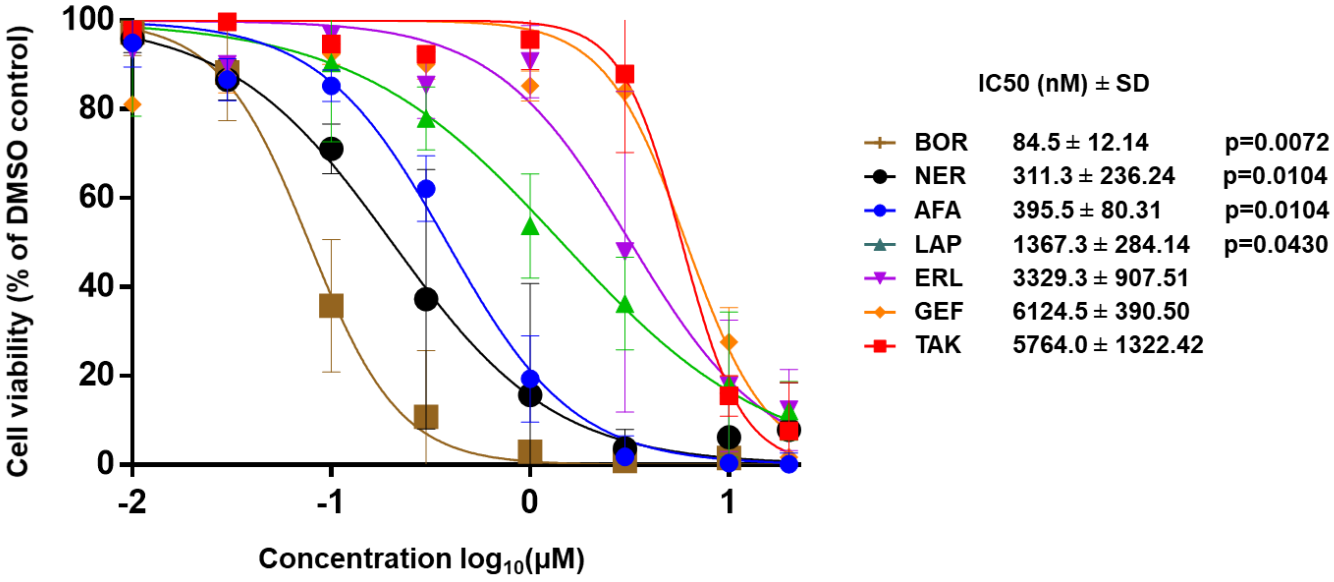


**Figure 4.29: TRIB2 selective inhibitors potently reduce cell viability in U937 cells.** MTT assays comparing the cytotoxicity of a panel of TRIB2 binding and non-binding EGFR/Her2 kinase inhibitors in U937 cells. U937 cells were dispensed in 96 well plates prior to the addition of varying concentrations of inhibitors the following day (0.1% DMSO v/v). The MTT assay was performed subsequent to 72 hours

exposure to inhibitors. IC50 values in nM ± SD derived from 3 independent experiments are shown. Statistical analysis confirmed a significant difference in cytotoxicity between afatinib and erlotinib (students t-test p value = 0.0104) bortezomib and erlotinib (p value = 0.0072), neratinib and elotinib (p value = 0.0104) and lapatinib and erlotinib (p value = 0.04).

## 4.11 Discussion

### 4.11.1 Characterised expression of TRIB2 in HeLa and U937 cells

Stable HeLa cells that expressed FLAG-tagged TRIB2 protein after induction with TET were generated, and TRIB2 expression was analysed by western blotting. Importantly, a novel polyclonal TRIB2 antibody allowed comparison of exogenous FLAG-tagged TRIB2 expressed in HeLa cells to endogenous TRIB2 expressed in U937 cells. Serendipitously, the quantity of TRIB2 expressed by TET induction in stable HeLa cells was similar to the amount observed in U937 cells (Figure 4.4C), which is useful for comparative purposes. Interestingly FLAG-TRIB2 was phosphorylated in HeLa cells, which was confirmed by incubation of the cellular lysate with lambda phosphatase (Figure 4.3). Indeed, from immunoblot analysis, a similar second band faint smeared band could also be observed just above the band corresponding to endogenous TRIB2 in U937 cells (Figure 4.4C). Speculatively, this could have indicated the presence of a TRIB2 phosphorylated form in U937 cells, although unfortunately this was not confirmed with a lambda phosphatase assay due to experimental time constraints.

In AGC kinases, including AKT, repositioning of the αC-helix to permit an active conformation is mediated by an *in cis* docking interaction between the C-terminal tail containing the HF motif and a hydrophobic groove between the αC-helix and β4 strand known as the PIF pocket [24, 295]. Both the HM motif and the αC-helix are disordered when AKT is in an inactive conformation, however, phosphorylation of Ser473 in HF motif of AKT helps to stabilise this active conformation, activating the kinase [42]. It would be interesting to use mass spectrometry analysis to elucidate potential TRIB2 phosphosites, as phosphorylation could serve a similar regulatory purpose. A regulatory interaction between the C-terminal tail and binding pocket near the αC-helix of TRIB1 has recently been elucidated. Biochemical analysis from Chapter 3 suggests that the TRIB2 C-terminal tail also forms interactions within the pseudokianse domain. It would be interesting to observe whether or not mutation of potential TRIB2 phosphosites disrupts or stabilises the interaction of C-terminal tail with the

pseudokinase domain. It was also previously reported that p70S6K, a member of the AGC kinase superfamily, phosphorylates TRIB2 causing degradation via Smurf1 [120] and mutation of Ser83 prevented degradation of TRIB2.

### 4.11.2 Regulation of TRIB2 stability by the proteasome

The turnover of both exogenous FLAG-TRIB2 expressed in HeLa cells and endogenous TRIB2 expressed in U937 cells was dependent on the proteasome (Figure 4.2 and 4.4). It was discovered that TRIB2 was rapidly degraded in the presence of the HSP90 inhibitor geldanamycin. In the presence of both geldanamycin and MG132 TRIB2 was stabilised (Figure 4.2). Inhibition of heat shock proteins has been a major focus of cancer research [296]. Association with the chaperone protein HSP90 can enhance the stability of many cellular proteins, including AKT and EGFR [297, 298]. The HSP90 inhibitor 17-allylamino-geldanamycin inhibited myeloma cell growth by destabilising AKT [297]. Upon HSP90 inhibition by geldanamycin, HER2 is polyubiquitinated and rapidly degraded [299], whereas EGFR is more slowly ubiquitinated with catalytic activity inhibited due to stabilisation of the EGFR monomer. It would be interesting to investigate the effects of heat shock protein inhibition in cell models where TRIB2 is a driver of disease.

In various cell lines, TRIB1 and TRIB2 have been reported to be unstable, which was suggested to be due to conserved destabilising motifs present in the small N-terminal PEST region [104, 120, 300]. However, when the N-terminal domain of TRIB2 was truncated and TRIB2 54-343 was expressed in HeLa cells, protein stability did not increase. Furthermore, TRIB2 54-343 was still stabilised by the proteasome inhibitor MG132 to a similar extent as WT-TRIB2 (Figure 4.10). These data suggest that the N-terminal domain of TRIB2 is not required for protein stability in these cell lines.

When the DQLVP E3 ligase-binding motif of TRIB2 was mutated to AQLAA, expression was similar to WT-TRIB2 and was still stabilised in the presence of proteasome inhibitors. An intact DQLVP motif was previously shown to be required for TRIB2 to target substrates for ubiquitination [112]. Mutation of the DQLVP motif to AQLAA stabilised C/EBPα *in vitro* and *in vivo* [112]. However, these data suggest that turnover of TRIB2 itself is unlikely to be directed through the binding of E3 ubiquitin ligases to the DQLVP motif.

### 4.11.3 Targeting of TRIB2 with the reversible dual EGFR/HER2 inhibitor lapatinib

Although the type I dual EGFR/HER2 kinase inhibitors lapatinib and TAK-285 stabilised TRIB2 *in vitro* when analysed by DSF, there did not seem to be a direct consequence on TRIB2 stability when analysed in HeLa cells. This does not, however, rule out intracellular binding. Compounds were exposed to TRIB2 expressing HeLa cells for only 4 hours. Perhaps an extended period of incubation is required to observe significant changes in levels of TRIB2. Ji and colleagues (2018) [301] discovered, by employing surface plasmon resonance (SPR), that the compound rutacecarpine bound to the active site of VEGF-2 with a K*d* of 0.4706 μM. However, it was only after 48 hours incubation with 5 and 10 μM of inhibitor with HUVEC cells that there was a modest detectable increase in levels of total VEGF-2. Unfortunately, the levels of TRIB2 in TET-induced HeLa cells begin to decrease after 24 hours (Figure 4.24). This is consistent with previous findings that TET has a half-life of around 24 hours in cell culture [302]. To circumvent this issue, CETSA analysis was used to elucidate intracellular compound binding. CETSA revealed that lapatinib did in fact convincingly increase the thermal stability of cellular TRIB2 by ~2 °C. This change in melting temperature is close to the thermal shift induced by lapatinib for *E. coli* purified TRIB2 *in vitro* (~3 °C) (section 3.8.1 Figure 3.23). It has been previously noted that conventional *in vitro* thermal shift assays with recombinant proteins purified from *E. coli* correlate with thermal shifts generated by CETSAs [292]. Thermal shifts generated from the purified poly (ADP-ribose) polymerase domain of PARP-1 analysed by differential static light scattering (DSLS), in the presence of cognate inhibitors (~10 °C), were replicated when analysed by CETSA [292].

In U937 cells, the amount of endogenous TRIB2 was not affected by lapatinib or the type I EGFR inhibitor erlotinib after 4 and 24 hours incubation at 10 μM. However, after 24 hours exposure, lapatinib caused a reduction in the amount of pSer473 AKT in U937 lysate. Perhaps, during this time the effects of an interaction between lapatinib and TRIB2 began to become apparent. In U937 cells 24 hour incubation with lapatinib did not lead to caspase-3 cleavage and the cell viability, assessed by Typan blue, was not affected. However after 72 hours, MTT assay analysis did reveal that lapatinib had enhanced cytotoxicity compared to control EGFR/HER2 inhibitors, which suggests that prolonged exposure of lapatinib had an effect on cell viability, perhaps mediated through interaction with TRIB2.

### 4.11.4 Targeting TRIB2 for proteasomal degradation with covalent kinase inhibitors

These studies focused on electrophilic type IV kinase inhibitors, and since they were likely to bind to TRIB2 via a covalent mechanism, comparative chemical and mutational analysis was amenable [303, 304]. At nanomolar concentrations, afatinib is a specific inhibitor of EGFR and HER2 in cells, however at low micromolar concentrations various other canonical kinases are inhibited due to off-target activity [11]. Moreover, osimertinib has off-targeted effects on both kinases [11] as well as non-kinases [305], including the lysosomal cathepsin proteases. In this chapter the cross-reactivity of afatinib had been exploited to target TRIB2 in cells. CETSA analysis revealed that TRIB2 was thermally destabilised in the presence of afatinib by between 2-3 °C (Figure 4.13), which was similar to thermal shifts observed by DSF. In whole cell assays TRIB2 was rapidly degraded in the presence of afatinib after 4 hours incubation. Interestingly, the dose dependent elimination of TRIB2 had a maximal effect between 10-15 µM, which is remarkably close to the reversible binding of K*d* of afatinib (16 µM) elucidated in chapter 3. The related inhibitor neratinib also induced TRIB2 degradation in HeLa cells.

The cellular mechanism by which TRIB2 stability is regulated is proteasome-based. Unlike lapatinib, covalent compounds such as afatinib binding caused degradation of TRIB2, the effect of which was reversed in the presence of proteasome but not lysosome/autophagy inhibitors. TRIB2 levels were also depleted in the presence of geldanamycin, the effect of which was also reversed in the presence of proteasome inhibitor, indicating a potential stabilising roles of a geldanamycin target on TRIB2. It was previously demonstrated that the binding of lapatinib and vemurafenib to HER2 can deprive the kinase of an interaction with the HSP90-CDC37 system, leading to time-dependent HER2 degradation at micromolar concentrations [306]. It can be speculated that an afatinib-induced conformational change might induce TRIB2 ubiquitination, or negatively regulate interaction with an unknown stabilising factor(s), such as heat shock protein chaperones [286, 307]. It was previously demonstrated that HSP90 does not bind to particular sequence motifs, but in fact associates with intrinsically unstable kinases [308]. TRIB1, TRIB2 and TRIB3 have been reported to be unstable [104, 120, 300], which has been a major challenge in understanding roles of Tribbles in cellular signalling. Therefore, exploring the potential mechanisms of

stabilisation of Tribbles pseudokinases through the HSP90 system could be a valuable endeavour.

### 4.11.5 A chemical genetics approach to elucidate on targeted binding of afatinib to TRIB2

It was hypothesised that mutation of Cys96 and 104 would negate the ability of afatinib to covalently bind to TRIB2. A THZ-derived covalent CDK inhibitor was found to bind covalently to Cys1039 of CDK12 resulting in protein destabilisation and cellular cytotoxicity [304]. HAP1 chronic myeloid leukaemia cells engineered to express a C1039S CDK12 mutation, using clustered regularly interspaced short palindromic repeats- (CRISPR)-cas9 technology, stabilised CDK12 and reversed compound induced cytotoxic effects. Similarly mutation of Cys96 and Cys104 to Ser in TRIB2 abolished destabilisation induced by afatinib. Both TRIB2 Cys-residues, targeted by afatinib, are uniquely located within the distorted αC-helix, which make it vulnerable to certain type IV inhibitors that were originally developed as nanomolar covalent inhibitors of the tyrosine kinases EGFR and HER2. Such dual-targeting suggests shared features between signalling-relevant (‘active’) conformations in the ATP-site of both TRIB2 (SLE-in) and EGFR/HER2 (DFG-in).

It can be asserted that C96/104S-TRIB2 reversibly binds to afatinib but covalent modification of Cys96 and 104 are necessary to induce degradation of TRIB2. Indeed, MST analysis, (see Section 3.8.2), confirmed a reversible binding K*d* of 16 μM to WT TRIB2. Further to this afatinib, has the potential to be developed as a TRIB2 specific ligand as the lack of equivalent Cys residues in other pseudokinases, including the related TRIB1, TRIB3 and STK40, likely prevents them from covalent modification. It was recently discovered that MLKL activity could also be regulated by a covalent compound that exerted its function by binding to a region distal to the active site. The compound necrosulfonamide targeted a unique Cys86 on the N-terminal coiled coil domain of MLKL, in turn preventing necroptosis in human cells [309]. This discovery presents the opportunity to exploit unique Cys residues both within and outside the ATP-binding site to develop target specific pseudokinase irreversible inhibitors.

HER3 was the first pseudokinase to be targeted by irreversible inhibitors. Afatinib has also been shown to bind to HER3, although the binding is reversible due to the presence of a Ser794 residue at the equivalent Cys797 in EGFR. However, an

alternate, unique, Cys721 residue in the roof of the ATP binding pocket has been exploited to which the compound TX2-121-1 irreversibly binds [62]. As well as inducing proteasomal degradation of HER3, TX2-121-1 perturbed the hetero-dimerization of HER3 with HER2 leading to reduced AKT and ERK phosphorylation. The covalent HER3 compound TX2-121-1 was generated by structure-guided hybridization between the most potent hits discovered from initial screening [310]. Alas, in the absence of a high-resolution TRIB2 pseudokinase crystal structure, the conformation(s) relevant for small molecule interaction are not yet known and structure guided design of novel TRIB2 ligands is not yet possible.

The TRIB2 COP1-binding site DQLVP to AQLAA mutant was proposed to be maintained in the 'SLE-in' conformation and destabilised due to the absence of the regulatory interaction between the C-terminal tail and pseudokinase domain *in vitro* (section 3.6). However, AQLAA and WT-TRIB2 had similar stability and expression levels in HeLa cells (Figure 4.14). Remarkably, AQLAA-TRIB2 was more sensitive to destabilisation in the presence of afatinib, suggesting that in the absence of the C-terminal tail, the Cys96 and 104 residues in the αC-helix are more readily primed for covalent modification. It would be interesting to mutate the Cys96 and 104 residues in the AQLAA-TRIB2 mutant to test this hypothesis.

### 4.11.6 Kinase inhibitors to investigate the roles of TRIB2 in cellular signalling

TRIB3 was previously shown to be able to target endogenous ACC for proteasomal-mediated degradation *in vivo* in adipose tissue [107]. In transiently transfected HeLa cells there was no evidence for degradation of ACC in the presence of TRIB2 (Figure 4.19). It was previously observed that TRIB3 had the ability to induce ACC degradation in HeLa cells but only when TRIB3 cDNA was co-transfected with the gene encoding the E3 ligase COP1 [285]. Perhaps in order to observe TRIB2 mediated effects on levels of ACC in HeLa, TET induced cells must also be transfected to express COP1. TET induced stable HeLa cells had lower levels of phosphorylated ACC than un-induced cells, suggestive of perhaps a preferential targeted ubiquitination of phosphorylated ACC (Figure 4.22). Conversely, it was previously demonstrated *in vitro* that the ability of TRIB1 to bind to C/EBPβ was negated when C/EBPβ was phosphorylated at Ser77 or Tyr79, which are within the Tribbles degron [105].

The effects of TRIB2 in U937 cells, in the context of targeted ubiquitination of C/EBPα and CDC25C, have been documented [102, 113]. TRIB2 in TET induced HeLa cells did not induce degradation of either C/EBPα or CDC25C (Figure 4.19). Again, perhaps this was due to the requirement of co-transfection to induce expression of both TRIB2 and the E3 ligase COP1 [285].

It was recently demonstrated that TRIB2 overexpression in various transiently transfected cell lines induced AKT phosphorylation at Ser473 but not Thr308 [103]. In this chapter I demonstrated that transiently transfected HeLa cells expressing TRIB2 had increased levels of pSer473 AKT (Figure 4.19). Stable TET induced HeLa cells also had increased levels of pSer473 AKT after a serum block and release procedure (Figure 4.24).WT-TRIB2 was degraded in the presence of afatinib which lead to decreased levels of pSer473 AKT. Conversely, using chemical genetics it was revealed that the C96/104S-TRIB2 mutant was completely resistant to afatinib, which resulted in maintained levels of pSer473 AKT in the presence of afatinib. This provides strong evidence for targeted activity of afatinib against TRIB2.

### 4.11.7 Targeting TRIB2 in a myeloid leukaemia cell model

The work in this chapter describes the use of novel ligands to elucidate TRIB2 functions in human cells and potential leads for the development of therapeutics where TRIB2 overexpression is a driver of disease [104]. Overexpression of TRIB1 and TRIB2 are associated with hematopoietic malignancies, as well as various solid cancers [104]. Levels of TRIB1 were found to be elevated in AML and myelodysplastic syndrome clinical samples due to gene amplifications and TRIB2 expression was shown to be increased in subsets of AML clinical samples characterised by abrogated C/EBPα function [311, 312]. These findings are supported by *in vivo* murine models, where TRIB2 overexpression in bone marrow progenitors caused fully penetrant and lethal AML [109].

A previous study established that a K177R TRIB2 mutant, that was not able to promote p42-C/EBPα degradation, was able to inhibit granulocyte differentiation in 32D cells [112], suggesting that other functions may be exerted by TRIB2 in haematological malignancies. Although there are reports that TRIB2 may regulate MAPK signalling, no differences in phopho-p44/42 MAPK activity in TRIB2 expressing 32D cells were

observed [112]. This result corroborates previous reports that TRIB1, TRIB2 and TRIB3 could not influence MAPK activation in hematopoietic cells [285].

U937 cells are highly sensitive to knockdown of TRIB2, making them a suitable model to probe TRIB2 function with small molecule inhibitors. The effects of TRIB2 on AKT signalling in U937 cells have not yet been described. In this chapter I have demonstrated that the rapid degradation of endogenous TRIB2 in the presence of afatinib resulted in concomitant loss of pSer473 AKT followed by caspase-3 cleavage. The covalent EGFR/HER2 inhibitor afatinib may represent a promising basis for the development of TRIB2 therapeutics in haematological malignancies where TRIB2 is overexpressed. Afatinib and neratinib exhibited submicromolar cytotoxicity in U937 cells, where other EFGR/HER2 inhibitors were 10-20 fold less potent, despite the fact that all compounds tested completely inhibited pERK. Only afatinib, and to a lesser extent lapatinib (only after 24 hours), caused a reduction in pSer473 AKT, which was proposed to be mediated through binding to TRIB2. Unfortunately dose response assays and immunoblot analyses were not performed in the presence of neratinib, but it can be argued that a reduction in the amount of TRIB2 and pSer473 AKT might be observed. No caspase-3 cleavage was observed after 24 hours incubation of U937 cells with lapatinib. However, of the reversible inhibitors, lapatinib was the most cytotoxic in MTT assay analyses.

Trypan blue assays revealed that afatinib and the clinical leukaemia therapeutic bortezomib had similar cytotoxicity after 24 hours, whereas other EGFR/HER2 inhibitors had no apparent effect. At 24 hours 10 μM afatinib completely eliminated TRIB2 in U937 cells, which coincided with caspase-3 cleavage, giving credence to the assertion that TRIB2 is a rate limiting factor in U937 cell survival. Although it cannot be ruled out that simultaneous effects of afatinib on both TRIB2 destabilisation and ERK/AKT pathway inhibition may be contributing to cellular phenotypes, there is a strong case that afatinib-binding is required for TRIB2 destabilisation and AKT regulation in HeLa and U937 cells. Indeed simultaneous elimination of TRIB2 and inhibition of the ERK-signalling pathway could be a polypharmacological asset, especially in TRIB2-dependent drug-resistance in tumour cells [103, 239].

# Chapter 5: Conclusions and Future investigations

## Conclusions

It is widely accepted that non-enzymatic components can control signalling outputs in normal physiology and disease, exemplified by the cellular activities of pseudokinases [313]. In chapter 3 of this thesis, I sought to target the cancer-associated pseudokinase TRIB2 with small molecules, initially with the aim of evaluating their biochemical properties *in vitro*. In order to discover novel TRIB2 chemical ligands, a relatively simple DSF thermal shift assay was employed [58]. Multiple chemical classes of small molecules originally reported to be specific dual EGFR/HER2 kinase inhibitors (but not monovalent EGFR inhibitors), were discovered to modulate TRIB2 thermal stability *in vitro*. One group of thienopyrimidine based type I ATP-competitive small molecule inhibitors were found to induce a stereotypical (positive) thermal shift by interacting with the pseudo-ATP binding site. A second group of quinazoline-based type IV EGFR/HER2 inhibitors were found to destabilise TRIB2, leading to the opposite (negative) thermal shift. Although initially unexpected, this was mechanistically explained by a Cys-based covalent binding mode, which caused the C-terminal tail of TRIB2 to become uncoupled from its own pseudokinase domain. Consistently, a more thermally-stable conformation of TRIB2, generated by intramolecular interaction between the C-terminal tail and the pseudokianse domain, was targeted by three clinically-approved type IV EGFR/HER2 inhibitors afatinib, neratinib and osimertinib *in vitro*. Synthetic stapled C-terminal tail peptides that compete with the TRIB2 C-terminal tail DQLVP sequence were also found to destabilise TRIB2, again likely by competing with the C-terminal tail for binding in the pseudokinase domain.

A combination of techniques presented in chapter 3 went on to confirm that afatinib and neratinib covalently bound to TRIB2 at Cys96 and Cys104 in the αC-helix. These two distinct Cys residues are not conserved in TRIB1, TRIB3 or the more distantly related pseudokinase STK40. Consistently, afatinib and neratinib did not modulate TRIB1 stability when analysed by DSF, or TRIB2 in which these Cys residues were mutated to Ser. It can, therefore, be argued that the occurrence of the two unique TRIB2 Cys residues exert a selectivity filter, which permits targeting of TRIB2 but not

TRIB1, TRIB3 or STK40, by covalent EGFR/HER2 inhibitors. If this is the case, then the differential effects of TRIB2 versus TRIB1 and TRIB3 in cellular signalling could potentially be analysed in appropriate experimental circumstances. As discussed in chapter 4, the electrophilic type IV EGFR/HER2 chemical ligands, which were amenable to comparative and mutational analysis were found to induce destabilisation and proteasome-mediated degradation of TRIB2 in human cells. Elimination of WT-TRIB2, in the presence of afatinib, correlated with decreased phosphorylation of AKT at Ser473, which correlates with AKT activity, in an inducible exogenous FLAG-TRIB2 expressing HeLa cell model. Conversely, the FLAG-C96/104S-TRIB2 mutant was significantly more resistant to afatinib-mediated degradation, and in turn, phosphorylation of pSer473 AKT was not inhibited. Analysis in a U937 leukaemia disease model revealed that endogenous TRIB2 was also destabilised, and the levels of pSer473 AKT decreased in-line with afatinib degradation, supporting the case that TRIB2 is targeted directly by afatinib in human cells. Furthermore, in U937 cells, upon depletion of TRIB2 and concomitant with a decrease in levels pSer473 AKT, afatinib also induced caspase-3-cleavge, suggestive of apoptosis. The viability of U937 cells also was assessed by MTT assays in the presence of selected EGFR/HER2 inhibitors and the leukaemia chemical therapeutic bortezomib. Afatinib and neratinib were nearly as effective as the clinical proteasome inhibitor bortezomib and were some 10-20 fold more effective than other EGFR and EGFR/HER2 inhibitors.

## 5.1 In vitro analysis of TRIB2 with small molecule kinase inhibitors

In this thesis I have employed various techniques, including DSF, MST and MS to establish that compounds from distinct designated chemical classes bind to TRIB2 *in vitro*. TRIB2 stabilising and destabilising cell-permeable compounds were initially discovered by DSF profiling, supporting the use of this technique to study compounds that target this, and other, pseudokinases with unusual nucleotide-binding sites [58]. I also attempted to establish TRIB2 compound binding affinity using ITC, but this was problematic because TRIB2 was not stable above 100 µM, and the compounds remained soluble under these conditions, to ~20 µM, as measured by UV-Vis spectroscopy (see Appendix). However, using MST I was able to establish an apparent the K*d* in the micromolar range for reversible binding of afatinib and TAK-

285. To corroborate these findings, molecular dynamics simulations revealed that the docked enamide moieties of both afatinib and neratinib were positioned between 3-5 Å from the Cys thiol functional groups specific to TRIB2, and remained stably bound for ~17 ns, which is believed to be favourable for covalent bond formation and is similar to the experimental parameters calculated for EGFR covalent modification [213]. By using mutational analysis *in vitro,* it was confirmed that covalent EGFR/HER2 inhibitors, including afatinib and neratinib, caused TRIB2 destabilisation by uncoupling the C-terminal tail from the pseudokinase domain upon covalent modification of Cys96 and Cys104 in the αC-helix. The strongest destabilising agent discovered from initial screening was a reversible PLK inhibitor (GW804482X), which induced destabilisation through an alternate mechanism that has yet to be elucidated. However, analysis of various truncation proteins and a TRIB2 K90M mutant suggested that reversibly binding compounds (both stabilising and destabilising) modulate TRIB2 stability by an interaction with pseudo-active site, although conformations relevant for binding remain unknown.

Allosteric release of the DQLVP motif occurs on C/EBPα substrate-binding in TRIB1 [105]. Analysis of TRIB1 revealed that binding of the substrate C/EBPα causes the C-terminal tail to uncouple from the pseudokinase domain, in turn causing the pseudokinase domain to adopt an SLE-in conformation, whereby the activation loop folds towards the αC-helix and forms a binding site for the C/EBPα degron. Isothermal titration calorimetry (ITC) revealed that maltose binding protein (MBP)-fused C/EBPα and C/EBPβ tribbles degron sequence peptides bound to TRIB1 with K*d* values of 11 and 15 μM respectfully [106]. Interestingly, phosphorylation of C/EBPβ at Ser77 and Tyr79, within the Tribbles degron, negatively regulated binding, as measured by fluorescence polarisation experiments [105]. This observation suggests that phosphorylation of C/EBP transcription factors might regulate their binding to TRIB1, depending on cell type or developmental stage. It would be interesting to repeat these experiments with TRIB2 to establish whether or not there is an analogous mechanism of regulation.

Interestingly, TRIB1 was not stabilised by the C/EBPα Tribbles degron peptide when assayed by DSF [105], perhaps because the global stability of TRIB1 did not change with binding to either the C/EBPα peptide or its own C-terminal tail. It would be interesting to see whether or not the pseudokinase domain alone of TRIB1 and TRIB2

can be stabilised by the C/EBPα peptide. Interestingly, Jamieson and colleagues (2018) [105] very recently demonstrated that some PKIS1 compounds stabilised TRIB1 in the presence of C/EBPα peptide, and that the stabilisation afforded by compound GW607049C, a previously described benzimidazole-based TIE-2/VEGF2 inhibitor, was prevented in the presence of C/EBPα peptide, potentially indicative of different binding conformations. I speculate that 'stabilising' compounds, such as lapatinib and TAK-285, might permit, or strengthen, an interaction between the C-terminal tail and the pseudokinase domain, therefore preventing TRIB2 from binding to substrates, or perhaps compete with substrates for binding in the pseudokinase domain. There are several crystal structures of TRIB1 in different conformations (and in complex with C/EBPα peptide substrate), which have recently been solved [105, 106]. Therefore, it seems feasible that in the near future TRIB1 (or TRIB2)-compound co-crystal structures will begin to emerge. This would give valuable insight into TRIB conformations relevant to compound binding for stabilising and destabilising ligands. It is worthy to note that the second most prominent class of TRIB2 stabilisers, discovered by DSF in my analysis, were benzimidazole TIE-2/VEGF2 inhibitors, which included the TRIB1 stabilising compound GW607049C. A relevant experiment, to be considered in the future, could employ TRIB2, and C/EBPα and/or C/EBPβ peptides to evaluate the structural effects, or dynamics, in the presence of selected inhibitors. It could be speculated that binding of afatinib/neratinib would uncouple the C-terminal tail from the pseudokinase domain and will either (1) enhance the binding of C/EBPα/C/EBPβ peptides or (2) cause binding of the C/EBPα/C/EBPβ peptides to be prevented. The former should result in no global change in protein stability and therefore no thermal shift in the presence of both compound and C/EBP peptide. In the latter case, there will be compound induced destabilisation. Florescence polarization experiments to observe whether or not titration of certain inhibitors can outcompete the binding of Fluorescence isothiocyanate- (FITC)-C/EBPα to TRIB2 would additionally be interesting to evaluate [105].

### *5.2* Investigation of TRIB2 protein-protein interactions *in vitro*

In Chapter 3 I confirmed that recombinant purified TRIB2 interacted with C/EBPα using GST pull down assays. A next logical future step will be to investigate the TRIB2-C/EBPα interaction in the presence of small molecule compounds, perhaps also using NMR or cryo-EM to probe the structure of the complexes. Perhaps different

compounds that offer alternate modes of binding will agonise or antagonise TRIB2 interaction with C/EBPα. Surface plasmon resonance (SPR) might be an alternative approach to determine K*d* values for C/EBP peptide binding. It would also be interesting to investigate binding between the TRIB2 C-tail containing the DQLVP motif and αC-helix using SPR in the presence of compounds. The pseudokinase domain (54-318) of TRIB2 could be immobilised by exploiting the 6His N-terminal tag and the affinity for purified TRIB2 C-terminal peptide (residues 319-343) could be elucidated.

It might be possible to assess C/EBPα degron peptide binding or C-terminal tail binding to TRIB2 in the presence/absence of compounds by using Alphascreen (Amplified Luminescent Proximity Homogeneous Assay Screen) technology. The AlphaScreen is an interaction based assay, which relies on the use of 'donor' and 'acceptor' beads that can bioconjugated. An interaction between the molecules leads to a proximity induced cascade of chemical reactions. On laser excitation of the donor bead, a reaction causes ambient oxygen to form the unstable singlet species, which can diffuse a maximum of 200 nm before conversion to back $O_2$. The generated singlet state oxygen molecules react with a chemiluminescer in the acceptor bead in turn activating fluorophores, which emit light at 520–620 nm [314]. For example, AlphaScreen was used to screen 14,500 compounds to find inhibitors which allosterically modulated the binding of a synthetic PRK2 hydrophobic motif peptide (conjugated to the donor bead) to the PIF-pocket of PDK1, which was bioconjugated to the Nickel acceptor beads via exploitation of a 6His tag [39].

Aside from C/EBPα, another substrate that TRIB2 has been reported to be a target for proteasome-mediated degradation in human cells is CDC25C, a dual phosphatase that activates CDK1 by specifically dephosphorylating residues Thr14 and Tyr15 [315]. TRIB2 was shown to bind to C/EBPα in pull down experiments. It would be interesting to repeat this experiment to observe whether or not TRIB2 can interact with recombinant CDC25C. Although, it has been reported that the majority of CDC25C, purified from *E. coli* resolved at around 220 kDa and was not present as 55 kDa monomer [316]. Additionally endogenous CDC25C immunoprecipitated from HeLa cells was observed at a complex above 200 kDa [316]. It would be interesting to observe whether or not TRIB2 interacted with the CDC25C tetramer *in vitro*. Indeed, CDC25C is differentially phosphorylated and activated by CDK1/cyclin B1,

CDK2/cyclin A2 and CDK2/cyclin E complexes [315, 317], which could potentially regulate interaction with TRIB2.

Size exclusion chromatography analysis of the pseudokinase domain of TRIB2 and the E3 ligase-binding site AQLAA-TRIB2 mutant suggested that these proteins form dimers. It is postulated that uncoupling of the C-terminal tail from the pseudokinase domain, in the absence of substrate, causes dimerization and serves as a regulatory function. Size exclusion chromatography coupled to multiangle light scattering (SEC-MALS) analysis could be used to help deduce whether or not the pseudokinase domain of TRIB2 dimerises after uncoupling of the C-terminal tail. C-related protein kinases (PRKs), of the AGC kinase superfamily, possess a HM motif in their C-terminal tail that does not form an intramolecular interaction with the PIF-pocket when the kinase domain forms an inactive homodimer [49]. Phosphorylation of the turn motif within the C-terminal tail promotes zipper-like association of the tail with the kinase domain, which results in HM binding to the PIF-pocket and stabilisation of the PRK2 active monomer [318]. Antibodies that bind to and sequester the HM motif in the C-terminal tail of PRK2 result in stabilisation of the inactive dimer [49].

### 5.2.1 Biophysical approaches for studying TRIB2

Circular dichroism (CD) can be used to help elucidate conformational changes, by observing changes in α-helical and β-sheet composition in the protein secondary structure that become modulated upon compound binding [319]. Drawing on the biophysical principles of thermal shift assays, compound binding to TRIB2 could be investigated using temperature-dependent CD (TdCD) profiling [320]. Measuring the temperature-dependent unfolding of proteins by TdCD in the absence and presence of inhibitors might lend additional support to conclusions derived from DSF analysis. For example, alterations in TRIB2 secondary structure would be more sensitive to temperature increase in the presence of destabilising agents such as afatinib and less sensitive in the presence of stabilising agents such as lapatinib. It would also be interesting observe the potential secondary structure changes upon dimerization of the TRIB2 pseudokinase domain.

An important aspect of future studies will be to chemically modify covalent EGFR/HER2 inhibitors such as afatinib, so that they have reduced affinity for their original targets, whilst ideally engineering a TRIB2 affinity in the nM region. Then,

synthesised compounds that eliminate or preserve interaction with EGFR/HER2 can be compared side-by-side in cells. In the latter case, simultaneous elimination of TRIB2 and inhibition of EGFR/HER2 signalling could be a polypharmacological asset, especially if TRIB2 expression is a contributing factor to drug-resistance, as reported for tumour cells [103]. In order to facilitate structure guided design for the development of potential TRIB2 inhibitors, structural information of TRIB2 bound to compounds would need to be generated. To date there is no NMR or crystallographic structural information available for TRIB2 and this is foremost due to the challenging nature of recombinant TRIB2 stability and propensity to aggregate *in vitro*. Previous endeavours to crystallise TRIB2 have met with failure. Nanobodies may potentially be used in future applications to stabilise WT TRIB2 and aid crystallisation [321]. Perhaps there might be more success in crystallising the hyper stable TRIB2 C104Y mutant, or fusing TRIB2 to C/EBPα, as reported recently for TRIB1 [105]. Thereupon molecular models replacing the Tyr back to a Cys *in silico* could be informative and produce a more accurate WT TRIB2 model and form the basis for the future structure guided design of potential ligands.

## 5.3 Small molecule kinase inhibitors for analysis of TRIB2 in human cells and *in vivo*

Type II EGFR/HER2 inhibitors such as lapatinib and TAK-285 stabilised the pseudokianse domain of TRIB2 in the presence and absence of the C-terminal tail. Type IV EGFR/HER2 inhibitors, including afatinib, neratinib and osimertinib, destabilised TRIB2 only in the presence of an intact DQLVP motif. On the other hand the PLK inhibitor GW804482X destabilised the pseudokianse domain of TRIB2, regardless of whether or not the C-terminal tail was present. Alternate modes of binding could stabilise different conformations and have versatile effects on TRIB2 signalling outputs in human cells. In the absence of $PIP_3$ the N-terminal domain of AKT containing the PH domain forms intramolecular interactions with the catalytic domain, stabilising an inactive conformation that sterically prevents it binding to and being phosphorylated at the activation loop Thr308 by PDK1 [322]. The compounds MK-2206 exploits this intramolecular inhibitory interaction within AKT and allosterically stabilises the interaction of the PH domain with catalytic domain [211]. This prevents

the PH domain form being sequestered by $PIP_3$. MK-2206, which is currently in numerous clinical trials for diverse types of cancers, was developed from compounds AKTi1 and AKTi2 [323]. AKTi-1 and AKTi-2 were discovered from screening to be selective for AKT1 and AKT2 and allosterically stabilise PH domain binding to the catalytic domain [323]. This inactive form of AKT also inhibits the intramolecular interaction of the C-terminal HM with the PIF-pocket in the αC-helix [211]. It is expected that future structural analysis will reveal detailed mechanisms of TRIB2 stabilisation and destabilisation and lead to the synthesis of inhibitors that specifically target various TRIB2 functions in human cells. The key effects of the AKT signalling pathway could be extended beyond pSer473, and the effects assessed on the downstream components TSC2 and mTORC1 .

Inhibitors afatinib and neratinib stimulate TRIB2 degradation in human cells at micromolar concentrations. Despite the high concentration required for TRIB2 degradation and signalling perturbation, covalent drugs have the potential to accumulate to relatively high concentrations in cells, which may be of physiological relevance for TRIB2 signalling in clinical circumstances. For example osimertinib has previously been shown to accumulate in lysosomes [214].

The effect of various compounds on C/EBPα stability in U937 cells could not be assessed due to time constraints, though it is expected that a loss of TRIB2 will be reflected by changes in C/EBPα stability. There are many other haematological cancer cell lines that could be employed to explore TRIB2 substrate ubiquitination in the presence of small molecule TRIB2 inhibitors. In U937 cells CRISPR/Cas9 technology could be utilised to mutate Cys96 and Cys104 of endogenously expressed TRIB2. It is hypothesised that C96/104S endogenous TRIB2 would not be as readily degraded in the presence of afatinib and neratinib, and therefore would result in levels of C/EBPα and pSer473 AKT being analogous to untreated cells. A role for TRIB2 in C/EBPα ubiquitination has been described in 32D cells [112]. It will be interesting to test whether or not TRIB2 destabilisation modulated C/EBPα stability in this cell line. Similarly TRIB2 was discovered to promote ubiquitination of CDC25C leading to proteasome-mediated degradation in these cells [324], which could be assessed in the presence of afatinib and neratinib. Mice that retrovirally express TRIB2 in hematopoietic stem cells develop fully penetrant, lethal AML [109]. It would be interesting to analyse the effects of various TRIB2 binding/non-binding EGFR/HER2

inhibitors in mice that have been reconstituted with hematopoietic stem cells retrovirally expressing either WT or C96/104S-TRIB2.

Finally, it will be interesting to obtain clinical samples from patients, for instance from the Lux-lung trials comparing afatinib and erlotinib in NSCLC with EGFR/HER2 activating mutations, and quantify TRIB2 expression levels after drug exposure *in vivo*. For example, levels of TRIB2 could be correlated with levels of C/EBPα and pSer473 AKT signalling in afatinib versus erlotinib treated NSCLC. ELISA-based procedures could be developed to quantify effects of these drugs on TRIB2 protein stability, as part of broader proteomics approaches to establish all of the intracellular targets of these compounds.

# Appendix

The following tables contain data from the TRIB2 PKIS1 DSF screen. Table 1 discloses all of the compounds tested, revealing average $\Delta T_m$ values. The most destabilising compounds along with information about their chemical structures and originally intended targets are disclosed in Table 2. Table 3 contains the same data as Table 2 but for the top TRIB2 stabilising compounds.

| Plate position | Compound code | ΔTm 1 | ΔTm 2 | average | st.dev |
|---|---|---|---|---|---|
| JMP-A1 | SB-630812 | -0.3 | -0.27 | -0.285 | 0.015 |
| JMP-A2 | GW831091X | -0.09 | 0 | -0.045 | 0.045 |
| JMP-A3 | GW700494X | 2.83 | 2.06 | 2.445 | 0.385 |
| JMP-A4 | GW461104B | 1.2 | 1.51 | 1.355 | 0.155 |
| JMP-A5 | GW796920X | -0.12 | 0.07 | -0.025 | 0.095 |
| JMP-A6 | GW632046X | 0.6 | 0.43 | 0.515 | 0.085 |
| JMP-A7 | GW627834A | 1.27 | 1.71 | 1.49 | 0.22 |
| JMP-A8 | GSK561866B | -0.03 | 0.24 | 0.105 | 0.135 |
| JMP-A9 | GW352430A | 0.21 | 0.25 | 0.23 | 0.02 |
| JMP-A10 | SB-734117 | 0.63 | 0.64 | 0.635 | 0.005 |
| JMP-B1 | GW620972X | -0.93 | -0.19 | -0.56 | 0.37 |
| JMP-B2 | SB-686709-A | 0.1 | 0.13 | 0.115 | 0.015 |
| JMP-B3 | GW578748X | 0.29 | 0.13 | 0.21 | 0.08 |
| JMP-B4 | GW572399X | 1.81 | 2.06 | 1.935 | 0.125 |
| JMP-B5 | GSK2163632A | -2.96 | -0.38 | -1.67 | 1.29 |
| JMP-B6 | GSK953913A | -0.01 | 0.22 | 0.105 | 0.115 |
| JMP-B7 | GSK180736A | 0.27 | 0.32 | 0.295 | 0.025 |
| JMP-B8 | SB-264866 | 0.32 | 0.29 | 0.305 | 0.015 |
| JMP-B9 | GW809897X | 1.63 | 1 | 1.315 | 0.315 |
| JMP-B10 | SB-361058 | 0.44 | 0.47 | 0.455 | 0.015 |
| JMP-C1 | GW829055X | 1.43 | 1.68 | 1.555 | 0.125 |
| JMP-C2 | GW434756X | -0.12 | 0.11 | -0.005 | 0.115 |
| JMP-C3 | GSK237700A | -0.36 | -0.55 | -0.455 | 0.095 |
| JMP-C4 | GW577921A | 0.77 | 0.03 | 0.4 | 0.37 |
| JMP-C5 | GW621970A | 0.3 | 0.36 | 0.33 | 0.03 |
| JMP-C6 | SB-741905 | 0.06 | 0.22 | 0.14 | 0.08 |
| JMP-C7 | SB-736290 | 0.11 | 0.03 | 0.07 | 0.04 |
| JMP-C8 | SB-742865 | 1.01 | 0.83 | 0.92 | 0.09 |
| JMP-C9 | GW874091X | 0.27 | 0.26 | 0.265 | 0.005 |
| JMP-C10 | SB-738561 | -1.22 | 0.34 | -0.44 | 0.78 |
| JMP-D1 | GW829115X | 0.05 | 0.28 | 0.165 | 0.115 |
| JMP-D2 | GW856804X | 0.96 | 1.15 | 1.055 | 0.095 |

| | | | | | |
|---|---|---|---|---|---|
| JMP-D3 | GW833373X | 1.05 | 0.91 | 0.98 | 0.07 |
| JMP-D4 | GW796921X | -0.02 | 0.28 | 0.13 | 0.15 |
| JMP-D5 | GSK586581B | 0 | 0.21 | 0.105 | 0.105 |
| JMP-D6 | SB-390527 | 0.24 | 0.42 | 0.33 | 0.09 |
| JMP-D7 | GSK571989A | -0.33 | 0.05 | -0.14 | 0.19 |
| JMP-D8 | GW784684X | 3.58 | 2.88 | 3.23 | 0.35 |
| JMP-D9 | GSK204925A | 0.22 | 0.72 | 0.47 | 0.25 |
| JMP-D10 | SB-236687 | 0.45 | -0.93 | -0.24 | 0.69 |
| JMP-E1 | GW829906X | 0.52 | 1.29 | 0.905 | 0.385 |
| JMP-E2 | GW813360X | 0.04 | 0.15 | 0.095 | 0.055 |
| JMP-E3 | GW680908A | 1.37 | 1.33 | 1.35 | 0.02 |
| JMPE4 | SKF-62604 | -0.11 | -0.07 | -0.09 | 0.02 |
| JMP-E5 | GSK1023156A | 0.77 | 0.24 | 0.505 | 0.265 |
| JMP-E6 | SB-751399 | 0.16 | 0.6 | 0.38 | 0.22 |
| JMP-E7 | GW574783B | 1.59 | 2.69 | 2.14 | 0.55 |
| JMP-E8 | GW641155B | 0.52 | 0.52 | 0.52 | 0 |
| JMP-E9 | GW301789X | 0.89 | 0.95 | 0.92 | 0.03 |
| JMP-E10 | GW607049B | 3.48 | 2.93 | 3.205 | 0.275 |
| JMP-F1 | GSK620503A | 0.1 | -0.36 | -0.13 | 0.23 |
| JMP-F2 | GW569530A | -2.56 | -1.87 | -2.215 | 0.345 |
| JMP-F3 | SB-264865 | -2.97 | 0.2 | -1.385 | 1.585 |
| JMP-F4 | GSK319347A | 0.39 | 0.6 | 0.495 | 0.105 |
| JMP-F5 | SB-739452 | 0.47 | 0.4 | 0.435 | 0.035 |
| JMP-F6 | GSK711701A | 0.14 | 0.65 | 0.395 | 0.255 |
| JMP-F7 | GW768505A | 1.31 | 1.14 | 1.225 | 0.085 |
| JMP-F8 | SB-814597 | 0.35 | 0.46 | 0.405 | 0.055 |
| JMP-F9 | GW837331X | 3.16 | 1.88 | 2.52 | 0.64 |
| JMP-F10 | SB-678557-A | 0.57 | 0.5 | 0.535 | 0.035 |
| JMP-G1 | GW775608X | 0.12 | 0.32 | 0.22 | 0.1 |
| JMP-G2 | GI261520A | 1.58 | 0.81 | 1.195 | 0.385 |
| JMP-G3 | SB-245392 | -0.19 | 0.09 | -0.05 | 0.14 |
| JMP-G4 | GSK317315A | 0.43 | 0.23 | 0.33 | 0.1 |
| JMP-G5 | GW817396X | 0.08 | 0.38 | 0.23 | 0.15 |
| JMP-G6 | GW785804X | 0.1 | 0.43 | 0.265 | 0.165 |
| JMP-G7 | SB-732881-H | 0.03 | 0.41 | 0.22 | 0.19 |
| JMP-G8 | GSK1173862A | 1.27 | 1.6 | 1.435 | 0.165 |
| JMP-G9 | GW301888X | 0.53 | 0.64 | 0.585 | 0.055 |
| JMP-G10 | GW843682X | 0.66 | 0.42 | 0.54 | 0.12 |
| JMP-H1 | GW405841X | 1.25 | 1.24 | 1.245 | 0.005 |
| JMP-H2 | SB-409513 | 0.07 | 0.19 | 0.13 | 0.06 |
| JMP-H3 | GSK619487A | 0.03 | 0.07 | 0.05 | 0.02 |
| JMP-H4 | GW410563A | 0.07 | 0.27 | 0.17 | 0.1 |
| JMP-H5 | GW784752X | 0.27 | 0.4 | 0.335 | 0.065 |
| JMP-H6 | SKF-86002 | 0.25 | 0.32 | 0.285 | 0.035 |

| | | | | | |
|---|---|---|---|---|---|
| JMP-H7 | SB-376719 | 0.34 | 0.33 | 0.335 | 0.005 |
| JMP-H8 | SB-223133 | 0.24 | 0.29 | 0.265 | 0.025 |
| JMP-H9 | GW708893X | 0.54 | 0.04 | 0.29 | 0.25 |
| JMP-H10 | GW759710A | 0.79 | 0.7 | 0.745 | 0.045 |
| JOJ-A1 | GW416469X | -1.26 | -0.97 | -1.115 | 0.145 |
| JOJ-A2 | SKF-86055 | -0.71 | 0.09 | -0.31 | 0.4 |
| JOJ-A3 | SB-682330-A | -1.14 | -1.04 | -1.09 | 0.05 |
| JOJ-A4 | SB-242719 | -0.55 | -0.85 | -0.7 | 0.15 |
| JOJ-A5 | SB-333612 | 0.18 | -0.13 | 0.025 | 0.155 |
| JOJ-A6 | GSK1030061A | -0.41 | -0.95 | -0.68 | 0.27 |
| JOJ-A7 | GSK1030059A | -0.6 | -0.58 | -0.59 | 0.01 |
| JOJ-A8 | GW799251X | 1.05 | -0.19 | 0.43 | 0.62 |
| JOJ-A9 | GW832467X | 0.2 | 0.51 | 0.355 | 0.155 |
| JOJ-A10 | GW296115X | 2.67 | 3.85 | 3.26 | 0.59 |
| JOJ-B1 | GW830263A | -0.27 | -0.11 | -0.19 | 0.08 |
| JOJ-B2 | GSK1751853A | -0.32 | -0.43 | -0.375 | 0.055 |
| JOJ-B3 | GW643971X | 0.84 | 0.3 | 0.57 | 0.27 |
| JOJ-B4 | SB-614067-R | 0.48 | -0.55 | -0.035 | 0.515 |
| JOJ-B5 | GW694590A | 3.6 | 3.3 | 3.45 | 0.15 |
| JOJ-B6 | SB-278538 | -1.06 | -1.31 | -1.185 | 0.125 |
| JOJ-B7 | SB-390523 | -0.53 | -0.06 | -0.295 | 0.235 |
| JOJ-B8 | GSK200398A | -0.55 | -0.29 | -0.42 | 0.13 |
| JOJ-B9 | GW829877X | -0.19 | 0.17 | -0.01 | 0.18 |
| JOJ-B10 | GW435821X | 0.63 | 0.58 | 0.605 | 0.025 |
| JOJ-C1 | GSK938890A | -1.42 | -3.46 | -2.44 | 1.02 |
| JOJ-C2 | GW445015X | 0.1 | -0.52 | -0.21 | 0.31 |
| JOJ-C3 | GW853609X | 3.48 | 2.86 | 3.17 | 0.31 |
| JOJ-C4 | SB-400868-A | -0.44 | -0.56 | -0.5 | 0.06 |
| JOJ-C5 | SB-739245-AC | -0.25 | -0.88 | -0.565 | 0.315 |
| JOJ-C6 | SB-226879 | -0.65 | -0.72 | -0.685 | 0.035 |
| JOJ-C7 | GSK1030062A | -0.62 | -0.7 | -0.66 | 0.04 |
| JOJ-C8 | GW300657X | 0.35 | -0.26 | 0.045 | 0.305 |
| JOJ-C9 | SB-633825 | -1.34 | -2.17 | -1.755 | 0.415 |
| JOJ-C10 | GSK1030058A | 0.38 | 0.44 | 0.41 | 0.03 |
| JOJ-D1 | GW810372X | -0.31 | 0.57 | 0.13 | 0.44 |
| JOJ-D2 | GW627512B | -0.33 | 0 | -0.165 | 0.165 |
| JOJ-D3 | SB-360741 | -0.12 | -0.5 | -0.31 | 0.19 |
| JOJ-D4 | GW580509X | -0.16 | -0.25 | -0.205 | 0.045 |
| JOJ-D5 | GW631581B | 1.1 | -0.12 | 0.49 | 0.61 |
| JOJ-D6 | GSK1000163A | -3.2 | 0.18 | -1.51 | 1.69 |
| JOJ-D7 | GW703087X | 3.01 | 3.59 | 3.3 | 0.29 |
| JOJ-D8 | GW869810X | 1.31 | 1.88 | 1.595 | 0.285 |
| JOJ-D9 | GW780159X | -0.66 | -0.55 | -0.605 | 0.055 |
| JOJ-D10 | SB-239272 | 0.31 | -0.27 | 0.02 | 0.29 |

| | | | | | |
|---|---|---|---|---|---|
| JOJ-E1 | GW612286X | -2.41 | -0.83 | -1.62 | 0.79 |
| JOJ-E2 | GW284408X | -1.45 | -1.17 | -1.31 | 0.14 |
| JOJ-E3 | GW450241X | -1.05 | -0.9 | -0.975 | 0.075 |
| JOJ-E4 | GSK300014A | 2.08 | 4.08 | 3.08 | 1 |
| JOJ-E5 | GW770220A | -0.97 | -0.67 | -0.82 | 0.15 |
| JOJ-E6 | GW785974X | -0.56 | -0.72 | -0.64 | 0.08 |
| JOJ-E7 | GW828525X | 1.55 | 2.82 | 2.185 | 0.635 |
| JOJ-E8 | GW406108X | -0.66 | 1.04 | 0.19 | 0.85 |
| JOJ-E9 | GW804482X | -3.41 | -3.63 | -3.52 | 0.395 |
| JOJ-E10 | GSK299115A | 0.02 | 0.93 | 0.475 | 0.455 |
| JOJ-F1 | GW290597X | -0.76 | -0.81 | -0.785 | 0.025 |
| JOJ-F2 | GW644007X | -0.84 | 0.26 | -0.29 | 0.55 |
| JOJ-F3 | GW831090X | -0.17 | -0.05 | -0.11 | 0.06 |
| JOJ-F4 | SB-409514 | -0.72 | -0.56 | -0.64 | 0.08 |
| JOJ-F5 | GW794726X | -0.13 | 0.17 | 0.02 | 0.15 |
| JOJ-F6 | GW827099X | 0.98 | 1.08 | 1.03 | 0.05 |
| JOJ-F7 | GW827106X | -0.05 | 0.11 | 0.03 | 0.08 |
| JOJ-F8 | GW846105X | 0.7 | 1.77 | 1.235 | 0.535 |
| JOJ-F9 | SB-738482 | 0.94 | 1.32 | 1.13 | 0.19 |
| JOJ-F10 | GW827396X | 2.68 | 3.19 | 2.935 | 0.255 |
| JOJ-G1 | SB-253228 | -2.45 | -0.28 | -1.365 | 1.085 |
| JOJ-G2 | GW300653X | 0.52 | 0.45 | 0.485 | 0.035 |
| JOJ-G3 | GW695874X | -1.08 | 0.01 | -0.535 | 0.545 |
| JOJ-G4 | GW575533A | 1.31 | -0.2 | 0.555 | 0.755 |
| JOJ-G5 | SB-657836-AAA | -2.54 | -0.61 | -1.575 | 0.965 |
| JOJ-G6 | GW807930X | 1.98 | 1.81 | 1.895 | 0.085 |
| JOJ-G7 | GSK943949A | -1.1 | -1.77 | -1.435 | 0.335 |
| JOJ-G8 | GW659386A | 2.33 | 3.11 | 2.72 | 0.39 |
| JOJ-G9 | GSK1511931A | -0.17 | -0.1 | -0.135 | 0.035 |
| JOJ-G10 | GSK969786A | 1.54 | 1.76 | 1.65 | 0.11 |
| JOJ-H1 | GW568326X | -2.48 | -0.07 | -1.275 | 1.205 |
| JOJ-H2 | GW861893X | 1.42 | 1.89 | 1.655 | 0.235 |
| JOJ-H3 | GW275944X | 2.5 | 1.23 | 1.865 | 0.635 |
| JOJ-H4 | GW278681X | 0.19 | -0.58 | -0.195 | 0.385 |
| JOJ-H5 | SB-711237 | -0.15 | 1.12 | 0.485 | 0.635 |
| JOJ-H6 | GW305178X | 0.1 | 1.6 | 0.85 | 0.75 |
| JOJ-H7 | GW445017X | -0.06 | -0.61 | -0.335 | 0.275 |
| JOJ-H8 | GW440139B | -0.65 | -0.52 | -0.585 | 0.065 |
| JOJ-H9 | GW651576X | -0.19 | -0.55 | -0.37 | 0.18 |
| JOJ-H10 | GW566221B | 1.96 | 1.44 | 1.7 | 0.26 |
| JOK-A1 | GSK182497A | 1.21 | 1.4 | 1.305 | 0.095 |
| JOK-A2 | GW778894X | -0.83 | -0.52 | -0.675 | 0.155 |
| JOK-A3 | SB-220455 | -1.1 | -1.4 | -1.25 | 0.15 |
| JOK-A4 | GW429374A | -0.16 | 0.05 | -0.055 | 0.105 |

| | | | | | |
|---|---|---|---|---|---|
| JOK-A5 | GW784307A | -0.54 | -0.52 | -0.53 | 0.01 |
| JOK-B1 | GW781673X | -1.53 | -0.99 | -1.26 | 0.27 |
| JOK-B2 | SB-592602 | -1.13 | -0.7 | -0.915 | 0.215 |
| JOK-B3 | SB-278539 | -1.25 | -1.24 | -1.245 | 0.005 |
| JOK-B4 | GSK2213727A | -0.73 | -0.77 | -0.75 | 0.02 |
| JOK-B5 | GW576484X | 1.97 | 2.06 | 2.015 | 0.045 |
| JOK-C1 | GSK238583A | -1.63 | -1.19 | -1.41 | 0.22 |
| JOK-C2 | GSK1392956A | -0.89 | -1.23 | -1.06 | 0.17 |
| JOK-C3 | SB-437013 | -1.59 | -1.55 | -1.57 | 0.02 |
| JOK-C4 | SB-242717 | -0.72 | -0.91 | -0.815 | 0.095 |
| JOK-D1 | GW827105X | 1.94 | 2.08 | 2.01 | 0.07 |
| JOK-D2 | GW830365A | -1.76 | -0.93 | -1.345 | 0.415 |
| JOK-D3 | GSK317354A | -0.48 | -0.86 | -0.67 | 0.19 |
| JOK-D4 | SB-742864 | -0.93 | -0.88 | -0.905 | 0.025 |
| JOK-E1 | GW441756X | -1.97 | -1.17 | -1.57 | 0.4 |
| JOK-E2 | GR105659X | -1.04 | -1.13 | -1.085 | 0.045 |
| JOK-E3 | SB-735465 | -1.06 | -0.99 | -1.025 | 0.035 |
| JOK-E4 | GW806742X | 2.59 | 2.69 | 2.64 | 0.05 |
| JOK-F1 | GW589933X | -0.75 | -1.04 | -0.895 | 0.145 |
| JOK-F2 | SB-750140 | -0.8 | -0.92 | -0.86 | 0.06 |
| JOK-F3 | GW549390X | -0.08 | 0.29 | 0.105 | 0.185 |
| JOK-F4 | GW458344A | -1.7 | -1.26 | -1.48 | 0.22 |
| JOK-G1 | GW810576X | -1.23 | -0.69 | -0.96 | 0.27 |
| JOK-G2 | GW772405X | -0.13 | 0.62 | 0.245 | 0.375 |
| JOK-G3 | GW282974A | -0.64 | -0.2 | -0.42 | 0.22 |
| JOK-G4 | SB-431533 | -0.37 | -0.8 | -0.585 | 0.215 |
| JOK-H1 | GW853606X | 0.82 | 0.72 | 0.77 | 0.05 |
| JOK-H2 | SB-732941 | -0.67 | -0.83 | -0.75 | 0.08 |
| JOK-H3 | GW581744X | -1.13 | -0.58 | -0.855 | 0.275 |
| JOK-H4 | SB-221466 | -0.53 | -0.41 | -0.47 | 0.06 |
| JOI-A1 | GW673715X | 1.75 | 2.32 | 2.035 | 0.285 |
| JOI-A2 | GW811761X | 1.02 | -0.2 | 0.41 | 0.61 |
| JOI-A3 | GW680975X | 0.89 | -0.02 | 0.435 | 0.455 |
| JOI-A4 | GSK605714A | 0.88 | 0.3 | 0.59 | 0.29 |
| JOI-A5 | GW782612X | -0.01 | 0.37 | 0.18 | 0.19 |
| JOI-B1 | GSK192082A | 2.74 | 1.72 | 2.23 | 0.51 |
| JOI-B2 | SB-707548-A | 4.01 | 3.55 | 3.78 | 0.23 |
| JOI-B3 | SB-285234-W | 0.81 | -0.27 | 0.27 | 0.54 |
| JOI-B4 | GR269666A | -0.27 | 0.14 | -0.065 | 0.205 |
| JOI-B5 | GW559768X | 0.7 | 0.38 | 0.54 | 0.16 |
| JOI-C1 | SB-675259-M | -0.32 | -0.21 | -0.265 | 0.055 |
| JOI-C2 | GSK718429A | 3.26 | 2.35 | 2.805 | 0.455 |
| JOI-C3 | GW572738X | 0.9 | -0.11 | 0.395 | 0.505 |
| JOI-C4 | GW621431X | 0.64 | -0.09 | 0.275 | 0.365 |

| | | | | | |
|---|---|---|---|---|---|
| JOI-C5 | GW416981X | 0.97 | 0.39 | 0.68 | 0.29 |
| JOI-D1 | GSK237701A | 0.54 | -1.87 | -0.665 | 1.205 |
| JOI-D2 | GW567808A | 2.72 | 2.37 | 2.545 | 0.175 |
| JOI-D3 | GSK605714A | 0.76 | -0.01 | 0.375 | 0.385 |
| JOI-D4 | GW561436X | 0.78 | -0.04 | 0.37 | 0.41 |
| JOI-D5 | GW607117X | 0.61 | 0.7 | 0.655 | 0.045 |
| JOI-E1 | GSK978744A | 0.64 | -0.54 | 0.05 | 0.59 |
| JOI-E2 | SB-744941 | 0.65 | 0.27 | 0.46 | 0.19 |
| JOI-E3 | GW574782A | 2.94 | 2.33 | 2.635 | 0.305 |
| JOI-E4 | GW575808A | 0.72 | 0.75 | 0.735 | 0.015 |
| JOI-E5 | GW654652X | 0.57 | 0.21 | 0.39 | 0.18 |
| JOI-F1 | GW513184X | 2.98 | 2.77 | 2.875 | 0.105 |
| JOI-F2 | GW622055X | 0.96 | 0.35 | 0.655 | 0.305 |
| JOI-F3 | GW589961A | 4.23 | 2.87 | 3.55 | 0.68 |
| JOI-F4 | GW569293X | 0.64 | -0.06 | 0.29 | 0.35 |
| JOI-F5 | GSK466317A | 0.76 | 0.67 | 0.715 | 0.045 |
| JOI-G1 | GW682841X | 0.65 | 0.22 | 0.435 | 0.215 |
| JOI-G2 | GSK1713088A | 2.95 | 2.58 | 2.765 | 0.185 |
| JOI-G3 | GW819230X | 0.9 | 0.21 | 0.555 | 0.345 |
| JOI-G4 | GW769076X | 1.03 | 0.33 | 0.68 | 0.35 |
| JOI-G5 | GW276655X | 0.99 | 0.68 | 0.835 | 0.155 |
| JOI-H1 | GW770249A | 4.06 | 3.13 | 3.595 | 0.465 |
| JOI-H2 | SB-242721 | 1.08 | -0.14 | 0.47 | 0.61 |
| JOI-H3 | GW642138X | 3.15 | 2.45 | 2.8 | 0.35 |
| JOI-H4 | GW820759X | 0.76 | 0.5 | 0.63 | 0.13 |
| JOI-H5 | GW819077X | 1.3 | 1.52 | 1.41 | 0.11 |
| JOI-A6 | GW680191X | -0.44 | -0.29 | -0.365 | 0.075 |
| JOI-A7 | GW583373A | 1.12 | 1.14 | 1.13 | 0.01 |
| JOI-A8 | GW335962X | -0.12 | -0.73 | -0.425 | 0.305 |
| JOI-A9 | GW301784X | -0.7 | -0.01 | -0.355 | 0.345 |
| JOI-A10 | GW824645A | -0.05 | 0.41 | 0.18 | 0.23 |
| JOI-B6 | GSK554170A | -3.58 | -0.21 | -1.895 | 1.685 |
| JOI-B7 | GSK1220512A | 0.01 | 0.48 | 0.245 | 0.235 |
| JOI-B8 | SB-253226 | -0.19 | -0.65 | -0.42 | 0.23 |
| JOI-B9 | GW282536X | -0.12 | -0.09 | -0.105 | 0.015 |
| JOI-B10 | GI98581X | -0.07 | 0.53 | 0.23 | 0.3 |
| JOI-C6 | GSK579289A | -0.57 | -0.5 | -0.535 | 0.035 |
| JOI-C7 | GW779439X | 0.79 | 0.87 | 0.83 | 0.04 |
| JOI-C8 | GW734508X | 0.37 | -0.46 | -0.045 | 0.415 |
| JOI-C9 | GW852849X | -0.59 | -0.47 | -0.53 | 0.06 |
| JOI-C10 | GW683134A | 3.66 | 3.6 | 3.63 | 0.03 |
| JOI-D6 | GW576924A | 1.11 | 1.35 | 1.23 | 0.12 |
| JOI-D7 | GW771127A | 0.07 | -0.15 | -0.04 | 0.11 |
| JOI-D8 | SB-210313 | 0.51 | -0.6 | -0.045 | 0.555 |

| | | | | | |
|---|---|---|---|---|---|
| JOI-D9 | GW580496A | 2.21 | 2.11 | 2.16 | 0.05 |
| JOI-D10 | GSK2219385A | -1.72 | 0.37 | -0.675 | 1.045 |
| JOI-E6 | GW633459A | 0.75 | 0.38 | 0.565 | 0.185 |
| JOI-E7 | GW795493X | 2.14 | 3.26 | 2.7 | 0.56 |
| JOI-E8 | GSK614526A | -0.2 | -0.5 | -0.35 | 0.15 |
| JOI-E9 | GW568377B | -0.34 | -0.02 | -0.18 | 0.16 |
| JOI-E10 | GW305074X | 2.55 | 1.29 | 1.92 | 0.63 |
| JOI-F6 | GSK466314A | -0.16 | -0.4 | -0.28 | 0.12 |
| JOI-F7 | SB-250715 | -1.93 | -0.42 | -1.175 | 0.755 |
| JOI-F8 | GSK1007102B | -0.47 | -1.07 | -0.77 | 0.3 |
| JOI-F9 | GW693917X | 3.12 | 4.37 | 3.745 | 0.625 |
| JOI-F10 | GSK2110236A | 0.07 | 0.78 | 0.425 | 0.355 |
| JOI-G6 | GW615311X | 0.51 | 0.64 | 0.575 | 0.065 |
| JOI-G7 | SB-284847-BT | -0.18 | -0.15 | -0.165 | 0.015 |
| JOI-G8 | GSK2220400A | 0.26 | -0.29 | -0.015 | 0.275 |
| JOI-G9 | GSK635416A | -0.22 | 0.1 | -0.06 | 0.16 |
| JOI-G10 | SB-251527 | -0.04 | 0.47 | 0.215 | 0.255 |
| JOI-H6 | GW621823A | 0.69 | 0.67 | 0.68 | 0.01 |
| JOI-H7 | SB-254169 | -0.05 | 0.07 | 0.01 | 0.06 |
| JOI-H8 | SB-610251-B | 0.84 | 0.8 | 0.82 | 0.02 |
| JOI-H9 | SB-693162 | -0.26 | -0.11 | -0.185 | 0.075 |
| JOI-H10 | GW701427A | 0.55 | 1.14 | 0.845 | 0.295 |
| JOH-A1 | GW809885X | -0.07 | 0.72 | 0.325 | 0.395 |
| JOH-A2 | GW678313X | -0.31 | 0.32 | 0.005 | 0.315 |
| JOH-A3 | GW782912X | -0.99 | -0.18 | -0.585 | 0.405 |
| JOH-A4 | GW694234A | 2.52 | 3.93 | 3.225 | 0.705 |
| JOH-A5 | GW432441X | -0.41 | -0.35 | -0.38 | 0.03 |
| JOH-A6 | SB-251505 | 0.06 | -0.14 | -0.04 | 0.1 |
| JOH-A7 | GW683109X | -0.12 | -0.04 | -0.08 | 0.04 |
| JOH-A8 | SB-735467 | 1.06 | -0.36 | 0.35 | 0.71 |
| JOH-A9 | GW785404X | 0.87 | -0.46 | 0.205 | 0.665 |
| JOH-A10 | GW743024X | 0.61 | 0.15 | 0.38 | 0.23 |
| JOH-B1 | GW572401X | -0.88 | 0.23 | -0.325 | 0.555 |
| JOH-B2 | GW280670X | -0.55 | 0.17 | -0.19 | 0.36 |
| JOH-B3 | GW407323A | 1.1 | 0.26 | 0.68 | 0.42 |
| JOH-B4 | GW282449A | -0.87 | -0.24 | -0.555 | 0.315 |
| JOH-B5 | SB-347804 | -0.07 | 0.75 | 0.34 | 0.41 |
| JOH-B6 | SB-242718 | 0.12 | -0.15 | -0.015 | 0.135 |
| JOH-B7 | GW616030X | 1.59 | -0.44 | 0.575 | 1.015 |
| JOH-B8 | SB-358518 | -0.26 | -0.07 | -0.165 | 0.095 |
| JOH-B9 | SB-737198 | -0.37 | -0.41 | -0.39 | 0.02 |
| JOH-B10 | GSK994854A | 0.81 | 0.54 | 0.675 | 0.135 |
| JOH-C1 | GW406731X | -0.95 | -0.03 | -0.49 | 0.46 |
| JOH-C2 | GW279320X | -1.07 | 0.22 | -0.425 | 0.645 |

| | | | | | |
|---|---|---|---|---|---|
| JOH-C3 | SB-698596-AC | -0.59 | 0.16 | -0.215 | 0.375 |
| JOH-C4 | GW794607X | -0.78 | 0.42 | -0.18 | 0.6 |
| JOH-C5 | SB-476429-A | -1.64 | -0.86 | -1.25 | 0.39 |
| JOH-C6 | GW817394X | -0.34 | 0.85 | 0.255 | 0.595 |
| JOH-C7 | GW693881A | 4.7 | 4.61 | 4.655 | 0.045 |
| JOH-C8 | SB-772077-B | -0.58 | -0.23 | -0.405 | 0.175 |
| JOH-C9 | SB-431542-A | 0.16 | 0.51 | 0.335 | 0.175 |
| JOH-C10 | GSK238063A | 1.22 | 1.63 | 1.425 | 0.205 |
| JOH-D1 | GW780056X | -0.86 | -0.01 | -0.435 | 0.425 |
| JOH-D2 | GW811168X | -0.46 | 1.35 | 0.445 | 0.905 |
| JOH-D3 | GW659893X | 3.96 | 3.72 | 3.84 | 0.12 |
| JOH-D4 | GW829874X | -0.62 | 0.51 | -0.055 | 0.565 |
| JOH-D5 | GSK270822A | -0.77 | 0.16 | -0.305 | 0.465 |
| JOH-D6 | GW396574X | 1.36 | 1.57 | 1.465 | 0.105 |
| JOH-D7 | SB-736302 | -0.37 | -0.17 | -0.27 | 0.1 |
| JOH-D8 | GSK269962B | 0.38 | 0.87 | 0.625 | 0.245 |
| JOH-D9 | GW632580X | 0 | 0.13 | 0.065 | 0.065 |
| JOH-D10 | GSK312948A | 0.12 | -0.11 | 0.005 | 0.115 |
| JOH-E1 | GSK248233A | -0.09 | -0.5 | -0.295 | 0.205 |
| JOH-E2 | GW442130X | -0.35 | 0.48 | 0.065 | 0.415 |
| JOH-E3 | GW693481X | -1.1 | 0.25 | -0.425 | 0.675 |
| JOH-E4 | GW679410X | -1.21 | 0.43 | -0.39 | 0.82 |
| JOH-E5 | GW805758X | -0.31 | 0.99 | 0.34 | 0.65 |
| JOH-E6 | GW458787A | 0.84 | 0.98 | 0.91 | 0.07 |
| JOH-E7 | GW830900A | -0.27 | 0.41 | 0.07 | 0.34 |
| JOH-E8 | GW445014X | -1.29 | -0.41 | -0.85 | 0.44 |
| JOH-E9 | SB-725317 | 0.05 | 0.43 | 0.24 | 0.19 |
| JOH-E10 | GW459057A | 0.4 | 0.2 | 0.3 | 0.1 |
| JOH-F1 | GW683768X | -0.43 | 0.23 | -0.1 | 0.33 |
| JOH-F2 | GW275616X | -0.88 | 0.23 | -0.325 | 0.555 |
| JOH-F3 | GW642125X | -0.41 | 0.57 | 0.08 | 0.49 |
| JOH-F4 | GW300660X | -0.66 | 0.67 | 0.005 | 0.665 |
| JOH-F5 | GW549034X | -1.03 | 0.09 | -0.47 | 0.56 |
| JOH-F6 | GW708336X | -0.66 | 0.28 | -0.19 | 0.47 |
| JOH-F7 | GW782907X | -1.07 | 0.7 | -0.185 | 0.885 |
| JOH-F8 | SB-743899 | -0.69 | -0.23 | -0.46 | 0.23 |
| JOH-F9 | GSK980961A | -0.74 | 0.22 | -0.26 | 0.48 |
| JOH-F10 | SB-590885-R | 0.15 | 0.02 | 0.085 | 0.065 |
| JOH-G1 | GSK949675A | -1.61 | -1.11 | -1.36 | 0.25 |
| JOH-G2 | GW786460X | -1.42 | 0.43 | -0.495 | 0.925 |
| JOH-G3 | GW876790X | -1.06 | 0.49 | -0.285 | 0.775 |
| JOH-G4 | GW427984X | -0.74 | 0.3 | -0.22 | 0.52 |
| JOH-G5 | GSK2186269A | -1.79 | -1.53 | -1.66 | 0.13 |
| JOH-G6 | GW684626B | -0.58 | 0.79 | 0.105 | 0.685 |

| | | | | | |
|---|---|---|---|---|---|
| JOH-G7 | GW806290X | -0.25 | -0.28 | -0.265 | 0.015 |
| JOH-G8 | GW445012X | -1.94 | -0.02 | -0.98 | 0.96 |
| JOH-G9 | GW711782X | -0.32 | 0.47 | 0.075 | 0.395 |
| JOH-G10 | GW576609A | 0.92 | 1.03 | 0.975 | 0.055 |
| JOH-H1 | GSK1819799A | 0.28 | 0.78 | 0.53 | 0.25 |
| JOH-H2 | GSK625137A | -1.09 | 0.28 | -0.405 | 0.685 |
| JOH-H3 | GW801372X | -1.25 | 0.66 | -0.295 | 0.955 |
| JOH-H4 | GSK317314A | -2.1 | 0.14 | -0.98 | 1.12 |
| JOH-H5 | GW284372X | 0.38 | 0.28 | 0.33 | 0.05 |
| JOH-H6 | GW701032X | -1.34 | 0.38 | -0.48 | 0.86 |
| JOH-H7 | SB-216385 | -0.55 | 0.47 | -0.04 | 0.51 |
| JOH-H8 | GW439255X | -0.51 | 0.95 | 0.22 | 0.73 |
| JOH-H9 | GW618013X | 0.44 | 0.76 | 0.6 | 0.16 |
| JOH-H10 | GSK1326255A | 2.16 | 2.18 | 2.17 | 0.01 |
| TRB2+ATP+EDTA | | 2.325 | 2.78 | 2.5525 | 0.2275 |
| | | | | | |

**Appendix Table 1: TRIB2 PKIS1 DSF screen data.**

| Compound | $\Delta T_m$ | Standard deviation | Compound information |
|---|---|---|---|
| GW804482X | -3.52 | 0.395 | Discovery of thiophene inhibitors of polo-like kinase. Bioorganic & Medicinal Chemistry Letters (2009), 19(3), 1018-1021. |
| GSK938890A | -2.44 | 1.02 | Aminofurazans as potent inhibitors of AKT kinase. Bioorganic & Medicinal Chemistry Letters (2009), 19(5), 1508-1511. |
| GW569530A | -2.215 | 0.345 | Discovery and Biological Evaluation of Potent Dual ErbB-2/EGFR Tyrosine Kinase Inhibitors: 6-Thiazolylquinazolines. Bioorganic & Medicinal Chemistry Letters (2003), 13(4), 637-640. |
| GSK554170A | -1.895 | 1.685 | Identification of 4-(2-(4-Amino-1,2,5-oxadiazol-3-yl)-1-ethyl-7-{[(3S)-3-piperidinylmethyl]oxy}-1H-imidazo[4,5-c]pyridin-4-yl)-2-methyl-3-butyn-2-ol (GSK690693), a Novel Inhibitor of AKT Kinase. Journal of Medicinal Chemistry (2008), 51(18), 5663-5679. |
| SB-633825 | -1.755 | 0.415 | Optimization of triarylimidazoles for Tie2: Influence of conformation on potency. Bioorganic & Medicinal Chemistry Letters (2007), 17(20), 5514-5517. |
| GSK2163632A | -1.67 | 1.29 | Optimization of a series of 4,6-bis-anilino-1H-pyrrolo[2,3-d]pyrimidine inhibitors of IGF-1R: elimination of an acid-mediated decomposition pathway. Bioorganic & medicinal chemistry letters (2009), 19(2), 373-7. |
| GSK2186269A | -1.66 | 0.13 | Optimization of a series of 4,6-bis-anilino-1H-pyrrolo[2,3-d]pyrimidine inhibitors of IGF-1R: elimination of an acid-mediated decomposition pathway. Bioorganic & medicinal chemistry letters (2009), 19(2), 373 |
| GW612286X | -1.62 | 0.79 | Discovery of 5-[[4-[(2,3-Dimethyl-2H-indazol-6-yl)methylamino]-2-pyrimidinyl]amino]-2-methyl-benzenesulfonamide (Pazopanib), a Novel and Potent Vascular Endothelial Growth Factor Receptor Inhibitor. Journal of Medicinal Chemistry (2008), 51(15), 4632-4640 |
| SB-657836-AAA | -1.575 | 0.965 | N-(3-Cyano-4,5,6,7-tetrahydro-1-benzothien-2-yl)amides as potent, selective, inhibitors of JNK2 and JNK3. Bioorganic & Medicinal Chemistry Letters (2007), 17(5), 1296-1301 |

| | | | |
|---|---|---|---|
| SB-437013 | -1.57 | 0.02 | Optimization of triarylimidazoles for Tie2: Influence of conformation on potency. Bioorganic & Medicinal Chemistry Letters (2007), 17(20), 5514-5517. |
| GW441756X | -1.57 | 0.4 | Discovery and in vitro evaluation of potent TrkA kinase inhibitors: oxindole and aza-oxindoles. Bioorganic & Medicinal Chemistry Letters (2004), 14(4), 953-957 |

**Apendix table 2: PKIS1 ligands with the most destabilising effect on TRIB2.**

| Compound | $\Delta T_m$ | Standard deviation | Compound information |
|---|---|---|---|
| GW837331X | 2.52 | 0.64 | Imidazo[5,1-f][1,2,4]triazin-2-amines as novel inhibitors of polo-like kinase 1. Bioorganic & Medicinal Chemistry Letters (2008), 18(23), 6214-6217 |
| GW567808A | 2.545 | 0.175 | Optimization and SAR for dual ErbB-1/ErbB-2 tyrosine kinase inhibition in the 6-furanylquinazoline series. Bioorganic & Medicinal Chemistry Letters (2006), 16(17), 4686-4691 |
| GW574782A | 2.635 | 0.305 | Optimization and SAR for dual ErbB-1/ErbB-2 tyrosine kinase inhibition in the 6-furanylquinazoline series. Bioorganic & Medicinal Chemistry Letters (2006), 16(17), 4686-4691 |
| GW806742X | 2.64 | 0.05 | Discovery of a novel and potent series of dianilinopyrimidineurea and urea isostere inhibitors of VEGFR2 tyrosine kinase. Bioorganic & Medicinal Chemistry Letters (2005), 15(15), 3519-352 |
| GW795493X | 2.7 | 0.56 | Orally active 4-amino-5-diarylurea-furo[2,3-d]pyrimidine derivatives as anti-angiogenic agent inhibiting VEGFR2 and Tie-2. Bioorganic & Medicinal Chemistry Letters (2007), 17(6), 1773-1778 |
| GW659386A | 2.72 | 0.39 | Discovery of Novel Benzimidazoles as Potent Inhibitors of TIE-2 and VEGFR-2 Tyrosine Kinase Receptors. Journal of Medicinal Chemistry (2007), 50(18), 4453-4470 |
| GSK1713088A | 2.765 | 0.185 | Optimization of 4,6-bis-anilino-1H-pyrrolo[2,3-d]pyrimidine IGF-1R tyrosine kinase inhibitors towards JNK selectivity. Bioorganic & Medicinal Chemistry Letters (2009), 19(2), 360-364 |
| GW642138X | 2.8 | 0.35 | Novel 4-aminofuro[2,3-d]pyrimidines as Tie-2 and VEGFR2 dual inhibitors. Bioorganic & Medicinal Chemistry Letters (2005), 15(9), 2203-2207. |
| GSK718429A | 2.805 | 0.455 | Knowledge-based design of 7-azaindoles as selective B-Raf inhibitors. Bioorganic & Medicinal Chemistry Letters (2008), 18(16), 4610-4614 |
| GW513184X | 2.875 | 0.105 | Novel pyrazolopyrimidine derivatives as GSK-3 inhibitors. Bioorganic & Medicinal Chemistry Letters (2004), 14(9), 2121-2125 |
| GW827396X | 2.935 | 0.255 | N-Phenyl-4-pyrazolo[1,5-b]pyridazin-3-ylpyrimidin-2-amines as Potent and Selective Inhibitors of Glycogen Synthase Kinase 3 with Good Cellular Efficacy. Journal of Medicinal Chemistry (2004), 47(19), 4716-4730 |
| GSK300014A | 3.08 | 1 | Thienopyrimidine-based dual EGFR/ErbB-2 inhibitors. Bioorganic & Medicinal Chemistry Letters (2009), 19(3), 817-820. CODEN: BMCLE8 ISSN:0960-894X. AN 2009:119140 CAPLUS |
| GW853609X | 3.17 | 0.31 | Discovery of thiophene inhibitors of polo-like kinase. Bioorganic & Medicinal Chemistry Letters (2009), 19(3), 1018-1021 |
| GW607049B | 3.205 | 0.275 | Discovery of Novel Benzimidazoles as Potent Inhibitors of TIE-2 and VEGFR-2 Tyrosine Kinase Receptors. Journal of Medicinal Chemistry (2007), 50(18), 4453-4470 |
| GW694234A | 3.225 | 0.705 | Discovery of Novel Benzimidazoles as Potent Inhibitors of TIE-2 and VEGFR-2 Tyrosine Kinase Receptors. Journal of Medicinal Chemistry (2007), 50(18), 4453-4470 |

| | | | |
|---|---|---|---|
| GW784684X | 3.23 | 0.35 | Thienopyrimidine-based dual EGFR/ErbB-2 inhibitors. Bioorganic & Medicinal Chemistry Letters (2009), 19(3), 817-820. CODEN: BMCLE8 ISSN:0960-894X. |
| GW296115X | 3.26 | 0.59 | Uings I J; Spacey G D; Bonser R W Effects of the indolocarbazole 3744W on the tyrosine kinase activity of the cytoplasmic domain of the platelet-derived growth factor beta-receptor. Cellular signalling |
| GW703087X | 3.3 | 0.29 | Alkynyl pyrimidines as dual EGFR/ErbB2 kinase inhibitors. Bioorganic & Medicinal Chemistry Letters |
| GW694590A | 3.45 | 0.15 | Discovery of Novel Benzimidazoles as Potent Inhibitors of TIE-2 and VEGFR-2 Tyrosine Kinase Receptors. Journal of Medicinal Chemistry (2007), 50(18), 4453-4470 |
| GW589961A | 3.55 | 0.68 | Discovery of Novel Benzimidazoles as Potent Inhibitors of TIE-2 and VEGFR-2 Tyrosine Kinase Receptors. Journal of Medicinal Chemistry (2007), 50(18), 4453-4470 |
| GW770249A | 3.595 | 0.465 | Orally active 4-amino-5-diarylurea-furo[2,3-d]pyrimidine derivatives as anti-angiogenic agent inhibiting VEGFR2 and Tie-2. Bioorganic & Medicinal Chemistry Letters (2007), |
| GW683134A | 3.63 | 0.03 | Discovery of Novel Benzimidazoles as Potent Inhibitors of TIE-2 and VEGFR-2 Tyrosine Kinase Receptors. Journal of Medicinal Chemistry (2007), 50(18), 4453-4470 |
| GW693917X | 3.745 | 0.625 | Discovery of Novel Benzimidazoles as Potent Inhibitors of TIE-2 and VEGFR-2 Tyrosine Kinase Receptors. Journal of Medicinal Chemistry (2007), 50(18), 4453-447 |
| SB-707548-A | 3.78 | 0.23 | Thousands of chemical starting points for antimalarial lead identification. Nature. 2010 May 20;465(7296):305-10. doi: 10.1038/nature09107 |
| GW659893X | 3.84 | 0.12 | Gw52s. Bioorganic & Medicinal Chemistry Letters (2006), 16(9), 2419-2422 |
| GW693881A | 4.655 | 0.045 | Thienopyrimidine-based dual EGFR/ErbB-2 inhibitors. Bioorganic & Medicinal Chemistry Letters |

**Appendix table 3: PKIS1 ligands with the greatest stabilising effect on TRIB2**

## UV absorbance to assess the solubility of compounds

ITC and NMR studies were limited by the poor solubility of the EGFR/HER2 inibitors proposed to bind to TRIB2. The compounds afatinib, neratinib, lapatinib, TAK-285 and erlotinib were assessed for their solubility in 20 mM Tris-HCl, 100 mM NaCl, 1 mM DTT and 2% DMSO (appendix Figure 1). Standard curves were generated by diluting known amounts of compound in 100% DMSO and reading UV absorbance at the particular compoudns wavelength of maximum absorption (λ max). ATP served as a control. The maximum concentration that could be detected by each compound in Tris buffer is indicated by a dotted line. The maximum solubilities calculated were as follows: afatinib 41.2 μM, neratinib 14.5 μM, lapatinib 17.9 μM, TAK-285 28.3 μM and erlotinib 25.9 μM.

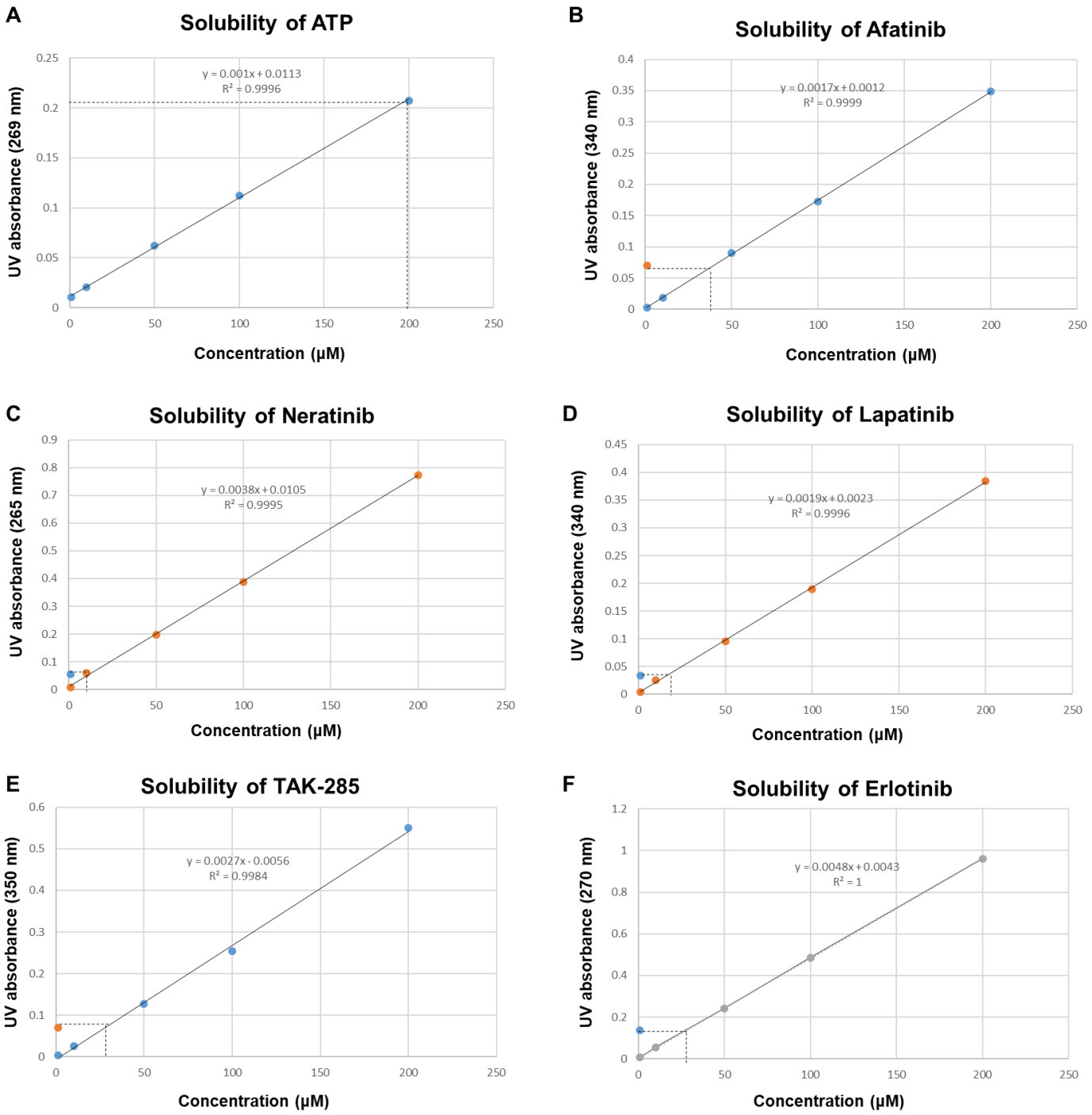


**Appendix Figure 1: Using UV absorbance to detect the maximum solubility of selected small molecule inhibitors.** Standard curves were generated by diluting the indicated compounds in DMSO and reading λ max using a NanoDrop. Compounds (A) ATP, (B) afatinib, (C) neratinib, (D) lapatinib, (E) TAK-285 and (F) erlotinib were then diluted in 20 mM Tris-HCl, 100 mM NaCl, 1 mM DTT and 2% DMSO to 200 μM. The insoluble compound was pelleted by centrifugation at 16,000 **g** for 20 minutes and the highest UV absorbance reading achieved for the supernatant was used to deduce the maximum solubility of each compound in biochemical assay buffer.

References


1. Crick, F.H., et al., *General nature of the genetic code for proteins.* Nature, 1961. **192**: p. 1227-32.
2. Bergman, J., *ATP: The Perfect Energy Currency for the Cell* CRSQ, 1999. **36**(1).
3. Manning, G., et al., *The protein kinase complement of the human genome.* Science, 2002. **298**(5600): p. 1912-34.
4. Kung, J.E. and N. Jura, *Structural Basis for the Non-catalytic Functions of Protein Kinases.* Structure, 2016. **24**(1): p. 7-24.
5. Byrne, D.P., D.M. Foulkes, and P.A. Eyers, *Pseudokinases: update on their functions and evaluation as new drug targets.* Future medicinal chemistry, 2017. **9**(2): p. 245-265.
6. Reiterer, V., P.A. Eyers, and H. Farhan, *Day of the dead: pseudokinases and pseudophosphatases in physiology and disease.* Trends in cell biology, 2014. **24**(9): p. 489-505.
7. Foulkes, D.M., et al., *Tribbles pseudokinases: novel targets for chemical biology and drug discovery?* Biochemical Society transactions, 2015. **43**(5): p. 1095-103.
8. Hari, S.B., E.A. Merritt, and D.J. Maly, *Conformation-selective ATP-competitive inhibitors control regulatory interactions and noncatalytic functions of mitogen-activated protein kinases.* Chemistry & biology, 2014. **21**(5): p. 628-35.
9. Jones, L.H., *Small-Molecule Kinase Downregulators.* Cell chemical biology, 2018. **25**(1): p. 30-35.
10. Xie, T., et al., *Pharmacological targeting of the pseudokinase Her3.* Nature chemical biology, 2014. **10**(12): p. 1006-12.
11. Klaeger, S., et al., *The target landscape of clinical kinase drugs.* Science, 2017. **358**(6367).
12. Zhang, J., P.L. Yang, and N.S. Gray, *Targeting cancer with small molecule kinase inhibitors.* Nature reviews. Cancer, 2009. **9**(1): p. 28-39.
13. Ferguson, F.M. and N.S. Gray, *Kinase inhibitors: the road ahead.* Nature reviews. Drug discovery, 2018.
14. Bailey, F.P., et al., *Going for broke: targeting the human cancer pseudokinome.* The Biochemical journal, 2015. **465**(2): p. 195-211.
15. Boudeau, J., et al., *Emerging roles of pseudokinases.* Trends in Cell Biology, 2006. **16**(9): p. 443-452.
16. Knighton, D.R., et al., *Structure of a peptide inhibitor bound to the catalytic subunit of cyclic adenosine monophosphate-dependent protein kinase.* Science, 1991. **253**(5018): p. 414-20.
17. Vandenabeele, P., et al., *Molecular mechanisms of necroptosis: an ordered cellular explosion.* Nature Reviews Molecular Cell Biology, 2010. **11**: p. 700.
18. Taylor, S.S. and A.P. Kornev, *Protein kinases: evolution of dynamic regulatory proteins.* Trends Biochem Sci, 2011. **36**(2): p. 65-77.
19. Umelo, I., et al., *Identification of a novel HER3 activating mutation homologous to EGFR-L858R in lung cancer.* Oncotarget, 2016. **7**(3): p. 3068-3083.
20. Yang, J., et al., *Crystal structure of an activated Akt/Protein Kinase B ternary complex with GSK3-peptide and AMP-PNP.* Nature Structural Biology, 2002. **9**: p. 940.
21. Huse, M. and J. Kuriyan, *The Conformational Plasticity of Protein Kinases.* Cell, 2002. **109**(3): p. 275-282.
22. Möbitz, H., *The ABC of protein kinase conformations.* Biochimica et Biophysica Acta (BBA) - Proteins and Proteomics, 2015. **1854**(10, Part B): p. 1555-1566.
23. Leroux, A.E., J.O. Schulze, and R.M. Biondi, *AGC kinases, mechanisms of regulation and innovative drug development.* Seminars in Cancer Biology, 2018. **48**: p. 1-17.
24. Kannan, N., et al., *The hallmark of AGC kinase functional divergence is its C-terminal tail, a cis-acting regulatory module.* Proc Natl Acad Sci U S A, 2007. **104**(4): p. 1272-7.
25. Biondi, R.M., et al., *High resolution crystal structure of the human PDK1 catalytic domain defines the regulatory phosphopeptide docking site.* EMBO J, 2002. **21**(16): p. 4219-28.

26. Yang, J., et al., *Molecular mechanism for the regulation of protein kinase B/Akt by hydrophobic motif phosphorylation.* Mol Cell, 2002. **9**(6): p. 1227-40.
27. Sicheri, F., I. Moarefi, and J. Kuriyan, *Crystal structure of the Src family tyrosine kinase Hck.* Nature, 1997. **385**: p. 602.
28. Xu, W., S.C. Harrison, and M.J. Eck, *Three-dimensional structure of the tyrosine kinase c-Src.* Nature, 1997. **385**: p. 595.
29. De Bondt, H.L., et al., *Crystal structure of cyclin-dependent kinase 2.* Nature, 1993. **363**: p. 595.
30. Jeffrey, P.D., et al., *Mechanism of CDK activation revealed by the structure of a cyclinA-CDK2 complex.* Nature, 1995. **376**: p. 313.
31. Kornev, A.P., et al., *Surface comparison of active and inactive protein kinases identifies a conserved activation mechanism.* Proc Natl Acad Sci U S A, 2006. **103**(47): p. 17783-8.
32. Kannan, N. and A.F. Neuwald, *Did protein kinase regulatory mechanisms evolve through elaboration of a simple structural component?* J Mol Biol, 2005. **351**(5): p. 956-72.
33. Bayliss, R., et al., *On the molecular mechanisms of mitotic kinase activation.* Open Biol, 2012. **2**(11): p. 120136.
34. Steichen, J.M., et al., *Global consequences of activation loop phosphorylation on protein kinase A.* J Biol Chem, 2010. **285**(6): p. 3825-32.
35. Nunes, Q.M., et al., *Fibroblast growth factors as tissue repair and regeneration therapeutics.* PeerJ, 2016. **4**: p. e1535.
36. Lemmon, M.A. and J. Schlessinger, *Cell signaling by receptor tyrosine kinases.* Cell, 2010. **141**(7): p. 1117-34.
37. Scheeff, E.D. and P.E. Bourne, *Structural evolution of the protein kinase-like superfamily.* PLoS Comput Biol, 2005. **1**(5): p. e49.
38. Pearce, L.R., D. Komander, and D.R. Alessi, *The nuts and bolts of AGC protein kinases.* Nature Reviews Molecular Cell Biology, 2010. **11**: p. 9.
39. Schulze, Jörg O., et al., *Bidirectional Allosteric Communication between the ATP-Binding Site and the Regulatory PIF Pocket in PDK1 Protein Kinase.* Cell Chemical Biology, 2016. **23**(10): p. 1193-1205.
40. Zhang, H., et al., *Molecular Mechanism of Regulation of the Atypical Protein Kinase C by N-terminal Domains and an Allosteric Small Compound.* Chemistry & Biology, 2014. **21**(6): p. 754-765.
41. Arencibia, J.M., et al., *AGC protein kinases: from structural mechanism of regulation to allosteric drug development for the treatment of human diseases.* Biochim Biophys Acta, 2013. **1834**(7): p. 1302-21.
42. Manning, B.D. and A. Toker, *AKT/PKB Signaling: Navigating the Network.* Cell, 2017. **169**(3): p. 381-405.
43. Toker, A. and S. Marmiroli, *Signaling specificity in the Akt pathway in biology and disease.* Advances in Biological Regulation, 2014. **55**: p. 28-38.
44. Alessi, D.R., et al., *Mechanism of activation of protein kinase B by insulin and IGF-1.* EMBO J, 1996. **15**(23): p. 6541-51.
45. Vanhaesebroeck, B., et al., *The emerging mechanisms of isoform-specific PI3K signalling.* Nature Reviews Molecular Cell Biology, 2010. **11**: p. 329.
46. Keshwani, M.M., et al., *Hydrophobic motif phosphorylation is not required for activation loop phosphorylation of p70 ribosomal protein S6 kinase 1 (S6K1).* J Biol Chem, 2011. **286**(26): p. 23552-8.
47. Lachmann, S., et al., *Regulatory domain selectivity in the cell-type specific PKN-dependence of cell migration.* PLoS One, 2011. **6**(7): p. e21732.
48. O'Sullivan, A.G., E.P. Mulvaney, and B.T. Kinsella, *Regulation of protein kinase C-related kinase (PRK) signalling by the TPα and TPβ isoforms of the human thromboxane A2 receptor: Implications for thromboxane- and androgen- dependent neoplastic and epigenetic responses*

*in prostate cancer.* Biochimica et Biophysica Acta (BBA) - Molecular Basis of Disease, 2017. **1863**(4): p. 838-856.
49. Bauer, A.F., et al., *Regulation of protein kinase C-related protein kinase 2 (PRK2) by an intermolecular PRK2-PRK2 interaction mediated by Its N-terminal domain.* J Biol Chem, 2012. **287**(24): p. 20590-602.
50. Balendran, A., et al., *A 3-phosphoinositide-dependent protein kinase-1 (PDK1) docking site is required for the phosphorylation of protein kinase Czeta (PKCzeta ) and PKC-related kinase 2 by PDK1.* J Biol Chem, 2000. **275**(27): p. 20806-13.
51. Bayliss, R., et al., *Structural Basis of Aurora-A Activation by TPX2 at the Mitotic Spindle.* Molecular Cell, 2003. **12**(4): p. 851-862.
52. Eyers, P.A., et al., *A novel mechanism for activation of the protein kinase Aurora A.* Curr Biol, 2003. **13**(8): p. 691-7.
53. Elkins, J.M., et al., *Crystal structure of human aurora B in complex with INCENP and VX-680.* J Med Chem, 2012. **55**(17): p. 7841-8.
54. Cheng, K.Y., et al., *The crystal structure of the human polo-like kinase-1 polo box domain and its phospho-peptide complex.* EMBO J, 2003. **22**(21): p. 5757-68.
55. Hubbard, S.R. and W.T. Miller, *Receptor tyrosine kinases: mechanisms of activation and signaling.* Current Opinion in Cell Biology, 2007. **19**(2): p. 117-123.
56. Ono, M. and M. Kuwano, *Molecular mechanisms of epidermal growth factor receptor (EGFR) activation and response to gefitinib and other EGFR-targeting drugs.* Clin Cancer Res, 2006. **12**(24): p. 7242-51.
57. Jura, N., et al., *Mechanism for activation of the EGF receptor catalytic domain by the juxtamembrane segment.* Cell, 2009. **137**(7): p. 1293-307.
58. Murphy, J.M., et al., *A robust methodology to subclassify pseudokinases based on their nucleotide-binding properties.* Biochem J, 2014. **457**(2): p. 323-34.
59. Mukherjee, K., et al., *CASK Functions as a Mg2+-independent neurexin kinase.* Cell, 2008. **133**(2): p. 328-39.
60. Bailey, F.P., et al., *The Tribbles 2 (TRB2) pseudokinase binds to ATP and autophosphorylates in a metal-independent manner.* Biochem J, 2015. **467**(1): p. 47-62.
61. Babon, J.J., et al., *The molecular regulation of Janus kinase (JAK) activation.* Biochem J, 2014. **462**(1): p. 1-13.
62. Xie, T., et al., *Pharmacological targeting of the pseudokinase Her3.* Nat Chem Biol, 2014. **10**(12): p. 1006-12.
63. Xu, B., et al., *WNK1, a novel mammalian serine/threonine protein kinase lacking the catalytic lysine in subdomain II.* J Biol Chem, 2000. **275**(22): p. 16795-801.
64. Zeqiraj, E., et al., *ATP and MO25alpha regulate the conformational state of the STRADalpha pseudokinase and activation of the LKB1 tumour suppressor.* PLoS Biol, 2009. **7**(6): p. e1000126.
65. Murphy, J.M., et al., *Insights into the evolution of divergent nucleotide-binding mechanisms among pseudokinases revealed by crystal structures of human and mouse MLKL.* Biochem J, 2014. **457**(3): p. 369-77.
66. Brennan, D.F., et al., *A Raf-induced allosteric transition of KSR stimulates phosphorylation of MEK.* Nature, 2011. **472**(7343): p. 366-9.
67. Lee, N., et al., *Comparative Interactomes of VRK1 and VRK3 with Their Distinct Roles in the Cell Cycle of Liver Cancer.* Mol Cells, 2017. **40**(9): p. 621-631.
68. Laurence, A., et al., *JAK Kinases in Health and Disease: An Update.* Open Rheumatol J, 2012. **6**: p. 232-44.
69. Ungureanu, D., et al., *The pseudokinase domain of JAK2 is a dual-specificity protein kinase that negatively regulates cytokine signaling.* Nat Struct Mol Biol, 2011. **18**(9): p. 971-6.

70. Lindauer, K., et al., *Prediction of the structure of human Janus kinase 2 (JAK2) comprising the two carboxy-terminal domains reveals a mechanism for autoregulation.* Protein Eng, 2001. **14**(1): p. 27-37.
71. Scott, L.M., et al., *JAK2 exon 12 mutations in polycythemia vera and idiopathic erythrocytosis.* N Engl J Med, 2007. **356**(5): p. 459-68.
72. Saharinen, P., K. Takaluoma, and O. Silvennoinen, *Regulation of the Jak2 tyrosine kinase by its pseudokinase domain.* Mol Cell Biol, 2000. **20**(10): p. 3387-95.
73. Min, X., et al., *Structural and Functional Characterization of the JH2 Pseudokinase Domain of JAK Family Tyrosine Kinase 2 (TYK2).* J Biol Chem, 2015. **290**(45): p. 27261-70.
74. Saharinen, P. and O. Silvennoinen, *The pseudokinase domain is required for suppression of basal activity of Jak2 and Jak3 tyrosine kinases and for cytokine-inducible activation of signal transduction.* J Biol Chem, 2002. **277**(49): p. 47954-63.
75. Haan, C., I. Behrmann, and S. Haan, *Perspectives for the use of structural information and chemical genetics to develop inhibitors of Janus kinases.* J Cell Mol Med, 2010. **14**(3): p. 504-27.
76. Kralovics, R., et al., *A gain-of-function mutation of JAK2 in myeloproliferative disorders.* N Engl J Med, 2005. **352**(17): p. 1779-90.
77. Dusa, A., et al., *JAK2 V617F constitutive activation requires JH2 residue F595: a pseudokinase domain target for specific inhibitors.* PLoS One, 2010. **5**(6): p. e11157.
78. Hammaren, H.M., et al., *ATP binding to the pseudokinase domain of JAK2 is critical for pathogenic activation.* Proc Natl Acad Sci U S A, 2015. **112**(15): p. 4642-7.
79. Mascarenhas, J. and R. Hoffman, *Ruxolitinib: the first FDA approved therapy for the treatment of myelofibrosis.* Clin Cancer Res, 2012. **18**(11): p. 3008-14.
80. Verstovsek, S., et al., *Ruxolitinib versus best available therapy in patients with polycythemia vera: 80-week follow-up from the RESPONSE trial.* Haematologica, 2016. **101**(7): p. 821-9.
81. Shi, F., et al., *ErbB3/HER3 intracellular domain is competent to bind ATP and catalyze autophosphorylation.* Proc Natl Acad Sci U S A, 2010. **107**(17): p. 7692-7.
82. Yarden, Y. and M.X. Sliwkowski, *Untangling the ErbB signalling network.* Nat Rev Mol Cell Biol, 2001. **2**(2): p. 127-37.
83. Zhang, N., et al., *HER3/ErbB3, an emerging cancer therapeutic target.* Acta Biochim Biophys Sin (Shanghai), 2016. **48**(1): p. 39-48.
84. Jaiswal, B.S., et al., *Oncogenic ERBB3 mutations in human cancers.* Cancer Cell, 2013. **23**(5): p. 603-17.
85. Naidu, R., et al., *Expression of c-erbB3 protein in primary breast carcinomas.* Br J Cancer, 1998. **78**(10): p. 1385-90.
86. Ma, J., et al., *Targeting of erbB3 receptor to overcome resistance in cancer treatment.* Molecular Cancer, 2014. **13**(1): p. 105.
87. Huang, S., et al., *Dual targeting of EGFR and HER3 with MEHD7945A overcomes acquired resistance to EGFR inhibitors and radiation.* Cancer Res, 2013. **73**(2): p. 824-33.
88. Lizcano, J.M., et al., *LKB1 is a master kinase that activates 13 kinases of the AMPK subfamily, including MARK/PAR-1.* The EMBO Journal, 2004. **23**(4): p. 833-843.
89. Huang, X., et al., *Important role of the LKB1-AMPK pathway in suppressing tumorigenesis in PTEN-deficient mice.* Biochem J, 2008. **412**(2): p. 211-21.
90. Pearce, Laura R., et al., *KSR2 Mutations Are Associated with Obesity, Insulin Resistance, and Impaired Cellular Fuel Oxidation.* Cell, 2013. **155**(4): p. 765-777.
91. Costanzo-Garvey, D.L., et al., *KSR2 is an essential regulator of AMP kinase, energy expenditure, and insulin sensitivity.* Cell Metab, 2009. **10**(5): p. 366-78.
92. Zhou, L., et al., *The Scaffold Protein KSR1, A Novel Therapeutic Target for the Treatment of Merlin-Deficient Tumors.* Oncogene, 2016. **35**(26): p. 3443-3453.
93. Murphy, James M., et al., *The Pseudokinase MLKL Mediates Necroptosis via a Molecular Switch Mechanism.* Immunity, 2013. **39**(3): p. 443-453.

94. Murphy, J.M., et al., *The pseudokinase MLKL mediates necroptosis via a molecular switch mechanism.* Immunity, 2013. **39**(3): p. 443-53.
95. Tang, B.L., *(WNK)ing at death: With-no-lysine (Wnk) kinases in neuropathies and neuronal survival.* Brain Res Bull, 2016. **125**: p. 92-8.
96. Piala, A.T., et al., *Chloride sensing by WNK1 involves inhibition of autophosphorylation.* Sci Signal, 2014. **7**(324): p. ra41.
97. Wilson, F.H., et al., *Human hypertension caused by mutations in WNK kinases.* Science, 2001. **293**(5532): p. 1107-12.
98. Sun, X., et al., *Down-regulation of WNK1 protein kinase in neural progenitor cells suppresses cell proliferation and migration.* J Neurochem, 2006. **99**(4): p. 1114-21.
99. Zhu, W., et al., *WNK1-OSR1 kinase-mediated phospho-activation of Na+-K+-2Cl- cotransporter facilitates glioma migration.* Mol Cancer, 2014. **13**: p. 31.
100. Haas, B.R., et al., *With-No-Lysine Kinase 3 (WNK3) stimulates glioma invasion by regulating cell volume.* Am J Physiol Cell Physiol, 2011. **301**(5): p. C1150-60.
101. Moniz, S., P. Matos, and P. Jordan, *WNK2 modulates MEK1 activity through the Rho GTPase pathway.* Cell Signal, 2008. **20**(10): p. 1762-8.
102. Liang, K.L., et al., *Human TRIB2 Oscillates during the Cell Cycle and Promotes Ubiquitination and Degradation of CDC25C.* Int J Mol Sci, 2016. **17**(9).
103. Hill, R., et al., *TRIB2 confers resistance to anti-cancer therapy by activating the serine/threonine protein kinase AKT.* Nat Commun, 2017. **8**: p. 14687.
104. Eyers, P.A., K. Keeshan, and N. Kannan, *Tribbles in the 21st Century: The Evolving Roles of Tribbles Pseudokinases in Biology and Disease.* Trends Cell Biol, 2017. **27**(4): p. 284-298.
105. Jamieson, S.A., et al., *Substrate binding allosterically relieves autoinhibition of the TRIB1 pseudokinase.* Science Signaling, 2018. **1**(1): p. 1.
106. Murphy, J.M., et al., *Molecular Mechanism of CCAAT-Enhancer Binding Protein Recruitment by the TRIB1 Pseudokinase.* Structure, 2015. **23**(11): p. 2111-21.
107. Qi, L., et al., *TRB3 links the E3 ubiquitin ligase COP1 to lipid metabolism.* Science, 2006. **312**(5781): p. 1763-6.
108. Johnson, P.F., *Molecular stop signs: regulation of cell-cycle arrest by C/EBP transcription factors.* J Cell Sci, 2005. **118**(Pt 12): p. 2545-55.
109. Keeshan, K., et al., *Tribbles homolog 2 inactivates C/EBPalpha and causes acute myelogenous leukemia.* Cancer Cell, 2006. **10**(5): p. 401-11.
110. Osada, S., et al., *DNA binding specificity of the CCAAT/enhancer-binding protein transcription factor family.* J Biol Chem, 1996. **271**(7): p. 3891-6.
111. Ellenberger, T., *Getting a grip on DNA recognition: structures of the basic region leucine zipper, and the basic region helix-loop-helix DNA-binding domains.* Current Opinion in Structural Biology, 1994. **4**(1): p. 12-21.
112. Keeshan, K., et al., *Transformation by Tribbles homolog 2 (Trib2) requires both the Trib2 kinase domain and COP1 binding.* Blood, 2010. **116**(23): p. 4948-57.
113. Rishi, L., et al., *Regulation of Trib2 by an E2F1-C/EBPalpha feedback loop in AML cell proliferation.* Blood, 2014. **123**(15): p. 2389-400.
114. Liang, K.L., et al., *TRIB2 regulates normal and stress-induced thymocyte proliferation.* Cell Discovery, 2016. **2**: p. 15050.
115. Hannon, M.M., et al., *Elevated TRIB2 with NOTCH1 activation in paediatric/adult T-ALL.* Br J Haematol, 2012. **158**(5): p. 626-34.
116. Wouters, B.J., et al., *Distinct gene expression profiles of acute myeloid/T-lymphoid leukemia with silenced CEBPA and mutations in NOTCH1.* Blood, 2007. **110**(10): p. 3706-3714.
117. Grandinetti, K.B., et al., *Overexpression of TRIB2 in human lung cancers contributes to tumorigenesis through downregulation of C/EBPα.* Oncogene, 2011. **30**: p. 3328.
118. Zhang, C., et al., *miR-511 and miR-1297 Inhibit Human Lung Adenocarcinoma Cell Proliferation by Targeting Oncogene TRIB2.* PLoS ONE, 2012. **7**(10): p. e46090.

119. Qiao, Y., Y. Zhang, and J. Wang, *Ubiquitin E3 ligase SCFβ-TRCP regulates TRIB2 stability in liver cancer cells.* Biochemical and Biophysical Research Communications, 2013. **441**(3): p. 555-559.
120. Wang, J., et al., *Impaired phosphorylation and ubiquitination by p70 S6 kinase (p70S6K) and Smad ubiquitination regulatory factor 1 (Smurf1) promote tribbles homolog 2 (TRIB2) stability and carcinogenic property in liver cancer.* J Biol Chem, 2013. **288**(47): p. 33667-81.
121. Wang, J., et al., *TRIB2 acts downstream of Wnt/TCF in liver cancer cells to regulate YAP and C/EBPalpha function.* Mol Cell, 2013. **51**(2): p. 211-25.
122. Zanella, F., et al., *Human TRIB2 is a repressor of FOXO that contributes to the malignant phenotype of melanoma cells.* Oncogene, 2010. **29**(20): p. 2973-82.
123. Song, J.J. and Y.J. Lee, *Dissociation of Akt1 from its negative regulator JIP1 is mediated through the ASK1–MEK–JNK signal transduction pathway during metabolic oxidative stress.* The Journal of Cell Biology, 2005. **170**(1): p. 61.
124. Du, K., et al., *TRB3: a tribbles homolog that inhibits Akt/PKB activation by insulin in liver.* Science, 2003. **300**(5625): p. 1574-7.
125. Eder, K., et al., *Tribbles-2 is a novel regulator of inflammatory activation of monocytes.* International Immunology, 2008. **20**(12): p. 1543-1550.
126. Nyfeler, B., S.W. Michnick, and H.-P. Hauri, *Capturing protein interactions in the secretory pathway of living cells.* Proceedings of the National Academy of Sciences of the United States of America, 2005. **102**(18): p. 6350-6355.
127. Zhang, J., P.L. Yang, and N.S. Gray, *Targeting cancer with small molecule kinase inhibitors.* Nature Reviews Cancer, 2009. **9**: p. 28.
128. Eyers, P.A., et al., *Conversion of SB 203580-insensitive MAP kinase family members to drug-sensitive forms by a single amino-acid substitution.* Chem Biol, 1998. **5**(6): p. 321-8.
129. Stefely, J.A., et al., *Mitochondrial ADCK3 employs an atypical protein kinase-like fold to enable coenzyme Q biosynthesis.* Mol Cell, 2015. **57**(1): p. 83-94.
130. Mukherjee, K., et al., *Evolution of CASK into a Mg2+-sensitive kinase.* Sci Signal, 2010. **3**(119): p. ra33.
131. Jura, N., et al., *Structural analysis of the catalytically inactive kinase domain of the human EGF receptor 3.* Proc Natl Acad Sci U S A, 2009. **106**(51): p. 21608-13.
132. Littlefield, P., et al., *Structural analysis of the EGFR/HER3 heterodimer reveals the molecular basis for activating HER3 mutations.* Sci Signal, 2014. **7**(354): p. ra114.
133. Littlefield, P., M.M. Moasser, and N. Jura, *An ATP-competitive inhibitor modulates the allosteric function of the HER3 pseudokinase.* Chem Biol, 2014. **21**(4): p. 453-8.
134. Fukuda, K., et al., *The pseudoactive site of ILK is essential for its binding to alpha-Parvin and localization to focal adhesions.* Mol Cell, 2009. **36**(5): p. 819-30.
135. Toms, A.V., et al., *Structure of a pseudokinase-domain switch that controls oncogenic activation of Jak kinases.* Nat Struct Mol Biol, 2013. **20**(10): p. 1221-3.
136. Bandaranayake, R.M., et al., *Crystal structures of the JAK2 pseudokinase domain and the pathogenic mutant V617F.* Nat Struct Mol Biol, 2012. **19**(8): p. 754-9.
137. Leroy, E., et al., *Uncoupling JAK2 V617F activation from cytokine-induced signalling by modulation of JH2 alphaC helix.* Biochem J, 2016. **473**(11): p. 1579-91.
138. Xie, T., et al., *Structural insights into RIP3-mediated necroptotic signaling.* Cell Rep, 2013. **5**(1): p. 70-8.
139. Christie, M., et al., *Structure of the PAN3 pseudokinase reveals the basis for interactions with the PAN2 deadenylase and the GW182 proteins.* Mol Cell, 2013. **51**(3): p. 360-73.
140. Artim, S.C., J.M. Mendrola, and M.A. Lemmon, *Assessing the range of kinase autoinhibition mechanisms in the insulin receptor family.* Biochem J, 2012. **448**(2): p. 213-20.
141. Senda, Y., N. Murata-Kamiya, and M. Hatakeyama, *C-terminal Src kinase-mediated EPIYA phosphorylation of Pragmin creates a feed-forward C-terminal Src kinase activation loop that promotes cell motility.* Cancer Sci, 2016. **107**(7): p. 972-80.

142. Tactacan, C.M., et al., *The pseudokinase SgK223 promotes invasion of pancreatic ductal epithelial cells through JAK1/Stat3 signaling.* Mol Cancer, 2015. **14**: p. 139.
143. Tanaka, H., H. Katoh, and M. Negishi, *Pragmin, a novel effector of Rnd2 GTPase, stimulates RhoA activity.* J Biol Chem, 2006. **281**(15): p. 10355-64.
144. Patel, O., et al., *Structure of SgK223 pseudokinase reveals novel mechanisms of homotypic and heterotypic association.* Nat Commun, 2017. **8**(1): p. 1157.
145. Agajanian, M., et al., *PEAK1 Acts as a Molecular Switch to Regulate Context-Dependent TGFbeta Responses in Breast Cancer.* PLoS One, 2015. **10**(8): p. e0135748.
146. Wang, Y., et al., *Pseudopodium-enriched atypical kinase 1 regulates the cytoskeleton and cancer progression [corrected].* Proc Natl Acad Sci U S A, 2010. **107**(24): p. 10920-5.
147. Ha, B.H. and T.J. Boggon, *The crystal structure of pseudokinase PEAK1 (Sugen kinase 269) reveals an unusual catalytic cleft and a novel mode of kinase fold dimerization.* J Biol Chem, 2018. **293**(5): p. 1642-1650.
148. Zeqiraj, E., et al., *Structure of the LKB1-STRAD-MO25 complex reveals an allosteric mechanism of kinase activation.* Science, 2009. **326**(5960): p. 1707-11.
149. Hackman, J.P., A.K. Vihola, and A.B. Udd, *The role of titin in muscular disorders.* Ann Med, 2003. **35**(6): p. 434-41.
150. Mayans, O., et al., *Structural basis for activation of the titin kinase domain during myofibrillogenesis.* Nature, 1998. **395**(6705): p. 863-9.
151. Bogomolovas, J., et al., *Titin kinase is an inactive pseudokinase scaffold that supports MuRF1 recruitment to the sarcomeric M-line.* Open Biol, 2014. **4**(5): p. 140041.
152. Tokarski, J.S., et al., *Tyrosine Kinase 2-mediated Signal Transduction in T Lymphocytes Is Blocked by Pharmacological Stabilization of Its Pseudokinase Domain.* J Biol Chem, 2015. **290**(17): p. 11061-74.
153. Scheeff, E.D., et al., *Structure of the pseudokinase VRK3 reveals a degraded catalytic site, a highly conserved kinase fold, and a putative regulatory binding site.* Structure, 2009. **17**(1): p. 128-38.
154. Durzynska, I., et al., *STK40 Is a Pseudokinase that Binds the E3 Ubiquitin Ligase COP1.* Structure, 2017. **25**(2): p. 287-294.
155. Nagano, K., et al., *Expression of Eph receptor A10 is correlated with lymph node metastasis and stage progression in breast cancer patients.* Cancer Med, 2013. **2**(6): p. 972-7.
156. Nagano, K., et al., *Eph receptor A10 has a potential as a target for a prostate cancer therapy.* Biochem Biophys Res Commun, 2014. **450**(1): p. 545-9.
157. Gu, Y., et al., *Expression of EphB6 in ovarian serous carcinoma is associated with grade, TNM stage and survival.* J Clin Pathol, 2016. **69**(5): p. 448-53.
158. Xu, D., et al., *EphB6 overexpression and Apc mutation together promote colorectal cancer.* Oncotarget, 2016. **7**(21): p. 31111-21.
159. Ma, T., et al., *Suppression of eIF2alpha kinases alleviates Alzheimer's disease-related plasticity and memory deficits.* Nat Neurosci, 2013. **16**(9): p. 1299-305.
160. Ye, J., et al., *The GCN2-ATF4 pathway is critical for tumour cell survival and proliferation in response to nutrient deprivation.* EMBO J, 2010. **29**(12): p. 2082-96.
161. Gibbons, A.V., et al., *Intestinal GUCY2C prevents TGF-beta secretion coordinating desmoplasia and hyperproliferation in colorectal cancer.* Cancer Res, 2013. **73**(22): p. 6654-66.
162. von Volkmann, H.L., et al., *An activating gucy2c mutation causes impaired contractility and fluid stagnation in the small bowel.* Scand J Gastroenterol, 2016. **51**(11): p. 1308-15.
163. Boye, S.E., *A Mini-review: Animal Models of GUCY2D Leber Congenital Amaurosis (LCA1).* Adv Exp Med Biol, 2016. **854**: p. 253-8.
164. Wood, L.D., et al., *Somatic mutations of GUCY2F, EPHA3, and NTRK3 in human cancers.* Hum Mutat, 2006. **27**(10): p. 1060-1.
165. Lin, S.C., Y.C. Lo, and H. Wu, *Helical assembly in the MyD88-IRAK4-IRAK2 complex in TLR/IL-1R signalling.* Nature, 2010. **465**(7300): p. 885-90.

166. Wang, H., et al., *A coding IRAK2 protein variant compromises Toll-like receptor (TLR) signaling and is associated with colorectal cancer survival.* J Biol Chem, 2014. **289**(33): p. 23123-31.
167. Goettel, J.A., et al., *KSR1 is a functional protein kinase capable of serine autophosphorylation and direct phosphorylation of MEK1.* Exp Cell Res, 2011. **317**(4): p. 452-63.
168. Roy, F. and M. Therrien, *MAP kinase module: the Ksr connection.* Curr Biol, 2002. **12**(9): p. R325-7.
169. Yan, F., et al., *Kinase suppressor of Ras-1 protects intestinal epithelium from cytokine-mediated apoptosis during inflammation.* J Clin Invest, 2004. **114**(9): p. 1272-80.
170. Zafrullah, M., et al., *Kinase suppressor of Ras transphosphorylates c-Raf-1.* Biochem Biophys Res Commun, 2009. **390**(3): p. 434-40.
171. Cavalieri, D., et al., *Analysis of gene expression profiles reveals novel correlations with the clinical course of colorectal cancer.* Oncol Res, 2007. **16**(11): p. 535-48.
172. Sarzani, R., *Ed 05-4 Natriuretic Peptides, Metabolic Syndrome and Hypertension: An Integrated View.* J Hypertens, 2016. **34 Suppl 1**: p. e187.
173. Kake, T., et al., *Chronically elevated plasma C-type natriuretic peptide level stimulates skeletal growth in transgenic mice.* Am J Physiol Endocrinol Metab, 2009. **297**(6): p. E1339-48.
174. Kuthe, A., et al., *Expression of guanylyl cyclase B in the human corpus cavernosum penis and the possible involvement of its ligand C-type natriuretic polypeptide in the induction of penile erection.* J Urol, 2003. **169**(5): p. 1918-22.
175. Tamura, N., et al., *Critical roles of the guanylyl cyclase B receptor in endochondral ossification and development of female reproductive organs.* Proc Natl Acad Sci U S A, 2004. **101**(49): p. 17300-5.
176. Wei, H., et al., *NRBP1 is downregulated in breast cancer and NRBP1 overexpression inhibits cancer cell proliferation through Wnt/beta-catenin signaling pathway.* Onco Targets Ther, 2015. **8**: p. 3721-30.
177. Larsson, J., et al., *Nuclear receptor binding protein 2 is induced during neural progenitor differentiation and affects cell survival.* Mol Cell Neurosci, 2008. **39**(1): p. 32-9.
178. Zhang, L., et al., *NRBP2 overexpression increases the chemosensitivity of hepatocellular carcinoma cells via Akt signaling.* Cancer Res, 2016.
179. Yamagishi, R., N. Hosoda, and S. Hoshino, *Arsenite inhibits mRNA deadenylation through proteolytic degradation of Tob and Pan3.* Biochem Biophys Res Commun, 2014. **455**(3-4): p. 323-31.
180. Dunn, N.R. and N.S. Tolwinski, *Ptk7 and Mcc, Unfancied Components in Non-Canonical Wnt Signaling and Cancer.* Cancers (Basel), 2016. **8**(7).
181. Kim, J.H., et al., *Protein tyrosine kinase 7 plays a tumor suppressor role by inhibiting ERK and AKT phosphorylation in lung cancer.* Oncol Rep, 2014. **31**(6): p. 2708-12.
182. Pearce, L.R., D. Komander, and D.R. Alessi, *The nuts and bolts of AGC protein kinases.* Nat Rev Mol Cell Biol, 2010. **11**(1): p. 9-22.
183. Pelletier, S., *SCYL pseudokinases in neuronal function and survival.* Neural Regen Res, 2016. **11**(1): p. 42-4.
184. Yoshida-Moriguchi, T., et al., *SGK196 is a glycosylation-specific O-mannose kinase required for dystroglycan function.* Science, 2013. **341**(6148): p. 896-9.
185. Kuo, P.L., et al., *STK31 is a cell-cycle regulated protein that contributes to the tumorigenicity of epithelial cancer cells.* PLoS One, 2014. **9**(3): p. e93303.
186. Yin, F.F., et al., *Serine/threonine kinases 31(STK31) may be a novel cellular target gene for the HPV16 oncogene E7 with potential as a DNA hypomethylation biomarker in cervical cancer.* Virol J, 2016. **13**: p. 60.
187. Veleva-Rotse, B.O., et al., *STRAD pseudokinases regulate axogenesis and LKB1 stability.* Neural Dev, 2014. **9**: p. 5.
188. Jackson, K.A., et al., *Aberrant STYK1 expression in ovarian cancer tissues and cell lines.* J Ovarian Res, 2009. **2**(1): p. 15.

189. Liu, Y., et al., *NOK/STYK1 promotes the genesis and remodeling of blood and lymphatic vessels during tumor progression.* Biochem Biophys Res Commun, 2016. **478**(1): p. 254-9.
190. Wang, Z., et al., *STYK1 promotes epithelial-mesenchymal transition and tumor metastasis in human hepatocellular carcinoma through MEK/ERK and PI3K/AKT signaling.* Sci Rep, 2016. **6**: p. 33205.
191. Bhoj, E.J., et al., *Mutations in TBCK, Encoding TBC1-Domain-Containing Kinase, Lead to a Recognizable Syndrome of Intellectual Disability and Hypotonia.* Am J Hum Genet, 2016. **98**(4): p. 782-8.
192. Guerreiro, R.J., et al., *Mutation of TBCK causes a rare recessive developmental disorder.* Neurol Genet, 2016. **2**(3): p. e76.
193. Liu, Y., X. Yan, and T. Zhou, *TBCK influences cell proliferation, cell size and mTOR signaling pathway.* PLoS One, 2013. **8**(8): p. e71349.
194. Kim, H.J., et al., *Structural and biochemical insights into the role of testis-expressed gene 14 (TEX14) in forming the stable intercellular bridges of germ cells.* Proc Natl Acad Sci U S A, 2015. **112**(40): p. 12372-7.
195. Mondal, G., et al., *Tex14, a Plk1-regulated protein, is required for kinetochore-microtubule attachment and regulation of the spindle assembly checkpoint.* Mol Cell, 2012. **45**(5): p. 680-95.
196. Grandinetti, K.B., et al., *Overexpression of TRIB2 in human lung cancers contributes to tumorigenesis through downregulation of C/EBPalpha.* Oncogene, 2011. **30**(30): p. 3328-35.
197. Yokoyama, T. and T. Nakamura, *Tribbles in disease: Signaling pathways important for cellular function and neoplastic transformation.* Cancer Sci, 2011. **102**(6): p. 1115-22.
198. Aime, P., et al., *Trib3 Is Elevated in Parkinson's Disease and Mediates Death in Parkinson's Disease Models.* J Neurosci, 2015. **35**(30): p. 10731-49.
199. Zhang, W., et al., *TRIB3 mediates glucose-induced insulin resistance via a mechanism that requires the hexosamine biosynthetic pathway.* Diabetes, 2013. **62**(12): p. 4192-200.
200. Tapias, A., et al., *Trrap-dependent histone acetylation specifically regulates cell-cycle gene transcription to control neural progenitor fate decisions.* Cell Stem Cell, 2014. **14**(5): p. 632-43.
201. Wang, J., et al., *Analysis of TRRAP as a Potential Molecular Marker and Therapeutic Target for Breast Cancer.* J Breast Cancer, 2016. **19**(1): p. 61-7.
202. Liu, M., et al., *Ulk4 Regulates Neural Stem Cell Pool.* Stem Cells, 2016. **34**(9): p. 2318-31.
203. Liu, M., et al., *Ulk4 Is Essential for Ciliogenesis and CSF Flow.* J Neurosci, 2016. **36**(29): p. 7589-600.
204. Brennan, D.F., et al., *A Raf-induced allosteric transition of KSR stimulates phosphorylation of MEK.* Nature, 2011. **472**: p. 366.
205. Liu, Y. and N.S. Gray, *Rational design of inhibitors that bind to inactive kinase conformations.* Nature Chemical Biology, 2006. **2**: p. 358.
206. Manley, P.W., et al., *Imatinib: a selective tyrosine kinase inhibitor.* European Journal of Cancer, 2002. **38**: p. S19-S27.
207. Byrne, D.P., D.M. Foulkes, and P.A. Eyers, *Pseudokinases: update on their functions and evaluation as new drug targets.* Future Med Chem, 2017. **9**(2): p. 245-265.
208. Han, Y., et al., *Structure of Human RNase L Reveals the Basis for Regulated RNA Decay in the IFN Response.* Science, 2014. **343**(6176): p. 1244-1248.
209. Cowan-Jacob, S.W., W. Jahnke, and S. Knapp, *Novel approaches for targeting kinases: allosteric inhibition, allosteric activation and pseudokinases.* Future Medicinal Chemistry, 2014. **6**(5): p. 541-561.
210. Schulze, J.O., et al., *Bidirectional Allosteric Communication between the ATP-Binding Site and the Regulatory PIF Pocket in PDK1 Protein Kinase.* Cell Chem Biol, 2016. **23**(10): p. 1193-1205.
211. Wu, W.I., et al., *Crystal structure of human AKT1 with an allosteric inhibitor reveals a new mode of kinase inhibition.* PLoS One, 2010. **5**(9): p. e12913.

212. Yun, C.H., et al., *The T790M mutation in EGFR kinase causes drug resistance by increasing the affinity for ATP.* Proc Natl Acad Sci U S A, 2008. **105**(6): p. 2070-5.
213. Chaikuad, A., et al., *The Cysteinome of Protein Kinases as a Target in Drug Development.* Angew Chem Int Ed Engl, 2018. **57**(16): p. 4372-4385.
214. Niessen, S., et al., *Proteome-wide Map of Targets of T790M-EGFR-Directed Covalent Inhibitors.* Cell Chemical Biology, 2017. **24**(11): p. 1388-1400.e7.
215. Soria, J.-C., et al., *Afatinib versus erlotinib as second-line treatment of patients with advanced squamous cell carcinoma of the lung (LUX-Lung 8): an open-label randomised controlled phase 3 trial.* The Lancet Oncology, 2015. **16**(8): p. 897-907.
216. Xie, T., et al., *Pharmacological Targeting of the Pseudokinase Her3.* Nature chemical biology, 2014. **10**(12): p. 1006-1012.
217. Hildebrand, J.M., et al., *Activation of the pseudokinase MLKL unleashes the four-helix bundle domain to induce membrane localization and necroptotic cell death.* Proc Natl Acad Sci U S A, 2014. **111**(42): p. 15072-7.
218. Hall, M.D., A. Simeonov, and M.I. Davis, *Avoiding Fluorescence Assay Interference-The Case for Diaphorase.* Assay Drug Dev Technol, 2016. **14**(3): p. 175-9.
219. Johnston, P.A., *Redox cycling compounds generate H2O2 in HTS buffers containing strong reducing reagents--real hits or promiscuous artifacts?* Curr Opin Chem Biol, 2011. **15**(1): p. 174-82.
220. Coan, K.E., et al., *Promiscuous aggregate-based inhibitors promote enzyme unfolding.* J Med Chem, 2009. **52**(7): p. 2067-75.
221. Hermann, J.C., et al., *Metal impurities cause false positives in high-throughput screening campaigns.* ACS Med Chem Lett, 2013. **4**(2): p. 197-200.
222. Rainard, J.M., G.C. Pandarakalam, and S.P. McElroy, *Using Microscale Thermophoresis to Characterize Hits from High-Throughput Screening: A European Lead Factory Perspective.* SLAS Discov, 2018. **23**(3): p. 225-241.
223. Seidel, S.A., et al., *Microscale thermophoresis quantifies biomolecular interactions under previously challenging conditions.* Methods, 2013. **59**(3): p. 301-15.
224. Pollack, S.J., et al., *A comparative study of fragment screening methods on the p38alpha kinase: new methods, new insights.* J Comput Aided Mol Des, 2011. **25**(7): p. 677-87.
225. Linke, P., et al., *An Automated Microscale Thermophoresis Screening Approach for Fragment-Based Lead Discovery.* J Biomol Screen, 2016. **21**(4): p. 414-21.
226. Martin, L.J., et al., *Structure-Based Design of an in Vivo Active Selective BRD9 Inhibitor.* J Med Chem, 2016. **59**(10): p. 4462-75.
227. Watzig, H., et al., *Data quality in drug discovery: the role of analytical performance in ligand binding assays.* J Comput Aided Mol Des, 2015. **29**(9): p. 847-65.
228. Seo, J., et al., *Retention of Native Protein Structures in the Absence of Solvent: A Coupled Ion Mobility and Spectroscopic Study.* Angewandte Chemie International Edition, 2016. **55**(45): p. 14173-14176.
229. Kitova, E.N., et al., *Reliable Determinations of Protein–Ligand Interactions by Direct ESI-MS Measurements. Are We There Yet?* Journal of The American Society for Mass Spectrometry, 2012. **23**(3): p. 431-441.
230. Konermann, L., et al., *Unraveling the mechanism of electrospray ionization.* Anal Chem, 2013. **85**(1): p. 2-9.
231. Göth, M. and K. Pagel, *Ion mobility–mass spectrometry as a tool to investigate protein–ligand interactions.* Analytical and Bioanalytical Chemistry, 2017. **409**(18): p. 4305-4310.
232. Elkins, J.M., et al., *Comprehensive characterization of the Published Kinase Inhibitor Set.* Nature Biotechnology, 2015. **34**: p. 95.
233. Nivón, L.G., R. Moretti, and D. Baker, *A Pareto-Optimal Refinement Method for Protein Design Scaffolds.* PLoS ONE, 2013. **8**(4): p. e59004.

234. Trott, O. and A.J. Olson, *AutoDock Vina: improving the speed and accuracy of docking with a new scoring function, efficient optimization and multithreading.* Journal of computational chemistry, 2010. **31**(2): p. 455-461.
235. Hanwell, M.D., et al., *Avogadro: an advanced semantic chemical editor, visualization, and analysis platform.* Journal of Cheminformatics, 2012. **4**(1): p. 17.
236. Savitski, M.M., et al., *Tracking cancer drugs in living cells by thermal profiling of the proteome.* Science, 2014. **346**(6205).
237. Li, K., F. Wang, and Z.W. Hu, *Targeting pseudokinase TRIB3 brings about a new therapeutic option for acute promyelocytic leukemia.* Mol Cell Oncol, 2017. **4**(4): p. e1337547.
238. Salazar, M., et al., *TRIB3 suppresses tumorigenesis by controlling mTORC2/AKT/FOXO signaling.* Mol Cell Oncol, 2015. **2**(3): p. e980134.
239. O'Connor, C., et al., *Trib2 expression in granulocyte-monocyte progenitors drives a highly drug resistant acute myeloid leukaemia linked to elevated Bcl2.* Oncotarget, 2018. **9**(19): p. 14977-14992.
240. Hammaren, H.M., A.T. Virtanen, and O. Silvennoinen, *Nucleotide-binding mechanisms in pseudokinases.* Biosci Rep, 2015. **36**(1): p. e00282.
241. Ferguson, F.M. and N.S. Gray, *Kinase inhibitors: the road ahead.* Nat Rev Drug Discov, 2018. **17**(5): p. 353-377.
242. Elkins, J.M., et al., *Comprehensive characterization of the Published Kinase Inhibitor Set.* Nat Biotechnol, 2016. **34**(1): p. 95-103.
243. Robertson, N.S. and D.R. Spring, *Using Peptidomimetics and Constrained Peptides as Valuable Tools for Inhibiting Protein(-)Protein Interactions.* Molecules, 2018. **23**(4).
244. Boivin, S., S. Kozak, and R. Meijers, *Optimization of protein purification and characterization using Thermofluor screens.* Protein Expr Purif, 2013. **91**(2): p. 192-206.
245. Vedadi, M., et al., *Chemical screening methods to identify ligands that promote protein stability, protein crystallization, and structure determination.* Proc Natl Acad Sci U S A, 2006. **103**(43): p. 15835-40.
246. Good, N.E., et al., *Hydrogen ion buffers for biological research.* Biochemistry, 1966. **5**(2): p. 467-77.
247. Santarino, I.B., S.C.B. Oliveira, and A.M. Oliveira-Brett, *Protein reducing agents dithiothreitol and tris(2-carboxyethyl)phosphine anodic oxidation.* Electrochemistry Communications, 2012. **23**: p. 114-117.
248. Lambrecht, M.A., et al., *Impact of extraction and elution media on non-size effects in size exclusion chromatography of proteins.* J Chromatogr A, 2015. **1415**: p. 100-7.
249. Carpenter, J.F., et al., *Potential inaccurate quantitation and sizing of protein aggregates by size exclusion chromatography: essential need to use orthogonal methods to assure the quality of therapeutic protein products.* J Pharm Sci, 2010. **99**(5): p. 2200-8.
250. Byrne, D.P., et al., *cAMP-dependent protein kinase (PKA) complexes probed by complementary differential scanning fluorimetry and ion mobility-mass spectrometry.* Biochem J, 2016. **473**(19): p. 3159-75.
251. Vedadi, M., et al., *Biophysical characterization of recombinant proteins: a key to higher structural genomics success.* J Struct Biol, 2010. **172**(1): p. 107-19.
252. Roy, A., A. Kucukural, and Y. Zhang, *I-TASSER: a unified platform for automated protein structure and function prediction.* Nat Protoc, 2010. **5**(4): p. 725-38.
253. Slobodan, V., et al., *Flavors of protein disorder.* Proteins: Structure, Function, and Bioinformatics, 2003. **52**(4): p. 573-584.
254. Fedorov, O., et al., *A systematic interaction map of validated kinase inhibitors with Ser/Thr kinases.* Proc Natl Acad Sci U S A, 2007. **104**(51): p. 20523-8.
255. Bunkoczi, G., et al., *Structural and functional characterization of the human protein kinase ASK1.* Structure, 2007. **15**(10): p. 1215-26.

256. Gaul, M.D., et al., *Discovery and biological evaluation of potent dual ErbB-2/EGFR tyrosine kinase inhibitors: 6-thiazolylquinazolines.* Bioorg Med Chem Lett, 2003. **13**(4): p. 637-40.
257. Rheault, T.R., et al., *Thienopyrimidine-based dual EGFR/ErbB-2 inhibitors.* Bioorg Med Chem Lett, 2009. **19**(3): p. 817-20.
258. Iyer, G.H., M.J. Moore, and S.S. Taylor, *Consequences of lysine 72 mutation on the phosphorylation and activation state of cAMP-dependent kinase.* J Biol Chem, 2005. **280**(10): p. 8800-7.
259. Honigberg, L.A., et al., *The Bruton tyrosine kinase inhibitor PCI-32765 blocks B-cell activation and is efficacious in models of autoimmune disease and B-cell malignancy.* Proc Natl Acad Sci U S A, 2010. **107**(29): p. 13075-80.
260. Jerabek-Willemsen, M., et al., *Molecular interaction studies using microscale thermophoresis.* Assay Drug Dev Technol, 2011. **9**(4): p. 342-53.
261. Schwartz, P.A., et al., *Covalent EGFR inhibitor analysis reveals importance of reversible interactions to potency and mechanisms of drug resistance.* Proc Natl Acad Sci U S A, 2014. **111**(1): p. 173-8.
262. Milani, M., et al., *DRP-1 is required for BH3 mimetic-mediated mitochondrial fragmentation and apoptosis.* Cell Death Dis, 2017. **8**(1): p. e2552.
263. Bruncko, M., et al., *Structure-Guided Design of a Series of MCL-1 Inhibitors with High Affinity and Selectivity.* Journal of Medicinal Chemistry, 2015. **58**(5): p. 2180-2194.
264. Cheng, H., S.K. Nair, and B.W. Murray, *Recent progress on third generation covalent EGFR inhibitors.* Bioorg Med Chem Lett, 2016. **26**(8): p. 1861-8.
265. Solca, F., et al., *Target binding properties and cellular activity of afatinib (BIBW 2992), an irreversible ErbB family blocker.* J Pharmacol Exp Ther, 2012. **343**(2): p. 342-50.
266. Trott, O. and A.J. Olson, *AutoDock Vina: improving the speed and accuracy of docking with a new scoring function, efficient optimization, and multithreading.* J Comput Chem, 2010. **31**(2): p. 455-61.
267. Bianco, G., et al., *Covalent docking using autodock: Two-point attractor and flexible side chain methods.* Protein Sci, 2016. **25**(1): p. 295-301.
268. Leshchiner, E.S., et al., *Direct inhibition of oncogenic KRAS by hydrocarbon-stapled SOS1 helices.* Proc Natl Acad Sci U S A, 2015. **112**(6): p. 1761-6.
269. Thomas, J.C., et al., *Inhibition of Ral GTPases Using a Stapled Peptide Approach.* J Biol Chem, 2016. **291**(35): p. 18310-25.
270. Fulton, M.D., et al., *Conformationally constrained peptides target the allosteric kinase dimer interface and inhibit EGFR activation.* Bioorg Med Chem, 2018. **26**(6): p. 1167-1173.
271. Zhang, J., P.L. Yang, and N.S. Gray, *Targeting cancer with small molecule kinase inhibitors.* Nat Rev Cancer, 2009. **9**(1): p. 28-39.
272. Schrage, Y.M., et al., *Kinome profiling of chondrosarcoma reveals SRC-pathway activity and dasatinib as option for treatment.* Cancer Res, 2009. **69**(15): p. 6216-22.
273. Drewry, D.H., T.M. Willson, and W.J. Zuercher, *Seeding collaborations to advance kinase science with the GSK Published Kinase Inhibitor Set (PKIS).* Curr Top Med Chem, 2014. **14**(3): p. 340-2.
274. Chaikuad, A., et al., *A unique inhibitor binding site in ERK1/2 is associated with slow binding kinetics.* Nat Chem Biol, 2014. **10**(10): p. 853-60.
275. Foulkes, D.M., et al., *Tribbles pseudokinases: novel targets for chemical biology and drug discovery?* Biochem Soc Trans, 2015. **43**(5): p. 1095-103.
276. Liang, K.L., et al., *Human TRIB2 Oscillates during the Cell Cycle and Promotes Ubiquitination and Degradation of CDC25C.* International journal of molecular sciences, 2016. **17**(9).
277. Salome, M., J. Campos, and K. Keeshan, *TRIB2 and the ubiquitin proteasome system in cancer.* Biochemical Society transactions, 2015. **43**(5): p. 1089-94.
278. O'Connor, C., et al., *The presence of C/EBPalpha and its degradation are both required for TRIB2-mediated leukaemia.* Oncogene, 2016. **35**(40): p. 5272-5281.

279. Sung, H.Y., et al., *Regulation of expression and signalling modulator function of mammalian tribbles is cell-type specific.* Immunol Lett, 2006. **104**(1-2): p. 171-7.
280. Kiss-Toth, E., et al., *Human tribbles, a protein family controlling mitogen-activated protein kinase cascades.* J Biol Chem, 2004. **279**(41): p. 42703-8.
281. Holmes, J.L. and R.S. Pollenz, *Determination of aryl hydrocarbon receptor nuclear translocator protein concentration and subcellular localization in hepatic and nonhepatic cell culture lines: development of quantitative Western blotting protocols for calculation of aryl hydrocarbon receptor and aryl hydrocarbon receptor nuclear translocator protein in total cell lysates.* Mol Pharmacol, 1997. **52**(2): p. 202-11.
282. Dickinson, J. and S.J. Fowler, *Quantification of Proteins on Western Blots Using ECL*, in *The Protein Protocols Handbook*, J.M. Walker, Editor. 2002, Humana Press: Totowa, NJ. p. 429-437.
283. Briggs, E.M., et al., *Long interspersed nuclear element-1 expression and retrotransposition in prostate cancer cells.* Mob DNA, 2018. **9**: p. 1.
284. Gomez-Martinez, M., D. Schmitz, and A. Hergovich, *Generation of stable human cell lines with tetracycline-inducible (Tet-on) shRNA or cDNA expression.* Journal of visualized experiments : JoVE, 2013(73): p. 10.3791/50171.
285. Dedhia, P.H., et al., *Differential ability of Tribbles family members to promote degradation of C/EBPalpha and induce acute myelogenous leukemia.* Blood, 2010. **116**(8): p. 1321-8.
286. Prodromou, C., *Mechanisms of Hsp90 regulation.* Biochem J, 2016. **473**(16): p. 2439-52.
287. Blank, M., et al., *Enhanced ubiquitinylation of heat shock protein 90 as a potential mechanism for mitotic cell death in cancer cells induced with hypericin.* Cancer Res, 2003. **63**(23): p. 8241-7.
288. Murtagh, J., H. Lu, and E.L. Schwartz, *Taxotere-induced inhibition of human endothelial cell migration is a result of heat shock protein 90 degradation.* Cancer Res, 2006. **66**(16): p. 8192-9.
289. Nalluri, S., et al., *EGFR signaling defines Mcl(-)1 survival dependency in neuroblastoma.* Cancer Biol Ther, 2015. **16**(2): p. 276-86.
290. Sundstrom, C. and K. Nilsson, *Establishment and characterization of a human histiocytic lymphoma cell line (U-937).* Int J Cancer, 1976. **17**(5): p. 565-77.
291. Liu, Q., et al., *Developing irreversible inhibitors of the protein kinase cysteinome.* Chem Biol, 2013. **20**(2): p. 146-59.
292. Martinez Molina, D., et al., *Monitoring drug target engagement in cells and tissues using the cellular thermal shift assay.* Science, 2013. **341**(6141): p. 84-7.
293. Savitski, M.M., et al., *Tracking cancer drugs in living cells by thermal profiling of the proteome.* Science, 2014. **346**(6205): p. 1255784.
294. Jafari, R., et al., *The cellular thermal shift assay for evaluating drug target interactions in cells.* Nat Protoc, 2014. **9**(9): p. 2100-22.
295. Leroux, A.E., J.O. Schulze, and R.M. Biondi, *AGC kinases, mechanisms of regulation and innovative drug development.* Semin Cancer Biol, 2018. **48**: p. 1-17.
296. Chatterjee, S. and T.F. Burns, *Targeting Heat Shock Proteins in Cancer: A Promising Therapeutic Approach.* Int J Mol Sci, 2017. **18**(9).
297. Zhang, Y., et al., *Destabilization of akt promotes the death of myeloma cell lines.* Biomed Res Int, 2014. **2014**: p. 190629.
298. Ahsan, A., et al., *Destabilization of the epidermal growth factor receptor (EGFR) by a peptide that inhibits EGFR binding to heat shock protein 90 and receptor dimerization.* J Biol Chem, 2013. **288**(37): p. 26879-86.
299. Xu, W., et al., *Sensitivity of mature Erbb2 to geldanamycin is conferred by its kinase domain and is mediated by the chaperone protein Hsp90.* J Biol Chem, 2001. **276**(5): p. 3702-8.
300. Soubeyrand, S., et al., *TRIB1 Is Regulated Post-Transcriptionally by Proteasomal and Non-Proteasomal Pathways.* PLoS One, 2016. **11**(3): p. e0152346.

301. Ji, L., M. Wu, and Z. Li, *Rutacecarpine Inhibits Angiogenesis by Targeting the VEGFR2 and VEGFR2-Mediated Akt/mTOR/p70s6k Signaling Pathway.* Molecules, 2018. **23**(8).
302. Gomez-Martinez, M., D. Schmitz, and A. Hergovich, *Generation of stable human cell lines with Tetracycline-inducible (Tet-on) shRNA or cDNA expression.* J Vis Exp, 2013(73): p. e50171.
303. Zhang, T., et al., *Covalent targeting of remote cysteine residues to develop CDK12 and CDK13 inhibitors.* Nat Chem Biol, 2016. **12**(10): p. 876-84.
304. Gao, Y., et al., *Overcoming Resistance to the THZ Series of Covalent Transcriptional CDK Inhibitors.* Cell Chem Biol, 2018. **25**(2): p. 135-142 e5.
305. Niessen, S., et al., *Proteome-wide Map of Targets of T790M-EGFR-Directed Covalent Inhibitors.* Cell Chem Biol, 2017. **24**(11): p. 1388-1400 e7.
306. Polier, S., et al., *ATP-competitive inhibitors block protein kinase recruitment to the Hsp90-Cdc37 system.* Nat Chem Biol, 2013. **9**(5): p. 307-12.
307. Schneider, C., et al., *Pharmacologic shifting of a balance between protein refolding and degradation mediated by Hsp90.* Proc Natl Acad Sci U S A, 1996. **93**(25): p. 14536-41.
308. Taipale, M., et al., *Quantitative analysis of HSP90-client interactions reveals principles of substrate recognition.* Cell, 2012. **150**(5): p. 987-1001.
309. Sun, L., et al., *Mixed lineage kinase domain-like protein mediates necrosis signaling downstream of RIP3 kinase.* Cell, 2012. **148**(1-2): p. 213-27.
310. Lim, S.M., et al., *Development of small molecules targeting the pseudokinase Her3.* Bioorg Med Chem Lett, 2015. **25**(16): p. 3382-9.
311. Rucker, F.G., et al., *Disclosure of candidate genes in acute myeloid leukemia with complex karyotypes using microarray-based molecular characterization.* J Clin Oncol, 2006. **24**(24): p. 3887-94.
312. Rothlisberger, B., et al., *TRIB1 overexpression in acute myeloid leukemia.* Cancer Genet Cytogenet, 2007. **176**(1): p. 58-60.
313. Reiterer, V., P.A. Eyers, and H. Farhan, *Day of the dead: pseudokinases and pseudophosphatases in physiology and disease.* Trends Cell Biol, 2014. **24**(9): p. 489-505.
314. Eglen, R.M., et al., *The Use of AlphaScreen Technology in HTS: Current Status.* Current Chemical Genomics, 2008. **1**: p. 2-10.
315. Aressy, B. and B. Ducommun, *Cell cycle control by the CDC25 phosphatases.* Anticancer Agents Med Chem, 2008. **8**(8): p. 818-24.
316. Franckhauser, C., A. Fernandez, and N.J. Lamb, *Purification and biochemical analysis of catalytically active human cdc25C dual specificity phosphatase.* Biochimie, 2013. **95**(7): p. 1450-61.
317. Hoffmann, I., et al., *Phosphorylation and activation of human cdc25-C by cdc2--cyclin B and its involvement in the self-amplification of MPF at mitosis.* EMBO J, 1993. **12**(1): p. 53-63.
318. Hauge, C., et al., *Mechanism for activation of the growth factor-activated AGC kinases by turn motif phosphorylation.* EMBO J, 2007. **26**(9): p. 2251-61.
319. Bertucci, C., M. Pistolozzi, and A. De Simone, *Circular dichroism in drug discovery and development: an abridged review.* Anal Bioanal Chem, 2010. **398**(1): p. 155-66.
320. Mayhood, T.W. and W.T. Windsor, *Ligand binding affinity determined by temperature-dependent circular dichroism: cyclin-dependent kinase 2 inhibitors.* Anal Biochem, 2005. **345**(2): p. 187-97.
321. Steyaert, J. and B. K Kobilka, *Nanobody stabilization of G protein coupled receptor conformational states.* Current opinion in structural biology, 2011. **21**(4): p. 567-572.
322. Parikh, C., et al., *Disruption of PH-kinase domain interactions leads to oncogenic activation of AKT in human cancers.* Proc Natl Acad Sci U S A, 2012. **109**(47): p. 19368-73.
323. Lindsley, C.W., et al., *Allosteric Akt (PKB) inhibitors: discovery and SAR of isozyme selective inhibitors.* Bioorg Med Chem Lett, 2005. **15**(3): p. 761-4.
324. Liang, K.L., et al., *Human TRIB2 Oscillates during the Cell Cycle and Promotes Ubiquitination and Degradation of CDC25C.* International Journal of Molecular Sciences, 2016. **17**(9): p. 1378.